Doctoral Thesis

Data assimilation to improve sea ice predictability in the Arctic Ocean

（北極海の海氷予測改善のためのデータ同化）

MUDUNKOTUWE HITIWADI VIDANELAGE DULINI YASARA MUDUNKOTUWA

（ドゥリニ　ヤサーラー　ムドゥンコトゥウェ）

Acknowledgement

The entire journey of the PhD program was very challenging, humbling and fun at the same time. There were many people who very kindly assisted me throughout this tough journey.

First, I would like to thank Professor Hajime Yamaguchi who was kind enough to accept me into his laboratory and have been supervising me by providing me with valuable advice, opportunities and financial assistance throughout these 3 years. Thank you very much for introducing me to such an interesting field like physical oceanography and constantly deepening my knowledge in the field with your valuable comments.

I acknowledge the support from my PhD committee Prof. S. Tabeta, Prof. T. Waseda Prof. H. Hasumi, and Assoc. Prof. D. Kitazawa for their valuable comments that enriched my thesis.

I would like to thank Dr. W.A. De Silva for all the kind support and advise during past three years. I would also like to thank Dr. J. Ono and Dr. N. Kimura for sharing data and providing me advise. I am grateful to all the wonderful lab members of Yamaguchi laboratory. Thank you for being so nice to me.

I acknowledge support from the Green Network of Excellence Program Arctic Climate Change Research Project (GRENE) and Arctic Challenge for Sustainability Research Project (ArCS) by the Japanese Ministry of Education, Culture, Sports, Science and Technology (MEXT) and a Kakenhi grant (no. 26249133) from the Japan Society for the Promotion of Science (JSPS).

I would also like to thank Prof. C. Kato and Dr. P. Samarakoon for teaching me how to do research and for providing me with recommendation letters.

With the end of PhD, I'm putting an end to my student life. I am ever so grateful to all the wonderful teachers in my life in Naritasan kindergarten, Taxila primary college, Devi Balika Vidyalaya, University of Moratuwa and University of Tokyo.

Life in Japan is challenging in many ways. I would like to thank all my friends who helped me to get used to life here. I would also like to thank all my Sri Lankan friends in Japan for all the support and good fun we had in Japan. I would also like to thank Gaba and all my students there. I learned a lot while teaching you.

I would like to thank all my friends who spared time to be in touch even though I am far away. I'm ever so grateful to wonderful Kalyana Mittas who helped me to keep calm and stay sane in these three years.

My family and extended family have always supported me throughout my life. I sincerely thank Amma, thatta, malli, aiya, Ranhawadi and all my extended family members for all the support and love. Nothing would've been possible if it wasn't for my wonderful husband who was supportive in every possible way. Thank you for being so encouraging in the darkest hours.

Finally, I would like to thank people of Sri Lanka and Japan for funding my studies for many years. Long live the free education in Sri Lanka. I will not take it for granted.

To

My parents who sacrificed everything in their lives to make sure I am granted with the right opportunities in life, and to My husband who would never let me give up.

Abstract

The Ice-POM model is used to predict sea ice conditions along the Arctic Sea Routes. However, the model-only-predictions aren't reliable due to the uncertainties in initial conditions and forcing data. The aim of this study is to overcome these drawbacks by introducing a data assimilation system to the Ice-POM model.

This study focuses on using data assimilation to improve the predictability of Ice-POM model. The aim of the study is to improve the model predictions such that it would produce better initial conditions for high-resolution models as well as sea route mapping models. Another objective is to use satellite observations of different sea ice variables. Sea ice concentration, sea ice thickness and sea ice velocity are assimilated in the study.

The study also focuses on testing several assimilation methods. Three-assimilation methods namely i) direct insertion method, ii) an improved nudging method and iii) an atmospheric forcing Kalman filter (based on ensemble Kalman filter) method are tested. The nudging method that is used, reflects the errors of both observations and the model. Atmospheric forcing Kalman filter method uses different atmospheric forcing data from different weather agencies in each ensemble member. The assimilated variables are sea ice concentration, sea ice thickness and sea ice velocity, which are assimilated individually and in combination. The assimilation time window is also varied using daily, weekly, monthly and yearly intervals.

Assimilating sea ice variables improved ocean and ice conditions as expected. It is evident from the changes in sea ice extent, sea ice thickness and ocean salinity. This is confirmed by comparing resulting ocean salinity with observations. While daily assimilation yields the best results, it is also evident that the weekly and monthly assimilation window can also produce sea ice extent predictions with acceptable accuracy compared to the model-only predictions in summer.

Non-assimilated sea ice variables have also been indirectly improved by assimilation. Improvements in sea ice variables are emphasized in the Barents Sea and near the pole. The assimilation results are used to initialize regional models. Regional model predictions show improvement in ice edge predictions in the melting and freezing season confirming the effectiveness of assimilation.

Table of Contents

List of tables

Abbreviations

AFKF- Atmospheric forcing Kalman filter

ASR - Arctic Sea Route

Conc. - Sea ice concentration

DI - Direct insertion method

EnKF - Ensemble Kalman filter method

NSR - Northern Sea Route

NU - Nudging method

NU-TC- Nudging method that uses nudging weight=1 and time constant=12 hours

NU1 –Nudging method 1

NU2-TC –Nudging method 2 that uses time constant =12 hours

SSS - Sea surface salinity

TC-Time constant

Thic. - Sea ice thickness

TIGGE-Historical THORPEX Interactive Grand Global Ensemble

Vel. - Sea ice velocity

List of figures

1. Introduction

This chapter presents research background and the motivation for this study.

1.1 Motivation

Arctic sea ice is a key component of the global climate system. It acts as a heat sink that keeps the Polar regions from warming by reflecting nearly 80% of sunlight back to the space. Having a higher albedo compared to open ocean, sea ice reduces the amount of heat absorbed by the ocean. Many ecosystems and indigenous cultures rely on sea ice for habitat and for nourishment. Sea ice also shields low lying coastal areas from erosion by ocean waves. It is also considered as a prominent indicator of global warming.

During the past few decades sea ice cover in the Arctic Ocean has been rapidly decreasing. It is evident from the average monthly Arctic sea ice extent produced by the National Snow and Ice Data center(NSIDC) from 1979 to 2015 (figure 1-1). The Inuit communities have also been observing this. “Solid ice has disappeared and there are no longer huge icebergs during autumn and winter. The ice now comes later and goes out earlier and it is getting thinner” (Wongittilin 2000).

There are various theories and hypothesis to explain this accelerated retreat of sea ice in the past few decades. Some of the valid theories are increased atmospheric warming (Rothrock 2005), ice albedo and ice feedback effect (Ikeda 2003), increased heat transportation from the Atlantic Ocean and the Pacific Ocean to the Arctic Ocean (Shimada 2006) (Steele 2008) intensification of Arctic Dipole effect (Ikeda 2009), and the enhanced upward heat flux from ocean resulting from changing wind fields (Watanabe 2013). According to several model predictions using Community Climate System Model 4.0 (CCSM4), there is significant probability of observing ice-free Arctic Ocean in summer within next few decades (Wang 2012) (Overland 2013)(figure 1-2).

While the changing sea ice cover has several implications on global climate system, it has also led to opening the Arctic Sea Routes (ASR) for an extended period. ASRs consist of two

main paths namely Northeastern passage that is also known as Northern Sea Route (NSR) and the Northwestern passage (figure 1-3).

Northern Sea Route runs between Kara Strait and Bering Strait along the Russian Federation. Northwestern passage is the route that connects Atlantic and Pacific Oceans, along the coastline of Alaska via waterways through Canadian archipelago and Baffin Bay. These routes can connect East Asia to Northern Europe and Northern America in a much shorter distance; the travel distance is shortened by about 40 percent from the commonly used southern shipping route. Therefore, navigation along the ASRs is economically appealing. However, it is also necessary to ensure the safety of the ships that travel along the ASRs. In order to navigate safely, it is important to know the sea ice conditions in the Arctic Ocean well in advance. Ice-POM model (De Silva 2013), (Fujisaki 2010) can be used to predict sea ice conditions along ASRs with middle and high resolution (25km, 2.5km).

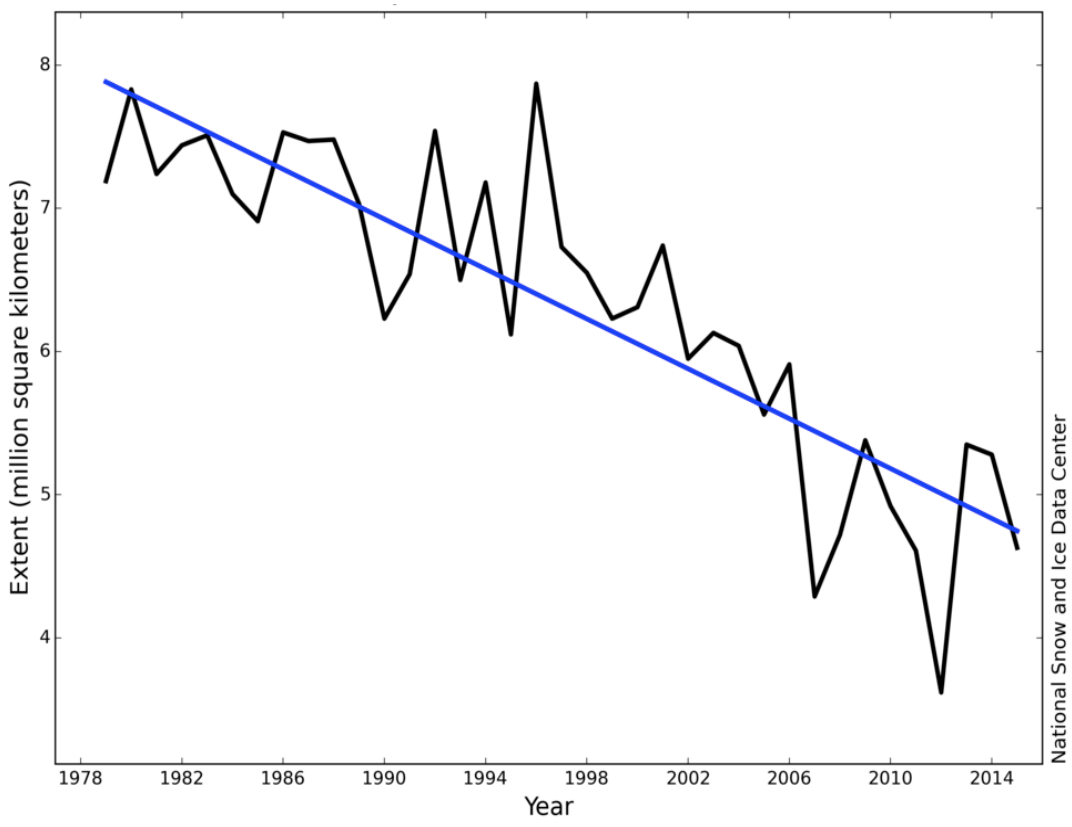

Figure 1-1: Average monthly Arctic sea ice extent in September (1979-2015) (National Snow and Ice Data Center 2015)

However, model only predictions are prone to produce faulty results due to uncertainties in initial conditions, uncertainties in forcing data, and the limitations of spatial and temporal resolution. Improving initial conditions in an ice-ocean coupled model is challenging due to the lack of sea ice observation data, ocean salinity and temperature observation data. Ice-POM model extracts its initial conditions for high-resolution models using the whole Arctic model with 25km resolution (figure 1-4). The focus of this study is to improve the whole Arctic model (25km) predictions using data assimilation. This would improve the initial conditions of the high-resolution model.

1.2 Research Background

Data assimilation is a widely used concept in numerical weather predictions to improve the model predictions using observation data. However, there are only a few studies available on data assimilation using satellite sea ice observations.

Lindsay et al. 2006 assimilated sea ice concentration and sea ice velocity covering whole Arctic region. However, the grid they have used is a coarse grid of 40km resolution. Lindsay et al. (2006) has also used a fixed value for observation errors irrespective of location and time, but in reality, the observation errors considerably vary with time and location.

Caya et al. (2010) have assimilated sea ice concentration and sea ice thickness. They have employed a coarse grid and the focus is only on Canadian East coast. Toyoda et al. (2011) has assimilated sea ice concentration. They have limited their domain to the East Siberian and the Beaufort seas. In a recent study Lindsay et al. (2012) have assimilated sea ice concentration and sea surface temperature. This study is only performed during summer. Scott et al. (2012) have assimilated sea ice concentration and sea surface temperature using 3D Variational (3DVAR) method. However, Scott's study is only performed from December 2006 to June 2007 avoiding summer. A study by Sakov et al. (2012) uses ensemble Kalman filter using TOPAZ4(a coupled ocean-sea ice data assimilation system for the Arctic Ocean) model using different sea ice observation products that are used in this thesis.

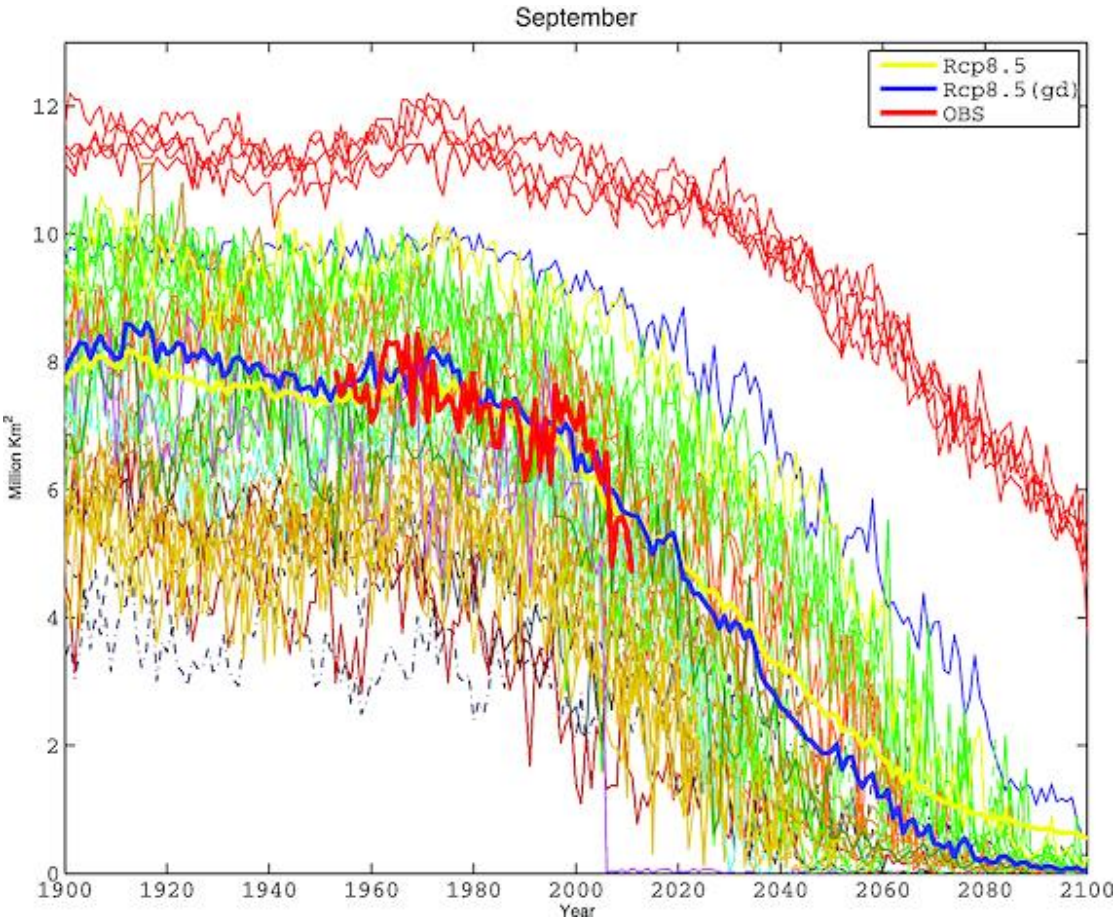

Figure 1-2: September Arctic sea ice extent from CMIP5 models for historical and RCP8.5 runs. Each thin colored line represents one ensemble member. Thick colored lines are the ensemble mean of all members (yellow), and ensemble means from seven selected models (blue), The thick red line is based on observations (HadleyISST_ice) as adjusted by Meier before 1979. Units are million square kilometers. (Wang 2012)

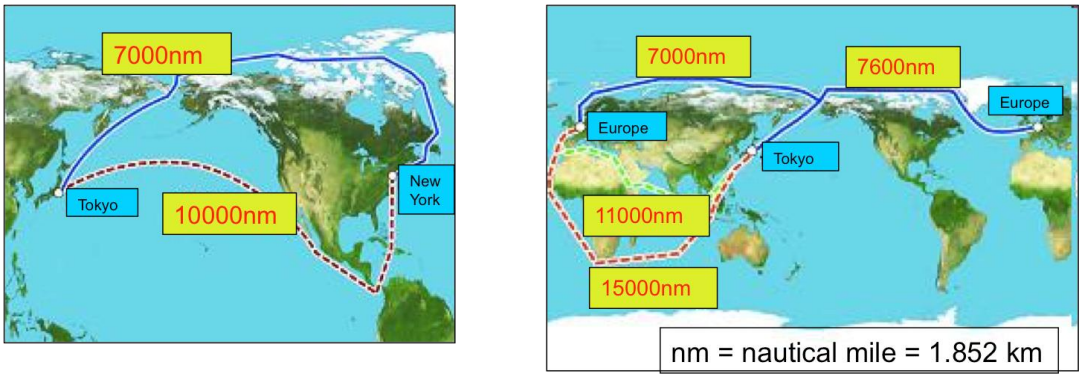

Figure 1-3: (a)(left) Northwest passage is shown in solid line. Conventional route is shown by the dotted line. (b)(right) Northeastern passage that is also known as northern shipping route is shown in solid line. The dotted lines show the conventional routes. (Weathernews 2008)

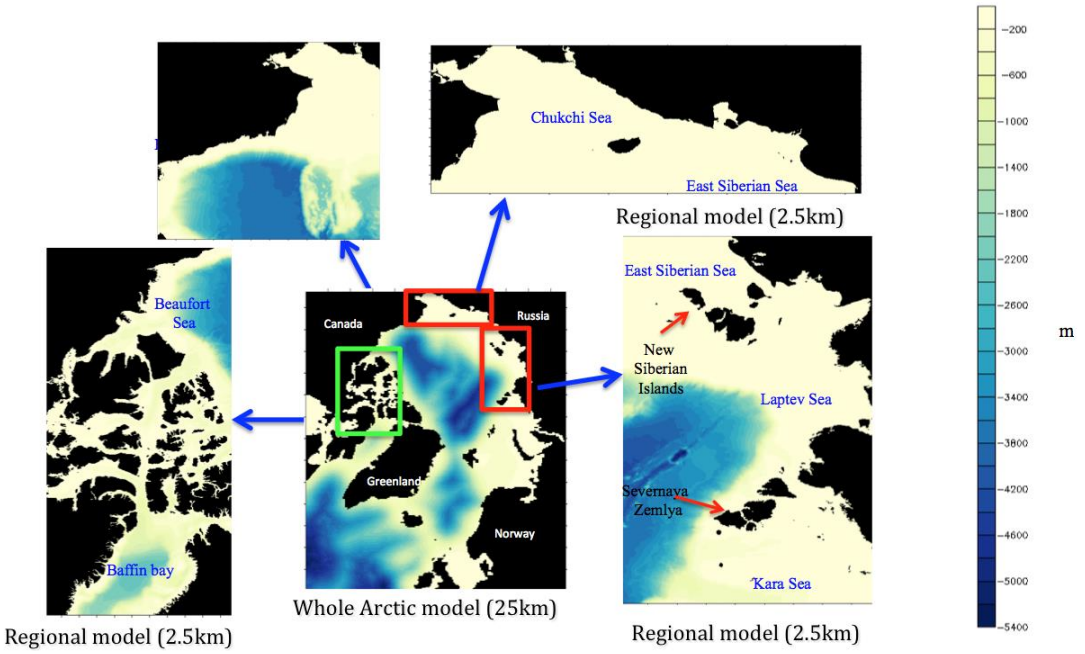

Figure 1-4: Initial conditions for 2.5km regional models are extracted from 25km whole arctic model (De Silva 2013)

Most of the commonly used methods in data assimilation of sea ice variables are nudging method, optimal interpolation method and the 3DVAR method with ensemble Kalman filter (Caya et al. 2010), (Lindsay et al. 2006), (Lindsay et al. 2012), (Scott et al. 2012). It can also be observed that most of the previous studies are only focusing on assimilating only one sea ice variable out of which the most common variable is the sea ice concentration.

An extensive literature survey is carried out. The summary of the literature survey is presented in table 1-1-a and 1-1-b. Table 1-1-c is the color code for table 1-1-a and 1-1-b. One of the conclusions from the study is that when more than one variable is assimilated, sea ice predictability improved significantly. In previous works nudging method and optimal interpolation methods aren't used for multiple variable assimilations. When a single variable is assimilated all methods produce similar results. In most of the studies observation errors and model errors are time independent. This thesis aims to create a more efficient data assimilation system for ice ocean coupled Ice-POM model.

1.3 Research objectives

The main objective of this study is to implement a data assimilation system into ice-ocean coupled Ice-POM model. The aim is to implement a data assimilation system into mid resolution (25km) model. This would consequently improve initial ice and ocean conditions of high-resolution (2.5 km) regional models. This study also focuses on evaluating the effectiveness of different assimilation methods in the Ice-POM model. The study also uses different observation products to that of previous studies.

- Introduce data assimilation into Ice-POM
    - Improve the initial conditions and boundary conditions of the high-resolution models by introducing data assimilation to mid resolution model.
- Assimilate different variables (single/multiple) and testing their effectiveness
    - Ice concentration, ice velocity, ice thickness
- Use different data assimilation methods and testing their effectiveness

  Direct insertion, nudging, Atmospheric forcing Kalman filter (AFKF)

1.4 Originality

This study is a first attempt to implement a data assimilation system to ice-POM model. In this study data assimilation is introduced to ice-POM model with the aim of accurately predicting the short-term sea ice distribution along the ASRs. Compared with the work mentioned above this study uses a model with better resolution (25km and 2.5km). The domain covers a large area including the Arctic Ocean, Greenland-Iceland-Norwegian (GIN) seas and the Northern Atlantic Ocean. Unlike other studies three sea ice variables, namely sea ice concentration, sea ice thickness and sea ice velocity are used in this study. This study uses three assimilation methods namely, direct insertion method, nudging method and atmospheric forcing Kalman filter method and the effectiveness of the methods are discussed comprehensively.

Table 1-1: Predictability improvement by assimilating different variables

Parameters	Ice conc.	Ice Velocity	Ice thickness	Ice concentration and thickness	Ice concentration and velocity	Ice concentration, brightness temperature	Ice thickness ,snow thickness
Accuracy improvement							

Table 1-1-b: Comparing different assimilation methods

Method	Nudging single variable	Optimal interpolation single variable	Ensemble Kalman filter single variable	Optimal interpolation multiple variables	Ensemble Kalman filter multiple
Accuracy improvement					
Computational complexity					
Computational time					

Table 1-1-c: color code for 1-1-a and 1-1-b

Low	
Medium	
High	

The study uses observation products that haven't been used in other mentioned studies. This study considers observation bias as well as model errors. Unlike most of the work discussed before, in this study observation bias as well as model errors are time dependent.

So far there hasn't been any comprehensive sensitivity study about different assimilation methods and the parameters that affects data assimilation in sea ice-ocean coupled computations. In this study assimilation time interval is also considered and its impact on the quality of resulting predictions are also considered. The effect on lead-time from different assimilation techniques and different variables is also investigated in this study.

1.5 Organization

This thesis is organized as follows. First chapter introduces the research background. Chapter two describes the ice ocean coupled Ice-POM model and presents the results of the model run. Assimilation methods and the process are presented in chapter three. Chapter four, five, and six present the results and discussions from three assimilation methods used. Chapter seven evaluates the impact of assimilation. Chapter eight presents the regional modeling and assimilation in the regional model. Conclusions section presents the summary of the important findings of this study and the future direction of the work.

2. Ice-POM Model

This chapter presents model description and assimilation method

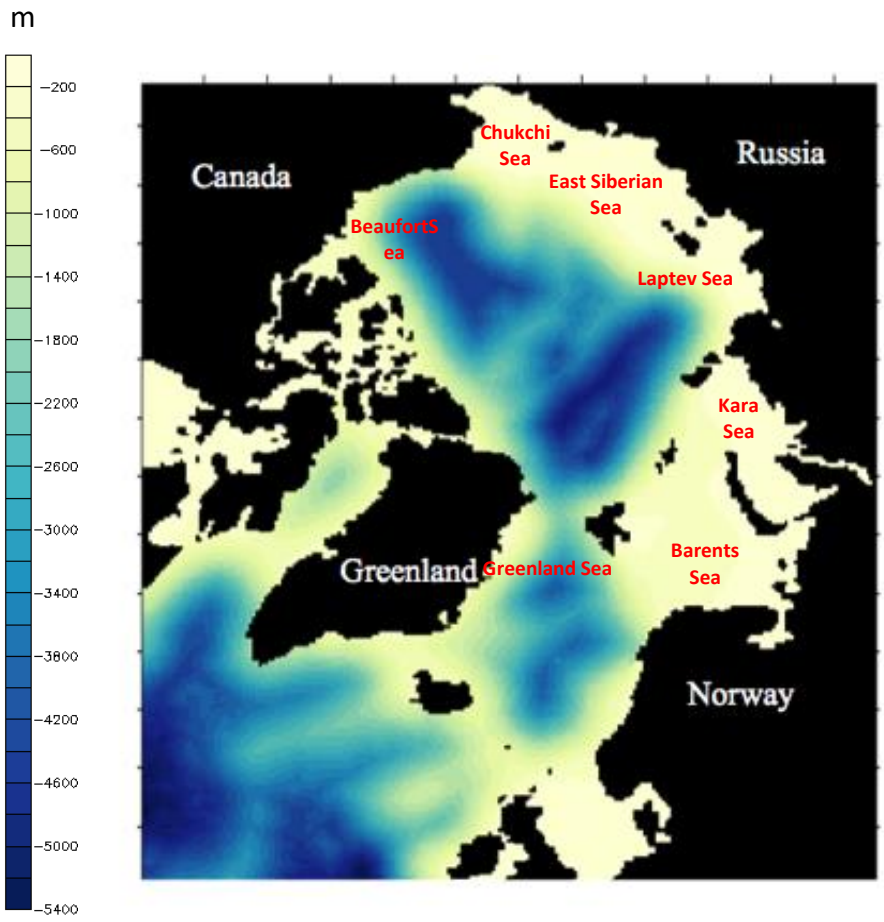

Figure 2-1: Model domain contains the entire Arctic Ocean (depth in m), Greenland-Iceland-Norwegian (GIN) seas and the Northern Atlantic Ocean (De Silva 2013)

2.1 Model Description

The ice-ocean coupled model, ice-POM that is used in this study is the model used by Fujisaki (2010) and De Silva (2013) for ice-ocean coupled computations. The ocean model of the ice-POM is based on Message Passing Interface (MPI) version of the Princeton Ocean Model (POM). The model variables, constants, and parameters of the ice-POM model are listed in table 2-1. In this thesis *a, i, s,* and *w* denote atmosphere, sea ice, snow and seawater respectively.

Table 2-1: Constants used in ice-POM model (De Silva 2013)

Symbol	Description	Values	Units
C_{Dai}	Air to ice drag coefficient	1.2×10^{-3}	
C_{Dwi}	Water to ice drag coefficient	5×10^{-3}	
C_{hio}	Turbulence ice ocean heat transfer coefficient	5×10^{-3}	
C_{lat}	Latent heat bulk transfer coefficient	1.75×10^{-3}	
c_{pa}	Specific heat of air	1004.0	J kg-1K-1
c_{pw}	Specific heat of seawater	4000.0	J kg-1K-1
C_{sen}	Sensible heat bulk transfer coefficient	1.75×10^{-3}	
G	Gravitational acceleration	9.81	ms-2
h_{min}	Minimum ice thickness	0.1	m
k_i	Thermal conductivity of ice	2.04	W m-1K-1
k_s	Thermal conductivity of snow	0.31	W m-1K-1
L_{melt}	Latent heat of fusion	3.3×10^5	J kg-1
L_{subl}	Latent heat of sublimation	2.8×10^6	J kg-1
L_{vap}	Latent heat of vaporization	2.5×10^6	J kg-1
n_{sub}	Number of elastic sub-cycles	50	
$P*$	Ice compressive strength	3×10^4	Pa
R	Radius of Earth	6371×10^3	m
S	Solar constant	1353	W m-2

S_I	Sea ice salinity	5.0	g kg-1
T_i^{melt}	Melting point of sea ice	273.05	K
T_s^{melt}	Melting point of snow	273.15	K
a_i	Albedo of sea ice	0.7	
a_s	Albedo of snow	0.9	
a_w	Albedo of seawater	0.1	
ε_i	Sea ice emissivity	0.97	
ε_s	Snow emissivity	0.99	
ε_w	Seawater emissivity	0.97	
κ	Von Karman constant	0.4	
ρ_a	Air density	1.247	kg m-3
ρ_i	Sea ice density	910	kg m-3
ρ_s	Snow density	330	kg m-3
ρ_w	Seawater density	1025.9	kg m-3
σ_b	Stefan-Boltzman constant	5.67×10^{-8}	Wm-2K-4

2.2 Ocean Model

The Ocean part of the coupled ice-ocean model is a parallel version of Princeton Ocean Model written using Message Passing Interface (MPI) language. The Coordinate system is a three-dimensional spherical coordinate system. The continuity equation and momentum equations are written in the s-coordinate system and spatially discretized using Arakawa C grid. Model domain contains the entire Arctic Ocean, Greenland-Iceland-Norwegian (GIN)

seas and the Northern Atlantic Ocean as shown in figure 2-1. The resolution of zonal and meridional grid are set to about 25km x 25km. The vertical grid is composed of *s*-coordinates system with 33 levels (Mellor 2002). The coordinate system of the model is rotated to the equator to avoid the singularity at the Pole. Top three *s*-levels are 1m in depth. Remaining 30 layers are composed of sigma coordinate system (figure 2-2). The bottom topography is created from Earth Topography 1 Arc-minute Gridded Elevation (ETOPO1) dataset. More details of the model description can be found in Princeton Ocean Model manual (Mellor 2002); (Mellor 2003) and in the PhD thesis of De Silva (2013)

Cartesian coordinate system (*x,y,z,t*) is transformed to the *s*-coordinate system(*s(x*, y*, k, t**)).

$$x = x^* \tag{2-1}$$

$$y = y^* \tag{2-2}$$

$$t = t^* \tag{2-3}$$

$$z = \eta(x^*, y^*, t^*) + s(x^*, y^*, k, t^*) \tag{2-4}$$

A continuous variable k is ranging from $1 \leq k \leq kb$. Where, kb = 33. It is discrete and will be the label of the numerical levels where *s*=0 at *k*=1. Surface elevation is η and $H_{x,y}$ is the bathymetry. In z-level system $s = \sigma(k)(H_{max} + \eta(x, y, t))$ and the sigma system $s = \sigma(k)(H_{x,y} + \eta(x, y, t))$. In z level system $\sigma(k) = (z - \eta)/(H_{max} + \eta)$. In sigma system $\sigma(k) = (z - \eta)/(H_{(x,y)} + \eta)$.

$$s_x = \frac{\partial s}{\partial x^*},\ s_y = \frac{\partial s}{\partial y^*} \tag{2-5 a,b}$$

$$\eta_x = \frac{\partial \eta}{\partial x^*},\ \eta_y = \frac{\partial \eta}{\partial y^*} \tag{2-6 a,b}$$

$$s_k = \frac{\delta s}{\delta k} \tag{2-7}$$

$$\frac{\partial k}{\partial x} = -(\eta_x + s_x)/s_k,\ \frac{\partial k}{\partial y} = -(\eta_y + s_y)/s_k \tag{2-8 a,b}$$

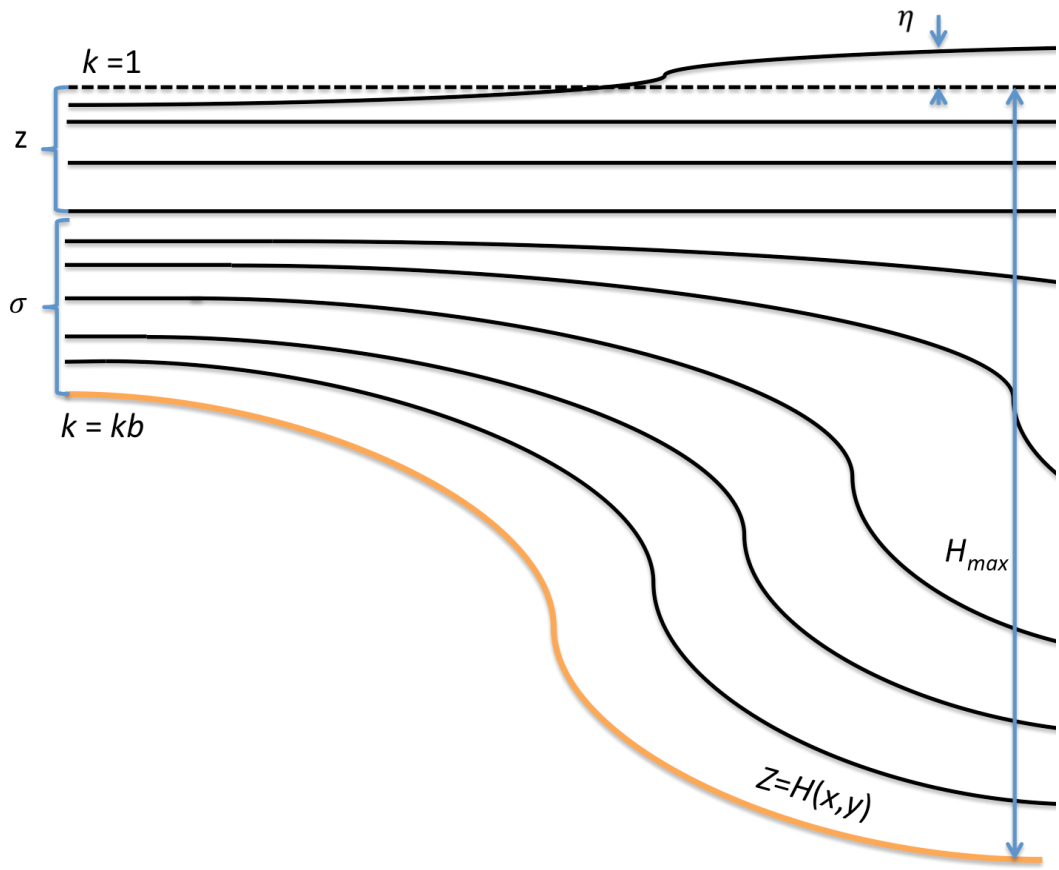

Figure 2-2: s-coordinate system

2.2.1 Governing equations of ocean model

The continuity and momentum equations are written in s-coordinate system and spatially discretized using Arakawa C grid. By dropping all the asterisks from independent and dependent variables the equations are presented in the format as described in detail by Mellor (2002).

$$\Im(\varphi) = \frac{\partial s_k \varphi}{\partial t} + \frac{\partial U s_k \varphi}{\partial x} + \frac{\partial V s_k \varphi}{\partial y} + \frac{\partial W \varphi}{\partial k} \qquad (2\text{-}9)$$

Where, φ is any given variable. The continuity equation is written as: $\Im(\varphi) = 0, where\ \ \varphi = 1$

$$\Im(1) = 0 \tag{2-10}$$

The conservation of momentum equations are written as follows.

$$\Im(U) - fVs_k + gs_k\frac{\partial\eta}{\partial x} + g\frac{s_k}{\rho_o}\int_k^0\left[s_k\frac{\partial\rho'}{\partial x} - (s_x + \eta_x)\frac{\partial\rho'}{\partial k'}\right]dk' = \frac{\partial}{\partial k}\left[\frac{K_M}{s_k}\frac{\partial U}{\partial k}\right] + \left(\frac{\partial s_k t_{xx}}{\partial x} + \frac{\partial s_k t_{xy}}{\partial y}\right) \tag{2-11}$$

$$\Im(V) - fUs_k + gs_k\frac{\partial\eta}{\partial y} + g\frac{s_k}{\rho_o}\int_k^0\left[s_k\frac{\partial\rho'}{\partial y} - (s_y + \eta_y)\frac{\partial\rho'}{\partial k'}\right]dk' = \frac{\partial}{\partial k}\left[\frac{K_M}{s_k}\frac{\partial V}{\partial k}\right] + \left(\frac{\partial s_k t_{xy}}{\partial x} + \frac{\partial s_k t_{yy}}{\partial y}\right) \tag{2-12}$$

Velocity components are *U, V* and *W* in zonal, meridional and vertical directions respectively. The gravity constant is *g* and *f* is the Coriolis parameter. The density is ρ and $\rho' = \rho - \bar{\rho}$. $K_M\ and\ K_H$ are vertical kinematic viscosity and vertical diffusivity. K_M, K_H and K_q are functions of a Richardson number dependent on density stratification (Mellor 2002). The terms t_{xx} , t_{xy}, t_{yy} are defined below.

$$t_{xx} = A_M(2\frac{\partial U}{\partial x}),\ t_{yy} = A_M(2\frac{\partial V}{\partial x}),\ t_{xy} = A_M(\frac{\partial U}{\partial y} + \frac{\partial V}{\partial x}) \tag{2-13 a, b, c}$$

$$q_{Tx} = A_H(\frac{\partial T}{\partial x}),\ q_{Ty} = A_H(\frac{\partial T}{\partial y}),\ q_{sx} = A_H(\frac{\partial S}{\partial x}),\ q_{Sy} = A_H(\frac{\partial S}{\partial y}) \tag{2-14 a, b, c, d}$$

A_M and A_H are horizontal viscosity and diffusivity respectively. They are calculated using equation 2-17 and 2-18. They are proportional to the horizontal grid size and velocity gradients. The proportional coefficient C is 0.2 (Smagorinsky 1963).

$$A_M = C\Delta x\Delta y\frac{1}{2}\left[\left(\frac{\partial U}{\partial x}\right)^2 + \frac{1}{2}\left(\frac{\partial V}{\partial x} + \frac{\partial U}{\partial y}\right)^2 + \left(\frac{\partial V}{\partial y}\right)^2\right]^{1/2} \tag{2-15}$$

$$A_H = 0.1A_M \tag{2-16}$$

The transportation equations for temperature *(T)* and salinity *(S)* are written as follows

$$\Im(T) = \frac{\partial}{\partial k}\left[\frac{K_H}{s_k}\frac{\partial T}{\partial k}\right] + \left(\frac{\partial s_k q_{Tx}}{\partial x} + \frac{\partial s_k q_{Ty}}{\partial y}\right) - \frac{\partial Rf}{\partial k} - R_t(T - T_o) \tag{2-17}$$

$$\Im(S) = \frac{\partial}{\partial k}\left[\frac{K_H}{s_k}\frac{\partial S}{\partial k}\right] + \left(\frac{\partial s_k q_{sx}}{\partial x} + \frac{\partial s_k q_{sy}}{\partial y}\right) - R_s(S - S_o) \quad (2\text{-}18)$$

where, radiation flux is *Rf*. R_t and R_s are restoring constants that restore temperature and salinity in a 30day cycle. Climatological temperature and salinity are T_o and S_o extracted from Polar Science Center Hydrographic Climatology (PHC3.0). Restoring term is only used in the spin up run. For model and assimilation run the term is set to zero.

In the ocean model, Turbulence kinetic energy (q^2) and Turbulence length scale (q^2l) are calculated using below equations in order to calculate Richardson number and there by calculate K_M and K_H.

$$\Im(q^2) = \frac{\partial}{\partial k}\left[\frac{K_q}{s_k}\frac{\partial q^2}{\partial k}\right] + \frac{2K_M}{s_k}\left[\left(\frac{\partial U}{\partial k}\right)^2 + \left(\frac{\partial V}{\partial k}\right)^2\right] + \frac{2g}{\rho_o}K_H\frac{\partial \bar{\rho}}{\partial k} - \frac{2s_k q^3}{B_1 l} + \left(\frac{\partial s_k q_{qx}}{\partial x} + \frac{\partial s_k q_{qy}}{\partial y}\right) \quad (2\text{-}19)$$

$$\Im(q^2 l) = \frac{\partial}{\partial k}\left[\frac{K_q}{s_k}\frac{\partial q^2 l}{\partial k}\right] + E_1 l\left(\frac{K_M}{s_k}\left[\left(\frac{\partial U}{\partial k}\right)^2 + \left(\frac{\partial V}{\partial k}\right)^2\right] + E_2\frac{g}{\rho_o}K_H\frac{\partial \rho^2}{\partial k}\right) - \frac{q^3\bar{W}}{B_1} + \left(\frac{\partial s_k q_{lx}}{\partial x} + \frac{\partial s_k q_{ly}}{\partial y}\right) \quad (2\text{-}20)$$

where,

$$q_{qx} = A_H\left(\frac{\partial q^2}{\partial x}\right),\ q_{qy} = A_H\left(\frac{\partial q^2}{\partial y}\right),\ q_{lx} = A_H\left(\frac{\partial q^2 l}{\partial x}\right),\ q_{ly} = A_H\left(\frac{\partial q^2 l}{\partial y}\right) \quad (2\text{-}21\ a,b,c,d)$$

B_1 is one of the turbulence closure constants which is set to be 16.6 (Mellor 2002). $E_1$and E_2 are set to be 0.5 and 0.2 (Mellor 2002). $\bar{W}$ is a wall proximity function. $\frac{\partial \bar{\rho}}{\partial k}$ is the vertical density gradient corrected for adiabatic lapse rate. More details of ice-Ocean model are explained in De Silva (2013), Mellor (2002) and Mellor (2003).

2.2.1 The Numerical Scheme

The model has a free surface and a split time step. The external mode portion of the model is two-dimensional and uses a short time step based on the CFL condition and the external

wave speed. The internal mode is three-dimensional and uses a long timestep based on the CFL condition and the internal wave speed. The external mode calculation results in updates for surface elevation η and the vertically averaged velocities in zonal and meridional directions, *ua*, *va*. The internal mode calculation results in updates for *U, V, T, S* and the turbulence quantities. Fig. 2-3 illustrates the time stepping process for the external and internal modes. It is assumed that everything is known at t^{n-1} and t^{n} (the previous leap frog time step having just been completed). Integrals involving the baroclinic forcing and the advective terms are supplied to the external mode along with the bottom stress, a process which is labeled "Feedback" in figure 2-3; their values are held constant during $t^{n} < t < t^{n+1}$. The external mode "leap frogs" many times, with the time step, *dte*, until $t = t^{n+1}$. Internal mode time step is set to be 30 times *dte*. The vertical time averaged velocities (*UTF, VTF*), and those from the previous time step (*UTB, VTB*), are time averages of the external variables. The internal and external modes have different truncation errors so that the vertical integrals of the internal mode velocity may depart slightly from (*ua*,*va*) during the course of a long integration. Therefore, internal velocities *U*, *V* are adjusted to be the mean of *UTF* and *VTF.*

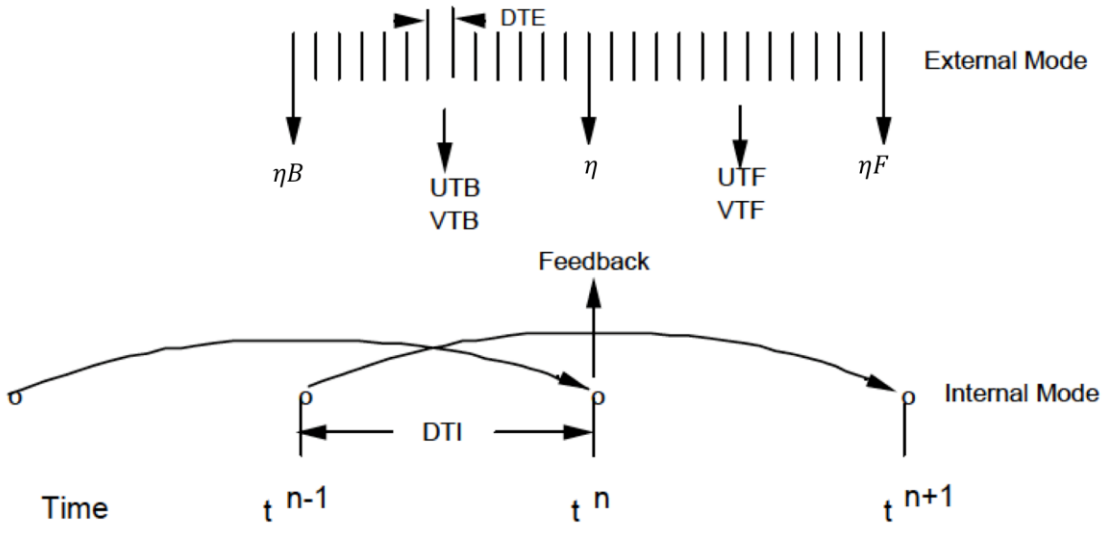

Figure 2-3: Internal external mode interaction (Mellor 2002)

The calculation of the three-dimensional (internal) variables is separated into a vertical diffusion time step and an advection plus horizontal diffusion time step. The former is implicit (to accommodate small vertical spacing near the surface) whereas the latter is explicit.

2.3 Ice Model

Ice-model is based on Fujisaki et al. (2010) and De Silva (2013). Ice is not entirely treated as a continuum body. Ice discrete characteristics are considered along the ice edge by introducing floe collision rheology (Sagawa 2007) into the conventional elastic-viscous-plastic rheology (Hunke 2001). Snow effect on ice is parameterized according to Zhang (1998). Snow is considered to be an insulated layer on the surface of ice. Sub-grid scale ice movements (semi-Lagrangeian movements) are introduced to the sea ice model to minimize the sea ice diffusion and improve the accuracy of ice edge locations (Rheem C.K. 1997).

2.3.1 Governing equations of ice model

In the sea ice dynamics model, two-dimensional momentum equations are solved in a curvilinear coordinate system as follows:

$$\rho_i hA \frac{\partial u_i}{\partial t} = F_\lambda + \tau_{ai\lambda} + \tau_{wl\lambda} + \rho_i hAf v_i - \rho_i hg \frac{1}{Rcos\phi} \frac{\partial H_o}{\partial \lambda} \quad (2\text{-}22)$$

$$\rho_i hA \frac{\partial v_i}{\partial t} = F_\phi + \tau_{ai\phi} + \tau_{wl\phi} - \rho_i hAf u_i - \rho_i hg \frac{1}{R} \frac{\partial H_o}{\partial \phi} \quad (2\text{-}23)$$

In these equations ρ_i, h, A, u_i, v_i, f, R and H_o are ice density, thickness, concentration, zonal and meridional velocities, Coriolis parameter, Earth radius and sea surface height respectively. λ and ϕ represent zonal (longitudinal) and meridional (latitude) directions respectively. τ_{ai} and τ_{wi} are air to ice stresses and ocean to ice stresses. They are calculated according to following equations.

$$\overrightarrow{\tau_{ai}} = \rho_a C_{Dai} |\overrightarrow{u_a} - \overrightarrow{u_i}| (\overrightarrow{u_a} - \overrightarrow{u_i}) \quad (2\text{-}24)$$

$$\overrightarrow{\tau_{wi}} = \rho_w C_{Dwi} |\overrightarrow{u_w} - \overrightarrow{u_i}| (\overrightarrow{u_w} - \overrightarrow{u_i}) \quad (2\text{-}25)$$

Where ρ_a, ρ_w, u_w, u_a C_{Dai}, $and\ C_{Dwi}$ are air density, sea water density upper surface ocean velocity, air velocity, air to ice drag coefficient and ocean to ice drag coefficient respectively. Arrow above represents the vector field.

Internal ice stress gradients $F_\lambda\ and\ F_\phi$ are calculated as the divergence of stress tensor σ (Zhang 1997). R is the radius of the earth.

$$F_\lambda = \frac{1}{R\ cos\phi}\frac{\partial \sigma_{\lambda\lambda}}{\partial \lambda} + \frac{1}{R}\frac{\partial \sigma_{\lambda\phi}}{\partial \phi} - \frac{2\sigma_{\lambda\phi} tan\phi}{R} \quad (2\text{-}26)$$

$$F_\phi = \frac{1}{R\ cos\phi}\frac{\partial \sigma_{\lambda\phi}}{\partial \lambda} + \frac{1}{R}\frac{\partial \sigma_{\phi\phi}}{\partial \phi} + \frac{(\sigma_{\lambda\lambda} - \sigma_{\phi\phi}) tan\phi}{R} \quad (2\text{-}27)$$

In most of the sea ice numerical models ice dynamic process is based on continuum approach, which is simple in application. Some models use discrete element techniques, which is computationally expensive. To answer these two problems, in this model the floe collision rheology (Sagawa 2007) is introduced into the conventional elastic-viscous-plastic rheology. This method can take the discrete characteristics of sea ice edge into account.

2.4 Thermodynamic Model

Ice is considered to be a horizontally homogeneous slab floating over seawater. Thermodynamics model incorporates ice growth. Ice thickness change, lateral growth and ice melting are modeled according to 0-layer thermodynamic model (Parkinson et al. 1979) that has been proposed by Semtner (1976). In the ice-POM model temperature and thermodynamically created thickness of sea ice are controlled by heat conduction through ice slab and balance of fluxes at upper and lower surfaces.

2.4.1 Surface heat flux calculation

Surface heat fluxes consist of, clear sky shortwave solar radiation F_{swo}, incoming longwave radiation F_{LE}, sensible heat flux F_{sen}, latent heat flux F_{lat}, outgoing longwave radiation F_{LO}, and heat input from ocean to ice bottom F_{wi}. The outgoing longwave radiation, sensible heat and latent heat fluxes are functions of surface temperature T_{sfc} and surface (snow, sea ice or water) properties.

2.4.1.1 Shortwave radiation

Empirical equations of clear sky shortwave radiation formulated by Zilman (Zillman 1972) is used in the model.

$$F_{swo} = \frac{S\,cos^2 Z}{(\cos Z + 2.7)vp \times 10^{-5} + 1.085 cosZ + 0.1} \tag{2-28}$$

$$cosZ = \sin \emptyset \sin \delta + \cos \emptyset \cos \delta \cos HA \tag{2-29}$$

$$\delta = 23.44° \frac{\pi}{180} \cos\left[(172 - J)\frac{\pi}{180}\right] \tag{2-30}$$

$$HA = (12 - H)\frac{\pi}{12} \tag{2-31}$$

Where, S is solar constant, Z is zenith angle, vp is vapor pressure, $\emptyset$ is latitude, δ is sun declination angle, J is days in year, HA is sun hour angle, and H is local time. The values of the constants are defined in table 2-1. The clear sky shortwave radiation is modified by introducing the effect of cloud cover (Laevastu 1960) as below.

$$F_{sw} = F_{swo}(1 - 0.6\,c^3) \tag{2-32}$$

Where c is total cloud cover, which varies between 0 and 1.

2.4.1.2 Incoming longwave radiation

Clear sky longwave radiation F_{LEo} is modeled according to Efimova theories (Efimova 1961)

$$F_{LEo} = \sigma_b T_a^4 (0.746 + 6.6 \times 10^{-5}\, vp) \tag{2-33}$$

Where, σ_b is Stefan-Boltzman constant and T_a is atmospheric temperature. This formulation is further modified by introducing cloud effect from the following equation (Parkinson 1979).

$$F_{LE} = F_{LEo}\,(1 + 0.275c) \tag{2-34}$$

2.4.1.3 Outgoing longwave radiation

The outgoing longwave radiation depends on the surface temperature T_{sfc} and surface emissivity (snow, ice or water) ε_{sfc}.

$$F_{LO} = \varepsilon_{sfc}\sigma T_{sfc}^4 \tag{2-35}$$

2.4.1.4 Sensible heat flux

The sensible heat flux is calculated by using the bulk aerodynamic formula (upward flux is considered as positive)

$$F_{sen} = \rho_a\, c_{pa} C_{sen} |U_a| \left(T_{sfc} - T_a\right) \tag{2-36}$$

$$|U_a| = \sqrt{{u_a}^2 + {v_a}^2} \tag{2-37}$$

Where U_a is wind speed, ρ_a is air density, T_a is air temperature, T_{sfc} is the surface temperature, C_{sen} is the turbulence heat transfer coefficient that is set as a constant and c_{pa} is specific heat of air.

2.4.1.5 Latent heat flux

The latent heat flux is calculated using aerodynamic bulk formula.

$$F_{lat} = \rho_a\, L_{sfc} C_{lat} |U_a| \left(q_{sfc} - q_a\right) \tag{2-38}$$

where C_{lat} is defined as latent heat bulk transfer coefficients, L_{sfc} is the surface latent heat of vaporization or sublimation, depending on the surface conditions explained in Haltiner(1957).

q_{sfc} and q_a are specific humidity at surface and atmosphere that are defined as,

$$q_{sfc} = \frac{0.622 \times vps}{P_a - 0.378 \times vps} \tag{2-39}$$

$$q_a = \frac{0.622 \times vp}{P_a - 0.378 \times vp} \tag{2-40}$$

Saturated vapor pressure vps is calculated from an empirical formula (Murray 1967).

$$vps = 611 \times 10^{\frac{a(T_{sfc}-273.16)}{(T_{sfc}-b)}} \text{ mb} \tag{2-41}$$

Where, (a,b)=(9.5,7.66) with the ice cover and (7.5, 35.86) without the ice cover

2.4.1.6 Heat flux from ocean to ice bottom

The turbulence heat flux from ocean to ice bottom (F_{wi}) is parameterized as,

$F_{wi} = \rho_w c_{pw} C_{hio} u^* (T_w - T_w^{frz})$ where, ρ_w and c_{pw} denote the density and the specific heat of seawater respectively. T_w and T_w^{frz} are the ocean uppermost layer temperature and associated freezing temperature. Ice bottom temperature (T_{btm}) is set to the ocean freezing temperature (T_w^{frz}). It's a function of salinity (S_w) as shown below. C_{hio} is turbulence heat transfer coefficient. The value of C_{hio} is set based on (McPhee 2008).

$$T_w^{frz} = 273.15 - 0.0575 \times S_w + 1.710523 \times {S_w}^{\frac{3}{2}} - 2.154996 \times {S_w}^2 \tag{2-42}$$

Where u^* denotes the friction velocity, which is given below.

$$u^* = \sqrt{\frac{\tau_w}{\rho_w}} \tag{2-43}$$

Where, τ_w is the sea surface stress calculated as below

$$\tau_w = (1 - A) \times \rho_a C_{Daw} \left|\overrightarrow{U_a}\right| \overrightarrow{U_a} + A \times \rho_w C_{Diw} \left|\overrightarrow{U_w} - \overrightarrow{U_\iota}\right| \left(\overrightarrow{U_w} - \overrightarrow{U_\iota}\right) \tag{2-44}$$

where U_w is the ocean velocity, U_i is the sea ice velocity, C_{Daw} is the drag coefficient between air and ice, C_{Diw} is the drag coefficient between ice and ocean.

2.4.2 Vertical formation of sea ice

Atmosphere to sea ice surface heat fluxes are changed according to the sea ice surface conditions such as surface albedo and emissivity. Snow covered sea ice surface flux (F_{as}) and snowless sea ice surface flux (F_{ai}) are calculated according to the surface temperature and surface properties. Energy fluxes of snow covered sea ice are presented in this section.

2.4.2.1 Snow free sea ice cover

The variation of ice thickness can be formulated as a system based on one-dimensional heat equation as below.

$$c_i \rho_i \frac{\partial T}{\partial t} = \frac{\partial}{\partial z}\left(k_i \frac{\partial T}{\partial z}\right) \tag{2-45}$$

By applying the boundary conditions at upper and lower surface to the equation 2-45, total variation of ice thickness at upper and lower surfaces are calculated.

Upper surface,

$$-L_{melt} \rho_i \frac{\partial h}{\partial t} = F_i - k_i \frac{\partial T}{\partial z}_{z=h_i} \; when \; T_{z=h_i} = T_i^{melt} \tag{2-46}$$

$$0 = F_i - k_i \frac{\partial T}{\partial z}_{z=h_i} \; when \; T_{z=h_i} < T_i^{melt} \tag{2-47}$$

Lower surface,

$$-L_{melt}\rho_i \frac{\partial h}{\partial t} = F_i - k_i \frac{\partial T}{\partial z}_{z=h_i} + F_{wi} \quad (2\text{-}48)$$

Vertical profile of temperature is assumed to be linear. c_i and k_i denote the specific heat and thermal conductivity respectively. Even though k_i is a function of salinity and temperature the range is relatively small. Therefore, the value obtained under 273.15K and 34 psu, which is 2.04 W/m/K, is used. When sea ice is not covered by snow, according to figure 2-4 surface heat fluxes are calculated.

$$F_{ai} = (1 - \alpha_i)F_{sw} + F_{LE} - F_{LO} - F_{sen} - F_{lat} \quad (2\text{-}49)$$

Conductive heat flux G_i is calculated by

$$G_i = \frac{k_i}{h_i} (T_{btm} - T_{sfc}) \quad (2\text{-}50)$$

The outgoing longwave radiation, F_{LO}, sensible heat flux F_{sen} and latent heat flux F_{lat} are nonlinear functions of surface temperature. Therefore, a new surface temperature is calculated using the iterative method while maintaining the energy balance at the upper surface:

$$T_{sfc} = T_p + \Delta T \quad (2\text{-}51)$$

Where, T_p is the surface temperature at the previous time step and ΔT is the variation. Energy balance at the upper surface is given below.

$$F_{ai} + G_i = \Delta Q \quad (2\text{-}52)$$

By applying the net surface heat flux derived from equation 2-49 and assuming zero net heat accumulation at the upper surface in equation 2-52 the following equation is obtained.

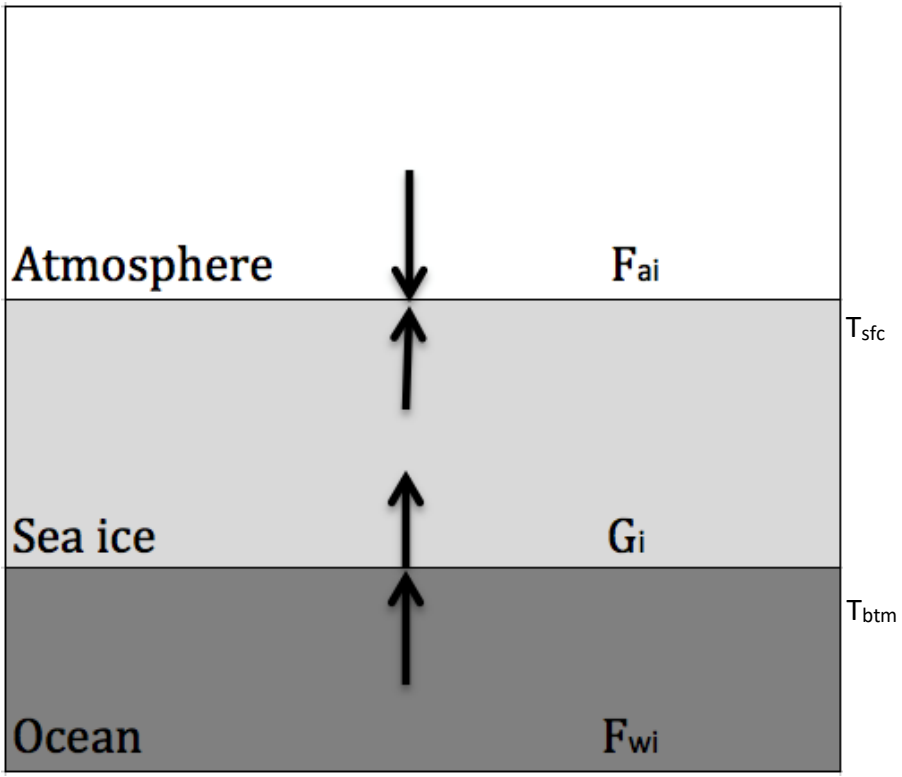

Figure 2-4 Schematic diagram of the energy fluxes in snow free sea ice (De Silva 2013)

$$(1-\alpha_i)F_{sw} + F_{LE} - F_{LO} - F_{sen} - F_{lat} + \frac{k_i}{h_i}(T_{btm} - T_{sfc}) = \Delta Q \tag{2-53}$$

Surface variation temperature is updated by,

$$\Delta T = \frac{(1-\alpha_i)F_{sw} + F_{LE} - F_{LO} - F_{sen} - F_{lat} + \frac{k_i}{h_i}(T_{btm} - T_p)}{4\varepsilon_i \sigma T_p^3 + \frac{k_i}{h_i} + \rho_a c_{pa} C_{sen} |U_a|} \tag{2-54}$$

If the updated temperature is greater than ice melting temperature, $\left(T_i^{melt}\right)$, then surface temperature is set to (T_i^{melt}). Excess heat is used to melt sea ice at the surface according to equation 2-55.

$$-\Delta h_i^{sfc} = \frac{\Delta t\left((1-\alpha_i)F_{sw} + F_{LE} - F_{LO} - F_{sen} - F_{lat} + \frac{k_i}{h_i}\left(T_{btm} - T_i^{melt}\right)\right)}{L_{melt}\rho_i} \tag{2-55}$$

Applying the energy balance at the bottom surface according to equation 2-47 can yield the bottom thickness as follows.

$$-\Delta h_i^{sfc} = \frac{\Delta t\left(F_{wi} - \frac{k_i}{h_i}(T_{btm} - T_{sfc})\right)}{L_{melt}\rho_i} \tag{2-56}$$

2.4.2.2 Snow covered sea ice

When sea ice is covered with snow (figure2-5), it is necessary to calculate snow ice interface temperature T_{si}. Total heat fluxes on the snow surface and the heat flux from ocean to ice bottom are F_{as} and F_{wi}.

Conductive heat fluxes through snow and sea ice are defined as

$$G_s = \frac{k_s}{h_s}\,(T_{si} - T_{sfc}\,) \tag{2-57}$$

$$G_i = \frac{k_i}{h_i}\,(T_{btm} - T_{si}\,) \tag{2-58}$$

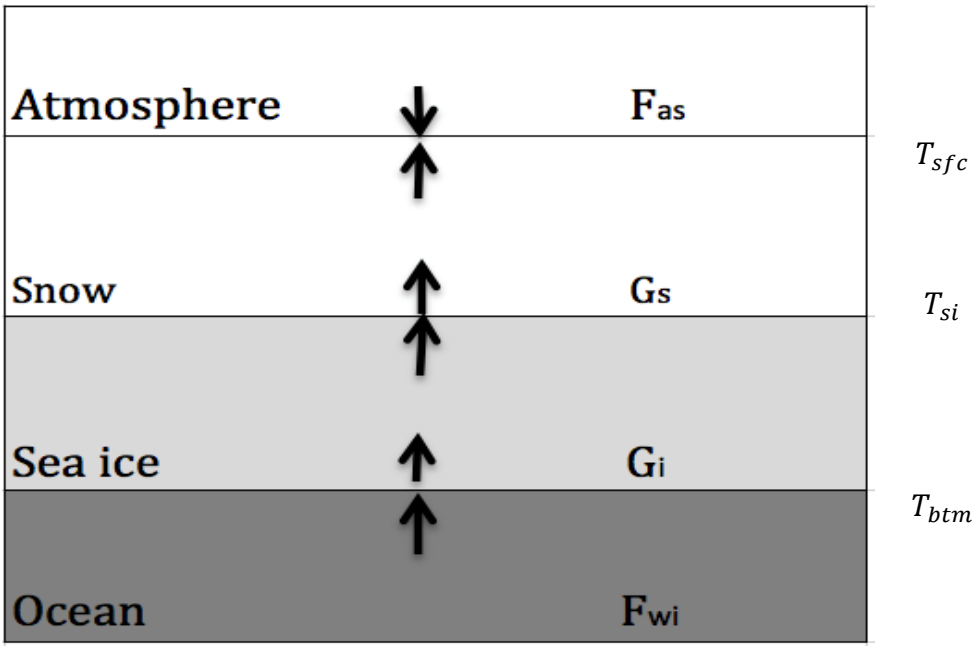

Figure 2-5: Schematic diagram of the energy fluxes at the snow-covered sea ice (De Silva 2013)

where k_s is thermal conductivity of snow. Interface energy balance is used to compute interface temperature. Accumulation of heat at the surface was ignored.

$$G_s = G_i \tag{2-59}$$

$$T_{si} = \frac{k_s h_i T_{sfc} + k_i h_s T_{btm}}{h_i k_s + h_s k_i} \tag{2-60}$$

The surface temperature is calculated using the same method as mentioned in snow free part (equation 2-47). Snow surface temperature is updated by the following equation.

$$\Delta T = \frac{(1-\alpha_s)F_{sw} + F_{LE} - F_{LO} - F_{sen} - F_{lat} + \frac{k_i k_s (T_{btm} - T_p)}{k_s h_i + k_i h_s}}{4\varepsilon_s \sigma T_p^3 + \frac{k_i k_s}{k_s h_i + k_i h_s} + \rho_a c_{pa} C_{sen} |U_a|} \tag{2-61}$$

When snow surface temperature is greater than melting point of snow (T_s^{melt}) the excess heat is used to melt snow. The snow melting depth is calculated according to

$$-\Delta h_i^{sfc} = \frac{\Delta t\left((1-\alpha_i)F_{sw} + F_{LE} - F_{LO} - F_{sen} - F_{lat} + \frac{k_s}{h_s}(T_{si} - T_s^{melt})\right)}{L_{melt}\rho_s} \tag{2-62}$$

The bottom surface melt is calculated according to snow free calculation (equation 2-55)

2.4.2.3 Lateral growth and melt of sea ice

In ice-POM model when the ocean mixed layer temperature drops below freezing point (super cooling) part of the water column (Δz_w) is frozen within one timestep. Total frozen volume within one timestep is defined as,

$$V_i^{frz} = \frac{\rho_w c_{pw} \Delta z_w \left(T_w^{frz} - T_w\right)}{\rho_i L_{melt}} \tag{2-63}$$

where, T_w^{frz} is the freezing temperature of water. The net heat flux from atmosphere to ocean can be led to melt the existing sea ice and snow. The net heat flux from atmosphere to ocean F_{aw} is defined as below.

$$F_{aw} = (1 - \alpha_w)F_{sw} + F_{LE} - F_{LO} - F_{sen} - F_{lat} \quad (2\text{-}64)$$

Where, α_w is seawater albedo. In the above equation, total heat available $(F_{aw}(1 - A))$ is used to melt sea ice laterally and warm the underneath ocean water. The fraction of total heat $(F_{aw}A(1 - A))$ is used to melt sea ice laterally according to (Parkinson 1979). A is sea ice concentration

In ice-POM model it is assumed that the ocean surface heat flux only changes the lateral concentration and does not affect the ice or snow thickness. The lateral melts of sea ice and snow concentration due to ocean heat flux is then defined as,

$$A^{melt} = \frac{F_{aw}A(1-A)dt}{(\rho_i h_i L_{melt} + \rho_s h_s L_{melt})} \quad (2\text{-}65)$$

Finally, new ice concentration and thickness due to the lateral melting and formation are formulated in following equations.

The new total volume of sea ice and snow defined in equation 2-66 and 2-67 respectively.

$$V_i = Ah_i + V_i^{frz} - h_i A^{melt} \quad (2\text{-}66)$$

$$V_s = (A_i - A^{melt})\, h_s \quad (2\text{-}67)$$

New concentration of ice and snow is defined as,

$$A^{new} = A - A^{melt} + min\left(\frac{V_i}{h_{min}}, 1 - A\right) \quad (2\text{-}68)$$

Equation 2-67 guarantees that sea ice concentration will not exceed 100%. New sea ice thickness and snow thickness are calculated according to following equations.

$$h_i^{new} = \frac{V_i}{A^{new}} \quad (2\text{-}69)$$

$$h_s^{new} = \frac{V_s}{A^{new}} \quad (2\text{-}70)$$

2.5 Model Run

This section presents the model computations prior to introduce data assimilation. It also provides details of the data that has been used, the basic set up of the spin up run, model run parameters and a validation of the model results.

2.5.1 Data Used

The model that is used in the study is an ice-ocean coupled model. It is forced with atmospheric conditions. The atmospheric forcing data are obtained from The European Centre for Medium-Range Weather Forecasts Re-Analysis Interim (ERA-interim) six hourly data sets. The data comes with the resolution of 0.75^o x 0.75^o. Mean sea level pressure, air velocity at 10m height, air temperature, humidity and total cloud cover are used. Precipitation is obtained from National Center for Environmental Prediction (NCEP) in 6 hourly reanalysis data sets.

The model initializes without any sea ice. Sea ice is created during the spin-up run. Sea surface salinity and sea surface temperature for spin-up run are obtained from Polar science center Hydrographic Climatology (PHC3.0) (Steele M. 2001) data using 30-day scale. It helps to prevent the model drifting from climatology. The salinity under sea ice is not restored by PHC3.0 data to avoid dampening the brine rejection by ice formation. WOA 2013 one-degree monthly average data provided by NOAA are used for inner ocean salinity and temperature. This data set is also used to set the boundary conditions.

2.5.2 Spin up

To create initial ice for the model run first, spin up run is performed. The model is spun up using the atmospheric forcing from 1979 cyclically for 12 years. Initial ocean conditions and ocean boundary conditions (temperature and salinity) are extracted from Polar science

center Hydrographic Climatology (PHC3.0) (Steele 2001) data. During the spin-up ocean temperature and salinity are restored with PHC3.0 climatology data set using 30-day time scale. Initial velocity at the boundaries are set to zero. By the end of 12 years the computation produces sea ice extent that is comparable to the observation. Comparison of the spin up sea ice extent with that of the observation is presented in figure 2-6 (Mudunkotuwa et al 2015).

2.5.3 Model integration

After the spin up run, model is integrated from 1979 to 2013 using the spin up results as initial conditions for the ocean and ice (figure 2-6). After this 33 years integration, resulting sea ice conditions and ocean structure is compared with available observations.

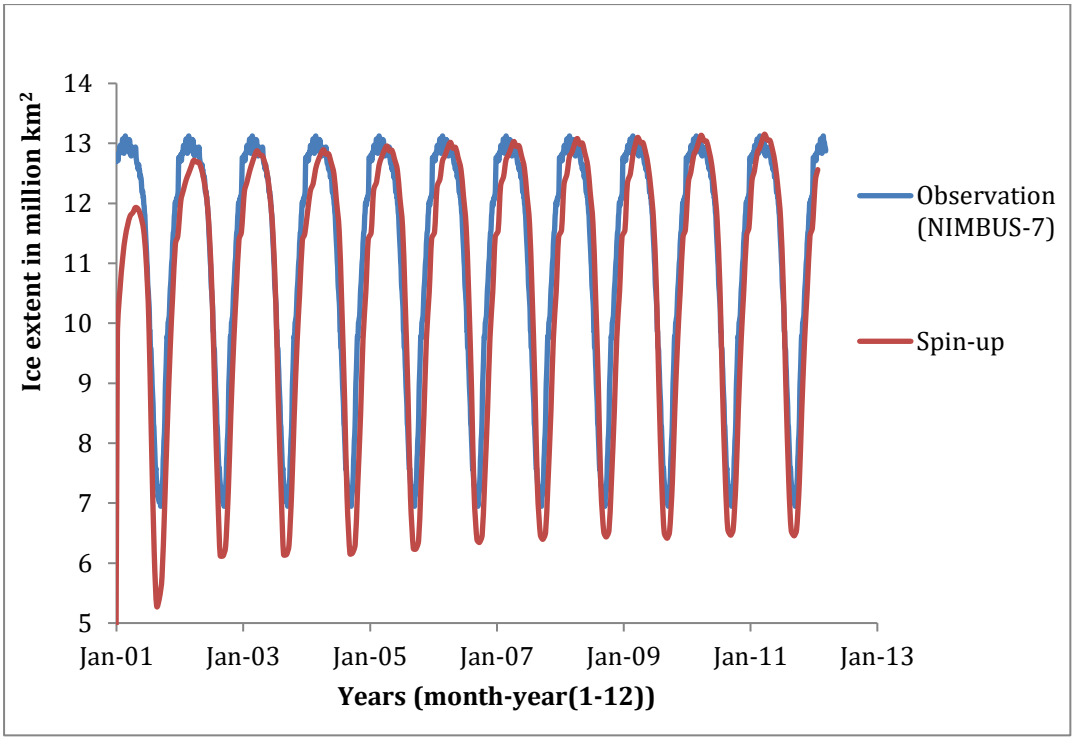

Figure 2-6: Time series of the sea ice extent in million square km from observation (in blue) and spin up run (in red) of 12 years using 1979 forcing data.

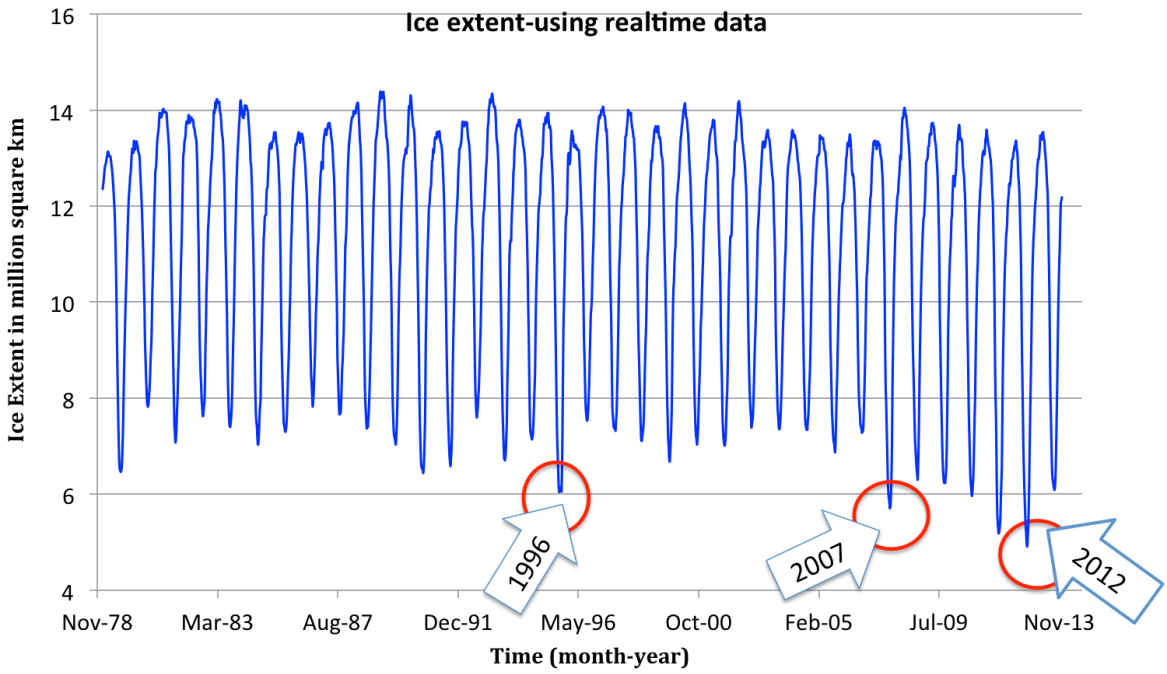

Figure 2-7: Time series of the sea ice extent from model integration (1979-2013) in million square km

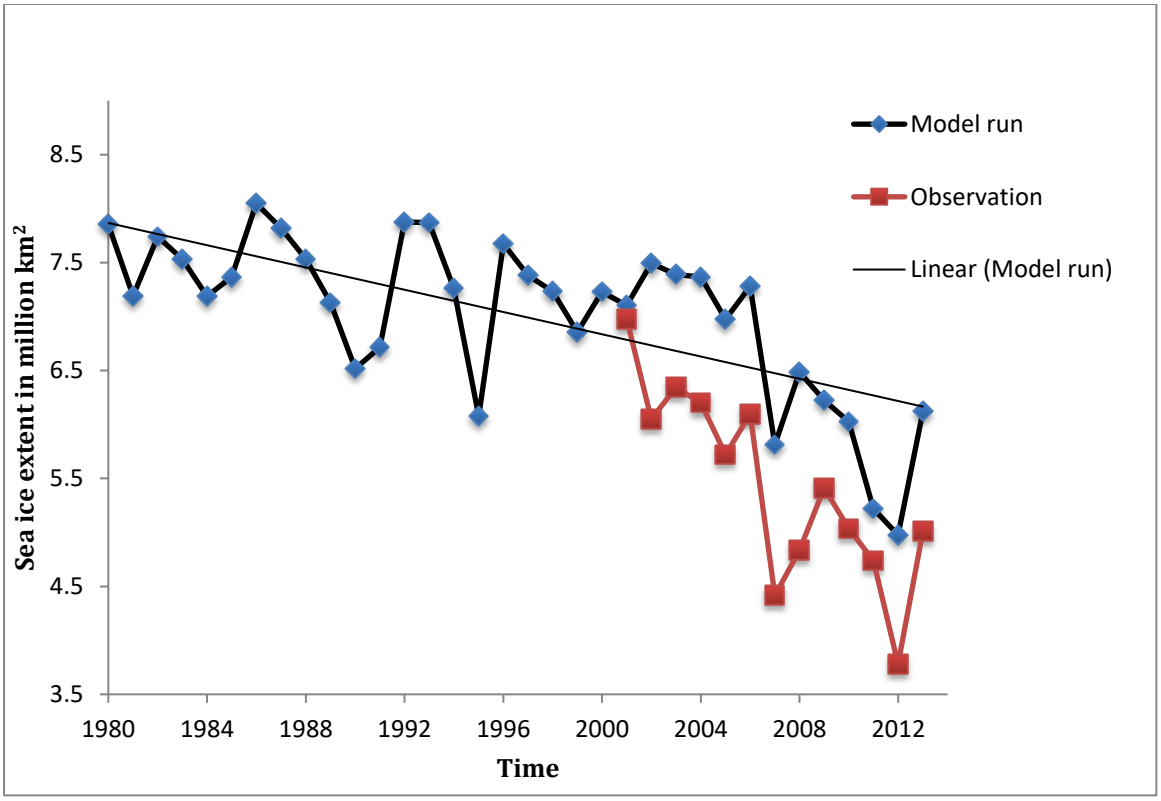

Figure 2-8: Average sea ice extent in September in million km²

Figure 2-7 demonstrates that the model well reproduces long-term trend of the sea ice extent including the ice extent minimums in 1996, 2007, and 2012. Figure 2-8 reproduces the sea ice extent minimum graph by NSIDC that is presented in chapter 1(figure 1-1). It compares model sea ice minimums with the satellite observations. It is clear that the model can reproduce the long-term trend. However, the model produces more ice in summer than the observation.

2.5.4 Model validation

For data assimilation experiments, year 2013 is selected. The following section validates the model behavior in the year 2013. It can be observed that the overall sea ice extent in the year 2013 is overestimated (figure 2-9). Sea ice extent in the Bering Sea (figure 2-10) and the Kara Sea are overestimated by the model (figure 2-11). The time series of sea ice extent in the Barents Sea is presented in figure 2-10. There are several reasons for discrepancies between the model sea ice extent and the observation sea ice extent. One of the reasons is the imperfections in ocean boundary conditions. PHC data set provides climatology data which is lower in temperature than the warming temperatures in the Atlantic Ocean. The imperfections in the ocean heat transportation expression that excludes warm water inflow from the Atlantic Ocean also contributes to the discrepancies in sea ice extent. Another reason is the simplified thermodynamic model that uses constant albedos and model disregarding melt pond phenomena. Coarseness of the model grid and disregard for ocean waves can also lead to discrepancies.

Sea ice thickness in the model is underestimated near the North Pole compared to observation (figure 2-12, 2-13). This could be explained by the overestimated sea ice velocity (figure 2-14, 2-15) in the same area that advects sea ice away from the North Pole. While total sea ice extent of model shows a yearlong average root mean squared difference (rmsd) of 1.28million km^2 with AMSR-2 observations, sea ice thickness in the polar area shows a large rmsd of 1.61m with Cryosat sea ice thickness observations in winter. Sea ice extent and sea ice thickness deviations must be addressed to accurately predict sea ice conditions along ASRs.

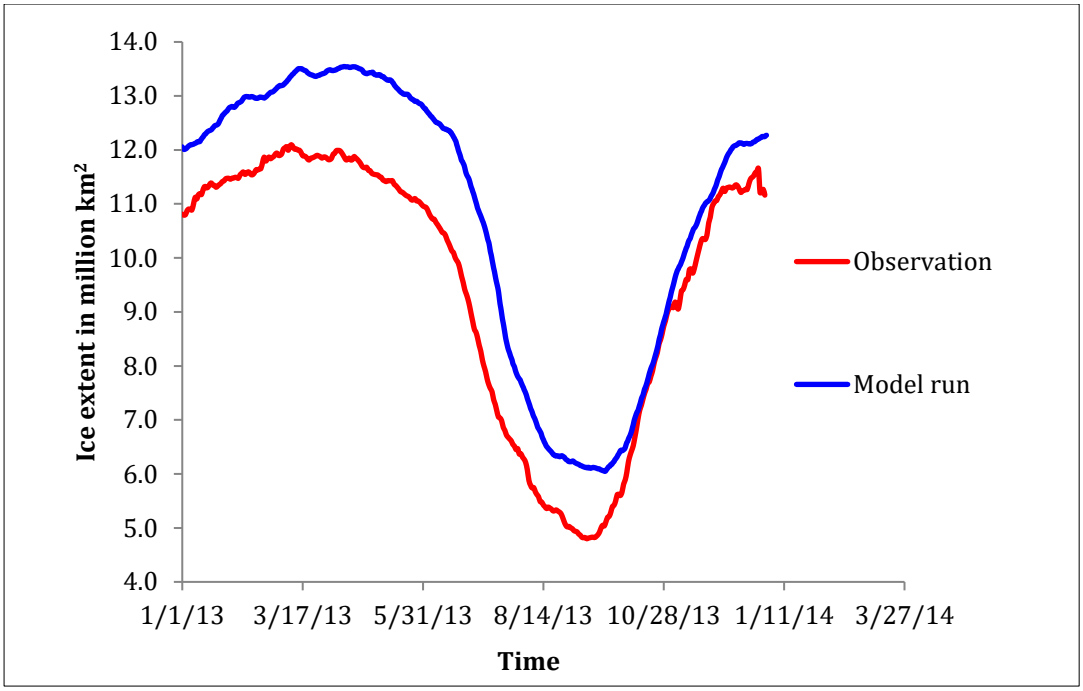

Figure 2-9: Time series of sea ice extent of model and AMSR-2 observation in million square km

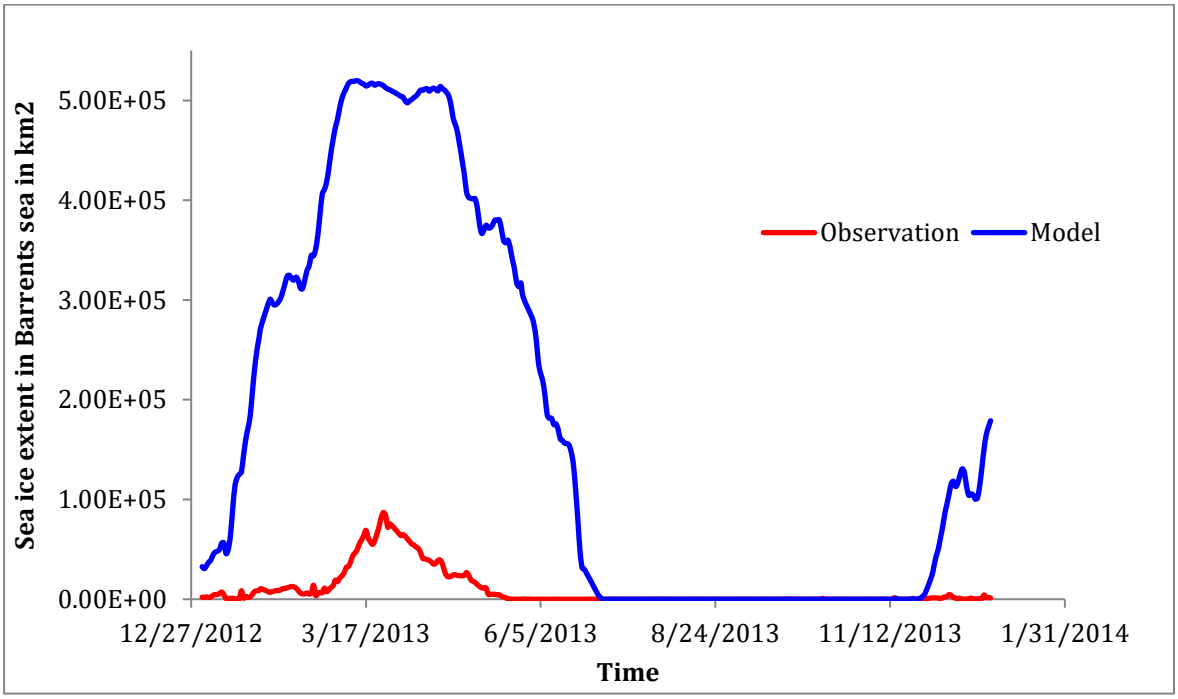

Figure 2-10: Time series of sea ice extent of model and AMSR-2 observation in million square km in Barents Sea

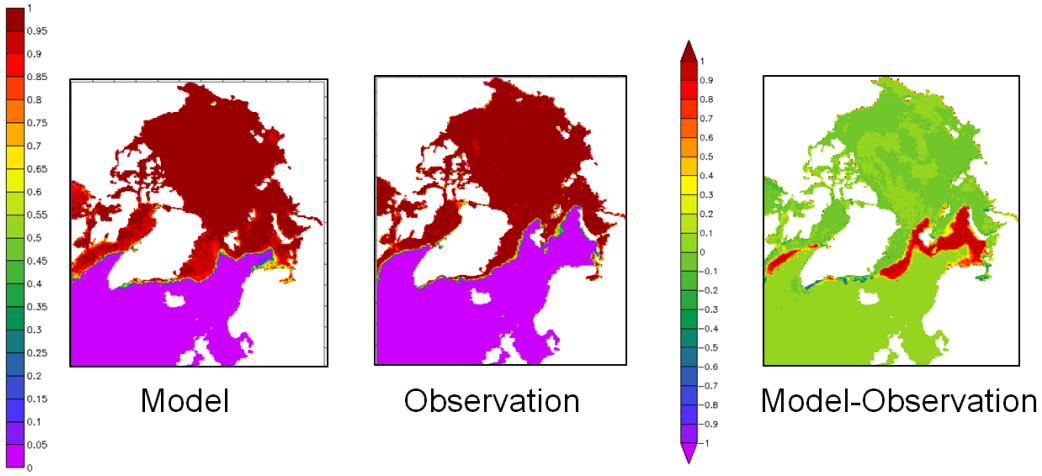

Figure 2-11: Comparison of sea ice concentration in winter. Model (left), observation (middle) and on right is the difference between model and observation (model-observation)

Even though Ice-POM model can reproduce sea ice conditions in the melting season using high-resolution models, its accuracy in the freezing season is not as high as in the melting season (De Silva 2013). Figure 2-16 presents sea ice extent in year 2005. The disparities between the model and the observations are due to exclusion of riverine inputs and the uncertainties of forcing data.

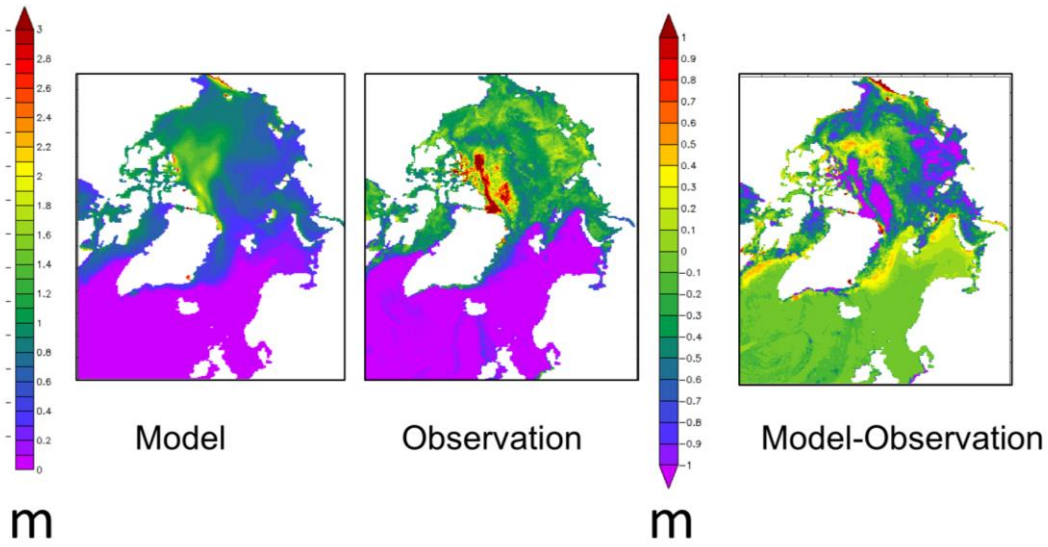

Figure2-12: Comparison of sea ice thickness (in m) in February. Observation from AMSR-2 (Krishfield 2014) data set (on left) model (on right)

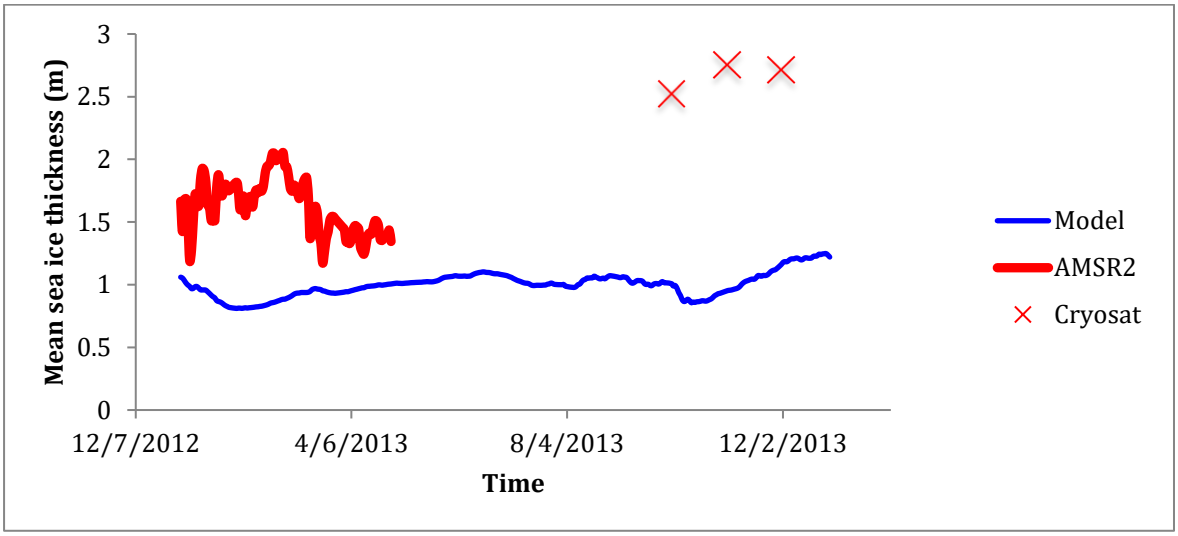

Figure 2-13: Time series of sea ice thickness of model and AMSR-2 observations and Cryosat observations in m

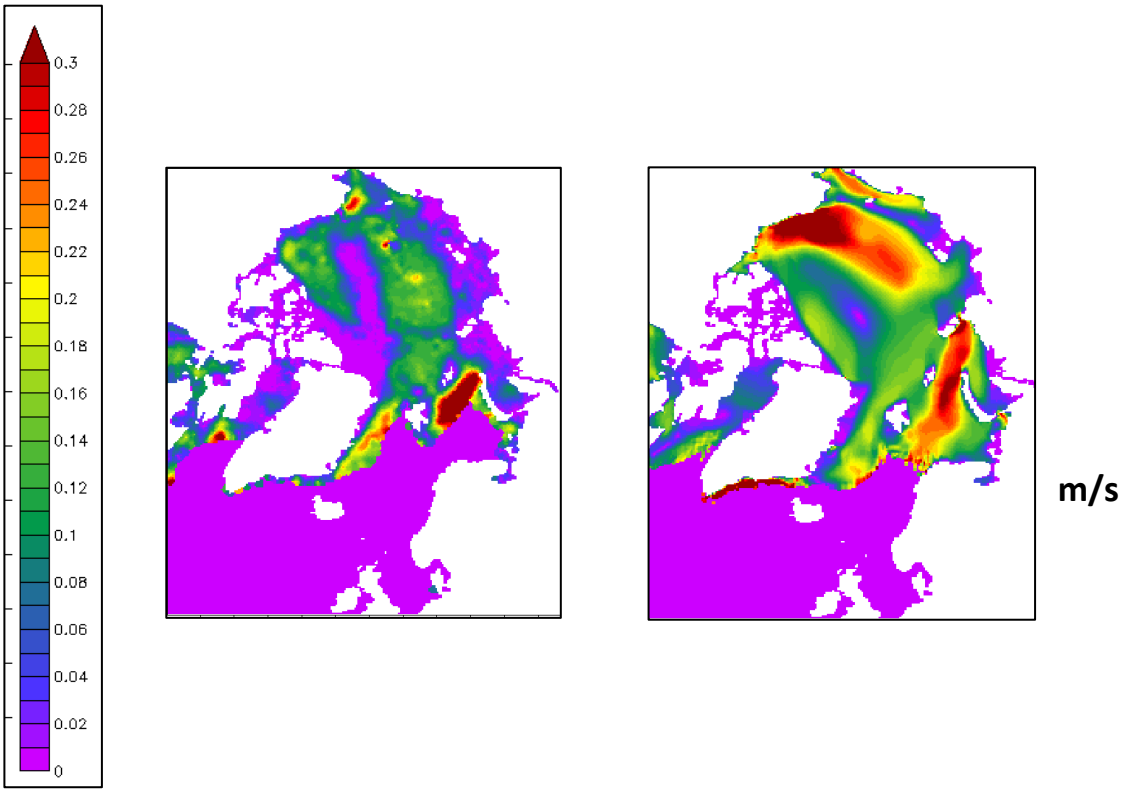

Figure 2-14: Comparison of sea ice velocity magnitude in m/s in February. Observation from Kimura (Kimura N. 2016) data set (on left) model (on right)

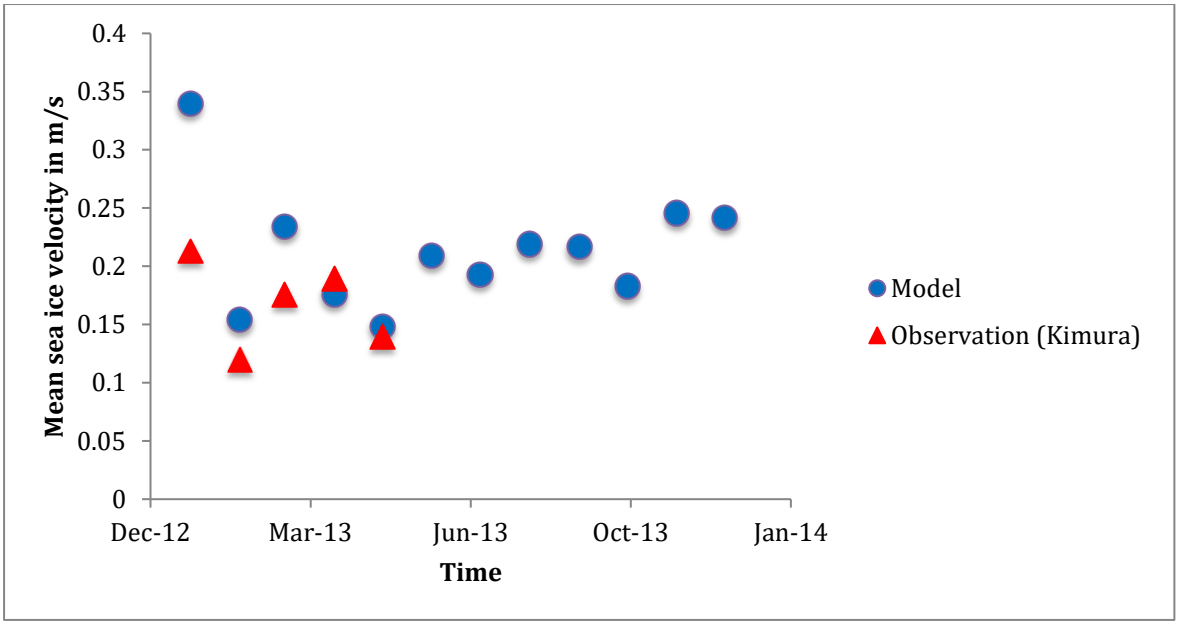

Figure 2-15: Time series of sea ice velocity magnitude of model and Kimura observation in m/s

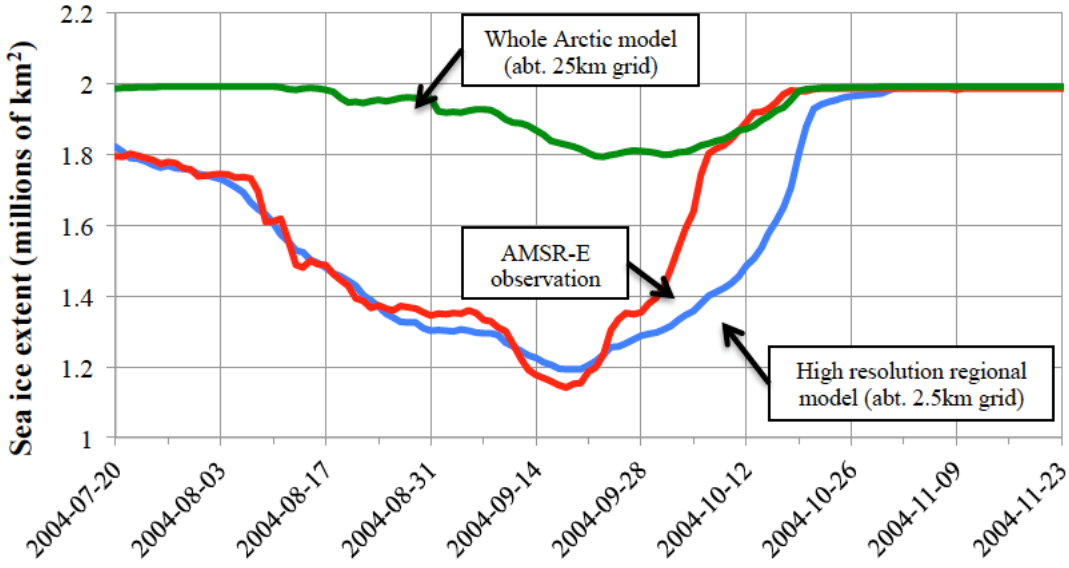

Figure 2-16: Comparison of sea ice extents between coarse grid computation, fine grid computation and AMSR-E observation. (De Silva 2013)

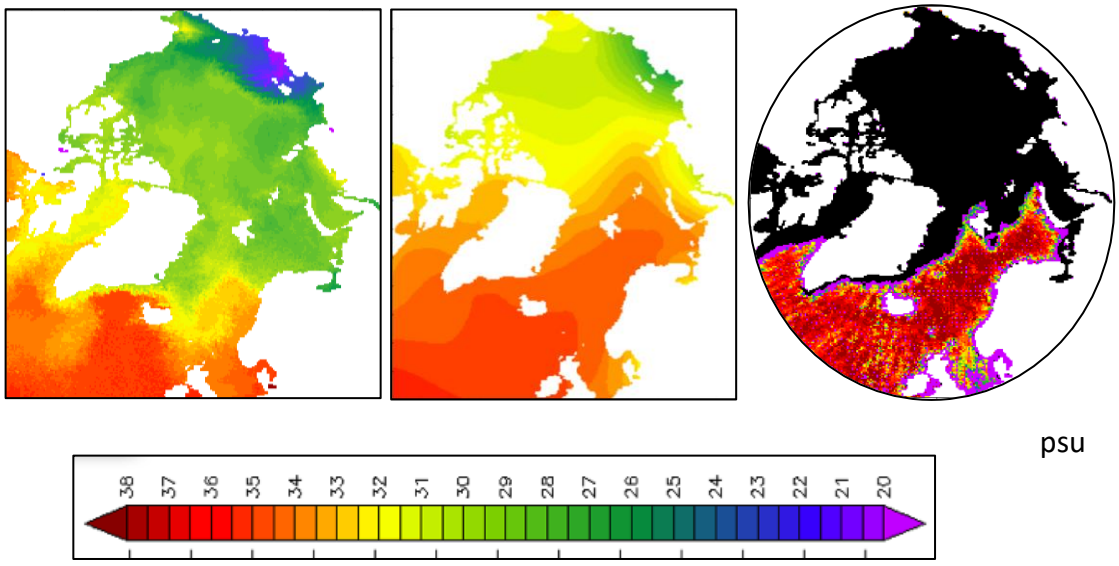

Figure 2-17: Comparison of sea surface salinity (psu) in February between model (left), PHC 3.0 data set (center) and observation from Aquarious data set (right)

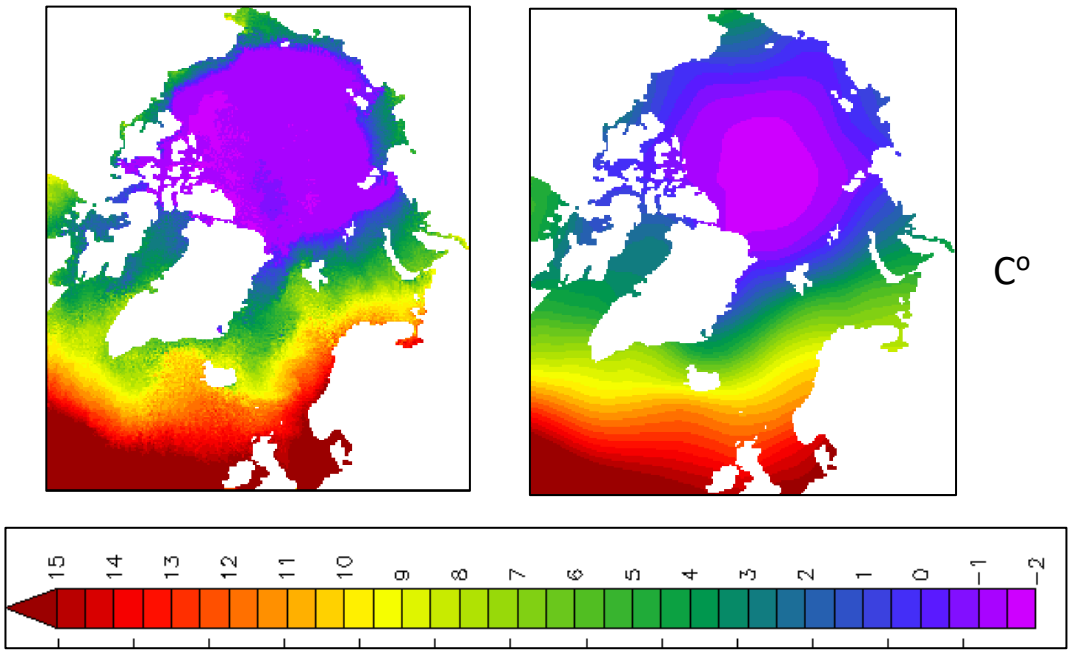

Figure 2-18: Comparison of sea surface temperature (C°) in September, between model (left) and PHC 3.0 data set (right)

Reproducibility of ocean conditions is also investigated. Even with a coarse grid of 25km the model is able to capture the general distribution of salinity in the Arctic Ocean. According to figure 2-17, the model underestimates sea surface salinity in some areas such as in the Barents Sea and East Siberian Sea.

There are disparities between the model predicted sea surface temperature and climatology data (figure 2-18). One of the reasons for this disagreement is the incompleteness of the ocean transportation expressions and imperfect ocean boundary conditions. Disparities could also arise due to overestimation in sea ice extent, along the ice edge sea surface temperature is underestimated (figure 2-18). However, sea surface temperature in the Norwegian Sea and upper Atlantic Ocean is higher than that of the PHC data. Not incorporating the effect of rapidly warming upper Atlantic Ocean in the climatology data set could also cause these disparities.

3. Data Assimilation Method

This chapter presents the data assimilation methods that are used in this study. Direct insertion method, nudging method and atmospheric forcing Kalman filter method are used in this study.

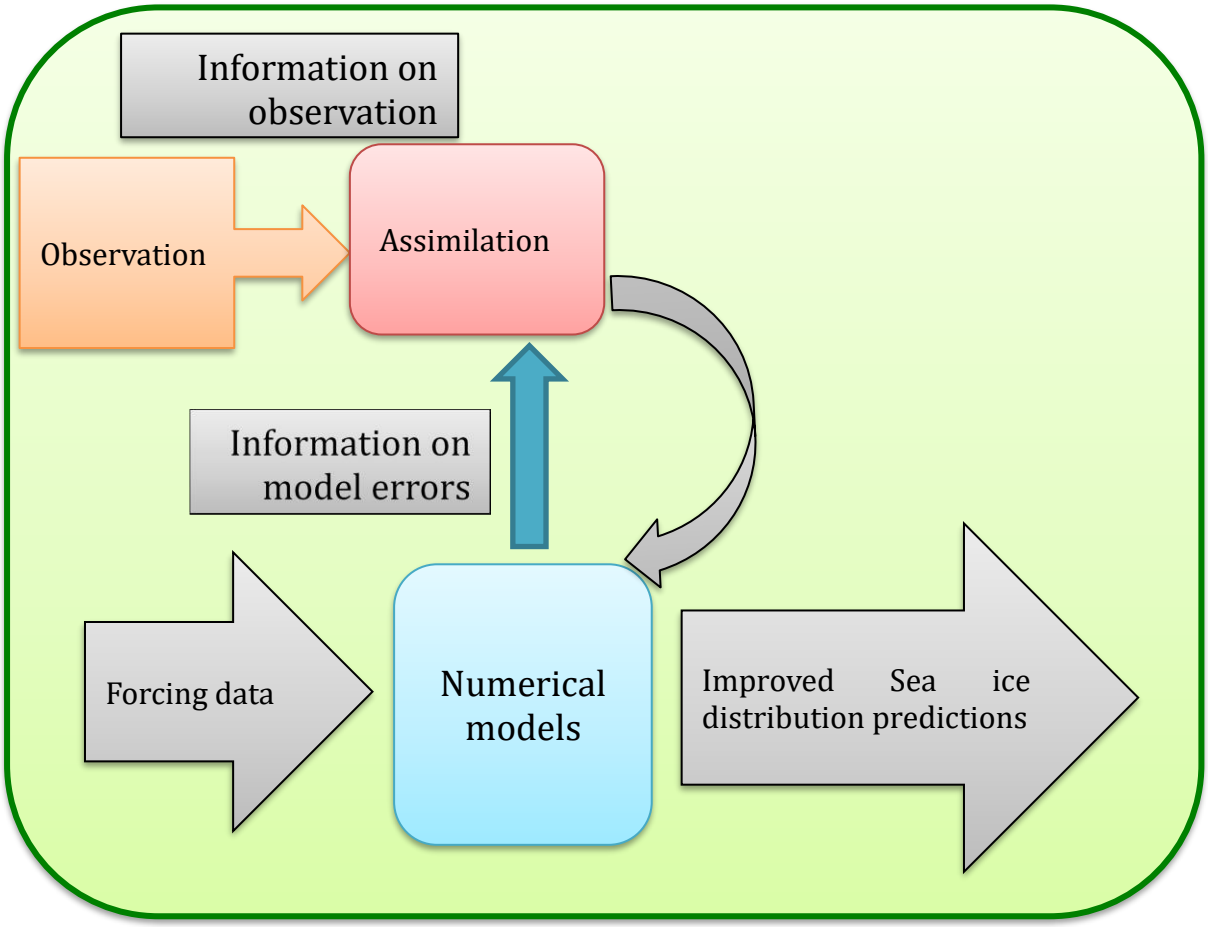

Figure 3-1: flow chart of data assimilation in a model

3.1 Introduction to data assimilation

Numerical models and satellite data are used to derive sea ice information. Numerical models are bound by the uncertainties of initial conditions, uncertainties of forcing data, temporal and spatial resolutions and the indeterministic features of the model. On the other hand, satellite observations are also limited by the instrument errors, spatial and

temporal resolutions, and uncertainties in converting algorithms. Data assimilation best combines model and observations (figure 3-1).

Data assimilation considers the uncertainties in models and observation to determine the true state of the system. It is widely used in numerical weather predictions. However there have only been few cases in assimilation of satellite sea ice observations. In this study three methods are used. Namely direct insertion method, nudging method and atmospheric forcing Kalman filter method (AFKF). Three variables are assimilated individually and simultaneously.

3.2 Data used in assimilation

Sea ice concentration data is obtained from the advanced microwave scanning radiometer 2 (AMSR2) onboard the GCOM-W satellite. Daily gridded sea ice concentration data set is extracted from Arctic Data Archive System (ADS) from the following website https://ads.nipr.ac.jp/. Daily sea ice thickness is calculated using Krishfield (2014) algorithm based on AMSR-2 satellite data. The gridded daily sea ice thickness data set is also obtained from ADS. Sea ice velocity data set is extracted from KIMURA Sea ice velocity data set (Kimura N. 2016). Sea ice concentration data are available in a daily interval for the year 2013. Sea ice thickness and sea ice velocity daily data sets are only available from January to May of 2013. Sea ice observation gridded data sets are available in 10km zonal and meridional resolution.

Very little is known about observation errors. In this study instrument errors and algorithm errors are considered. They are incorporated according to the equation below.

$$\sigma^2_{\text{observation}} = \sigma^2_{instrument} + \sigma^2_{algorithm} \quad (3\text{-}1)$$

The error variance of the observation varies considerably with time and location. Therefore, different values are selected for the ice edge and the other areas.

Table 3-1: Observation error variance

	Sea ice concentration	Sea ice thickness	Sea ice velocity
summer $\sigma_{algorithm}$	0.1~0.2	Not used in summer	Not used in summer
winter $\sigma_{algorithm}$	0.01~0.08	15cm	Zonal = 1.46 cm/s Meridional=1.35 cm/s
sea ice edge $\sigma_{algorithm}$	0.05~0.15	42cm	Zonal = 1.46 cm/s Meridional=1.35 cm/s
summer $\sigma_{instrument}$	0.1	Not used in summer	Not used in summer
winter $\sigma_{instrument}$	0.025	3.75cm	Zonal and meridional =0.05cm/s
sea Ice edge $\sigma_{instrument}$	0.125	12.5cm	Zonal and meridional =1.875cm/s

Table 3-2: Observation bias

	Sea ice concentration along the ice edge	Sea ice thickness	Sea ice velocity
Bias	-0.05	+10cm	0

Error variance values are higher in summer since the observations are not reliable in the summer. All the used values are listed in table 3-1. Observation instrument errors are calculated according to the instrumentation errors provided by JAXA (2014).

Sea ice concentration is derived using NASA team 2 ice concentration algorithm (NT2). The uncertainty values are obtained from Ludovic et al. (2014). Sea ice concentration uncertainties are provided in a range since uncertainties are larger in Fram Strait and smaller in the Chukchi Sea (Ludovic et al. 2014). Sea ice thickness is computed using Krishfield et al. (2014) algorithm. The error variance and bias are obtained from Ono et al. (2016). The error variance and the bias of sea ice velocity are obtained from Kimura et al. (2016).

To compare the experiment results with independent data sets that are not used in the experiments, Aquarius L3 Weekly Polar-Gridded Sea Surface Salinity data from National Snow and Ice Data Center (NSIDC), Ocean salinity of the Fram Strait and Barents Sea from Kawasaki and Hasumi, (2015) data set and monthly averaged sea ice thickness data set derived from Cryosat-2 are used. Different atmospheric forcing from several weather agencies differentiates ensemble members that are used in the atmospheric forcing Kalman filter method assimilation (AFKF). They are obtained from Historical THORPEX Interactive Grand Global Ensemble (TIGGE) forecast data archive system (Table 3-3).

3.3 Direct insertion method

Direct insertion is the most fundamental method that is used in data assimilation. During assimilation experiments the model estimates are nudged to new estimates with the following relationship (equation 3-2).

$$\psi^a = \psi^f + K(d - \psi^f) \tag{3-2}$$

K is the weighting. ψ is the prognostic variable; in this study variables are sea ice concentration, sea ice thickness or sea ice velocity. ψ^a is the analysis estimate, ψ^f is the background state and d is observation. In direct insertion experiments K is set to 1.

The observation data sets are interpolated to the model grid using inverse distance interpolation considering the nearest four observation points. Sea ice concentration sea ice thickness and Sea ice velocity are assimilated daily and are integrated for 24 hours.

In the coupled Ice-POM model direct insertion is introduced as a subroutine that is highlighted in the flowchart (figure 3-2). Observation data is introduced after updating ocean variables and sea ice variables. Both ocean variables and ice variables are updated after assimilation before starting the next time step.

Table 3-3: TIGGE (THORPEX (The Observing System Research and Predictability Experiment) Grand Global Ensemble) forecast data set

Weather Agency	**Resolution**
CMA (China Meteorological Administration)	12 hourly, $0.75° \times 0.75°$ lon, lat
CMC (Canadian Meteorological Centre)	12 hourly, $0.75° \times 0.75°$ lon, lat
ECMWF (European Center for Medium Range Weather Forecasting)	6 hourly, $0.75° \times 0.75°$ lon, lat
FRA (Meteo France)	12 hourly, $0.75° \times 0.75°$ lon, lat
JMA (Japanese Meteorological Agency)	6 hourly, $0.75° \times 0.75°$ lon, lat
NCEP (National Centre for Environmental Prediction)	6 hourly, $0.75° \times 0.75°$ lon, lat
UK (Met office)	12 hourly, $0.75° \times 0.75°$ lon, lat

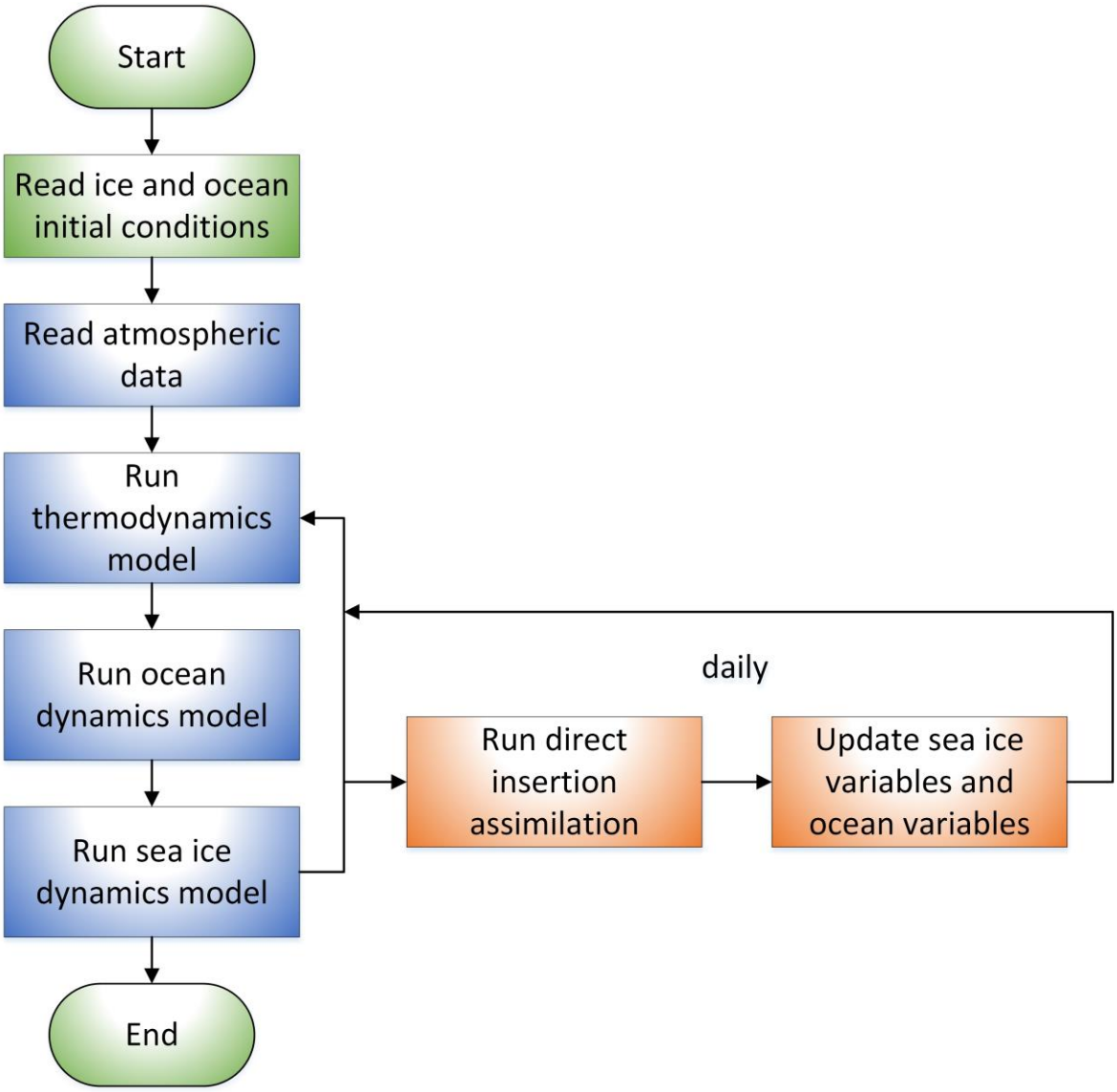

Figure 3-2: Ice POM model flow chart with direct insertion assimilation

When the model variables are changed according to the observations, non-assimilated ice variables and ocean variables are also affected by these changes. Therefore, some corrections are done to rectify discrepancies between assimilated and non-assimilated ice and ocean variables. These corrections are discussed in detail in section 3.6. As a result of assimilation in some areas sea ice is introduced or removed from the cells. These changes demand for modifications in the ocean temperature and salinity. It is also necessary to set accurate values for ice variables in those cells.

The impact of assimilation time interval is also studied. Yearly, monthly, weekly and daily assimilation intervals are examined. These time interval experiments are done only for sea ice concentration assimilation, since the other data sets aren't available throughout the year.

3.4 Nudging (Newtonian relaxation) method

Even though direct insertion method is simple in formulation and application, direct insertion makes large fluctuations in the computations, which in some cases lead to dominate over model estimate. Nudging method can overcome this issue by introducing observations into the model in a controlled manner. The prognostic equation is written as bellow.

$$\psi^a = \psi^f + \frac{\mathrm{K}}{\tau}(d - \psi^f) \tag{3-3}$$

Where, τ is the time relaxation coefficient that does not have a time dimension. K is the nudging weight. A sensitivity analysis was done for both τ and *K*, which will be discussed in chapter 5. Experiments with smaller τ make fluctuations in the assimilated variables while experiments with larger τ incorporate observations more smoothly.

3.4.1 Nudging method-1

A separate set of experiments was performed in order to consider the observation error. In those experiments, *K* was formulated according to Lindsay (2006). The optimal least square value of the weighting is formulated as in equation 3-4.

$$\mathrm{K} = \frac{\mathrm{R}^2_{\mathrm{model}}}{\mathrm{R}^2_{\mathrm{model}} + \mathrm{R}^2_{\mathrm{obs}}} \tag{3-4}$$

$\mathrm{R}^2_{\mathrm{model}}$ is the error variance of the model estimate and $\mathrm{R}^2_{\mathrm{obs}}$ is the error variance of the observation. The model error covariance is assumed to be zero. Errors are assumed to be

unbiased and normally distributed. The values used for observation errors are explained in section 3.2.

The model error variance is modeled as a function of observed quantity and model estimate and is assumed to be proportional to the power of their difference.

$$R^2_{model} = \langle(\psi_{truth} - \psi_{model})^{\alpha}\rangle = r|d - H\psi_i^f|^{\alpha} \quad (3\text{-}5)$$

Where r adjusts the dimension; r=1 is used. The weight *K* is formulated as,

$$\mathrm{K} = \frac{|d - \psi^f|^{\alpha}}{|d - \psi^f|^{\alpha} + \mathrm{R}^2_{\mathrm{obs}}} \quad (3\text{-}6)$$

Lindsay (2006) has used α =6 in their study. Different values were tried for α and due to numerical stability, α =2 is selected for this study. The observation data sets are interpolated to the model grid using inverse interpolation considering the nearest four observation points around a model grid cell. The intermittent approach (Bloom 1996) is used to assimilate sea ice concentration, sea ice velocity and sea ice thickness. They are assimilated daily and are integrated for 24 hours. In the coupled Ice-POM model nudging is introduced as a subroutine that is highlighted in the flowchart (figure 3-3). Observation data is introduced after updating ocean variables and sea ice variables. Both ocean variables and ice variables are updated after assimilation before starting the next time step.

When the model variables are changed according to the observations, non-assimilated variables are also affected by these changes. Therefore, some corrections are done to rectify discrepancies between assimilated and non-assimilated variables. These corrections are discussed in detail in section 3.6.

3.4.2 Nudging method-2

Lindsay (2006) method uses $|d - H\psi_i^f|^{\alpha}$ to be the model error variance. One of the issues with this method is that it assumes observations to be unbiased but in reality,

observations could be biased. In nudging method-2 correction to bias is introduced. In equation 3-5, model error variance is set to be $|d \quad - H\psi_i^f|^\alpha$. Therefore, as an improvement to the formulation the model error variance is altered to be

$$R_{model}^2 = \langle(\psi_{truth} - \psi_{model})^2\rangle \; = r|(d \quad + d_{bias}) - \psi_i^f|^\alpha \tag{3-7}$$

Where, d_{bias} is set to be the bias of the observation and r adjusts the dimension; r=1 is used. The values used for observation bias are listed in table3-2. This method yields *K* as

$$\mathrm{K} = \frac{|(d \quad + d_{bias}) - \psi_i^f|^\alpha}{|(d \quad + d_{bias}) - \psi_i^f|^\alpha + \mathrm{R}_{\mathrm{obs}}^2} \tag{3-8}$$

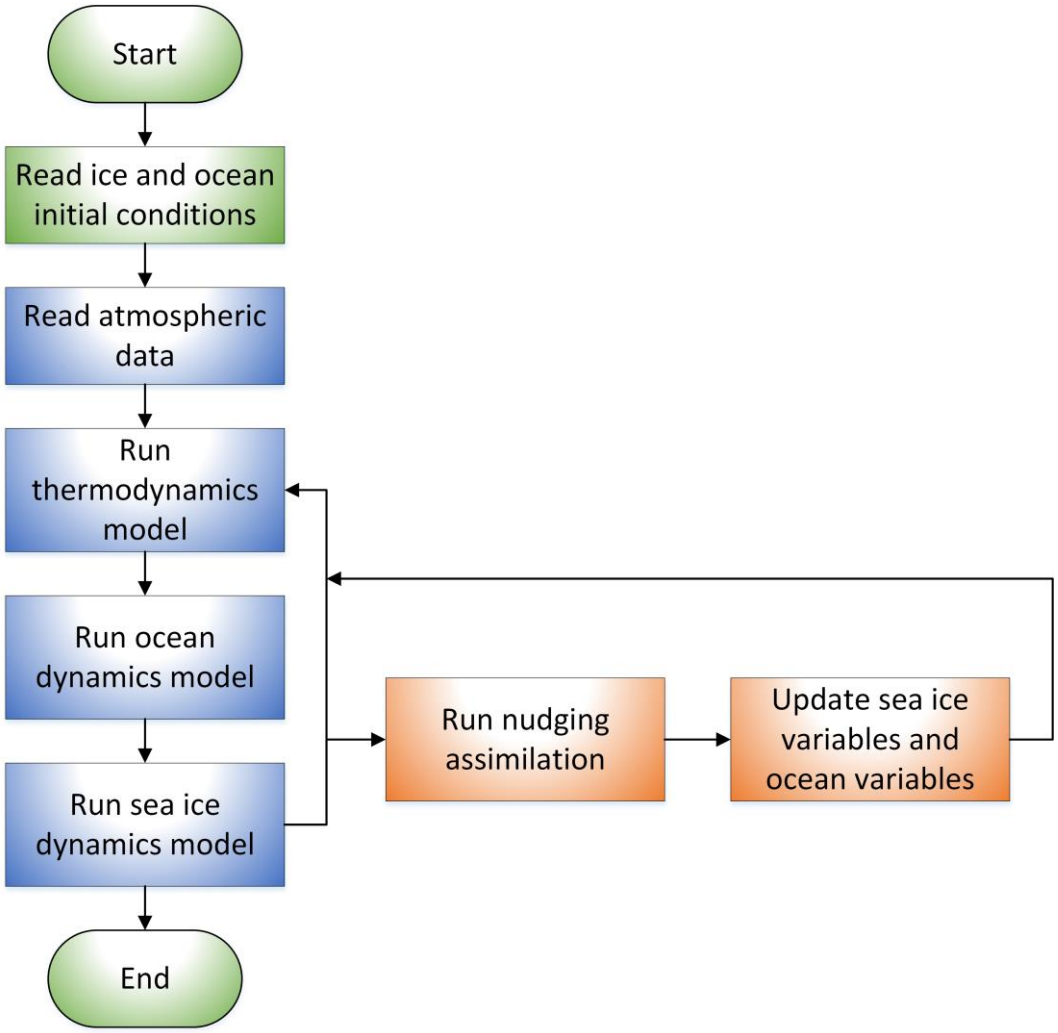

Figure 3-3: Ice-POM model flow chart with nudging assimilation

An experiment is performed assimilating sea ice concentration, sea ice thickness and sea ice velocity simultaneously. In the model, nudging method -2 is introduced as a subroutine that is highlighted in the flowchart (figure 3-3).

Corrections for non-assimilated sea ice variables and ocean variables are introduced similar to the nudging method-1.

3.5 Atmospheric Forcing Kalman Filter method (AFKF)

This section presents the atmospheric forcing Kalman filter method

3.5.1 Atmospheric forcing Kalman filter method justification

In an ice-ocean coupled model, atmospheric forcing directly affects the accuracy of predictions. Especially, precipitation data is directly related to the sea ice formulation process. However, different atmospheric data sets including reanalysis data sets show large differences in the Arctic region. In a study that evaluates seven atmospheric products over the Arctic, Lindsay et al. (2014) shows that there are large variations in atmospheric data sets in Arctic. According to the study, different products show large variations in sea level pressure over Greenland. Wind speed shows variations in most parts of Arctic Ocean where the differences are higher in the winter. Precipitation data also varies over North Atlantic and North Pacific Ocean. In a similar study that compares ERA reanalysis data and NCEP reanalysis data sets in Arctic region, Zhang (2016) shows that there is a significant difference in surface pressure and surface winds in these two data sets that are most commonly used as forcing data in many sea ice prediction models.

Large variance can be observed in the atmospheric forecast obtained from different agencies in which different weather agencies performing more skillfully in different geographical areas depending upon their access to field observations in different areas (Broman 2016). In a study that investigated the impact of surface observations over the Arctic Ocean on reanalysis, has observed that uncertainty regarding atmospheric data sets exist due to lack of observational data. (Inoue, 2013 and Inoue,2015).

The nudging method formulates the model error covariance as in equation 3-7, where the true state is defined as $d \quad + d_{bias}$. However, this description is imperfect. Model error covariance matrix (P_e^f) in Kalman filter is defined in terms of the true state as

$$P_e^f = \overline{(\psi^f - \psi^t)\ (\psi^f - \psi^t)^T} \tag{3.9}$$

where ψ^f is model forecast and ψ^t is the true state (Evensen, 2009).

Ensemble numerical predictions are widely used recently due to their better predictability skills compared to single computations. These ensemble predictions are performed using different atmospheric forcing data sets or by differentiating initial conditions (De Silva, 2016). Model errors largely depend upon the inaccuracies in forcing data. In a computation that uses ensemble of multiple atmospheric data sets, the spread of the ensemble is proportional to the uncertainties in model prediction. Hence this spread could be an indicator of the model error variance.

In atmospheric forcing Kalman filter method an ensemble of multiple atmospheric data is used. Since there are significant differences in the atmospheric data sets, the true state is assumed to be the mean of the ensemble prediction. Therefore, the true state is considered to be $\overline{\psi^f}$, the ensemble mean of the prognostic variable. In each ensemble member, the model is forced using different atmospheric forecast data from seven atmospheric agencies given in table 3-3 (figure 3-5). Hence, this method is named as atmospheric forcing Kalman filter method.

3.5.2 Formulation of Atmospheric forcing Kalman filter

The equation 3.9 is revised as below to use ensemble mean as the truth.

$$P_e^f = \overline{(\psi_i^f - \overline{\psi^f})\ (\psi_i^f - \overline{\psi^f})^T} \tag{3.10}$$

Observation error variance used to assimilate sea ice observations are selected based on table3-1. Different values are selected for ice edge and other areas as stated above in

Newtonian relaxation method. Observation variance is also varied according to the season. Higher values are selected during summer due to the unreliability of satellite observations in summer.

Observation errors and model errors are assumed to be uncorrelated, yielding a diagonal matrix, which is trivial to invert in equation 3-11. In this study ψ_i^f is model forecast of the ensemble member $\mathrm{i} \in \{1,2 \ldots \mathrm{N}\}$. *H* is a linear operator that transfers the model state to the observation space. K_e is the Kalman gain, which is given in equation 3-11. The updated state estimate (ψ_i^a) is given in equation 3-12, where d is observation.

$$K_e = P_e^f H^T (H P_e^f H^T + R)^{-1} \quad (3\text{-}11)$$

$$\psi_i^a = \psi_i^f + K_e (d - H\psi_i^f) \quad (3\text{-}12)$$

Analyzed model state covariance (P_e^a) is given in equation 3-13.

$$P_e^a = (I - K_e H) P_e^f \quad (3\text{-}13)$$

The method used is inspired by the Ensemble Kalman filter method (Evensen 2009). However, the key difference between the two methods is that the atmospheric forcing Kalman filter formulates the ensemble by using different atmospheric data sets, instead of observation perturbation that is often used in ensemble Kalman filter method.

Even though the error variance is assumed to be non-correlated the impact of non-correlated variables are considered through corrections. It prevents the discrepancies between assimilated and non-assimilated variables. This is explained in section 3.6.

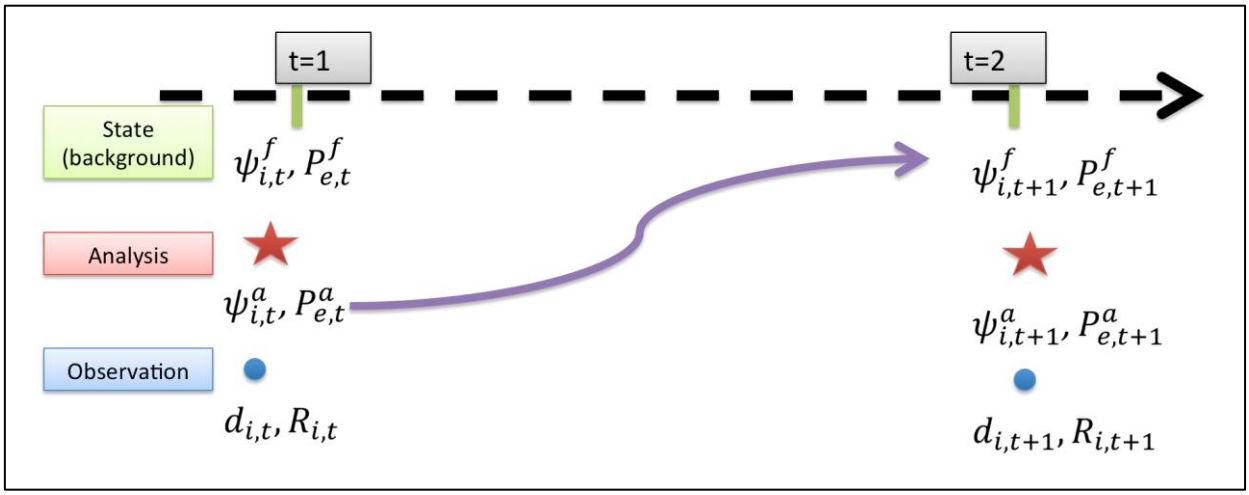

Figure 3-4 Atmospheric forcing Kalman filter diagram $\psi = prognostic\ variable$, $\psi_i^a = analysis\ estimate$, $\psi_i^f = model\ state$, $\overline{\psi^f} = ensemble\ average$, $d_i = observations$, H= observation operator, $P_e^a = Analysis\ error\ covar$, $P_e^f = Model\ error\ covariance$, i = ensemble number

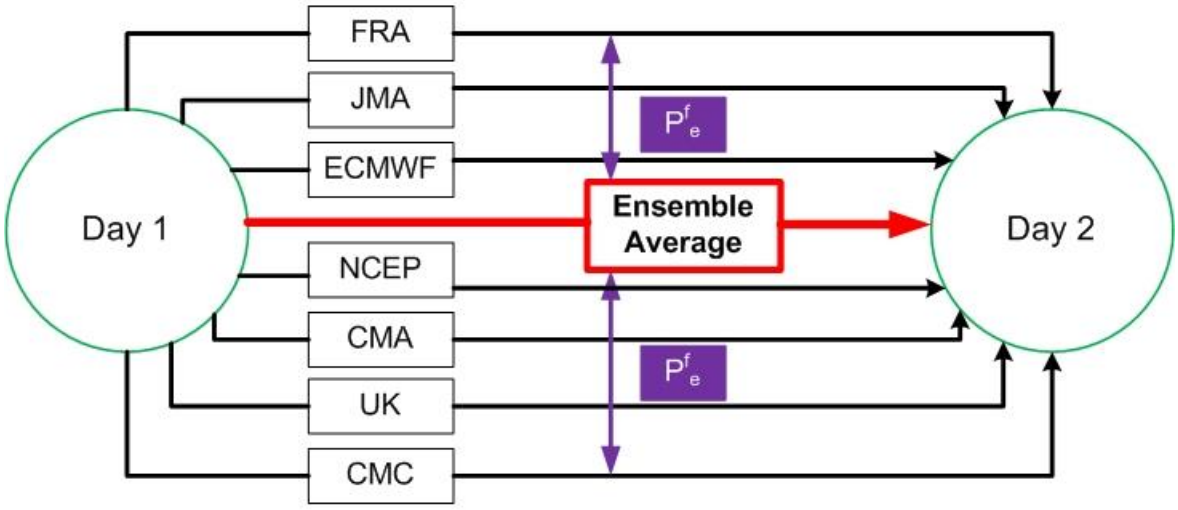

Figure 3-5 Atmospheric Forcing Kalman Filter diagram

3.5.3 Atmospheric forcing Kalman filter program architecture

The AFKF program structure is more complex than that of direct insertion method and the nudging method. Seven ensemble members run parallel while sharing the background estimate (ψ_i^f) values (figure 3-6). There is a main file-sharing hub that collects output data

from each ensemble member. There is one lead ensemble member that computes the error covariance matrix (P_e^f) by accessing the data in main file sharing hub. This happens in three steps. During the first step ensemble1 waits for all the ensemble members to finish their computation for one assimilation cycle (figure3-7). At the end of each assimilation cycle (one day) all the ensemble members share the output data (ψ_i^f) into main file sharing hub. During the last step, while the other ensemble members wait, the ensemble one computes error covariance matrix (P_e^f). (figure 3-8).

3.6 Corrections for non-assimilated variables

Some corrections are done to adjust the non-assimilated variables to avoid discrepancies and numerical instabilities. A similar criterion is used for direct insertion, nudging and atmospheric forcing Kalman filter method.

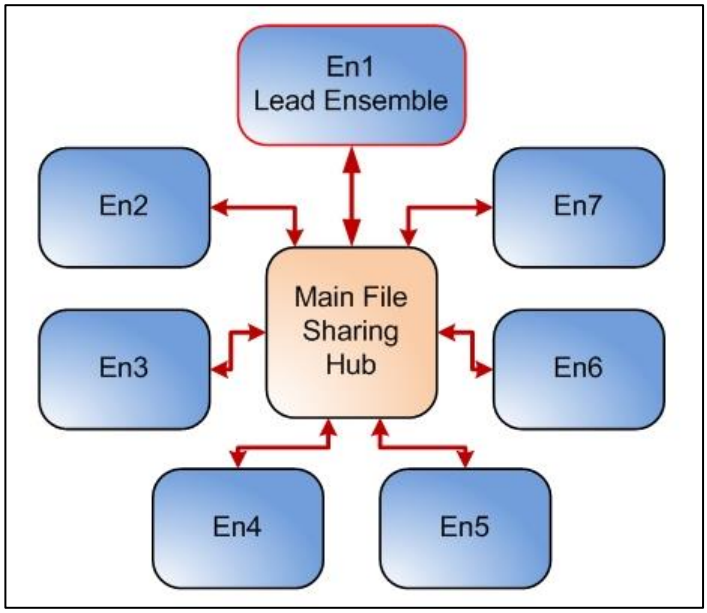

Figure3-6: AFKF program structure: Seven ensemble members run parallel while sharing the analysis estimate

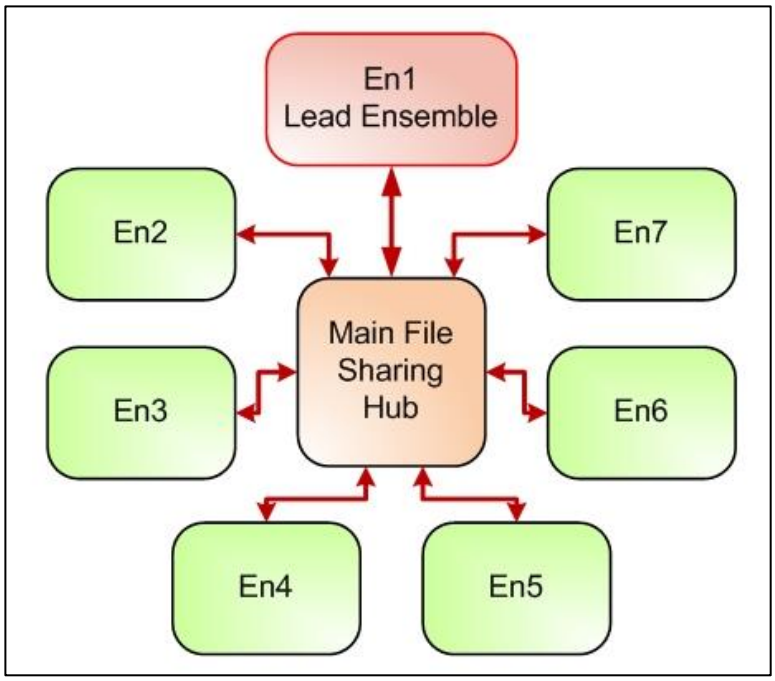

Figure 3-7: step1 ensemble1 waits for all the ensemble members to finish their computation for one assimilation cycle

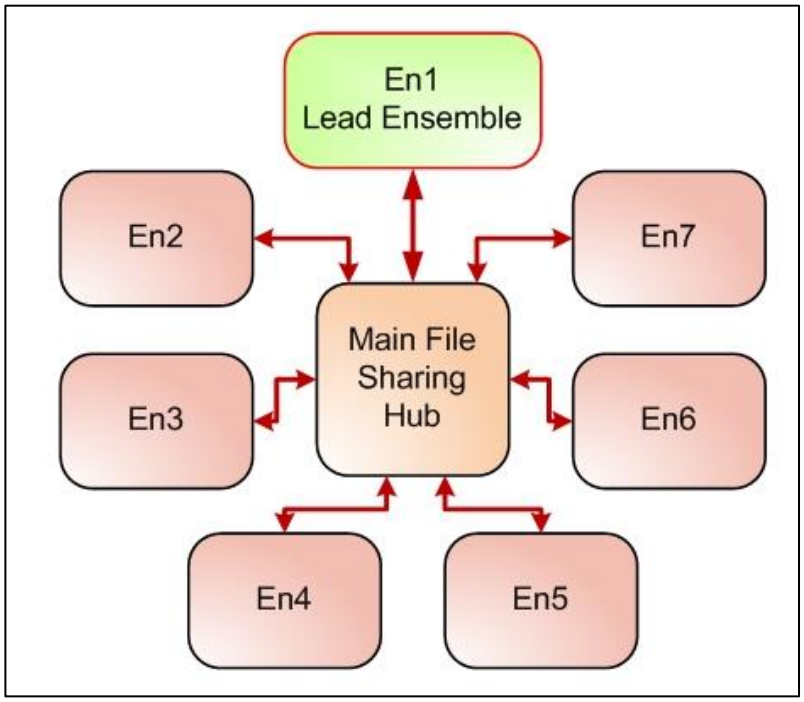

Figure 3-8: step 3 while the other ensemble members wait, the ensemble one computes error covariance matrix (P_e^f)

3.6.1 Sea ice concentration assimilation correction

Two scenarios are considered while assimilating sea ice concentration. When the analysis estimate (ψ_i^a) sea ice concentration value is positive while background estimate (ψ_i^f) sea ice concentration value is zero, model creates ice in the cell. Sea ice thickness, sea ice velocity and sea surface temperature are set to be the average of the four neighboring cells while the maximum thickness of created ice is set to be 0.5m and the minimum is set to 0.1m to avoid immediate melting (equations 3-14, 3-15, 3-16). Sea surface temperature and the ocean temperature of the top three 1m vertical layers are set to be the maximum of freezing temperature as in equation 3-17 (figure-3-9). When the analysis estimate (ψ_i^a) of sea ice concentration value is zero while background estimate (ψ_i^f) of sea ice concentration value is positive model removes ice, the values of other sea ice variables (sea ice thickness and sea ice velocity) are set to zero (equation 3-18, 3-19, 3-20) Ocean temperature of all the vertical layers is also set to a minimum freezing temperature if the temperature is below freezing temperature as in equation 3-21 (figure 3-10).

$$if\ (conc_{i,j}^a > 0\ and\ \ conc_{i,j}^f\ = 0\ )then$$

$$thic_{i,j}^a = (thic_{i+1,j}^f + \ thic_{i-1,j}^f + \ thic_{i,j+1}^f + \ thic_{i,j-1}^f)/4\ , thic(\max)_{i,j}^a = 0.5m, thic(\min)_{i,j}^a = 0.1m \quad (3\text{-}14)$$

$$uvel_{i,j}^a = (uvel_{i+1,j}^f + \ uvel_{i-1,j}^f + \ uvel_{i,j+1}^f + \ uvel_{i,j-1}^f)/4 \quad (3\text{-}15)$$

$$vvel_{i,j}^a = (vvel_{i+1,j}^f + \ vvel_{i-1,j}^f + \ vvel_{i,j+1}^f + \ vvel_{i,j-1}^f)/4 \quad (3\text{-}16)$$

$$Tocean(\max)_{i,j,(1\sim3)}^a = Tocean_{freezing} \quad (3\text{-}17)$$

$$if\ (conc_{i,j}^a = 0\ and\ \ conc_{i,j}^f > 0\ )then$$

$$thic_{i,j}^a = 0 \quad (3\text{-}18)$$

$$uvel_{i,j}^a = 0 \quad (3\text{-}19)$$

$$vvel_{i,j}^a = 0 \quad (3\text{-}20)$$

$$Tocean(\min)_{i,j,(1\sim33)}^a = Tocean_{freezing} \quad (3\text{-}21)$$

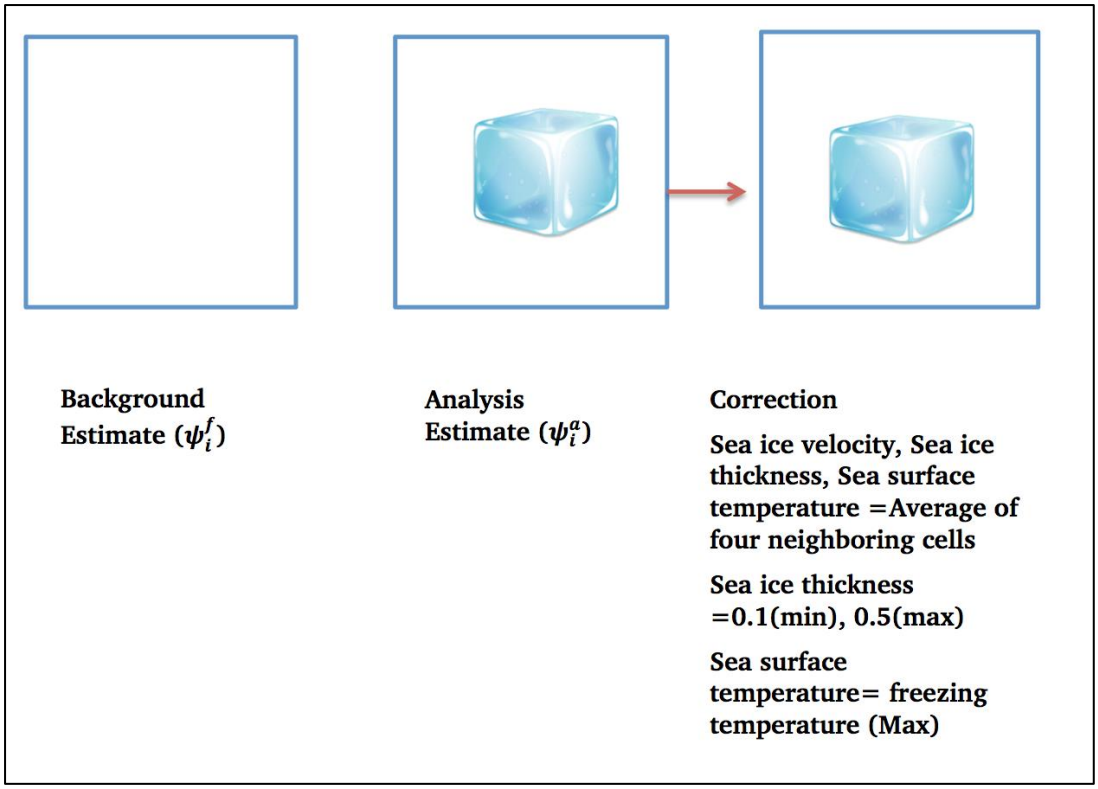

Figure 3-9: Corrections when the analysis estimate (ψ_i^a) sea ice concentration value is positive while background estimate (ψ_i^f) sea ice concentration value is zero

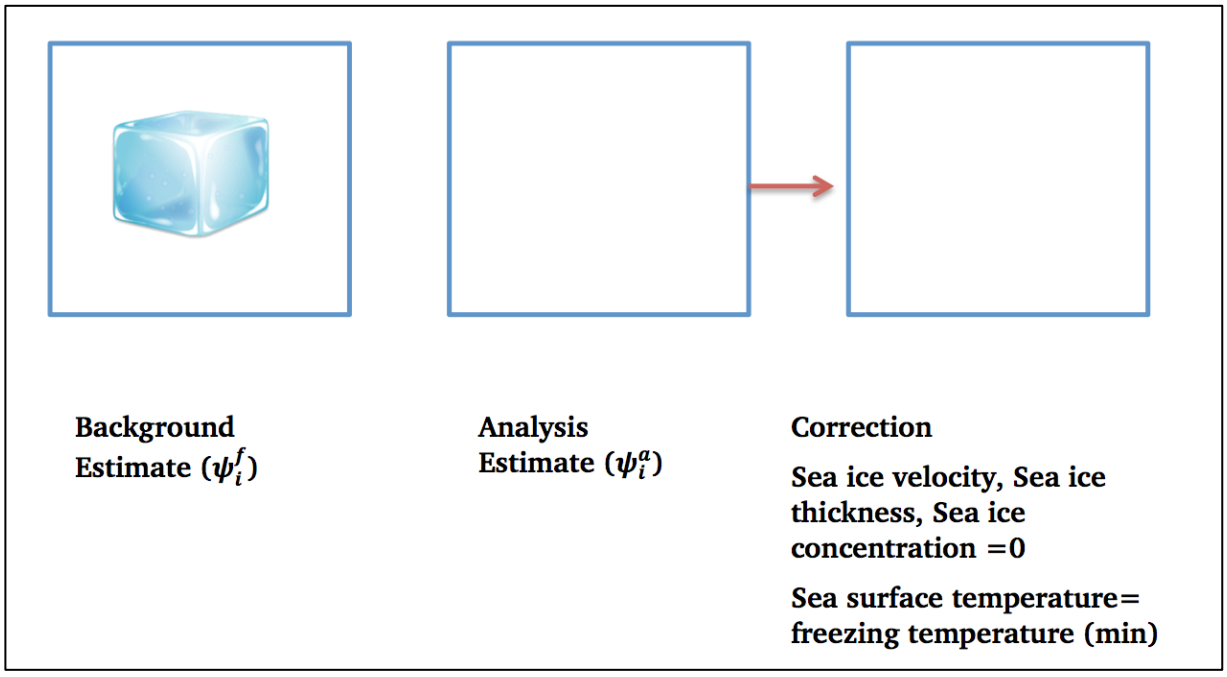

Figure 3-10: Corrections when the analysis estimate (ψ_i^a) sea ice concentration value is zero while background estimate (ψ_i^f) sea ice concentration value is positive

3.6.2 Sea ice thickness assimilation correction

Two scenarios are considered while assimilating sea ice thickness. When the analysis estimate (ψ_i^a) of sea ice thickness value is positive while background estimate (ψ_i^f) of sea ice thickness value is zero, model creates ice in the cell. Sea ice concentration, sea ice velocity and sea surface temperature are set to be the average of the four neighboring cells (equation 3-22, 3-23, 3-24). Sea surface temperature and the ocean temperature of the top three 1m vertical layers are set to be the maximum of freezing temperature as in equation (equation 3-25) (figure-3-11). When the analysis estimate (ψ_i^a) sea ice thickness value is zero while background estimate (ψ_i^f) sea ice thickness value is positive model removes ice, the values of other sea ice variables (sea ice concentration and sea ice velocity) are set to zero (equation 3-26, 3-27, 3-28). Ocean temperature of all the vertical s-layers is also set to a minimum freezing temperature if the temperature is below freezing temperature (equation 3-29), (figure 3-12).

$$if\ (thic_{i,j}^a > 0\ and\ \ thic_{i,j}^f\ = 0\ )then$$

$$conc_{i,j}^a = (conc_{i+1,j}^f + conc_{i-1,j}^f + conc_{i,j+1}^f + conc_{i,j-1}^f)/4 \quad (3\text{-}22)$$

$$uvel_{i,j}^a = (uvel_{i+1,j}^f + uvel_{i-1,j}^f + uvel_{i,j+1}^f + uvel_{i,j-1}^f)/4 \quad (3\text{-}23)$$

$$vvel_{i,j}^a = (vvel_{i+1,j}^f + vvel_{i-1,j}^f + vvel_{i,j+1}^f + vvel_{i,j-1}^f)/4 \quad (3\text{-}24)$$

$$Tocean(\max)_{i,j,(1\sim3)}^a = Tocean_{freezing} \quad (3\text{-}25)$$

$$if\ (thic_{i,j}^a = 0\ and\ \ thic_{i,j}^f > 0\ )then$$

$$conc_{i,j}^a = 0 \quad (3\text{-}26)$$

$$uvel_{i,j}^a = 0 \quad (3\text{-}27)$$

$$vvel_{i,j}^a = 0 \quad (3\text{-}28)$$

$$Tocean(\min)_{i,j,(1\sim33)}^a = Tocean_{freezing} \quad (3\text{-}29)$$

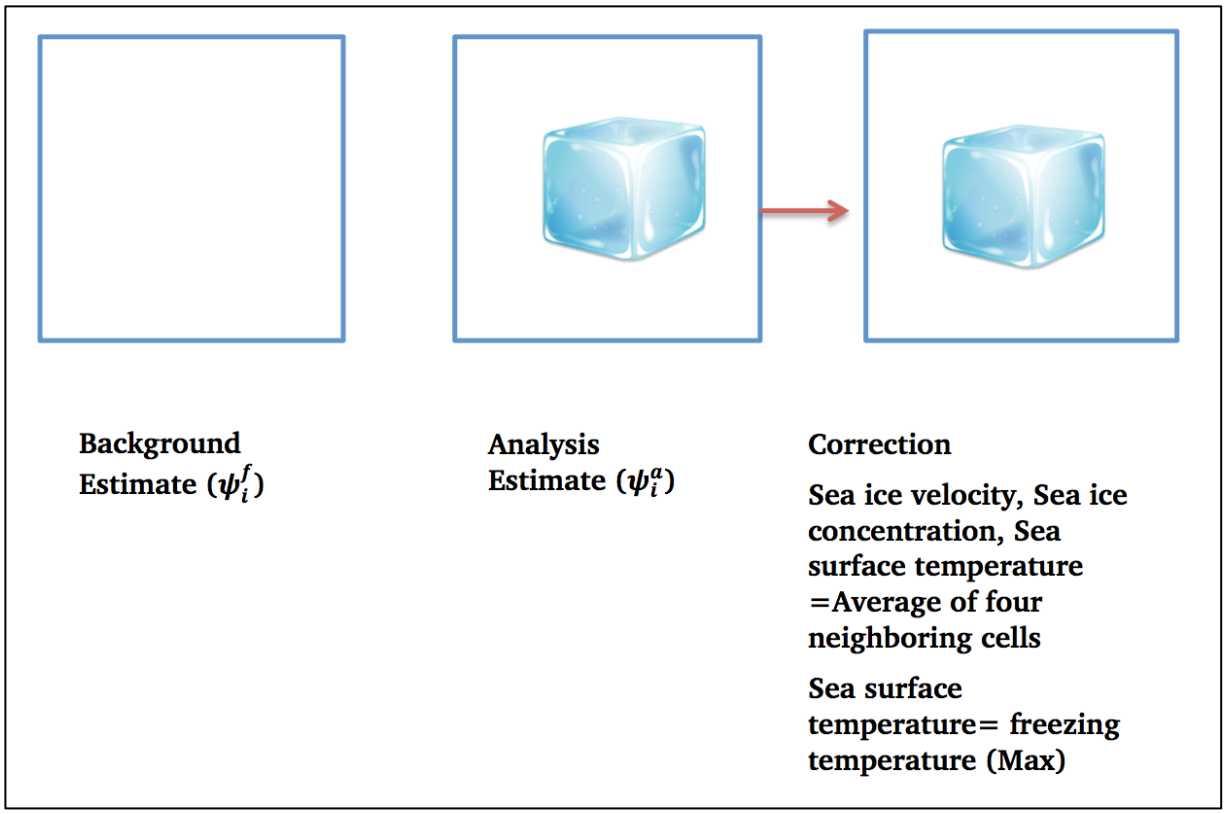

Figure 3-11: Corrections when the analysis estimate (ψ_i^a) sea ice thickness value is positive while background estimate (ψ_i^f) sea ice thickness value is zero

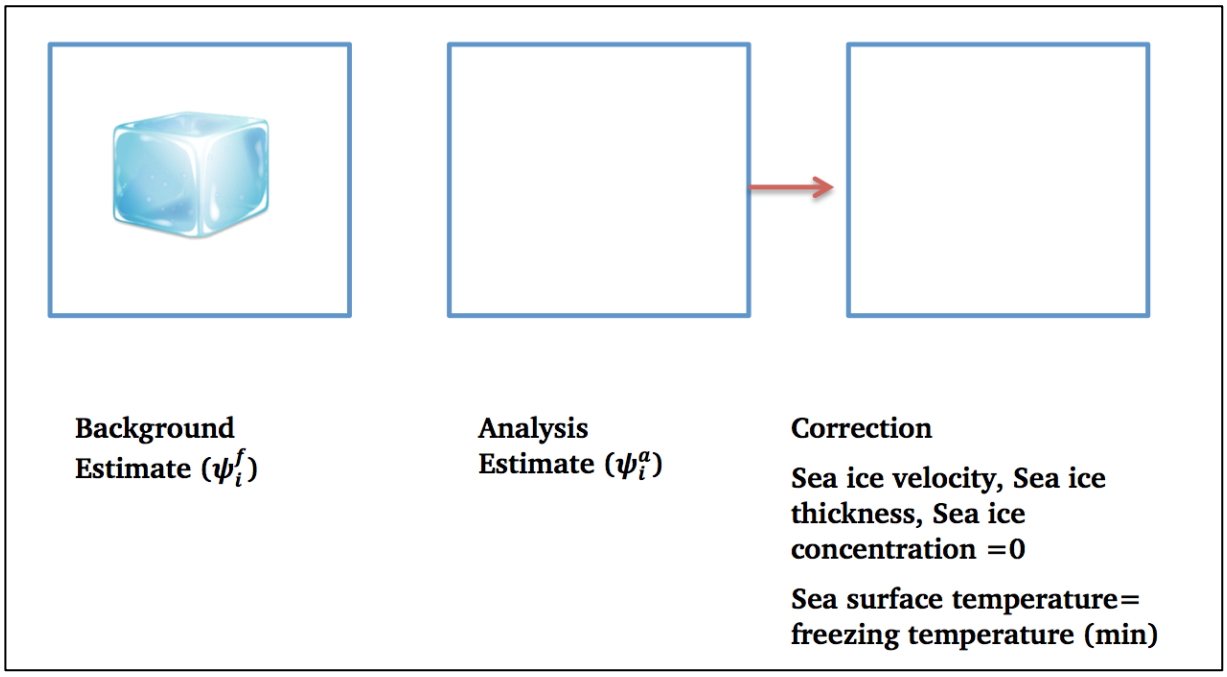

Figure 3-12: Corrections when the analysis estimate (ψ_i^a) sea ice thickness value is zero while background estimate (ψ_i^f) sea ice thickness value is positive

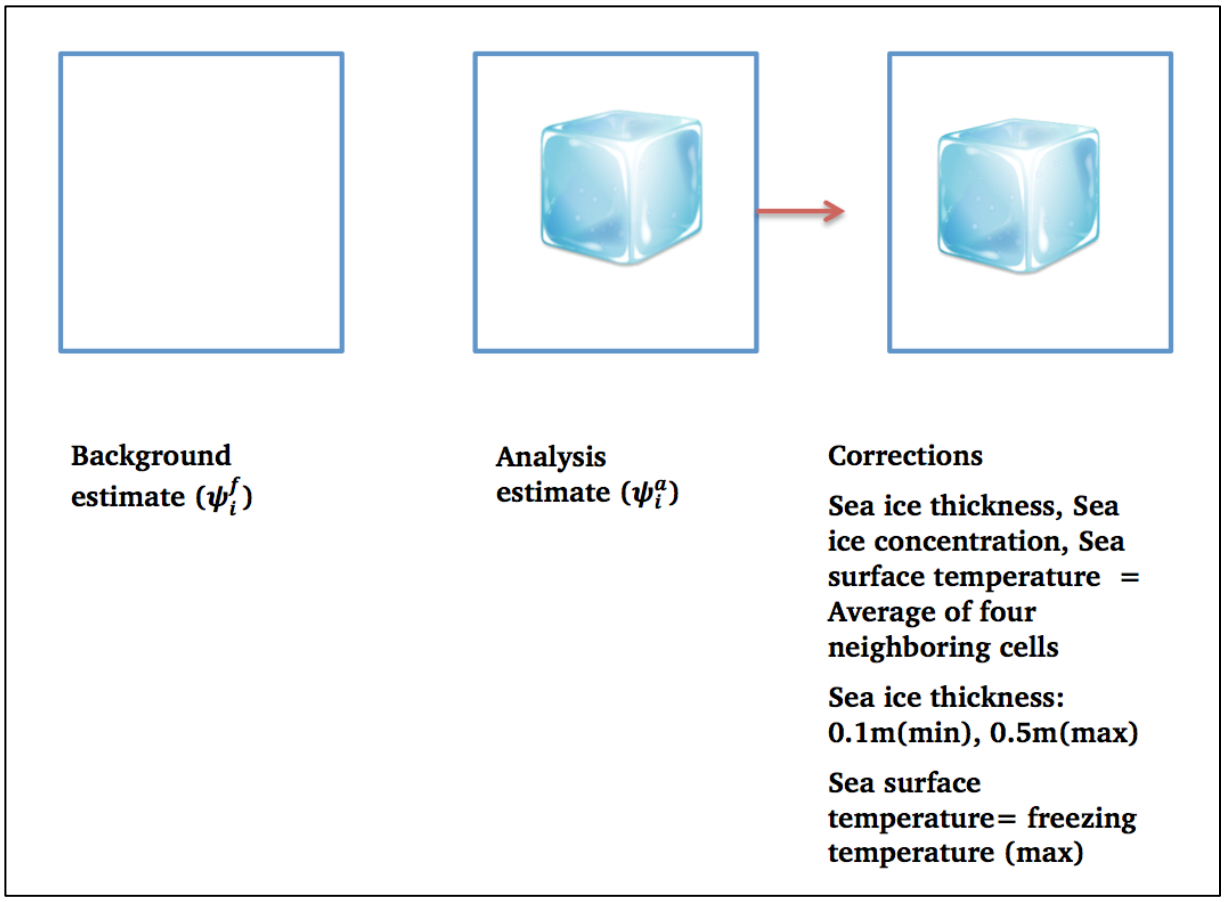

Figure 3-13: Corrections when the analysis estimate (ψ_i^a) sea ice velocity value is positive while background estimate (ψ_i^f) sea ice velocity value is zero

3.6.3 Sea ice velocity assimilation correction

When the analysis estimate (ψ_i^a) of sea ice velocity value is positive while background estimate (ψ_i^f)of sea ice concentration value is zero, model creates ice in the cell. Sea ice concentration, sea ice thickness and sea surface temperature are set to be the average of the four neighboring cells (equation 3-30, 3-31). Sea surface temperature and the ocean temperature of top 3 vertical layers are set to be the maximum of freezing temperature (equation 3-32) (figure-3-13). It isn't possible to do correction when the analysis estimate (ψ_i^a) of sea ice velocity value is zero since having zero velocity doesn't correspond to an ice-free situation. Therefore, no corrections are done in this situation.

$$\text{if } (|uvel_{i,j}^f| > 0 \ \ or \ |vvel_{i,j}^f| > 0 \ and \ \ conc_{i,j}^f \ = 0 \ )then$$

$$conc_{i,j}^{a} = (conc_{i+1,j}^{f} + conc_{i-1,j}^{f} + conc_{i,j+1}^{f} + conc_{i,j-1}^{f})/4 \quad (3\text{-}30)$$

$$thic_{i,j}^{a} = (thic_{i+1,j}^{f} + thic_{i-1,j}^{f} + thic_{i,j+1}^{f} + thic_{i,j-1}^{f})/4 \, , thic(\max)_{i,j}^{a} = 0.5m, thic(\min)_{i,j}^{a} = 0.1m \quad (3\text{-}31)$$

$$Tocean(\max)_{i,j,(1\sim3)}^{a} = Tocean_{freezing} \quad (3\text{-}32)$$

4. Direct Insertion Method

This section presents the results from direct insertion method. Direct insertion method is used as a feasibility study to see how Ice-POM model responds to data assimilation. Several experiments are executed. Sea ice concentration, sea ice thickness and sea ice velocity are assimilated. There are two other experiments that are executed to study the effect of assimilation time interval and to examine the effectiveness of assimilating each variable by investigating the lead time.

4.1 Sea ice concentration direct assimilation (DI-Conc.)

In this experiment sea ice concentration gridded data based on AMSR-2 satellite are assimilated daily. Satellite observations are introduced each day at midnight. Assimilation experiment is executed for the year 2013. An average of ascend and descend data are used. Inverse distance interpolation is used to interpolate observation data into the model grid using nearest 4 points. Corrections for the non-assimilated variables are done according to the detail discussed in section 3.6.

Sea ice concentration assimilation has improved sea ice extent significantly. For the year 2013, the model over predicts sea ice extent. Assimilation is able to bring the model towards observation. From figure 4-1, it is evident that it takes about 3 months to adjust the ocean conditions to reflect the changes of the sea ice concentration.

Figure 4-2 gives a closer look of how the assimilation is getting nudged towards the observation. Large fluctuations can be observed when observations are introduced directly into the model.

Figure 4-3 shows how the concentration is distributed in February and September. It is evident that the model over produces sea ice in the Barents Sea and the Greenland Sea in winter compared to the model. In summer model produces more ice in the Laptev Sea compared to AMSR-2 observation. Since direct insertion assimilation directly uses observation data, sea ice concentration of the assimilation overlaps with the AMSR-2 observations.

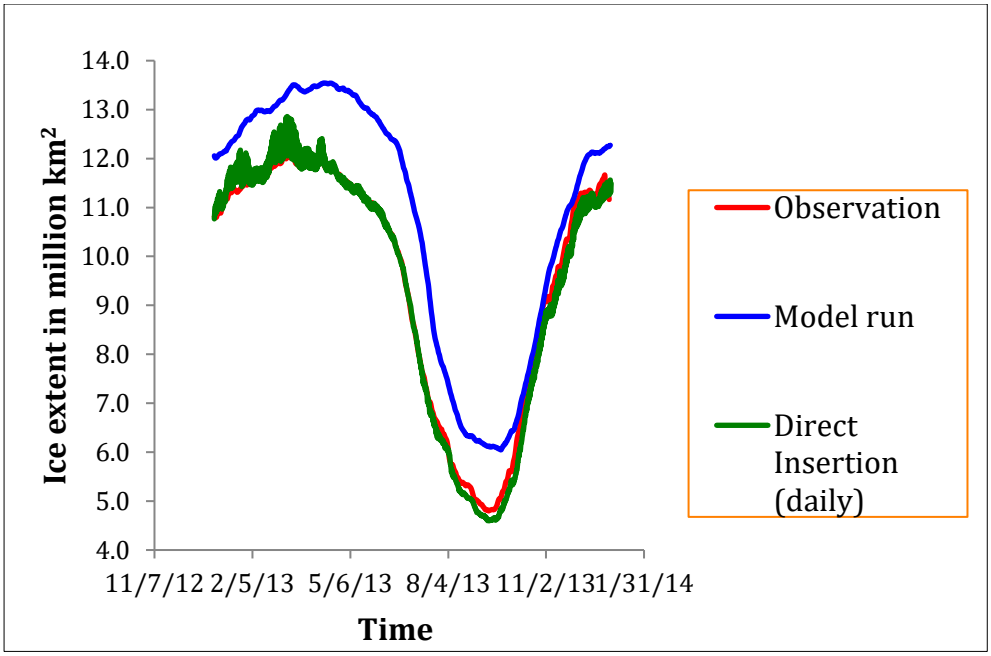

Figure 4-1: Sea ice extent time series from DI-Conc experiment compared with model and observation

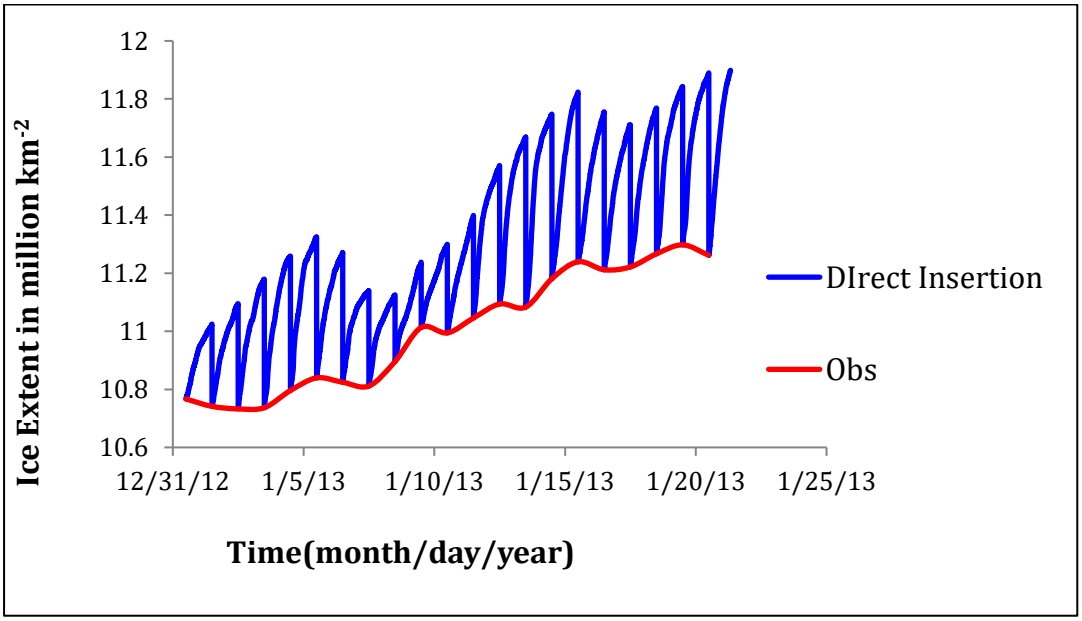

Figure 4-2: time series of sea ice extent from DI-Conc (magnified view)

Sea ice concentration assimilation has also improved the sea ice thickness. Ice-POM model underestimates sea ice thickness near the pole and the Canadian basin as already discussed in section 2.5.4. However, with the assimilation sea ice thickness has increased near the pole. Figure 4-4 represents the sea ice thickness distribution in the whole area. Compared to the model, in assimilation sea ice thickness has increased in the area.

Mean sea ice thickness of the area designated in figure 4-5 is plotted in figure 4-6. It can be observed that the assimilation increases sea ice thickness higher than that of the observation. The direct insertion method induces rapid changes in the model leading to an over estimation of the sea ice thickness.

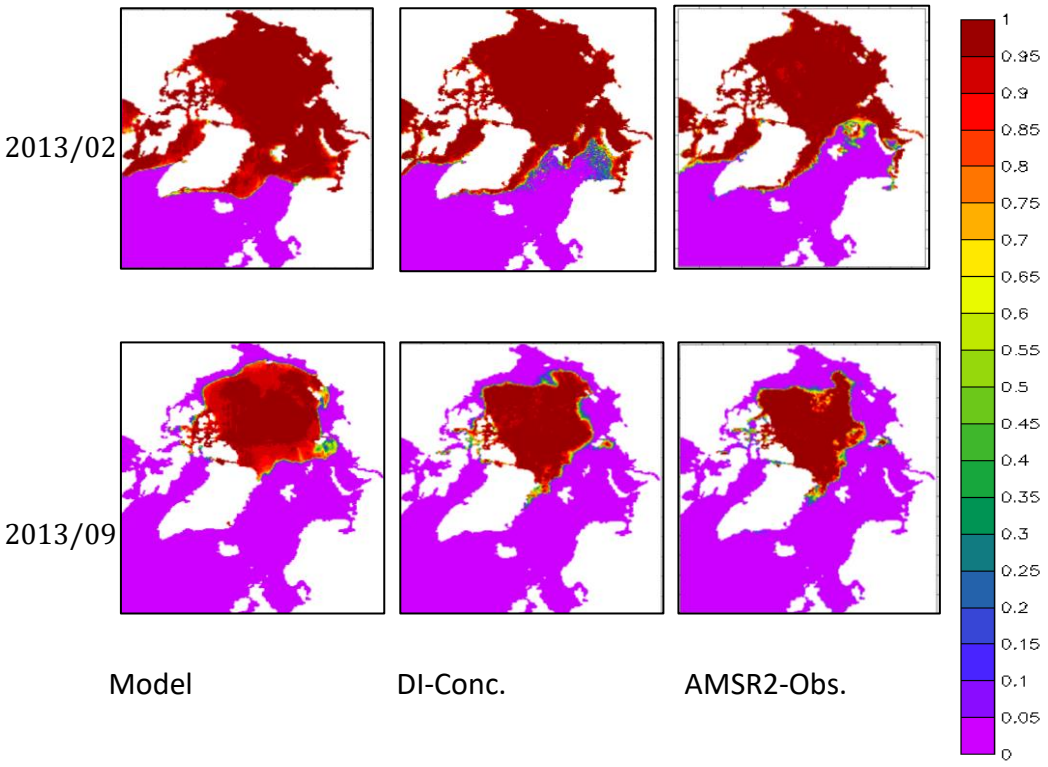

Figure 4-3: Spatial coverage of sea ice extent in February (above) and September (below)

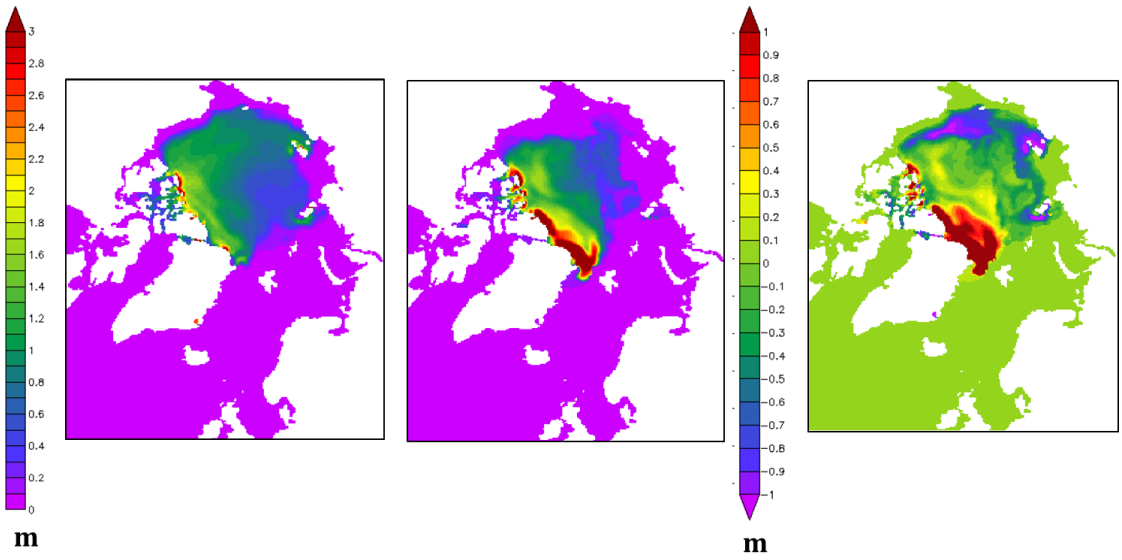

Figure 4-4: Sea ice thickness from model (left) DI-Conc assimilation (center) sea ice thickness difference(m) (DI-Conc - Model) in September 2013(right)

Sea ice thickness and sea ice velocity are interrelated; where in areas with higher sea ice velocity sea ice thickness decreases. The reason for the increased sea ice thickness in this experiment is that sea ice velocity in the polar area (figure 4-5) has declined with the assimilation. In the model sea ice velocity is higher than that of the assimilation. This is evident from the mean sea ice velocity magnitude plotted in figure 4-7 and the sea ice velocity distribution plotted in figure 4-8. This higher velocity makes the sea ice advect away from the pole reducing sea ice thickness near the pole.

Effect on ocean variables is also investigated. The model under predicts sea surface salinity in the Kara and the Barents Sea (figure 4-9). However, assimilation run shows higher salinity in the area compared to the model. The model overestimates sea ice concentration in the Barents Sea. Assimilation can increase the salinity in the Barents Sea for two reasons. Assimilation removes sea ice from the Barents Sea. As a result, freshwater content in the Barents Sea is reduced resulting in an increased sea surface salinity in the Barents Sea. Evaporation in open ocean can also lead to increased salinity in the area.

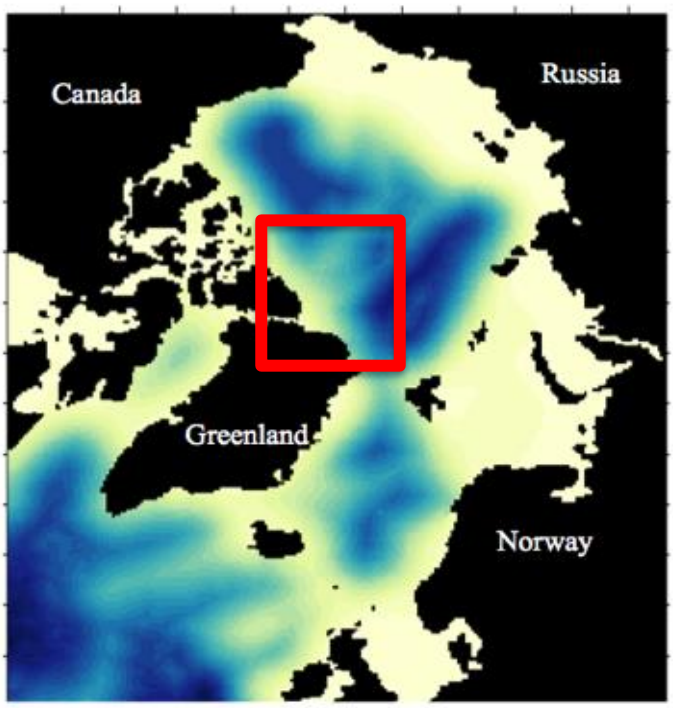

Figure 4-5: Polar area used for comparison

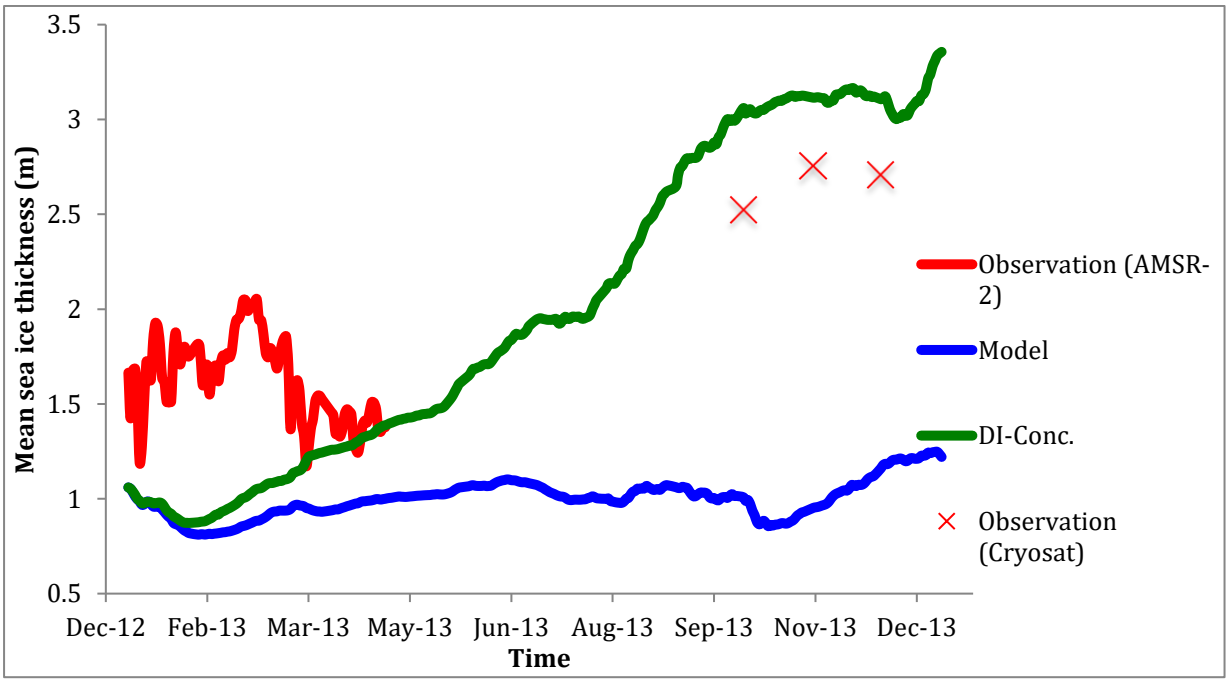

Figure 4-6: Comparison of sea ice thickness in polar area shown in figure 4-5 between AMSR2 observation (daily), Model run, DI-Conc assimilation and Cryosat monthly average data.

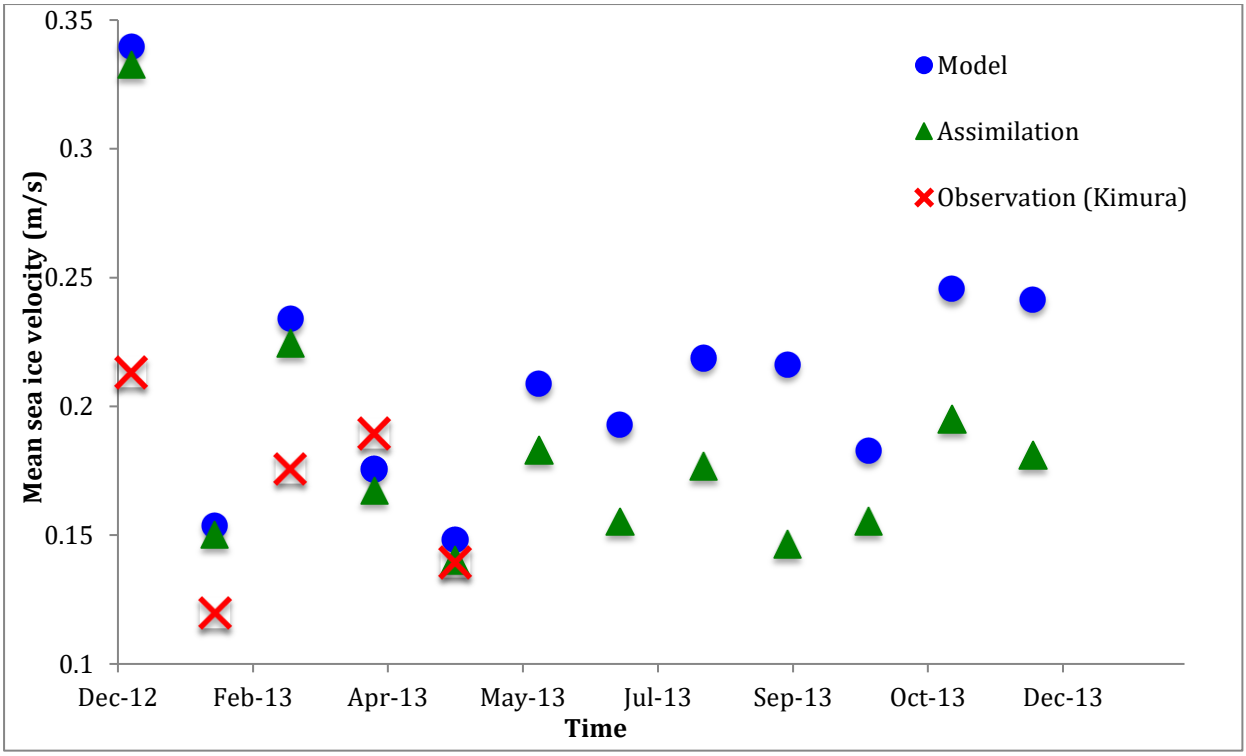

Figure 4-7: Comparison of sea ice velocity m/s in polar area shown in figure 4-5 between Kimura observation set, model run and DI-Conc

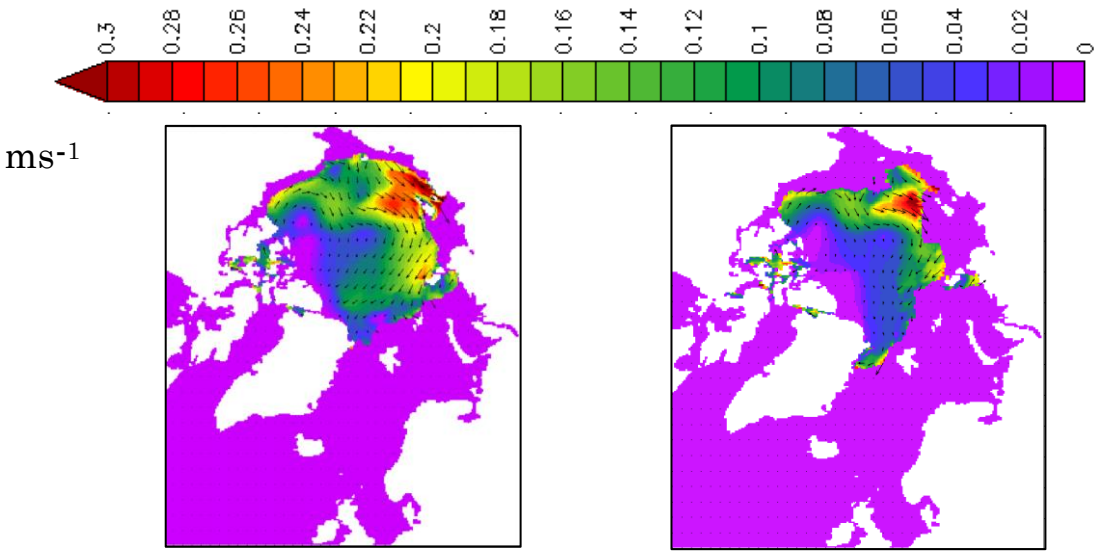

Figure 4-8: Model sea ice velocity (left) and Assimilation sea ice velocity (right) in September

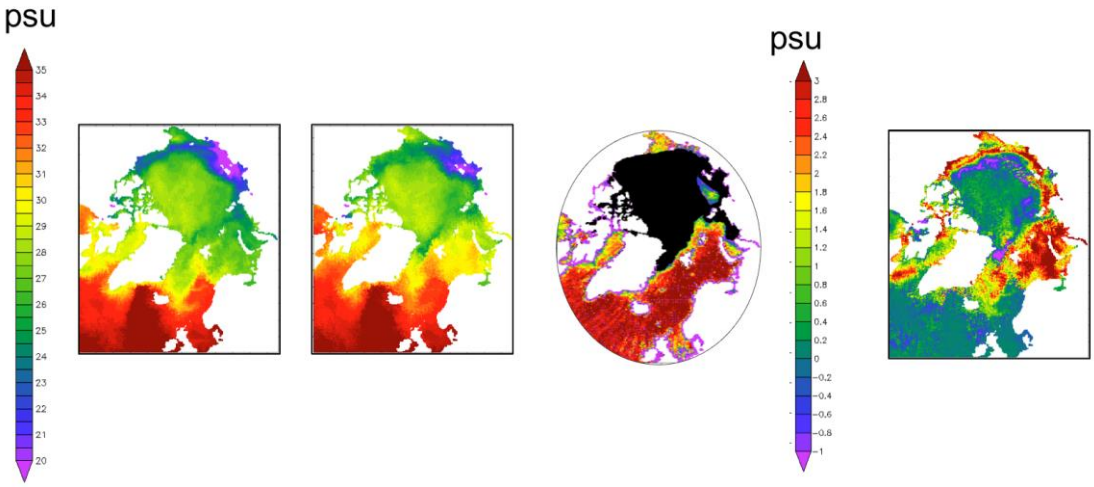

Figure 4-9: from left sea surface salinity in psu of model, assimilation(DI-Conc), Observation-Aquarius data set (area in black is where there is no data), salinity difference (assimilation-model) respectively in September

4.2 Sea ice thickness direct insertion assimilation (DI-thic.)

In this experiment sea ice thickness gridded data (Krishfield 2014) based on AMSR-2 satellite are assimilated daily. Satellite observations are introduced each day at midnight. Assimilation experiment is executed for the winter of year 2013, since the thickness data set is not reliable in summer. Inverse distance interpolation is used to interpolate observation data into the model grid using nearest 4 points. Corrections for the non-assimilated variables are done according to the detail discussed in section 3.6.

Sea ice thickness assimilation has improved sea ice thickness significantly. The model under predicts sea ice thickness near the pole as discussed in section 2.5.4. It is also confirmed in figure 4-10(left). With direct insertion sea ice thickness is greatly improved (figure 4-10-right).

Sea ice thickness assimilation has also indirectly improved sea extent (figure 4-11). The reason for this is the corrections that are done for sea ice extent as explained in section 3.6.

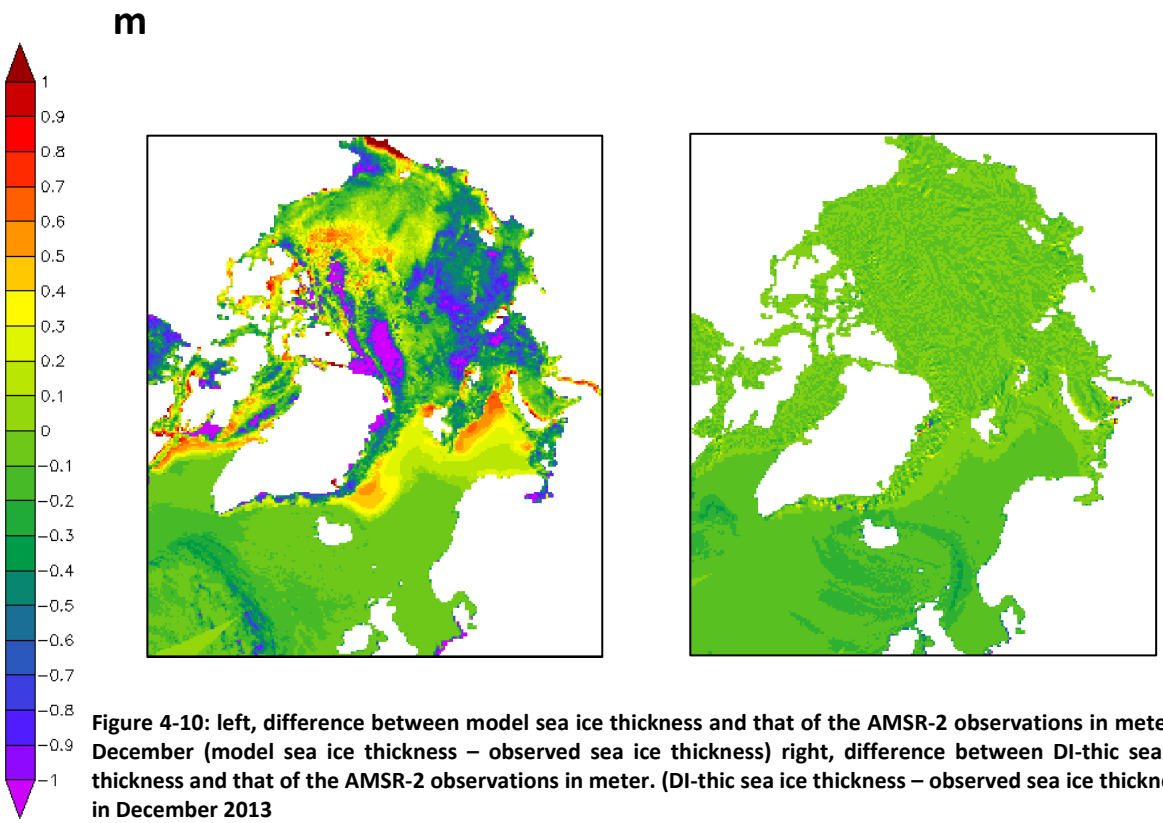

Figure 4-10: left, difference between model sea ice thickness and that of the AMSR-2 observations in meter in December (model sea ice thickness – observed sea ice thickness) right, difference between DI-thic sea ice thickness and that of the AMSR-2 observations in meter. (DI-thic sea ice thickness – observed sea ice thickness) in December 2013

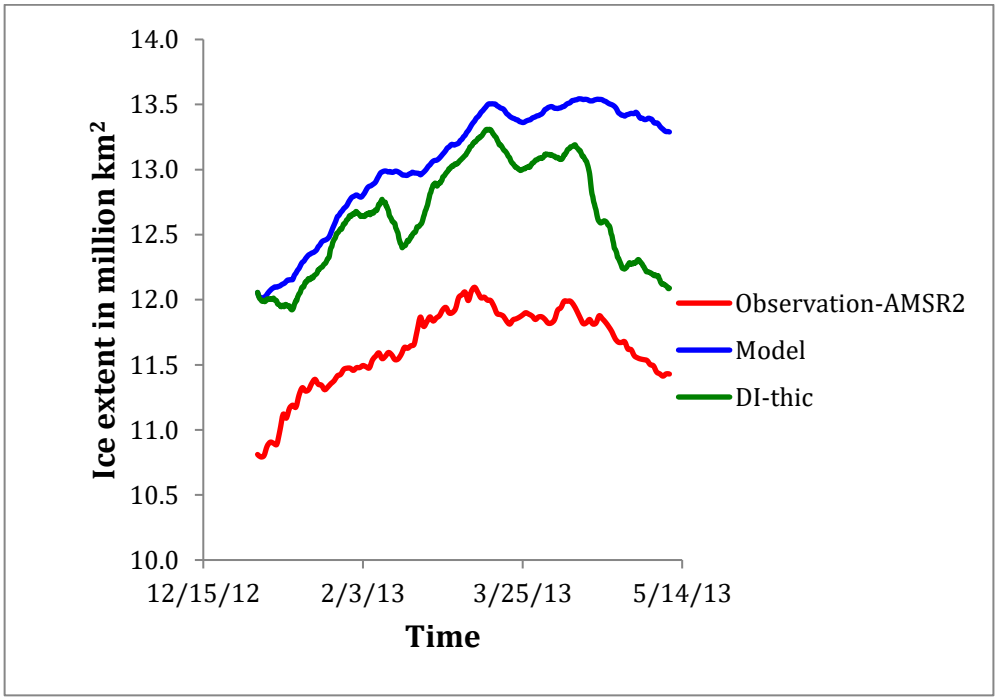

Figure 4-11: Sea ice extent time series from DI-Thic. compared with model and observation

4.3 Sea ice velocity direct insertion assimilation (DI-Vel.)

In this experiment sea ice velocity gridded data (Kimura N. 2016) based on AMSR-2 satellite are assimilated daily. Satellite observations are introduced each day at midnight. Assimilation experiment is executed for the winter of year 2013, since the data set is not reliable during summer. Inverse distance interpolation is used to interpolate observation data into the model grid using nearest 4 points. Corrections for the non-assimilated variables are done according to the detail discussed in section 3.6.

Sea ice velocity experiment does not yield much improvement to sea ice extent (figure 4-12). This is mainly because it isn't possible to do substantial corrections to other variables when sea ice velocity is assimilated as already mentioned in section 3.6. This is mainly because zero velocity does not correspond to zero sea ice concentration or sea ice thickness.

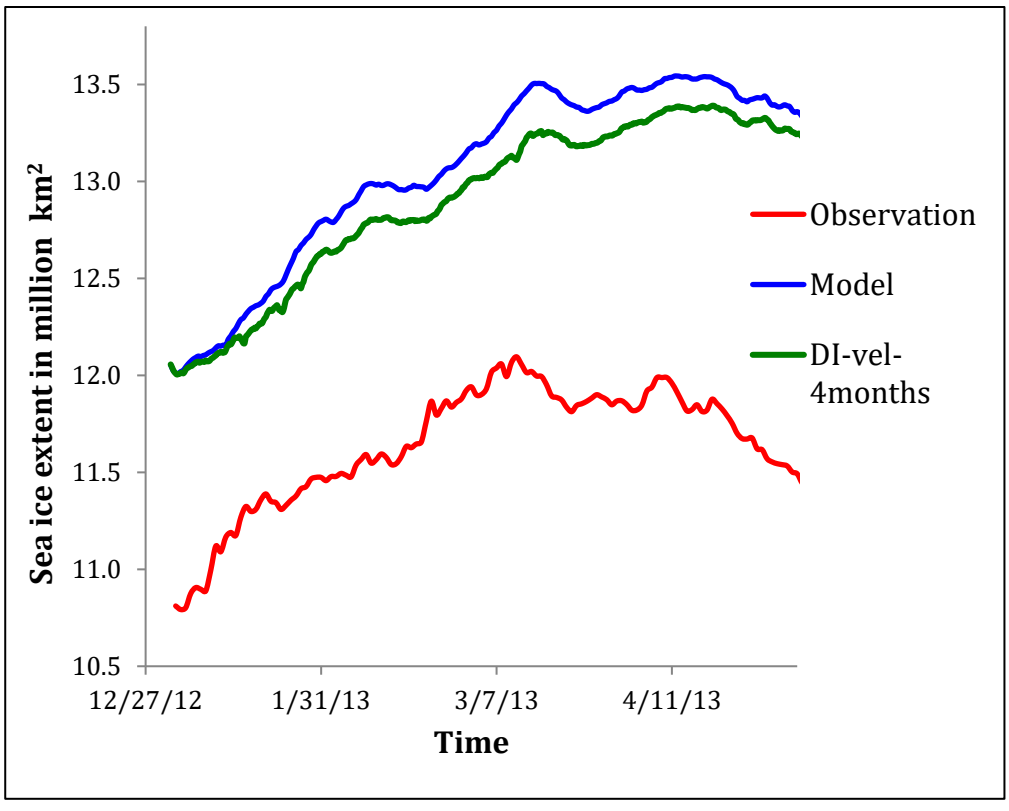

Figure 4-12: Sea ice extent time series from DI-Vel. compared with model and observation

4.4 Assimilation time interval

Observation data sets are available in different time intervals. Some data sets such as AMSR2 sea ice concentration data set are available in a daily interval. Some data sets such as NSIDC Aquarius sea surface salinity data set are available in a weekly interval. There are other data sets such as PHC 3.0 data set and Cryosat sea ice thickness data set that are available as a monthly average. Therefore, an experiment was carried out to investigate the effect of assimilation time interval. Assimilation time interval is varied in the study. Sea ice concentration data are assimilated in daily, weekly, monthly and yearly intervals.

Figure 4-13 represents the ice extent from daily assimilation. As can be expected the ice extent is comparable to the observed sea ice extent. It is also evident that the predicted sea ice extent from weekly (Figure 4-14) and monthly assimilations (Figure 4-15) can produce comparable sea ice extent to that of the observation in the winter. This is advantageous in predicting sea ice extent for the Arctic Sea Routes since the routes are operating only during the summer. Weekly and monthly observation data are available more widely than that of daily observations.

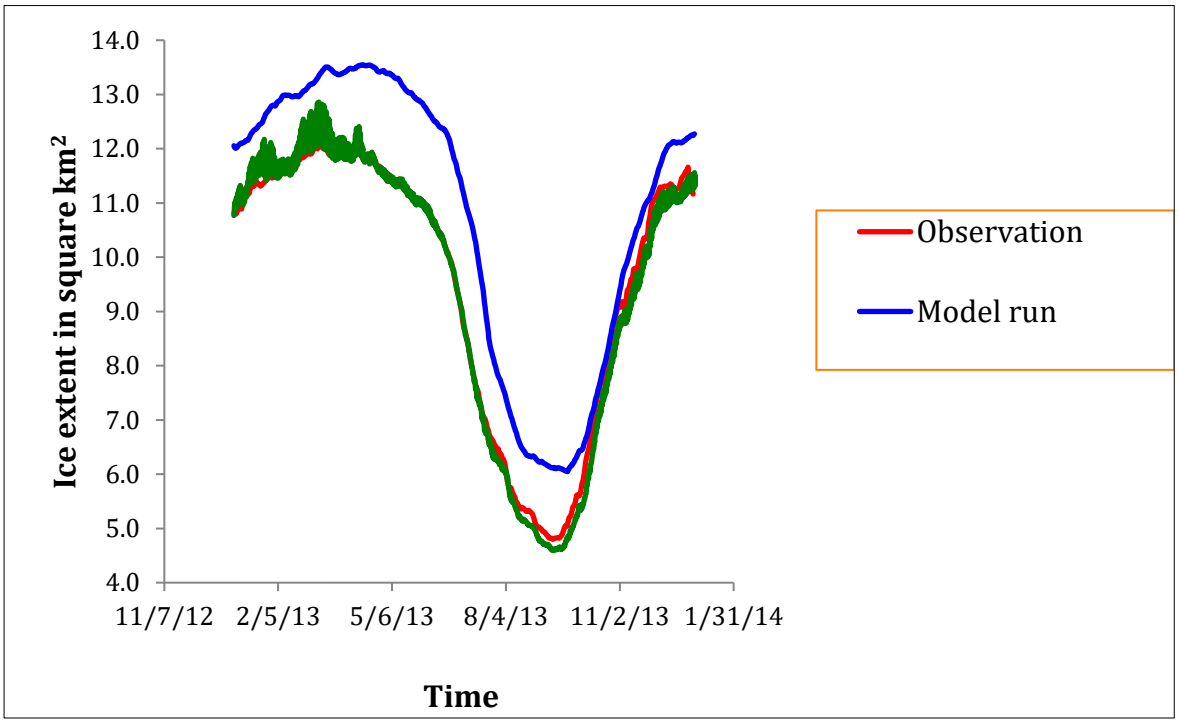

Figure 4-13: Sea ice extent time series from sea ice concentration assimilation – daily

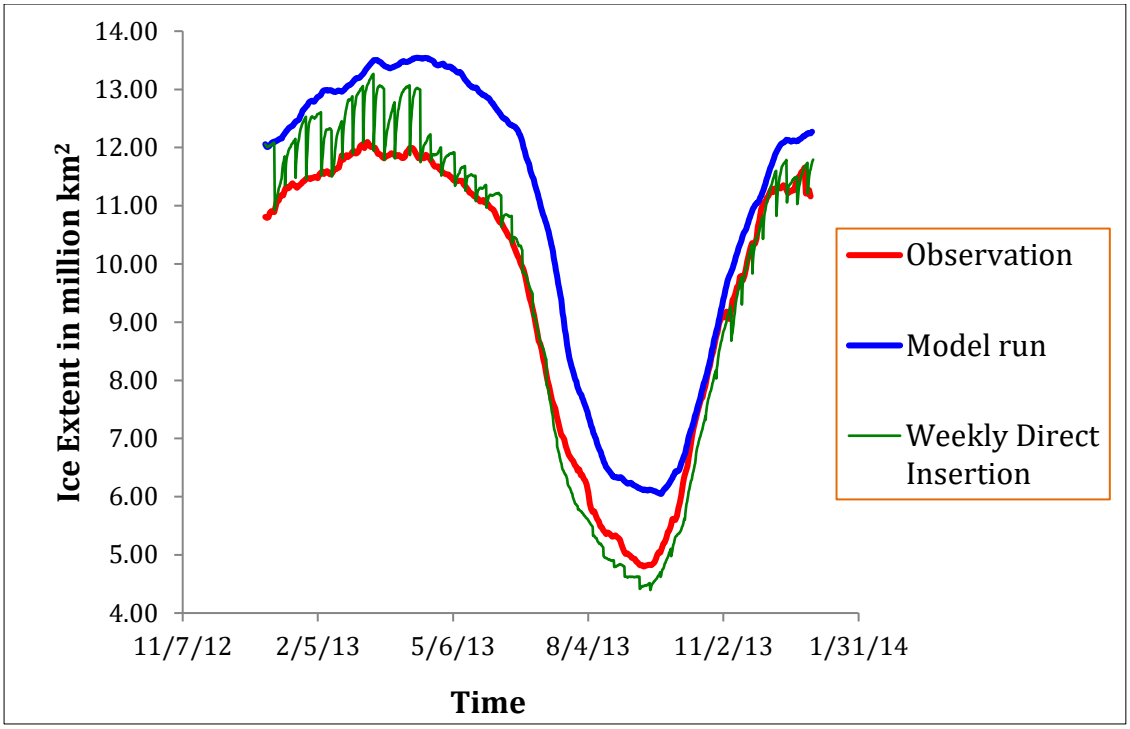

Figure 4-14: Sea ice extent time series from sea ice concentration assimilation – weekly

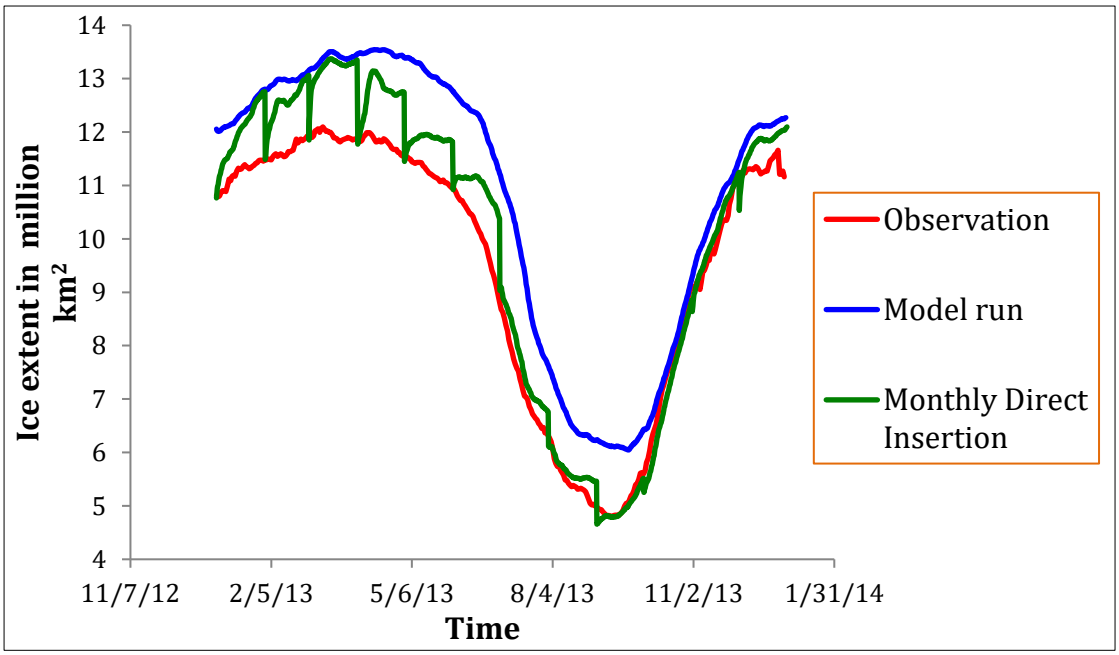

Figure 4-15: Sea ice extent time series from sea ice concentration assimilation – monthly

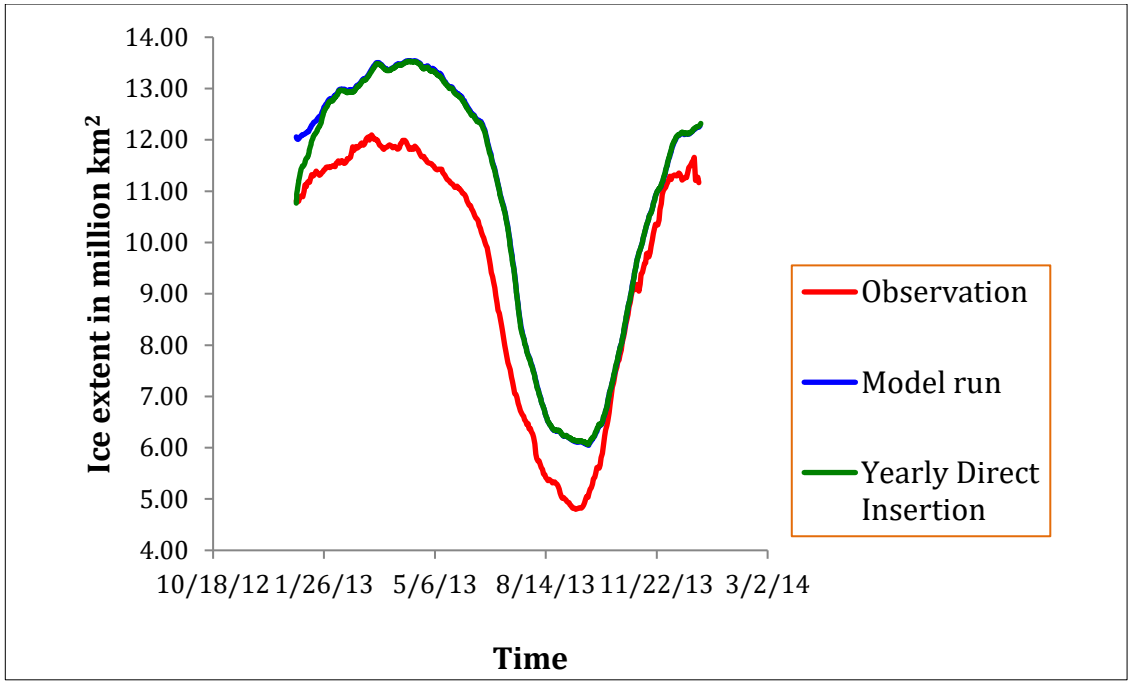

Figure 4-16: Sea ice extent time series from sea ice concentration assimilation – yearly

It can also be seen that yearly-assimilated experiment's ice extent (Figure 4-16) has moved back to the model ice extent after three weeks. This is occurring because it takes about three months to adjust the ocean conditions according to the changes in observed concentration.

4.5 Assimilation forecast (lead time)

Four experiments are carried out to investigate the effectiveness of assimilation. Lead-time is observed using different sea ice variables. Assimilation is seized after four months to investigate the effectiveness of each variable as to improve initial conditions. Sea ice concentration, sea ice thickness and sea ice velocity are assimilated for four months. Time duration used is four months since sea ice velocity and sea ice thickness data sets are reliable only during winter. Figure 4-17 confirms the effectiveness of sea ice concentration assimilation. Even after assimilation experiment is seized sea ice concentration assimilation continues to produce sea ice extent that is more in line with the observations compared to the model. This is mainly because sea ice concentration is directly related to sea ice extent. Therefore, Figure 4-17 clearly indicates that sea ice concentration assimilation can produce

better sea ice extent compared to sea ice velocity assimilation and sea ice thickness assimilation.

Another experiment is performed to investigate how lead time changes with time. In the first experiment DI-Conc assimilation is relaxed after four months of assimilation. In the second experiment DI-Conc. assimilation is relaxed after six months. Running through the melting season improves the accuracy of sea ice extent considerably according to figure 4-18. The bias of the model is a maximum in the melting season.

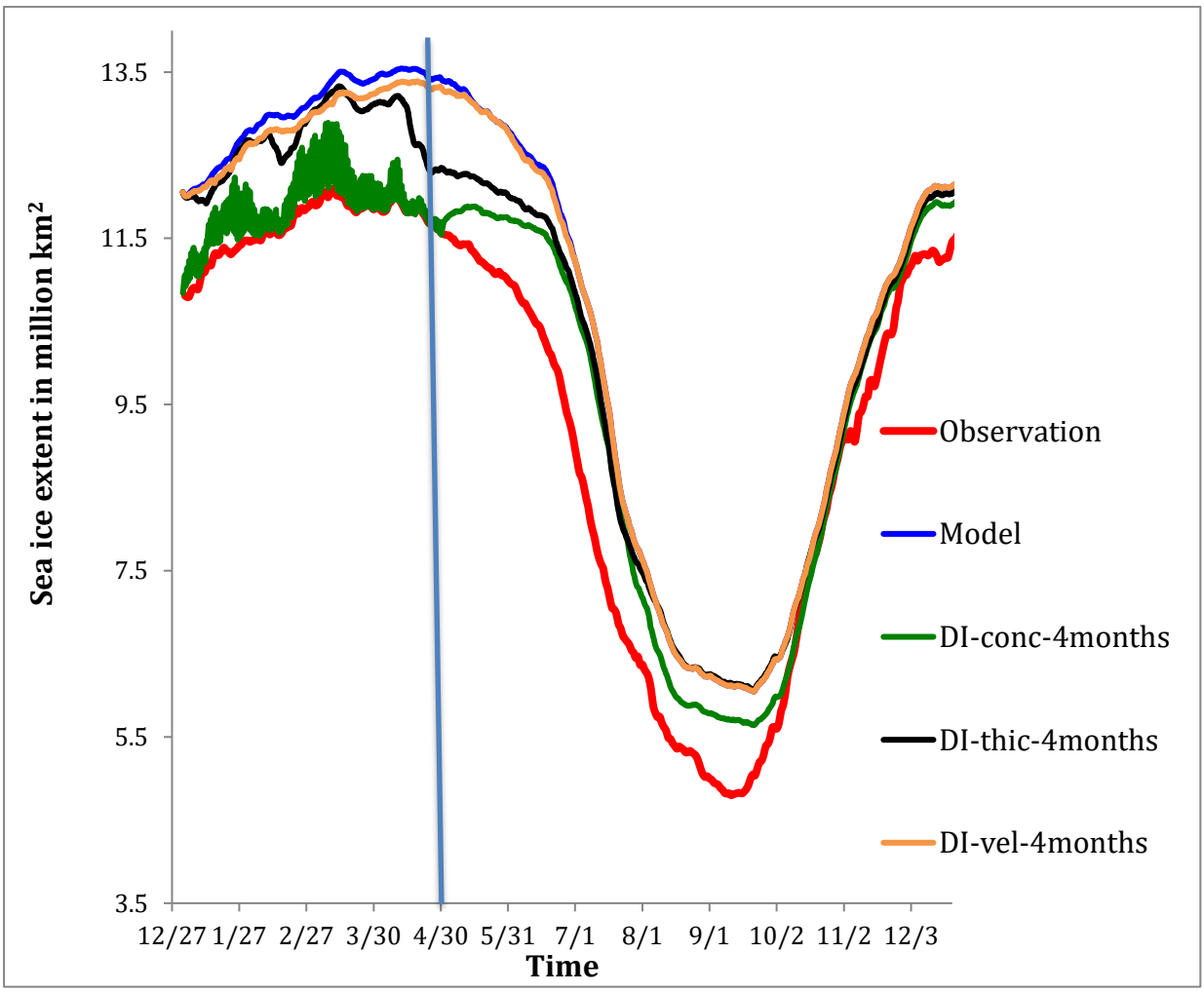

Figure 4-17: Time evolution of total sea ice extent from AMSR2 satellite observation, model prediction, DI-conc-4months, DI-thic-4months and DI-vel-4months experiments

Therefore, running the assimilation through the melting season shows more improvement. This shows that the assimilation can improve forecasting skill of the model. It also shows that longer the assimilation run, more accurate is the forecast.

According to the direct insertion experiments it is confirmed that the model predictions are significantly improved with assimilation.

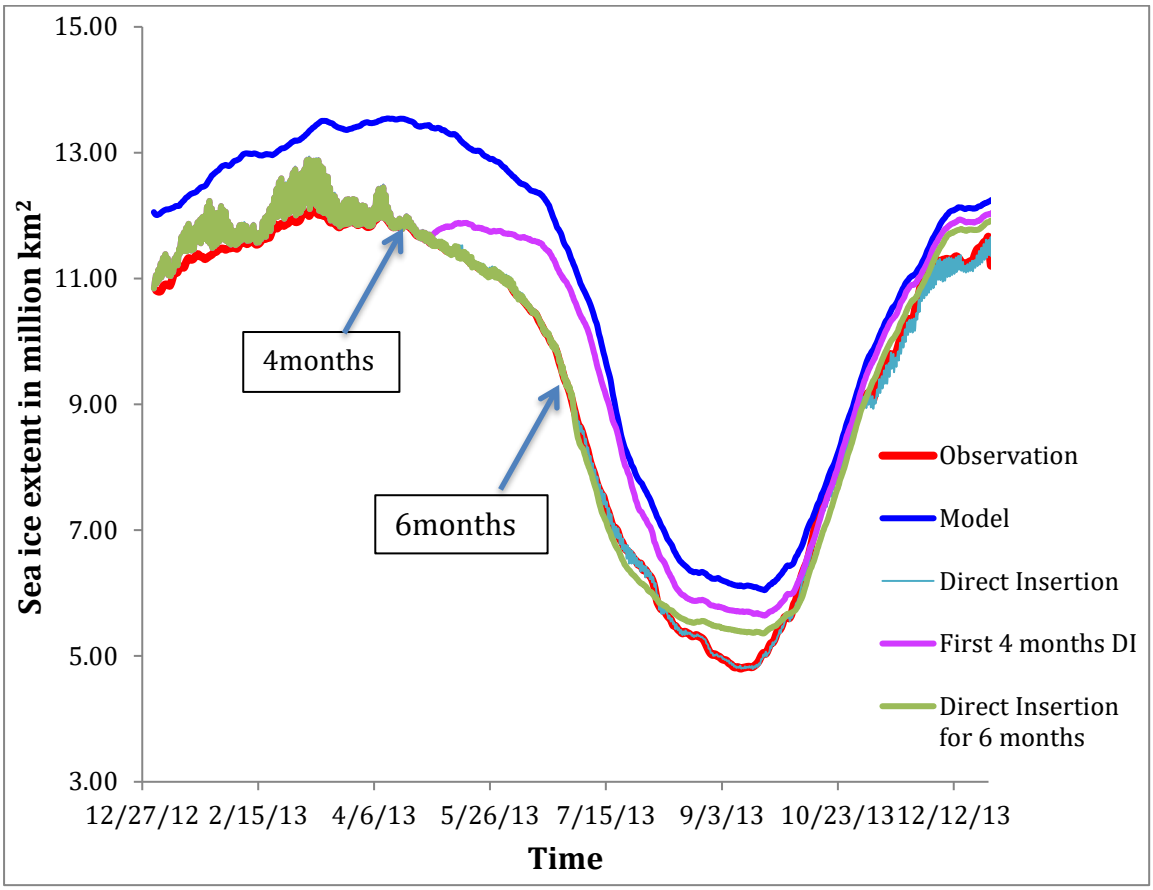

Figure 4-18: Time evolution of total sea ice extent from AMSR2 satellite observation, model prediction, DI-conc-4months and DI-Conc-6months

5. Nudging Method

This section presents the results from nudging method. Nudging method is a widely used assimilation method due to its simplicity and effectiveness. Observation errors are introduced through nudging experiments. Several experiments are executed. Sea ice concentration, sea ice thickness and sea ice velocity are assimilated. They are assimilated individually as well as simultaneously.

5.1 Nudging weight

In the preliminary study direct insertion method is used with the nudging weight(*K*) equals to one in equation 5.1. τ is the time constant. By varying *K* between 0 and 1, it is possible to change the influence on results from model and the observations, however once the observations are introduced due to initial variability, the assimilation behaves differently from the model even when the nudging weight is as low as 0.1.

$$\psi^a = \psi^f + \frac{\mathrm{K}}{\tau}(d \quad - \psi^f) \tag{5-1}$$

In this experiment nudging weight is changed from 0.1 to 1 in 0.1 intervals. In these experiments observations are introduced in one timestep ($\tau = 1$). All the other conditions are identical for all the experiments. Two sets of experiments are executed. One set of experiments is completed from assimilating sea ice concentration. The other set of experiments is completed from assimilating sea ice thickness.

5.1.1 Sea ice concentration assimilation using different nudging weights

From figure 5-1, it is evident that in the sea ice concentration assimilation, all the experiments produce results that are closer to observations. Nudging weight doesn't show a notable effect on sea ice extent. When nudging weight is closer to 1, sea ice extent is getting closer to observation after four months. On the other hand, when nudging weight is closer to 0, sea ice extent approaches observation after six months.

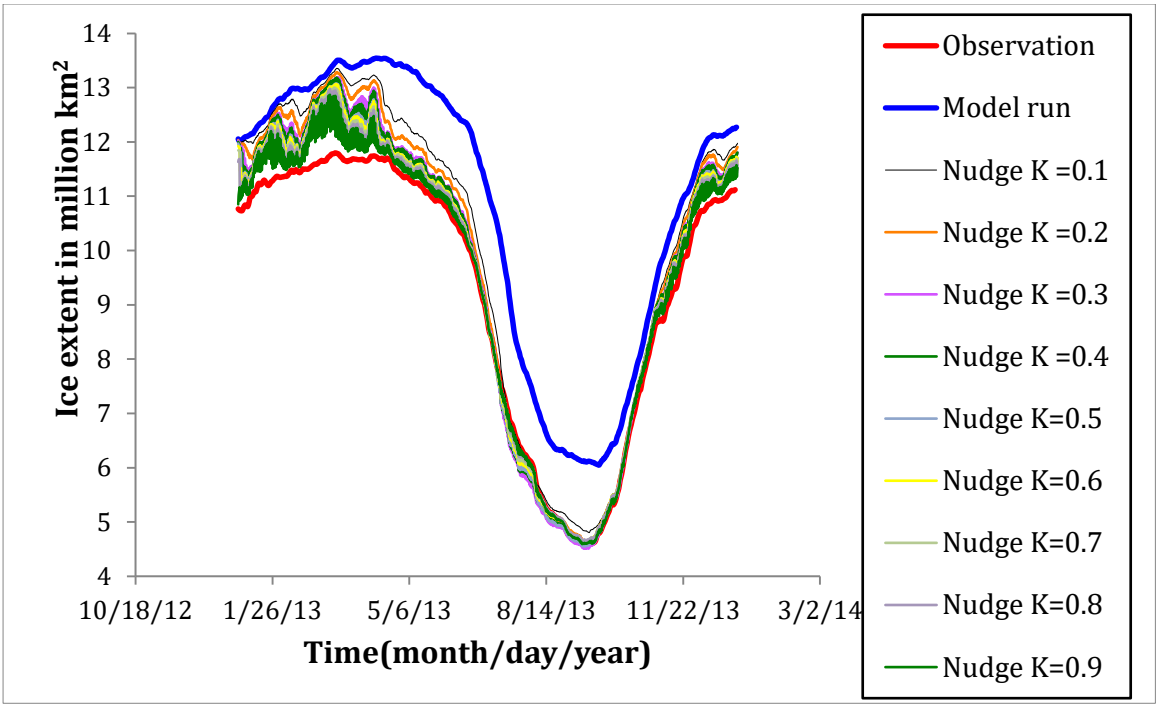

Figure 5-1: Sea ice extent time series from sea ice concentration assimilation using different nudging weights.

It can be observed that it takes a longer time for the experiments with lower weight to reach observations. After this initial period, all the experiments produce similar results. Even though the assimilated variable is not considerably sensitive to the nudging weight, non-assimilated variables are sensitive to nudging weight.

This can be observed by figure 5-2. We can see that from the same set of experiments in which sea ice concentration is assimilated, sea ice thickness shows considerable sensitivity to the nudging weight. When the weight is closer to one sea ice thickness near the pole is increased as was discussed in section 4.1.

5.1.2 Sea ice thickness assimilation using different nudging weights

The same effect can be observed in the sea ice thickness assimilation experiments with varying nudging weight. Figure 5-3 presents sea ice extent results from different sea ice thickness assimilation experiments.

Similar to sea ice concentration assimilation, in the beginning of the assimilation run the difference between observation and assimilation is high. This is because of the over prediction of sea ice in the model due to poor representation of incoming warm water

inflow from the Atlantic Ocean. However, after four months sea ice extent is getting closer to observation after observed sea ice thickness is assimilated in to the model. Similar trend can be observed in sea ice extent assimilation as well. This time is taken to modify the ocean conditions according to sea ice observations. As can be expected when the nudging weight is closer to one sea ice extent gets closer to the observations. We can see a clear difference between different nudging weights.

5.2 Nudging time constant

When observations are directly introduced into the model large fluctuations can be observed in the results. To minimize the shock and to improve the numerical stability, nudging time constant τ is introduced. When τ is small, observations are introduced into the model in a few time steps resulting large fluctuations in the model.

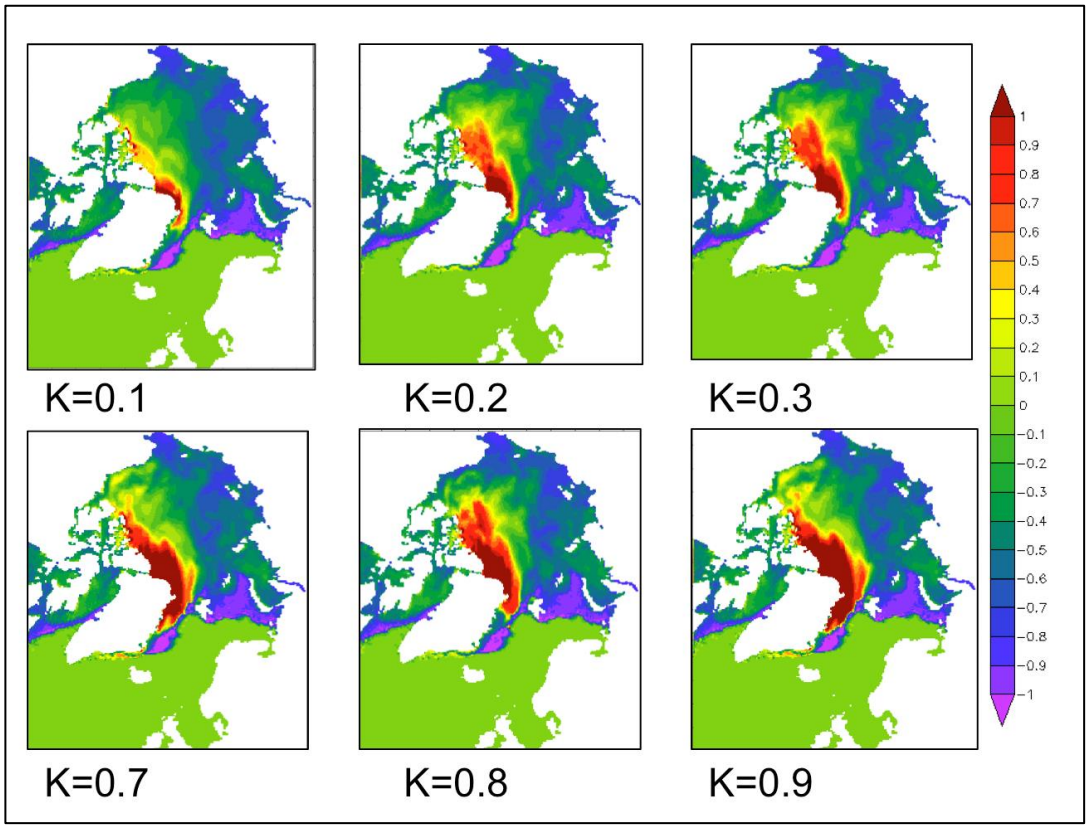

Figure 5-2: Sea ice thickness (assimilation -model) form sea ice concentration assimilation using different weights in December in meter

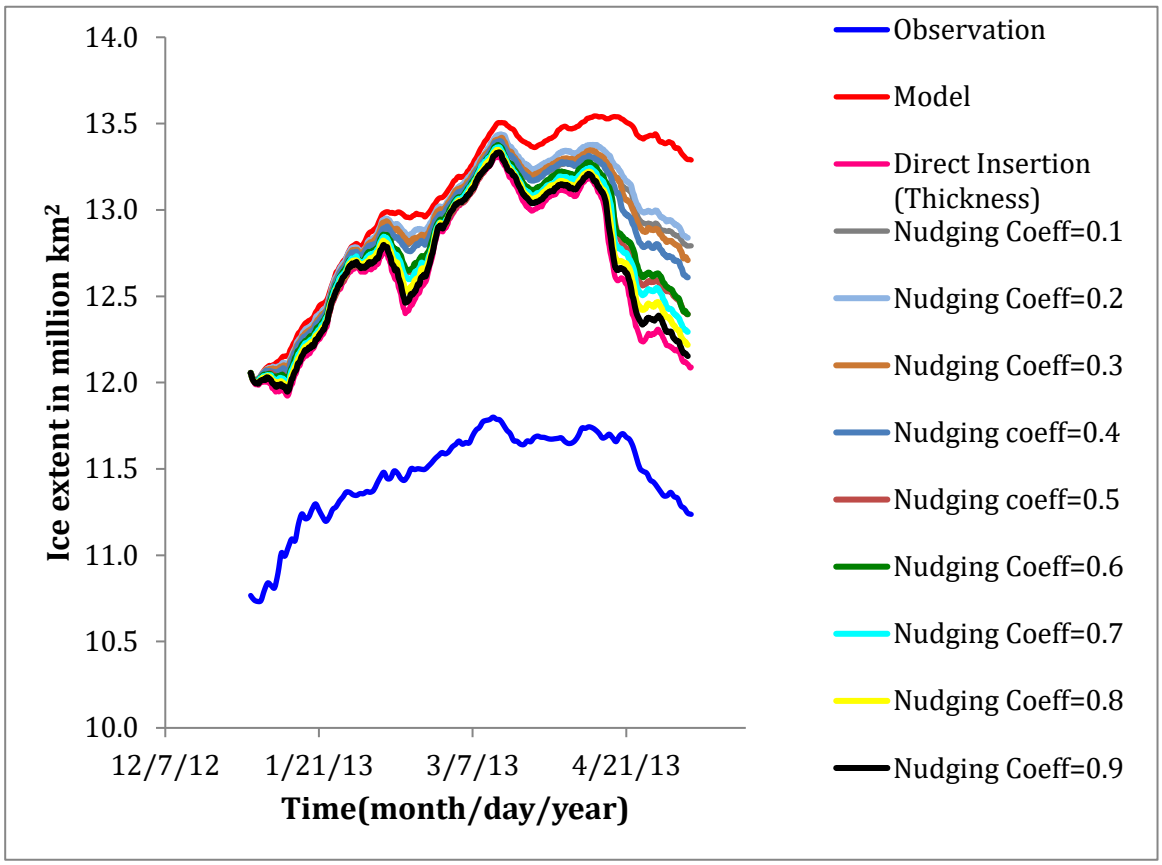

Figure 5-3: Sea ice extent time series from sea ice thickness assimilation using different nudging weights.

When τ is large, observations are introduced in a long period. If τ is too large model doesn't notice the nudging term.

In this experiment, different values were tried for τ. Observations are introduced in one timestep, in 30 timesteps (2 hours), in 75 timesteps (5 hours), and in 180 timesteps (12 hours). These experiments are identified with a tag of "NU-TC". In all these experiments nudging weight *K* is set to be 1. From figure 5-4 it can be observed that with larger τ , model reaches observations more slowly. Figure 5-5 shows the overall effect of τ. Initial fluctuations in sea ice extent have reduced because τ is introduced . $\tau = 180$ time constant is more effective in this case.

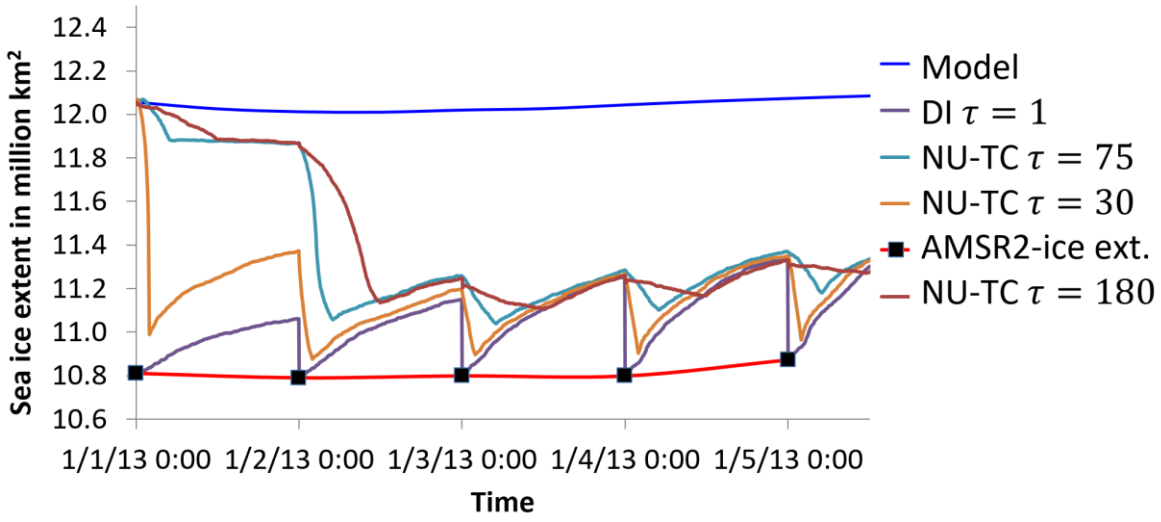

Figure 5-4: Sea ice extent during the first 1800 timesteps from different experiments using different τ.

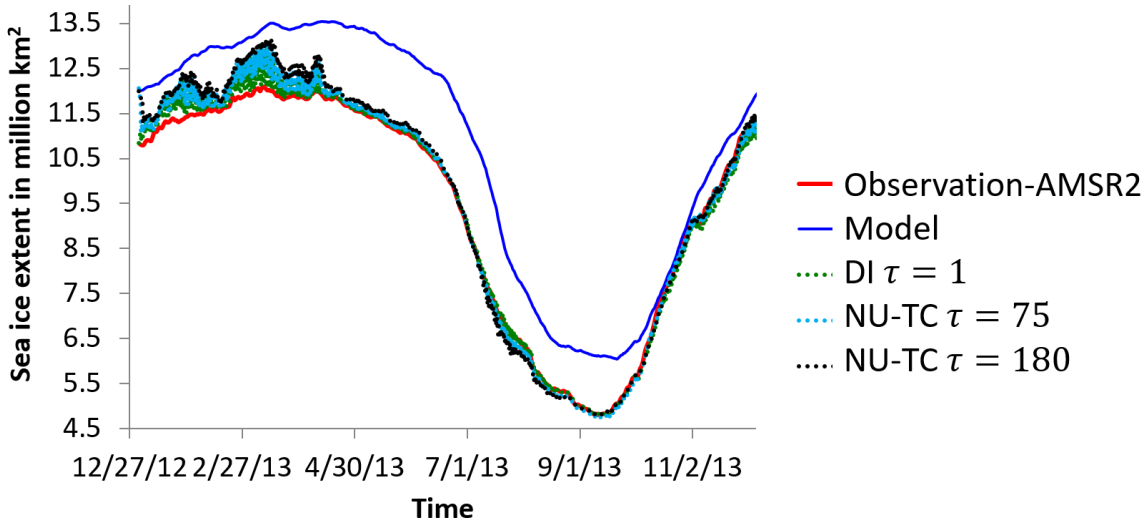

Figure 5-5: Time series of sea ice extent during year 2013 from different experiments using different τ

The rest of the experiments were executed using time constant equal to 180 (12 hours,) since it incorporates observations into the model more smoothly as discussed above. According to figure 5-6, the assimilation experiment is able to reproduce sea ice-extent for the whole year, which is in line with the observation. Since observation errors are not considered the assimilation overlaps with the observation. Figure 5-7 presents local sea ice thickness in polar area.

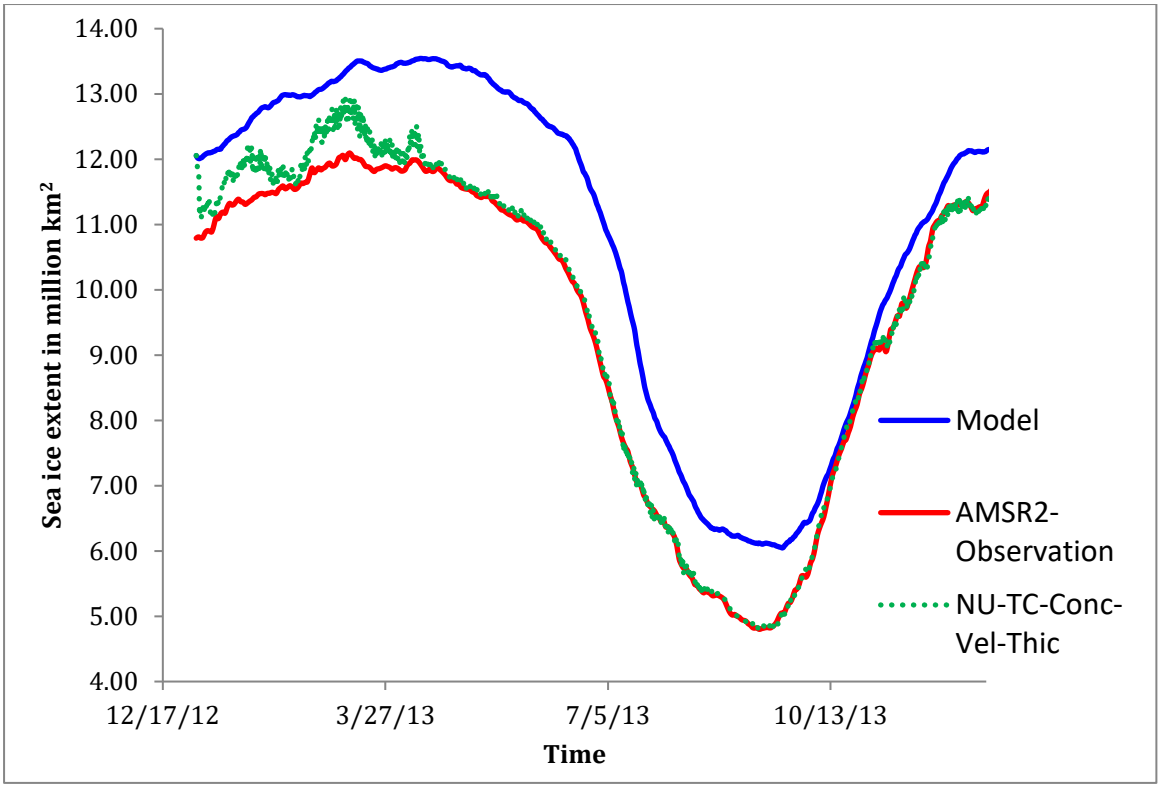

Figure 5-6: Sea ice extent from NU-TC-Conc-Vel-Thic, Model and AMSR2 observation

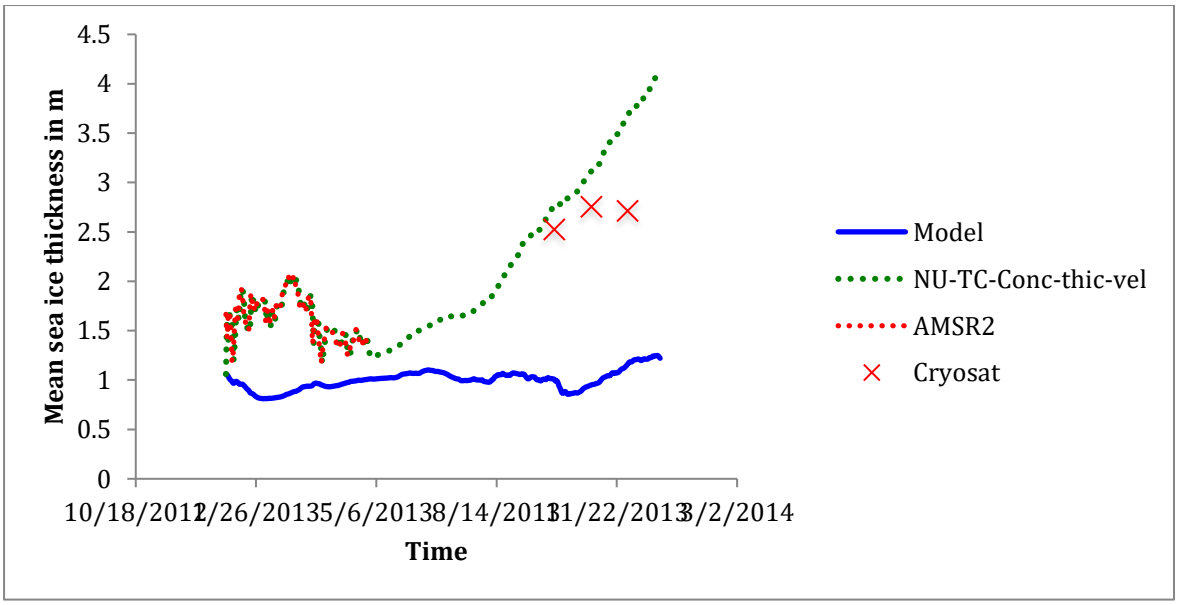

Figure 5-7: Comparison of mean sea ice thickness in polar area shown in figure 4-5 between AMSR2 observation (daily), Model run, NU-TC-Conc-thic-vel assimilation and Cryosat monthly averaged data.

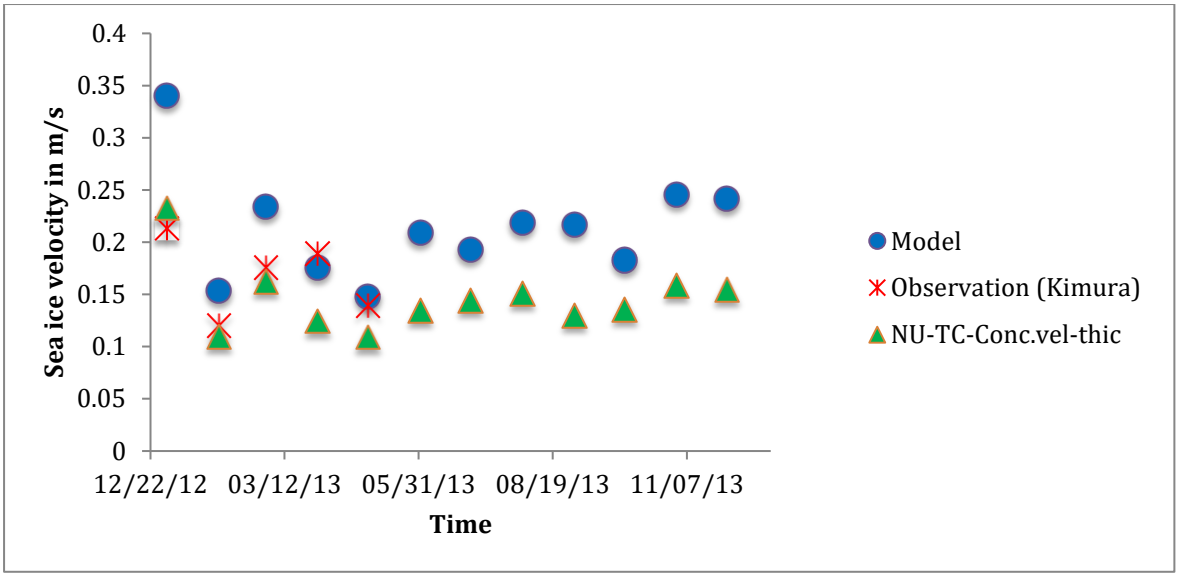

Figure 5-8: Monthly mean sea ice velocity in (m/s) from model, Kimura-observation and NU-TC-Conc-Vel-Thic assimilation

The reason for this increased sea ice thickness is the reduced velocity in the polar area shown in figure 5-8. Reduced velocity prevents sea ice from advecting. This can be observed in figure 5-8 where velocity is compared with model and the Kimura (2016) velocity set. Since any observation errors are not considered in this experiment the effect of observations overrides in the model. This has led to overestimating sea ice thickness and under estimation of sea ice velocity.

5.3 Nudging method 1 experiments

This section presents nudging experiments that are performed according to Lindsay (2006) method discussed in section 3.4.1 with time constant τ=1. These experiments are identified with a tag of "NU1".

5.3.1 Sea ice concentration nudging assimilation (NU1-Conc.)

In this experiment sea ice concentration, gridded data based on AMSR-2 satellite are assimilated daily. Satellite observations are introduced each day at midnight. Assimilation experiment is executed for the year 2013. An average of ascend and descend data are used.

Inverse distance interpolation is used to interpolate observation data into the model grid using nearest 4 points around a cell. Corrections for the non-assimilated variables are done according to the detail discussed in section 3.6.

Sea ice concentration assimilation has improved sea ice extent significantly (figure 5-9). For the year 2013, the model over predicts sea ice extent. Assimilation is able to nudge the model towards observation.

Sea ice concentration assimilation has also improved the sea ice thickness. Ice-POM model under predicts sea ice thickness near the pole (Figure 5-10). Nudging computation is able to improve the accuracy of sea ice thickness as shown in figure 5-11. The reason for this improved sea ice thickness is that sea ice velocity is improved with the assimilation. In the model sea ice velocity is higher than that of the assimilation (figure 5-12). This higher velocity makes sea ice advect away from the pole reducing sea ice thickness near the pole.

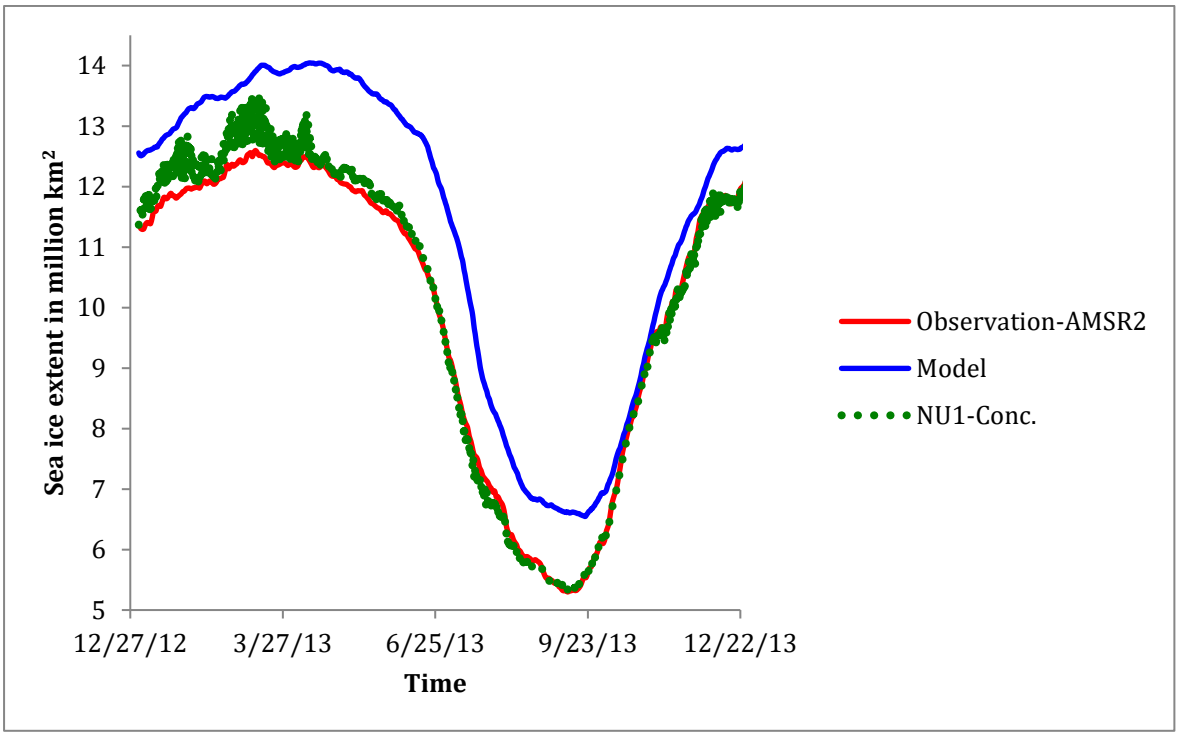

Figure 5-9: Time evolution of total sea ice extent from AMSR2 satellite observation, model prediction, DI-Conc and NU1-Conc

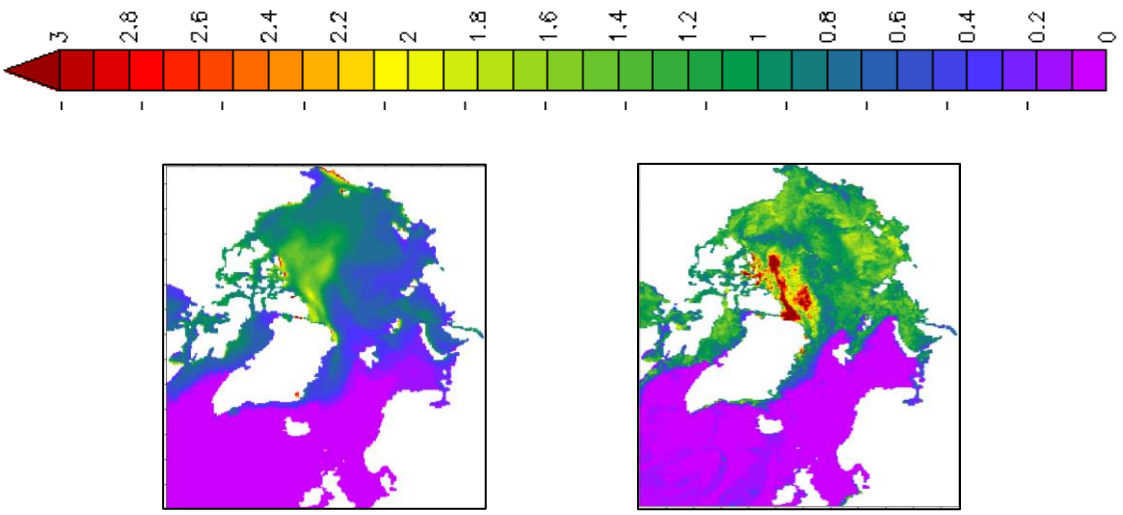

Figure 5-10: Sea ice thickness in meter in February, model (on left) observation (on right)

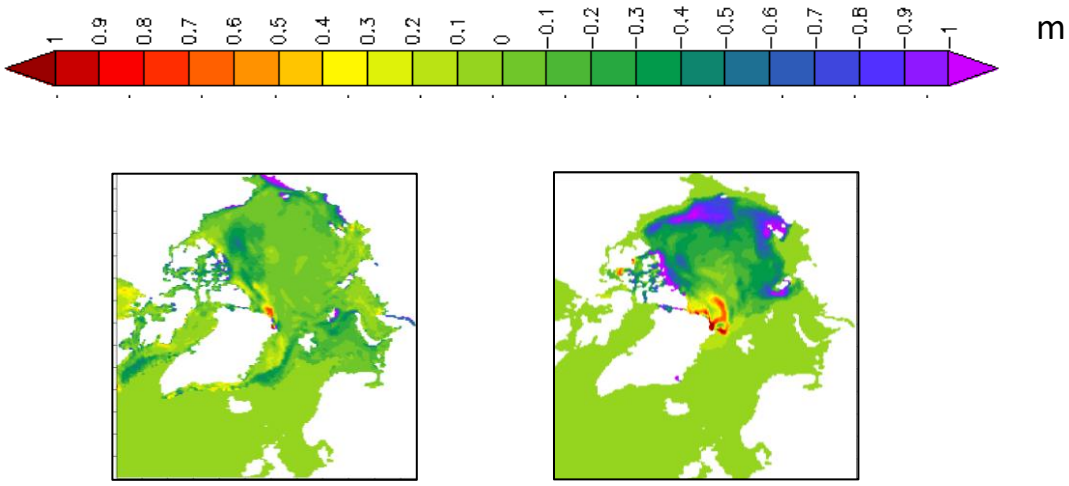

Figure 5-11: Difference between sea ice thickness of NU1-conc and model in meter. February on left. (NU1-conc sea ice thickness - model sea ice thickness). Difference between sea ice thickness of NU1-conc and model in meter. September on right. (NU1-conc sea ice thickness - model sea ice thickness)

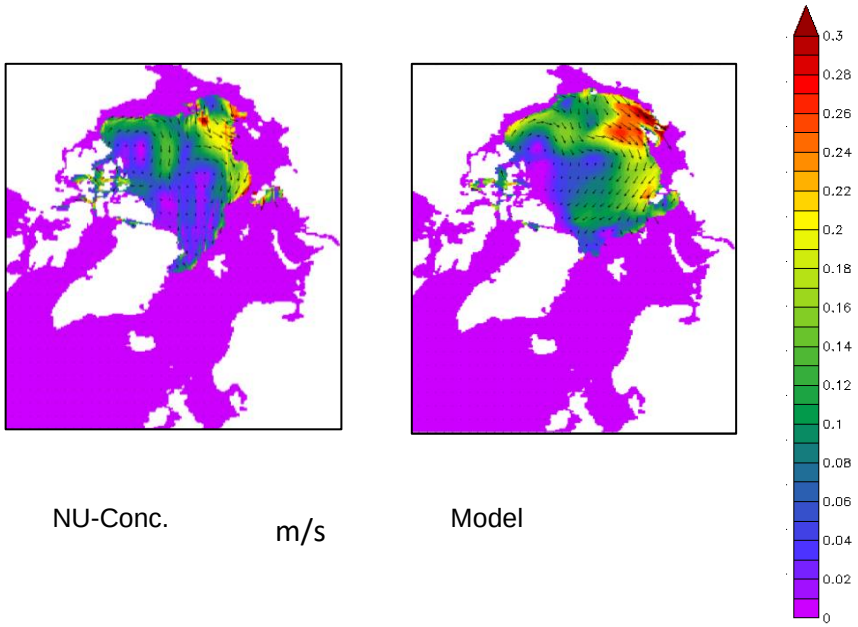

Figure 5-12: Model sea ice velocity (right) and assimilation sea ice velocity(m/s) (left) in September

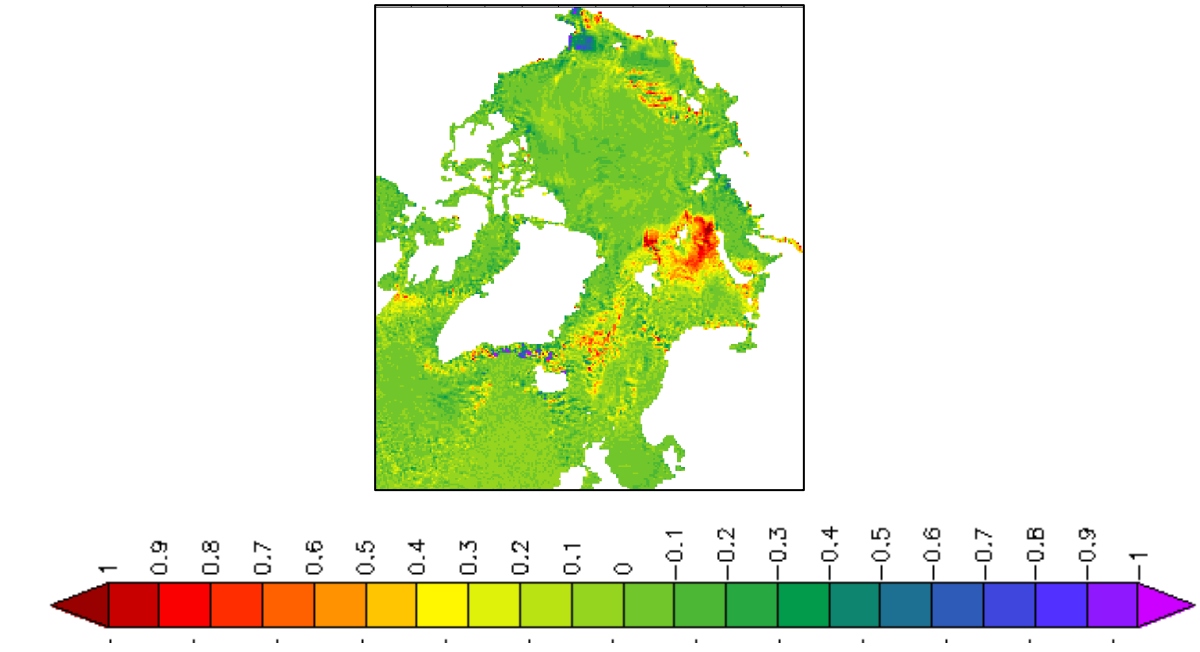

Figure 5-13: Sea surface salinity difference in psu (SSS NU-Conc - SSS model)

Impact on ocean variables is also investigated. The model under predicts sea surface salinity in the Kara and Barents Sea as discussed in section 2.5.4. With the improved sea ice extent sea surface salinity in these areas is improved (figure 5-13). Assimilation can increase the salinity in the Barents Sea for two reasons. Assimilation run removes sea ice from the Barents Sea. As a result, freshwater content in the Barents Sea is reduced resulting in an increased sea surface salinity in the Barents Sea. Evaporation in open ocean can also lead to increased salinity in the area.

5.3.2 Sea ice thickness nudging assimilation (NU1-Thic.)

In this experiment sea ice thickness gridded data (Krishfield 2014) based on AMSR-2 satellite are assimilated daily. Satellite observations are introduced each day at midnight. Assimilation experiment is executed for the year 2013 winter since the thickness data set is not reliable in summer. Inverse distance interpolation is used to interpolate observation data into the model grid using nearest 4 points around a cell. Corrections for the non-assimilated variables are done according to the detail discussed in section 3.6.

Sea ice thickness assimilation has improved sea ice thickness as can be seen in figure 5-14. The model under predicts sea ice thickness near the pole as discussed in section 2.2.2.

Sea ice thickness assimilation has also improved sea ice extent (figure 5-15). The reason for this is the corrections that are done for sea ice extent as explained in section 3.6. Since the improvement to sea ice extent is not as significant as in the sea ice concentration assimilation, sea surface salinity is not greatly affected by the sea ice thickness nudging assimilation (figure 5-16).

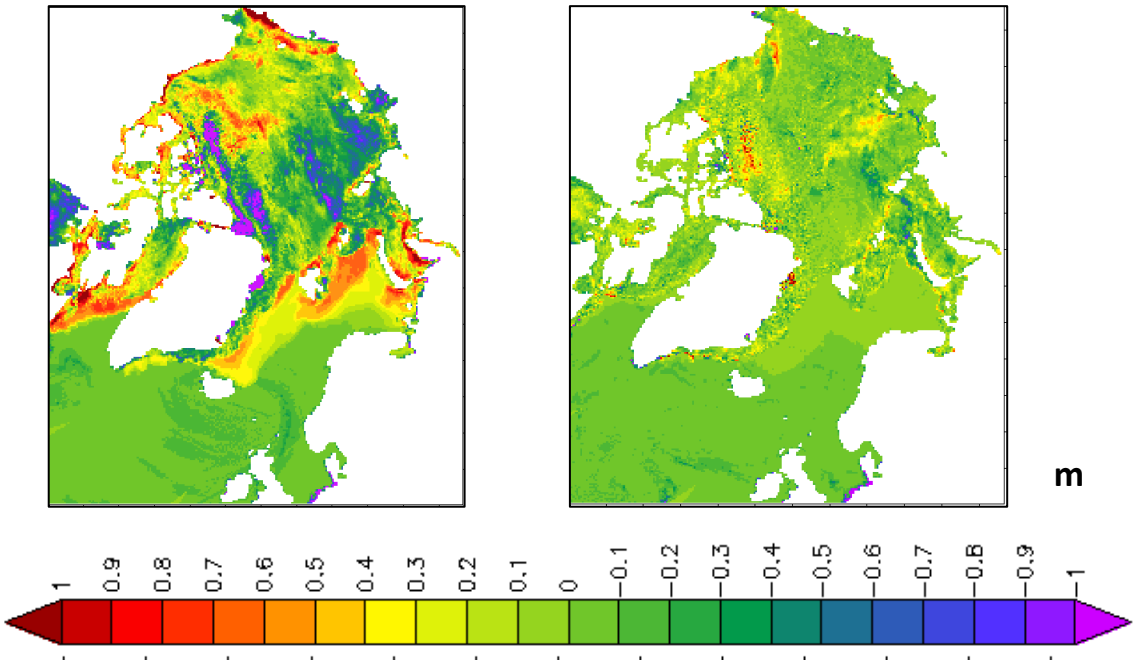

Figure 5-14: left, difference between model sea ice thickness and that of the AMSR-2 observations in meter in April (model sea ice thickness – observed sea ice thickness) right, difference between DI-thic sea ice thickness and that of the AMSR-2 observations in meter. (NU1-Thic. sea ice thickness – observed sea ice thickness)

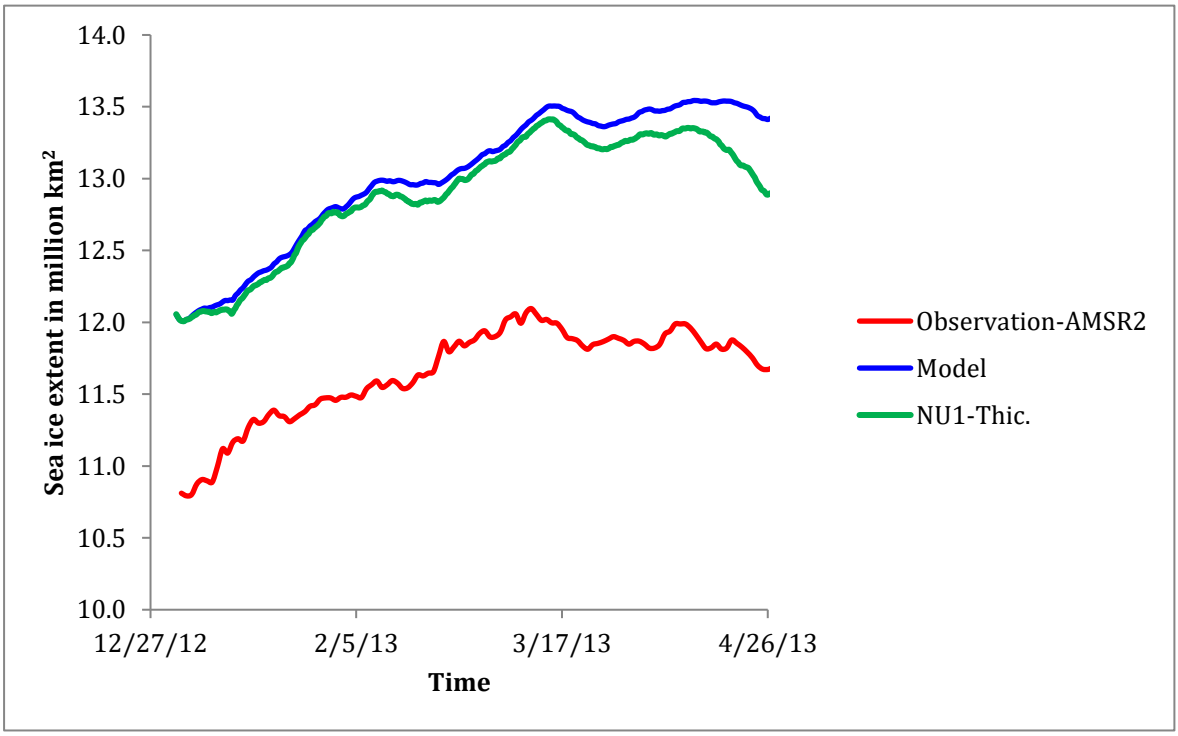

Figure 5-15: Sea ice extent time series from NU1-Thic., model and observation

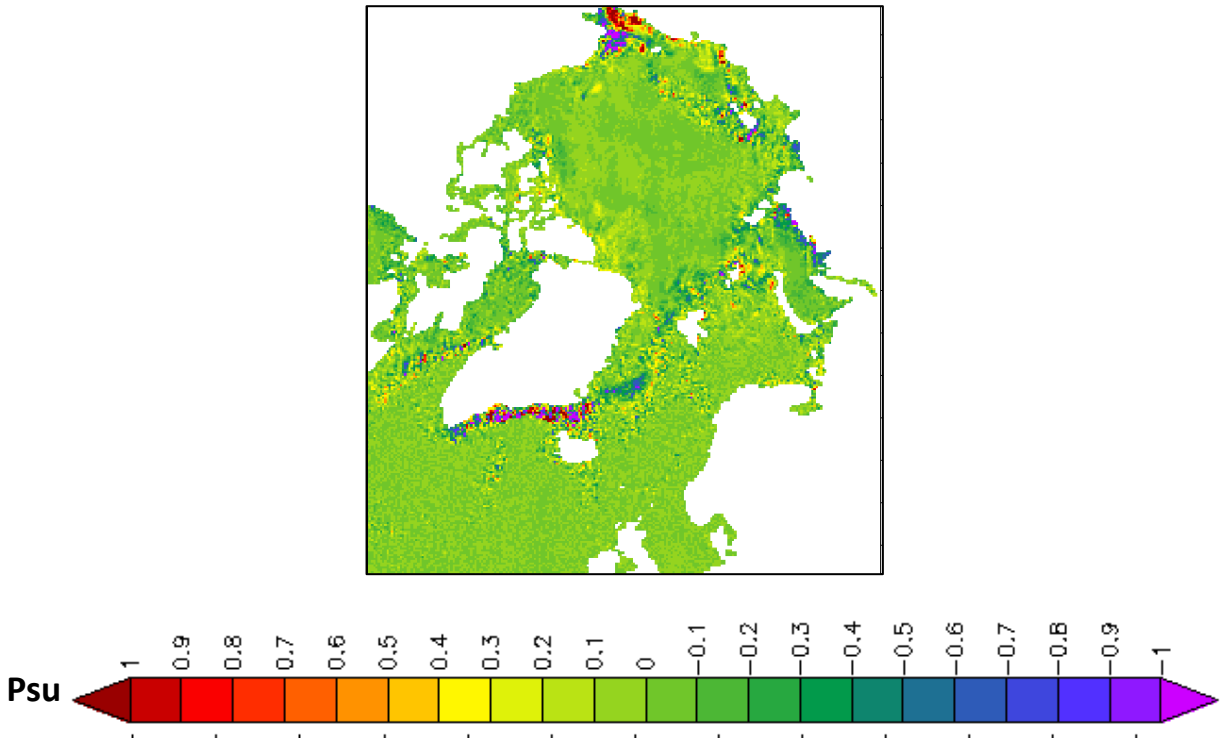

Figure 5-16: Sea surface salinity difference in psu February (SSS NU1-Thic - SSS model)

5.3.3 Sea ice concentration and thickness nudging assimilation (NU1-Conc.-Thic.)

In this experiment sea ice concentration and sea ice thickness are assimilated simultaneously. Sea ice concentration and thickness gridded data (Krishfield 2014) based on AMSR-2 satellite are assimilated daily. Satellite observations are introduced each day at midnight. Assimilation experiment is executed for the year 2013 winter since the thickness data set is not reliable in summer.

Sea ice extent is improved with the NU1-Conc.-Thic. Assimilation as can be seen in figure 5-17. Since sea ice thickness is assimilated, sea ice thickness is also improved by this assimilation (figure 5-18). Compared to the model, assimilation thickness is much closer to the observations. Since sea ice extent is significantly improved by the assimilation, consequently sea surface salinity is also improved as a result of assimilation (figure 5-19).

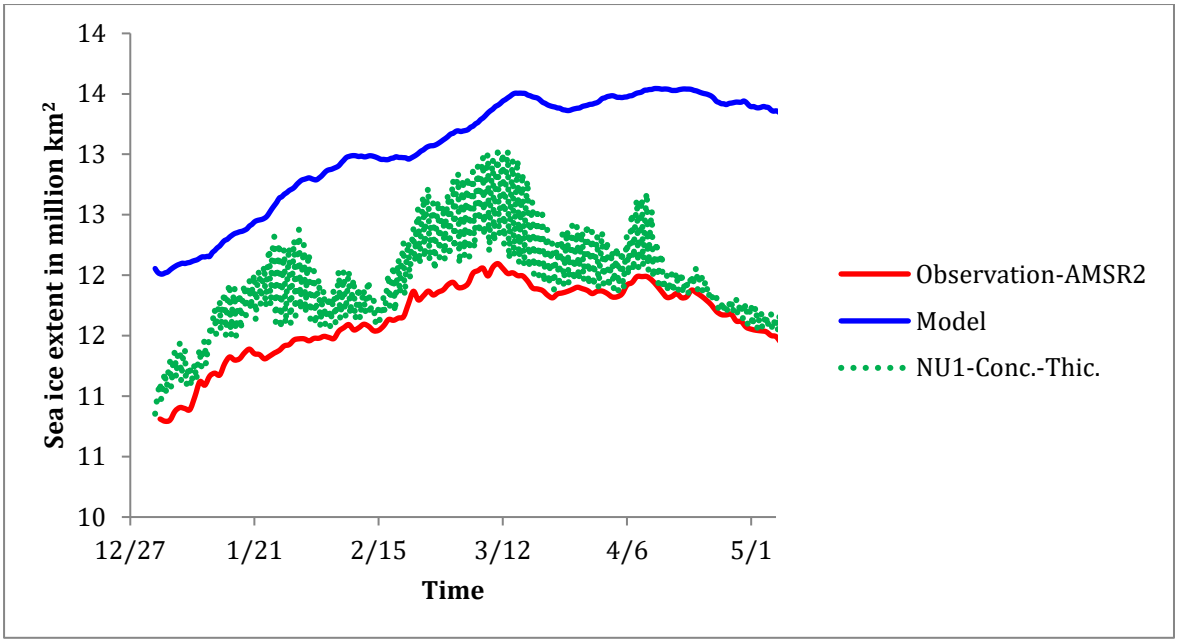

Figure 5-17. Sea ice extent time series from NU1-Conc.-Thic. assimilation, AMSR-2 observation and model.

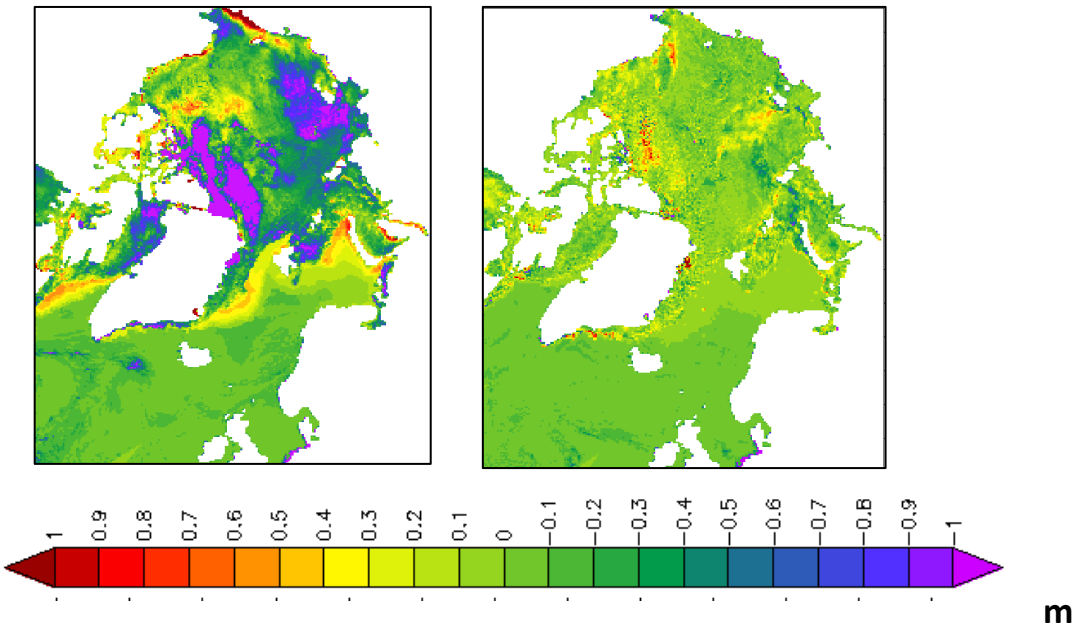

Figure 5-18: left, difference between model sea ice thickness and that of the AMSR-2 observations in meter in February (model sea ice thickness – observed sea ice thickness) right, difference between NU1-Conc.-Thic. sea ice thickness and that of the AMSR-2 observations in meter. (NU1-Conc.-Thic. sea ice thickness – observed sea ice thickness)

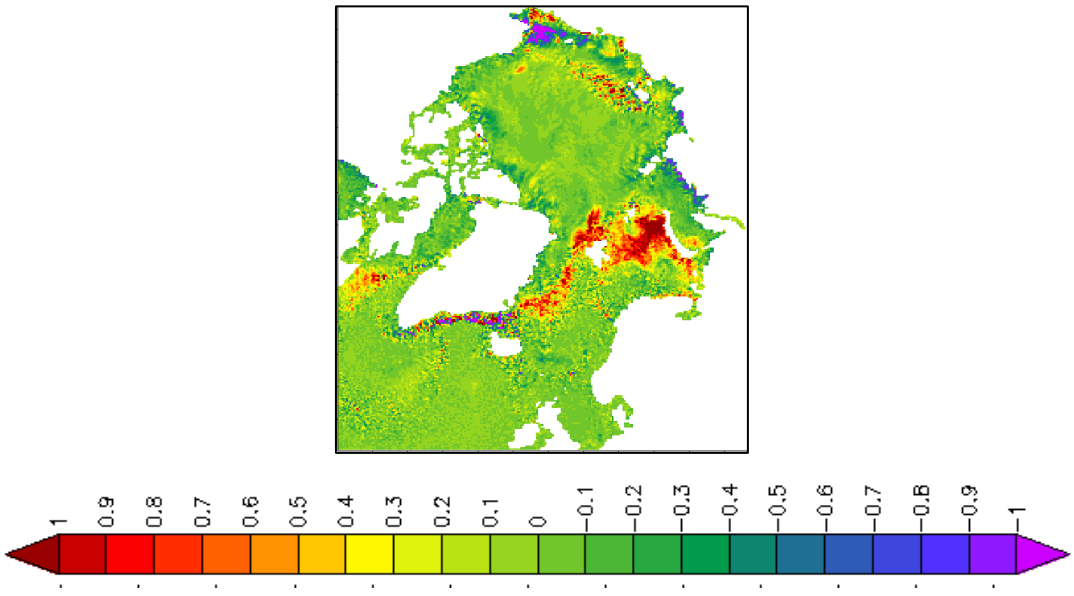

Figure 5-19: Sea surface salinity difference in psu (SSS NU1-Conc.-Thic - SSS model)

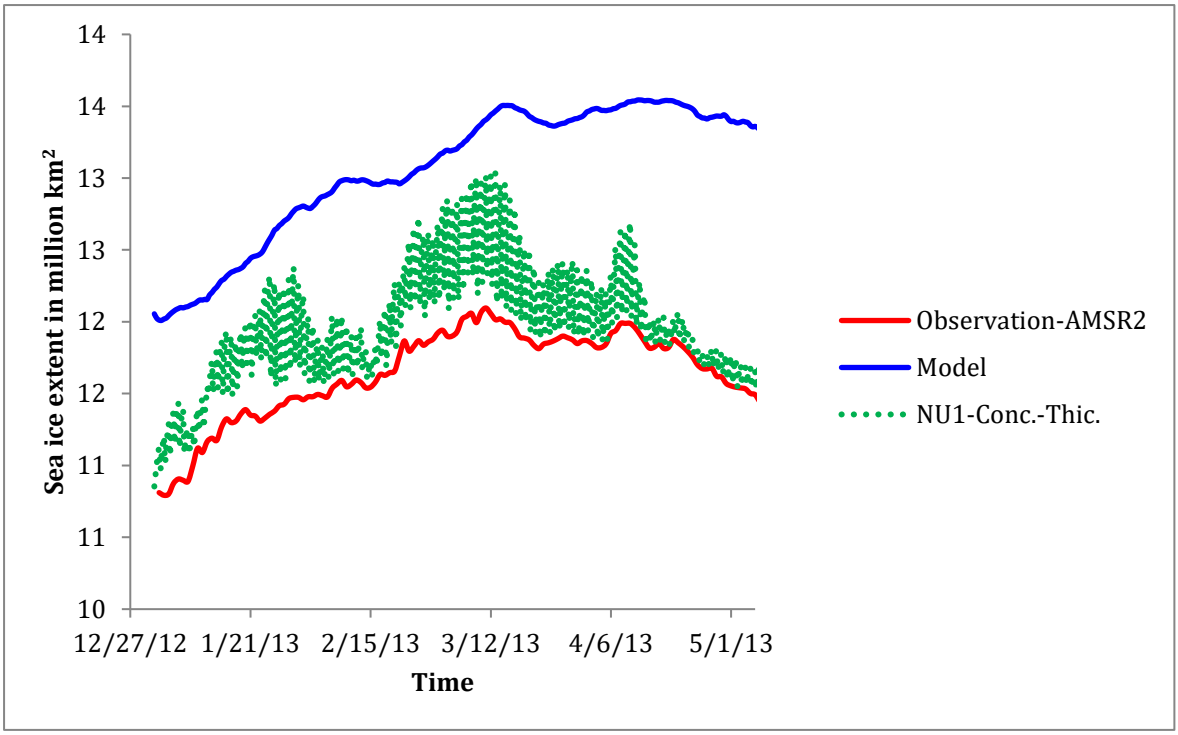

Figure 5-20: Sea ice extent time series from NU1-Conc.-Vel. Assimilation, Observation and Model.

5.3.4 Sea ice concentration and velocity nudging assimilation (NU1-Conc.-Vel.)

In this experiment sea ice concentration and sea ice velocity are assimilated simultaneously. Sea ice concentration and velocity gridded data (Kimura N. 2016) based on AMSR-2 satellite are assimilated daily. Satellite observations are introduced each day at midnight. Assimilation experiment is executed for the year 2013 winter since the velocity data set is not reliable in summer. Sea ice extent is improved with the assimilation since sea ice concentration is assimilated (figure 5-20).

Sea ice concentration assimilation has also improved sea ice thickness. Ice-POM model under predicts sea ice thickness near the pole as already discussed in section 2.2.2. NU1-Conc.-Vel. computation is able to improve the accuracy of sea ice thickness as shown in figure 5-21. The reason for this improved sea ice thickness is that sea ice velocity is improved with the assimilation.

Effect on ocean variables is also investigated. The model under predicts sea surface salinity in the Kara and the Barents Seas (figure 5-22). However, with the improved sea ice extent sea surface salinity in these areas is improved (figure 5-22) as discussed in section 5.3.3.

5.3.5 Nudging method-1 comparison

In this section all the experiments from nudging method-1 experiments are compared. Figure 5-23 compares sea ice extent from different experiments. It is evident that the experiments that assimilated sea ice concentration have improved sea ice extent better than the other experiments. All three experiments NU1-Conc, NU1-Conc.-Thic., NU1-Conc.-Vel shows similar results.

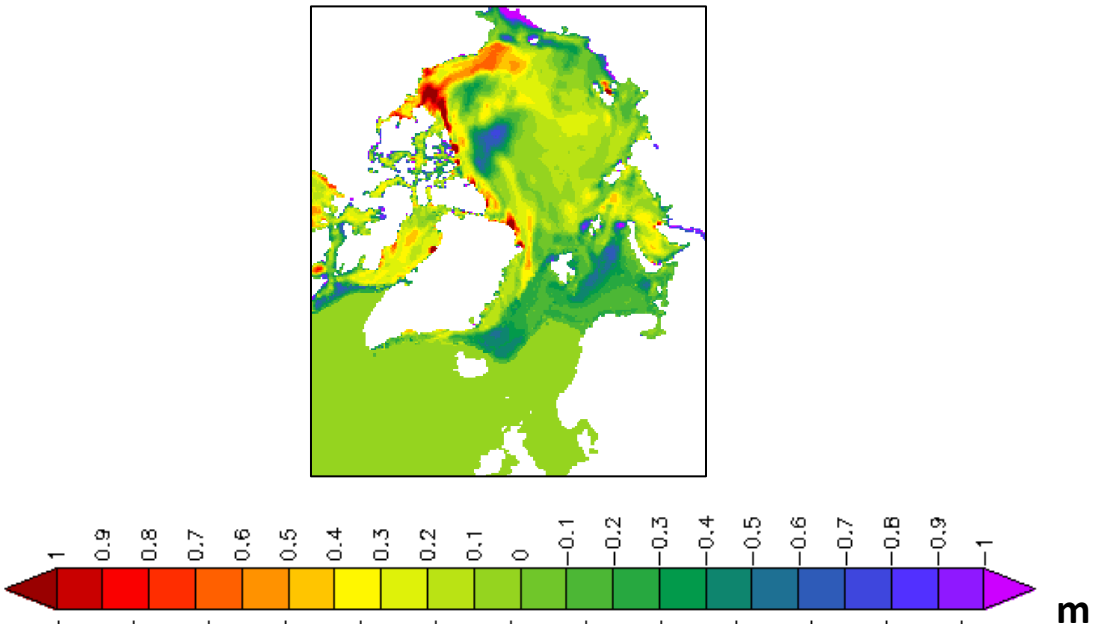

Figure 5-21: Difference between sea ice thickness of NU1-Conc.-Vel. and model in meter in winter. (NU1-Conc.-Vel. sea ice thickness - model sea ice thickness)

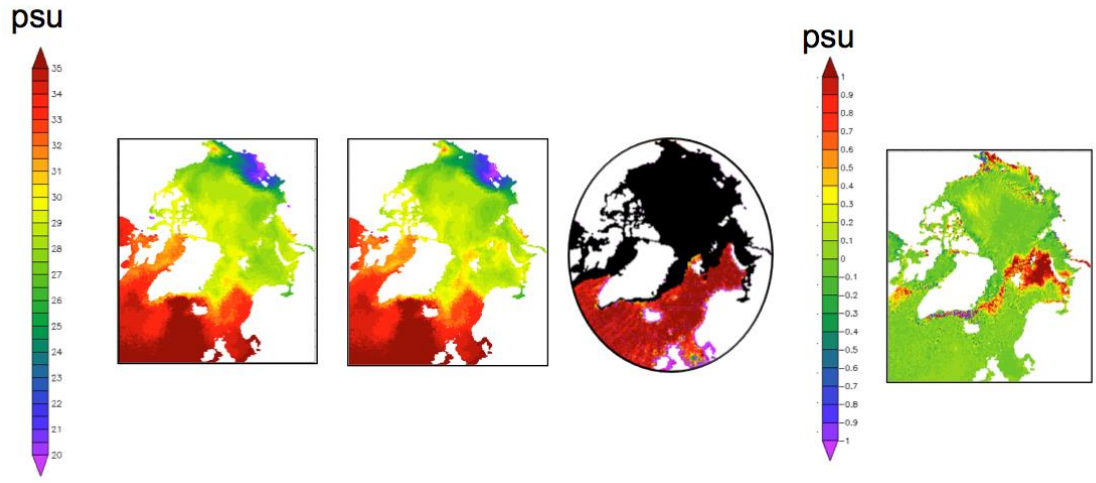

Figure 5-22: from left Sea surface salinity in psu of model, assimilation(NU1-Conc-Vel), Observation-Aquarius data set(area in black is where there is no data), salinity difference (assimilation-model) respectively in February

Thickness assimilation produces better results compared to velocity assimilation. This can be explained from the corrections that are done to non-assimilated variables. As discussed

in section 3.6 with sea ice velocity assimilation it's not possible to do corrections when sea ice velocity is zero.

5.4 Nudging method-2 experiments

This section presents nudging experiments that are performed according to the method described in section 3.4.2. This method provides a modification to Lindsay (2006) method by introducing observation bias. Experiments are carried out using a time constant $\tau = 180$. Figure 5-24 presents the sea ice extent from the experiment. Since this method corrects the observation bias, unlike direct insertion method sea ice extent from this experiment is close but not the same as assimilated AMSR-2 observation.

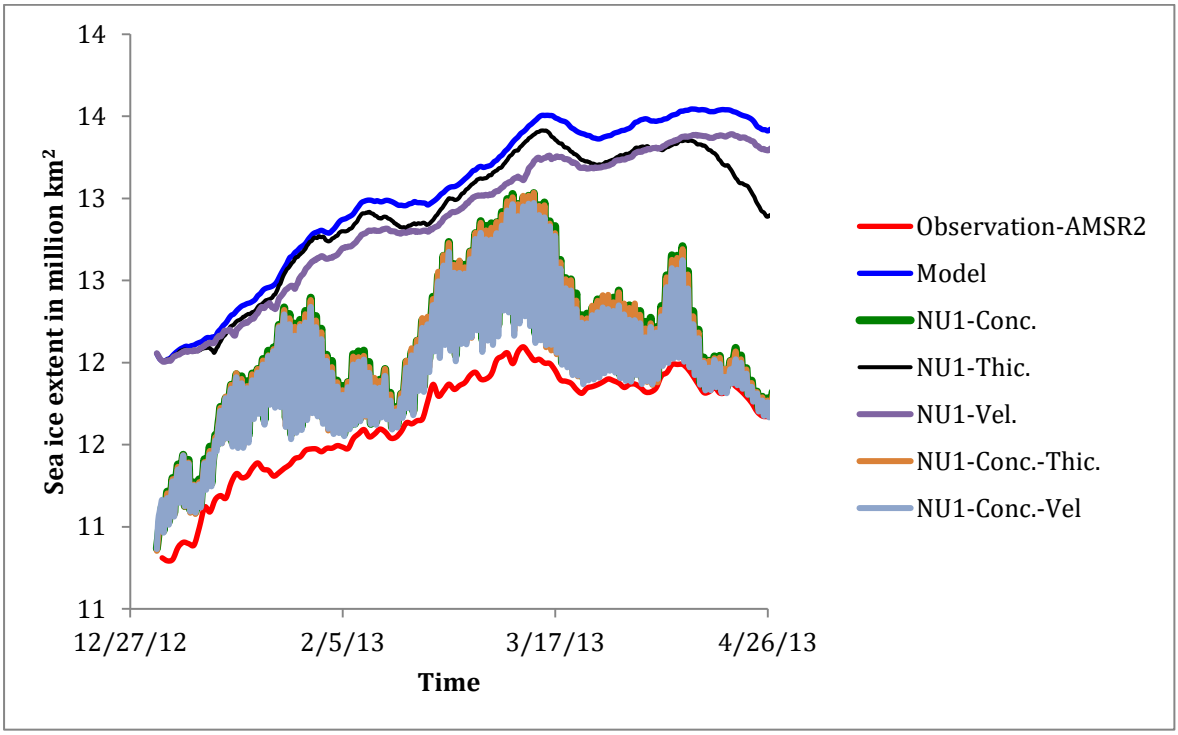

Figure 5-23: Sea ice extent time series from different nudging method-1 experiments

Sea ice thickness of Canadian basin and the polar area designated in figure 4-5 is presented in figure 5-25. Figure 5-26 shows the mean squared difference between NU2 sea ice thickness and the Cryosat sea ice thickness observation in the same area.

Sea ice thickness in the polar area has increased as a result of assimilation (figure 5-25). Reduced sea ice velocity (figure 5-27) in the same area directly relates to this sea ice thickness rise in the area.

However, this experiment shows that sea ice thickness has increased to a value greater than that of the Cryosat data. According to Chevallier (2016), over prediction of sea ice thickness is a common weakness in currently available data assimilation schemes due to lack of a proper mechanism to introduce or remove sea ice as a result of modifications that are done by the assimilation.

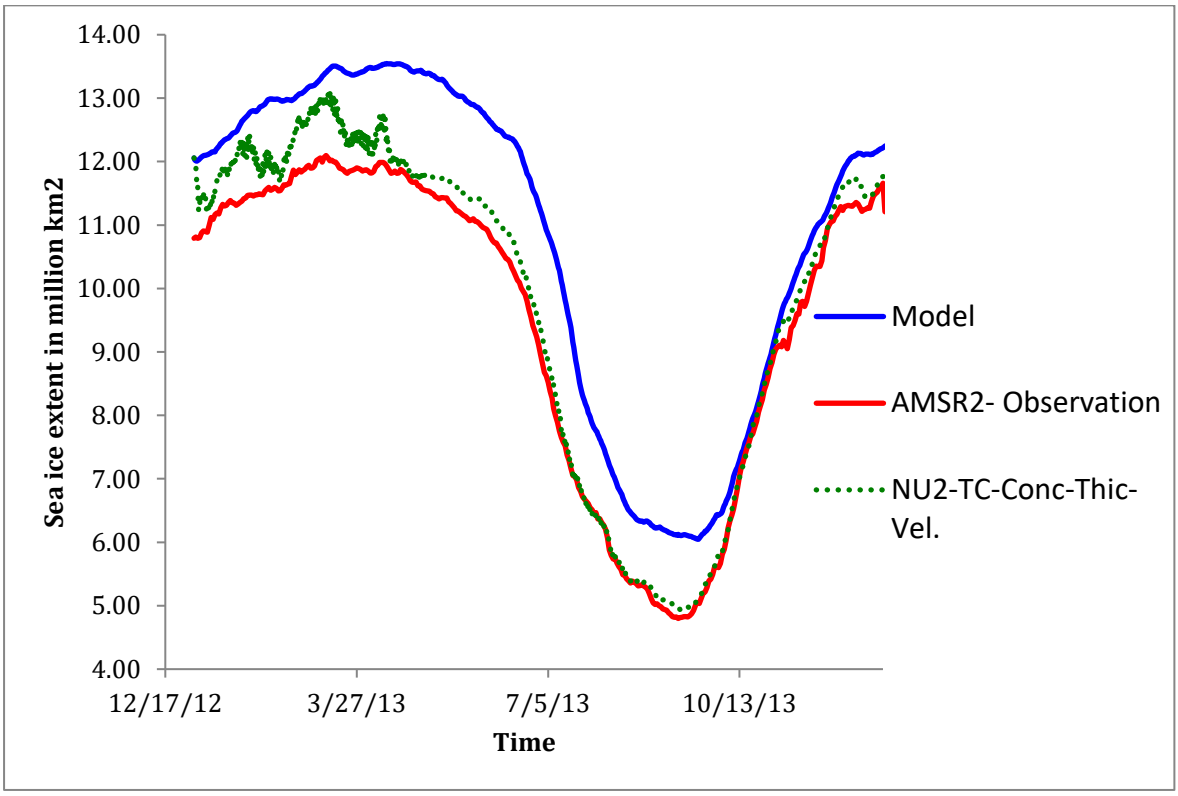

Figure 5-24: Sea ice extent from nudging method 2 experiments, model and AMSR2 observation

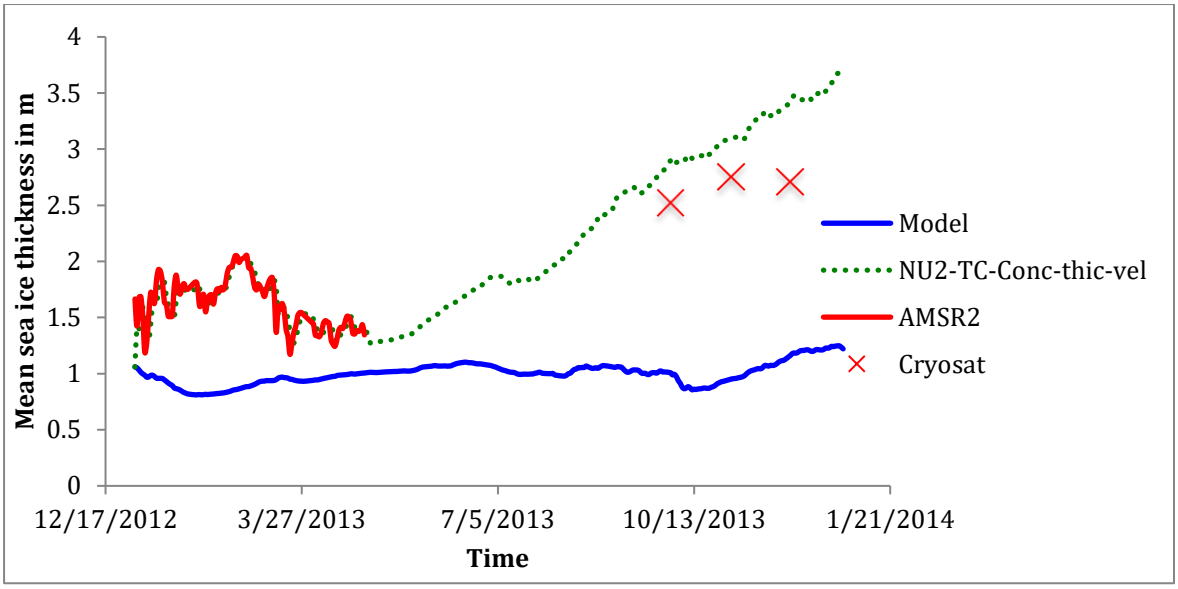

Figure 5-25: Mean sea ice thickness in polar area (Figure5-4) from nudging 2 experiments, AMSR2 observation, Cryosat monthly averaged observation and the model

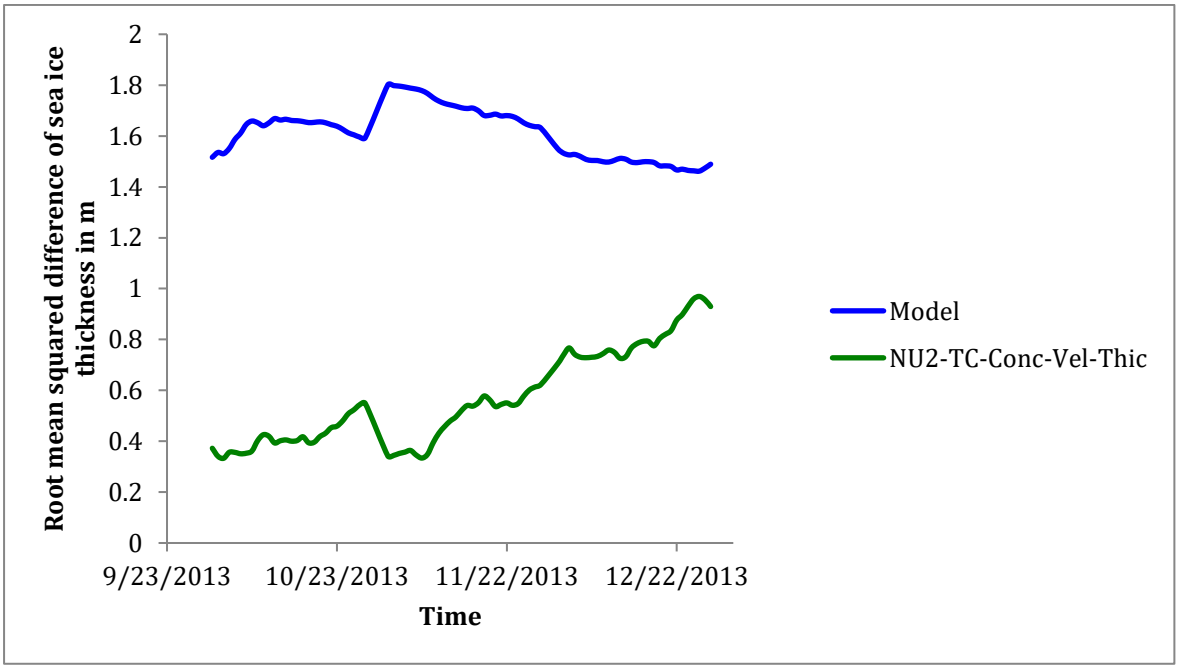

Figure 5-26: Root mean squared difference of sea ice thickness between Cryosat sea ice thickness data and the experiments in polar area (Figure 5-4) from nudging 2 experiment and the model free run

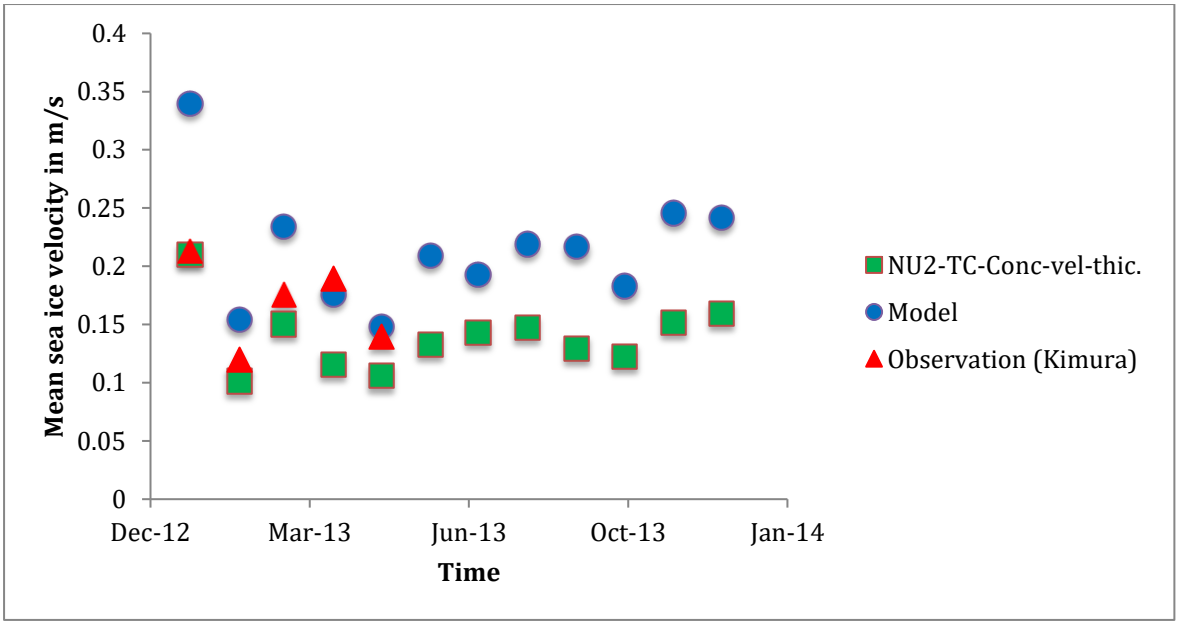

Figure 5-27: Mean sea ice velocity magnitude in the Polar area (figure 5-4) from nudging 2 experiment, model and the observation.

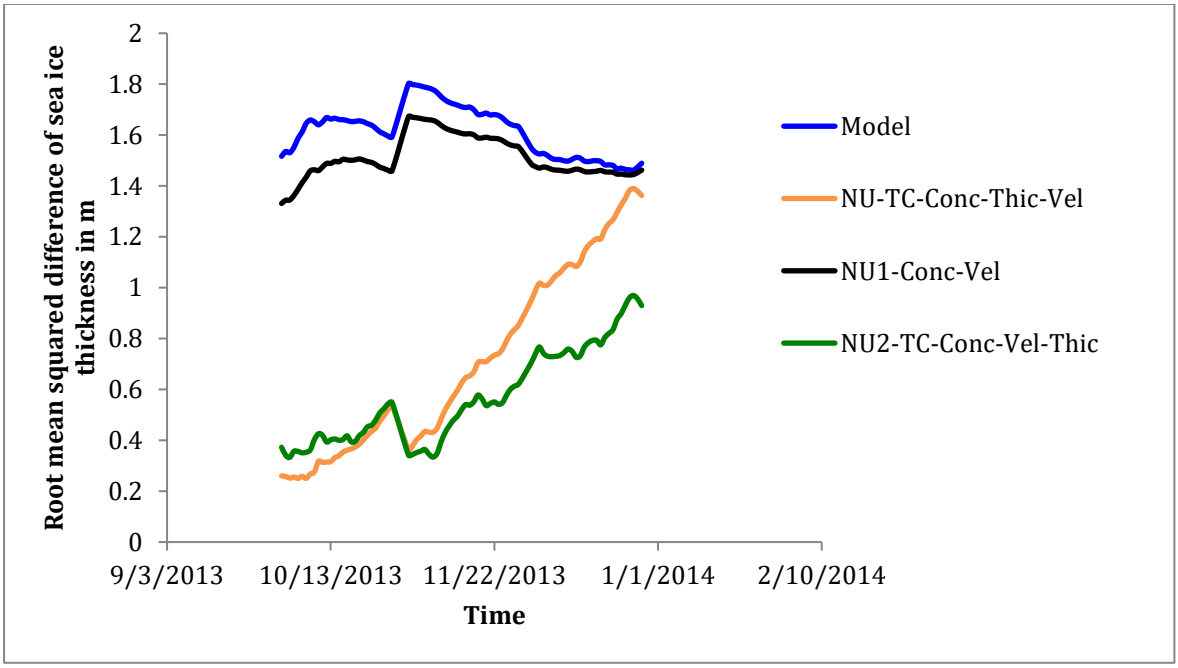

Figure 5-28: Comparison of root mean squared difference of mean sea ice thickness in the polar area between cryostat dataset and other datasets; model free run, nudging1, nudging 2 and nudging with time constant methods

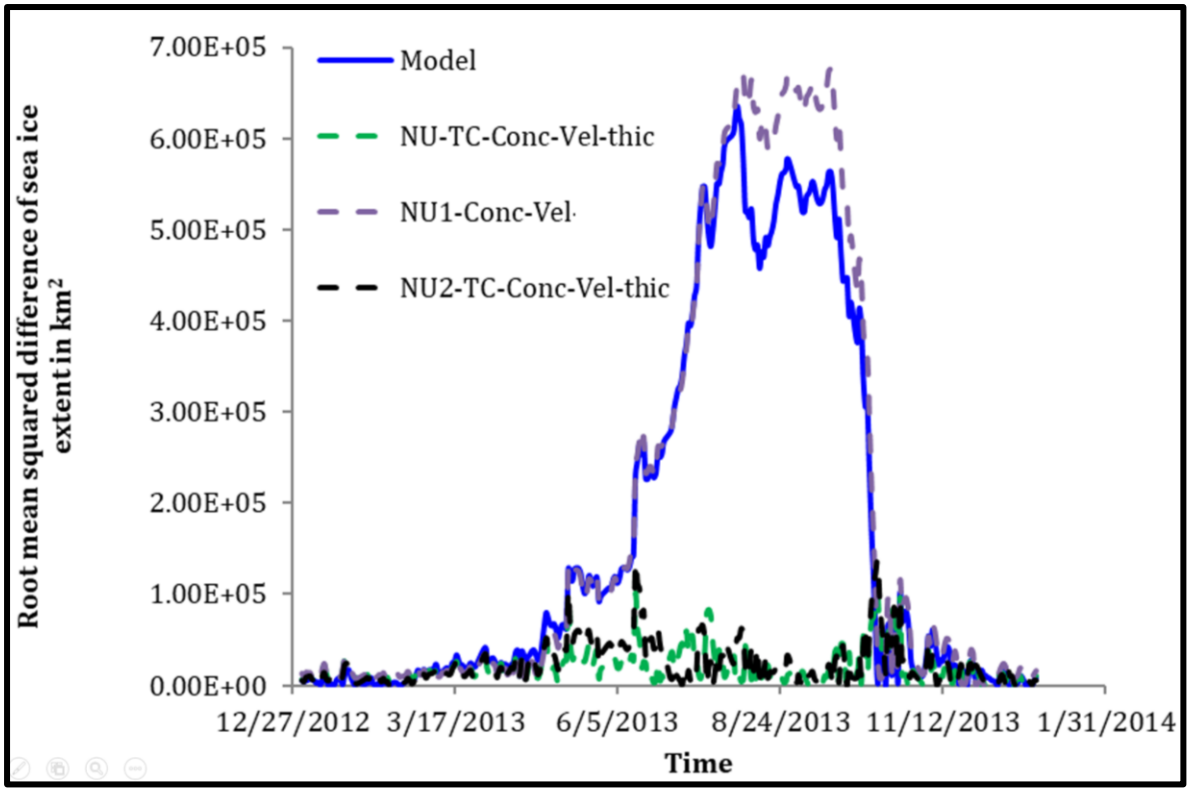

Figure 5-29: Comparison of root mean squared difference of mean sea ice extent in the Laptev Sea between AMSR2 dataset and other datasets; model free run, nudging1, nudging 2 and nudging with time constant methods

5.5 Nudging methods comparisons

This section presents a comparison between the results from different nudging methods. Comparisons are carried out locally since most of the differences are observed more clearly locally. Three experiments are considered for comparison. NU- uses a time constant of $\tau = 180$ (12 hours). It doesn't consider observation error; therefore, the nudging weight is 1. NU1 method considers observation error variance however the time constant used is 1. NU2 method considers both observation error variance as well as the observation bias. It incorporates observations in to the model in $\tau = 180$ (12 hours).

It can be seen in figure5-28, that NU method and the NU2 shows similarities in predicting sea ice thickness in the polar region. Over predicting sea ice thickness in the polar regions as time progresses is a common fault in many existing sea ice models that use data assimilation. This could be observed in NU1 method(figure5-28) where the assimilation

error is very close to model error. It can also be observed that NU- method and NU2 methods follows a similar trend in the sea ice thickness prediction error in the polar region. However, as time progresses NU method deviates from the independent observation data set more than NU2 estimate. The similarity at the beginning in the above two methods is possibly due to the incorporation of time constant in the assimilation. This shows that the time constant has a stronger impact on model estimate than the observation error or bias.

Similar trend can be seen in figure 5-29 where NU method and NU2 methods produces similar sea ice extent in Laptev sea while NU1 prediction is close to the model prediction. This highlights the importance of time constant in nudging assimilations.

6. Atmospheric Forcing Kalman Filter method

This section presents the results from atmospheric forcing Kalman filter method (AFKF). Observation errors are also considered in AFKF method. Several experiments are executed assimilating sea ice concentration, sea ice thickness and sea ice velocity individually and simultaneously.

6.1 Ensemble forcing

As discussed in section 3.5, AFKF method formulates the model error variance using the uncertainties of atmospheric data. In these AFKF experiments only seven ensemble members are used. Seven data sets from seven different weather agencies are used to differentiate ensemble members.

The accuracy of atmospheric forcing is a key driver of the accuracy of sea ice predictions in an ice-ocean coupled model. However different atmospheric data sets including reanalysis data sets show large difference in the Arctic region. Different data sets produced by different weather agencies have higher predictability skills in geographical areas where those agencies have access to more observational data. Therefore, the spread of the ensemble prediction is an indicator of the uncertainties in the model.

These atmospheric forecast data obtained from TIGGE data set vary significantly. This can be observed in atmospheric pressure, atmospheric velocity, atmospheric temperature, relative humidity and total cloud cover over the whole Arctic domain (figure 2-1) excluding landmasses. (from figure 6-1 to figure 6-6). Large variance can be observed in humidity, total cloud cover and temperature. This variance helps the ensemble to spread properly.

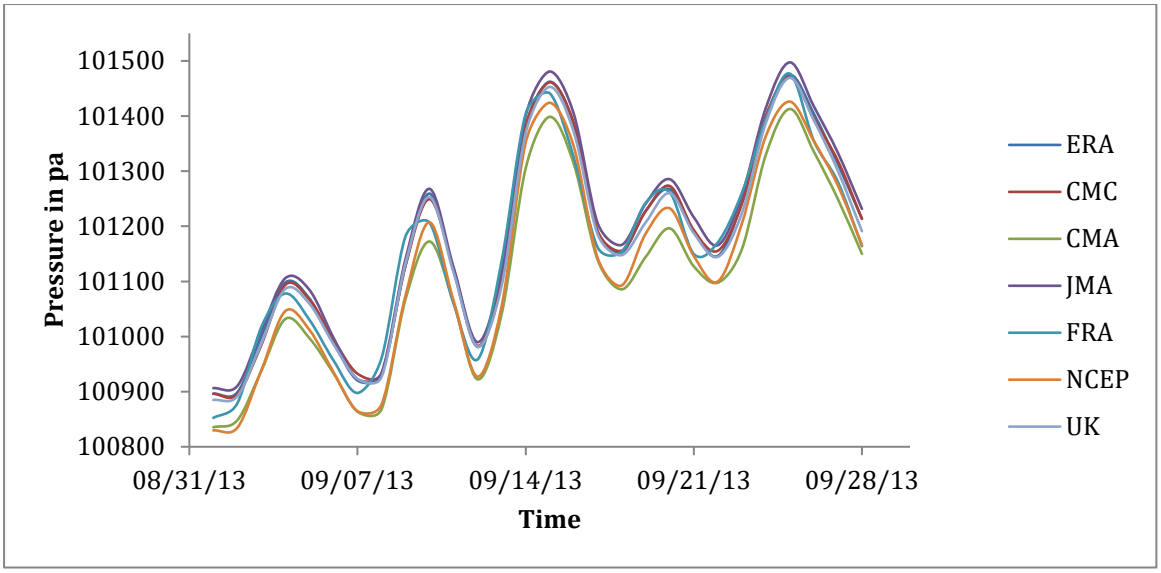

Figure 6-1: Atmospheric pressure in Pascal in September from TIGGE data set

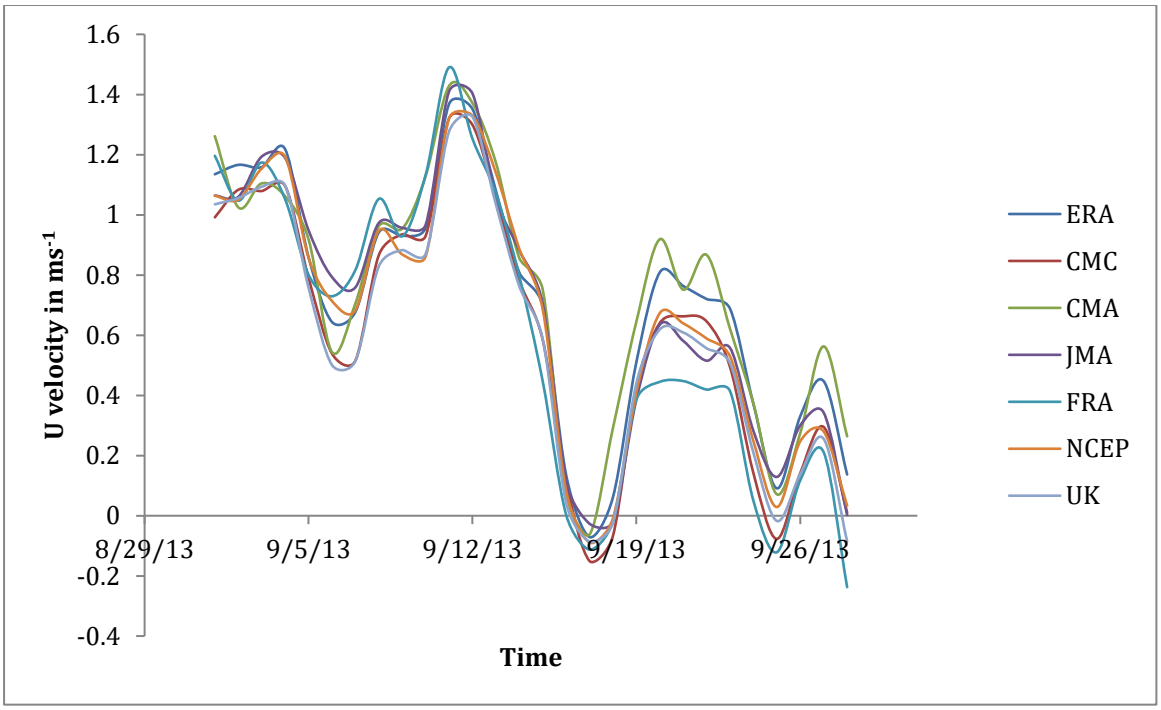

Figure 6-2: Atmospheric zonal velocity in m/s in September from TIGGE data set

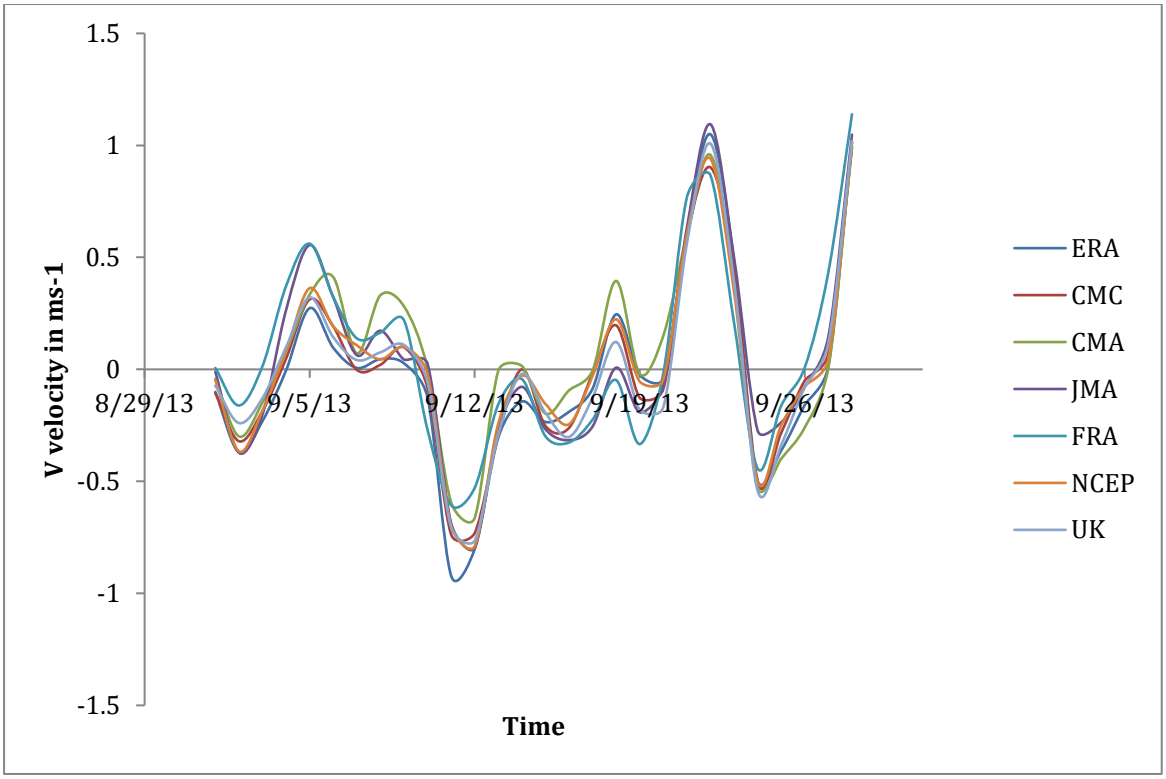

Figure 6-3: Atmospheric meridional velocity in m/s in September from TIGGE data set

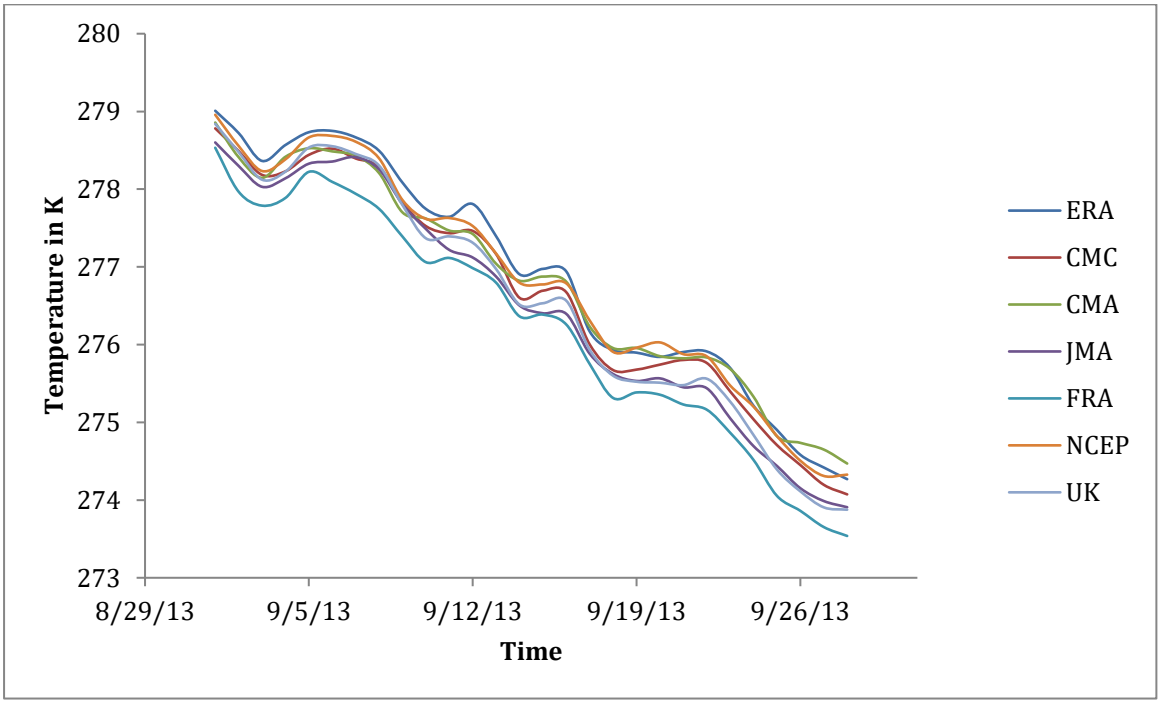

Figure 6-4: Atmospheric temperature in Kelvin in September from TIGGE data set

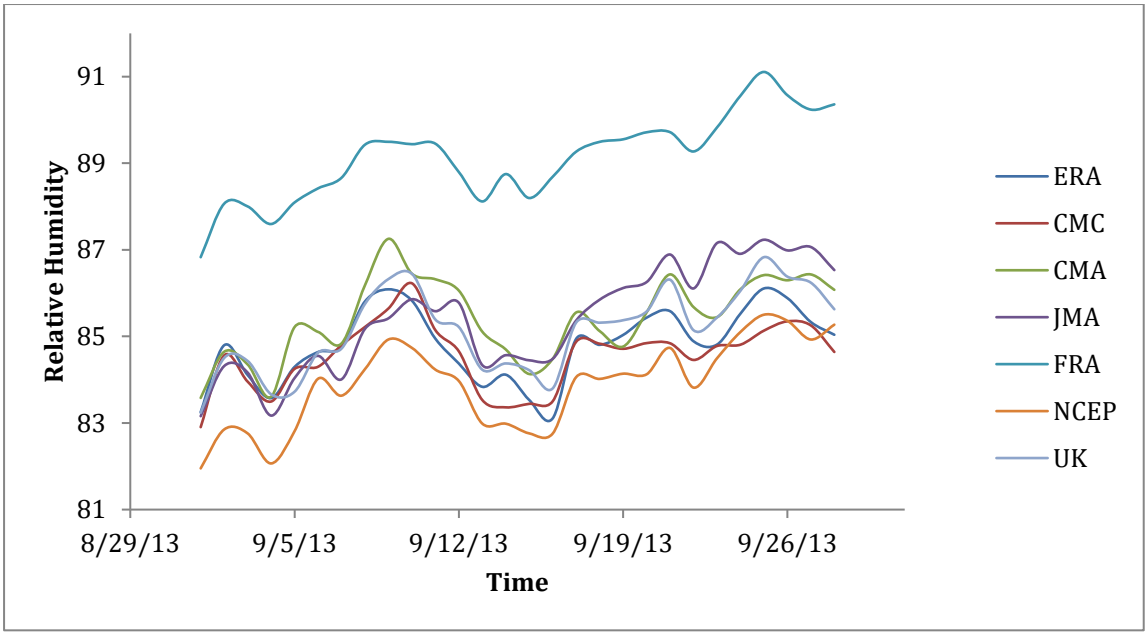

Figure 6-5: Relative humidity in September from TIGGE data set

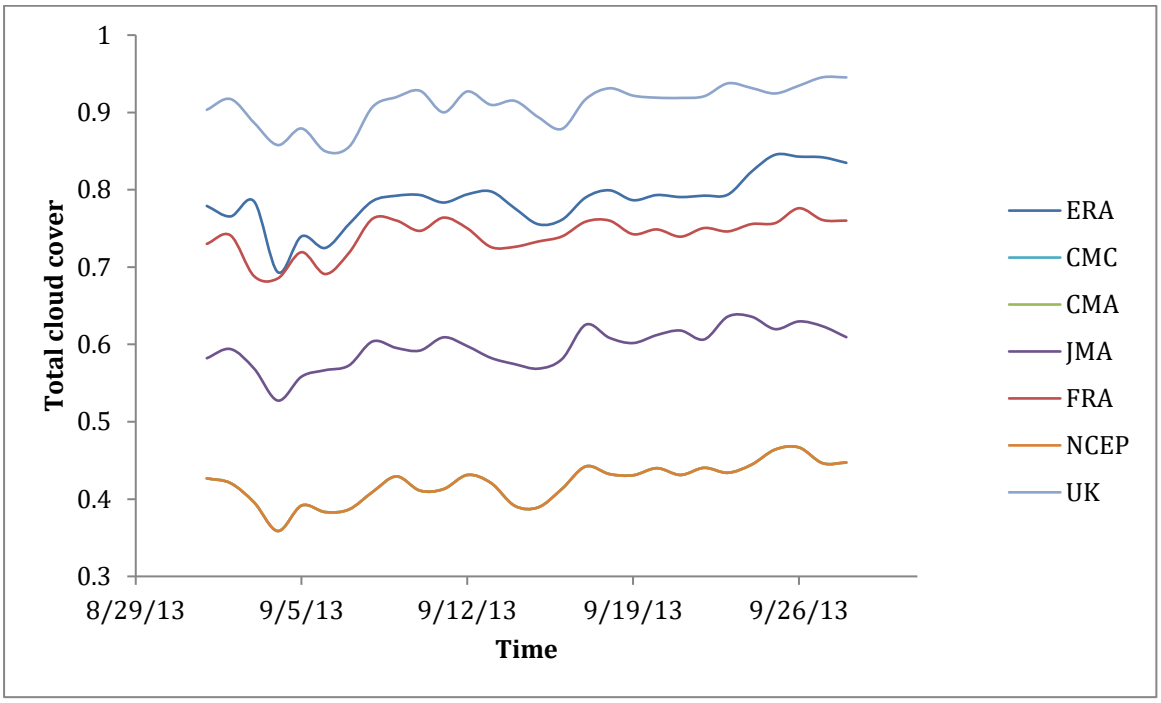

Figure 6-6: Total cloud cover in September from TIGGE data set

6.2 Sea ice concentration AFKF assimilation

In this experiment sea ice concentration gridded data based on AMSR-2 satellite are assimilated daily. Satellite observations are introduced each day at midnight. Assimilation experiment is executed for the year 2013. Corrections for the non-assimilated variables are done according to the detail discussed in section 3.6. Sea ice concentration assimilation is able to reproduce sea ice extent that is close to observation. Figure 6-7 presents the ensemble spread. Ensemble spread is large in the beginning and converges with time. Figure 6-7 shows that the observation is within the ensemble spread. It confirms the accuracy of the ensemble computation.

Sea ice concentration AFKF assimilation not only has improved sea ice extent but also it has improved sea ice thickness.

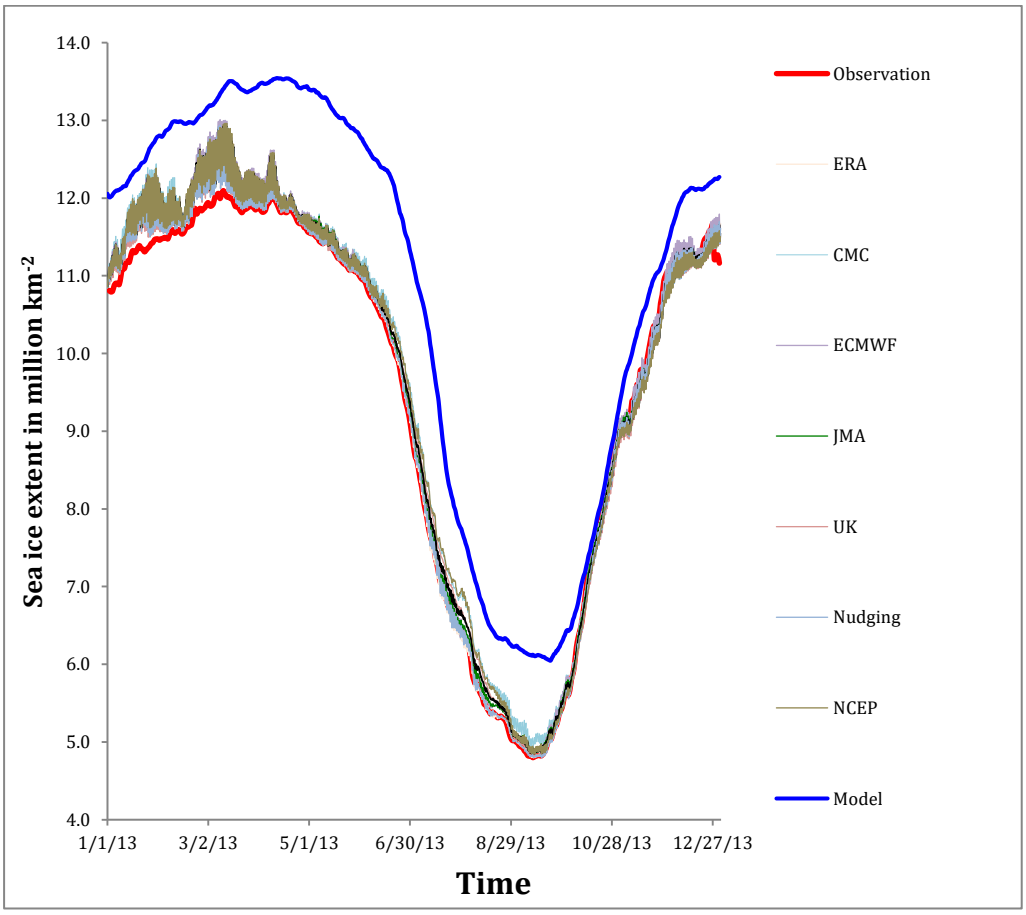

Figure 6-7: Ensemble spread – sea ice extent from different ensemble members.

Figure 6-8 compares sea ice thickness results from nudging and AFKF method. It shows that ensemble computation outperforms the nudging computations with regards to sea ice thickness predictability.

This improved sea ice thickness can be attributed to sea ice velocity in assimilation. Compared to the model and nudging-1 assimilation, AFKF predicted velocity is lower near the pole (figure 6-9). Ocean variables are also affected by the assimilation. AFKF method has improved sea surface salinity in the Barents Sea as shown in (figure 6-10).

6.3 Sea ice concentration and thickness AFKF assimilation

In this experiment sea ice concentration and sea ice thickness are assimilated simultaneously. Sea ice concentration and thickness gridded data (Krishfield 2014) based on AMSR-2 satellite are assimilated daily.

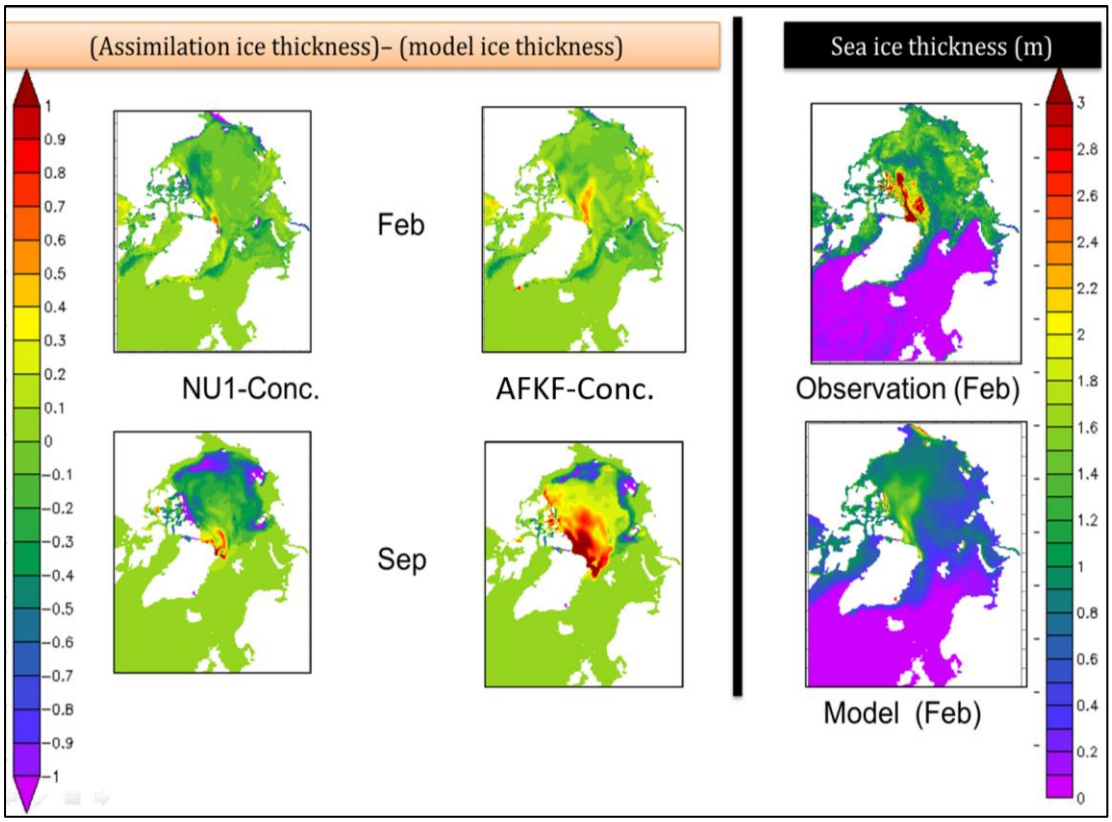

Figure 6-8: Sea ice thickness difference in meters (assimilation –model) on left. Observation sea ice thickness in meter on right (top). Model sea ice thickness in meter on left (bottom)

Satellite observations are introduced each day at midnight. Assimilation experiment is executed for the year 2013 winter since the thickness data set is not reliable in summer.

This experiment has improved sea ice extent and sea ice thickness significantly. This is presented in figure 6-11 and figure 6-12. Compared to sea ice extent from nudging-1 method, sea ice extent from AFKF method shows less variance since it's influenced by seven ensemble members (figure 6-11). Nudging-2 method also shows less variance since time constant is introduced in the experiment, however sea ice extent from nudging2 method is further away from the observation.

Sea ice thickness from assimilation is comparable with that of the observations (figure 6-12). Sea surface salinity is improved in the Barents Sea after assimilation (figure 6-13).

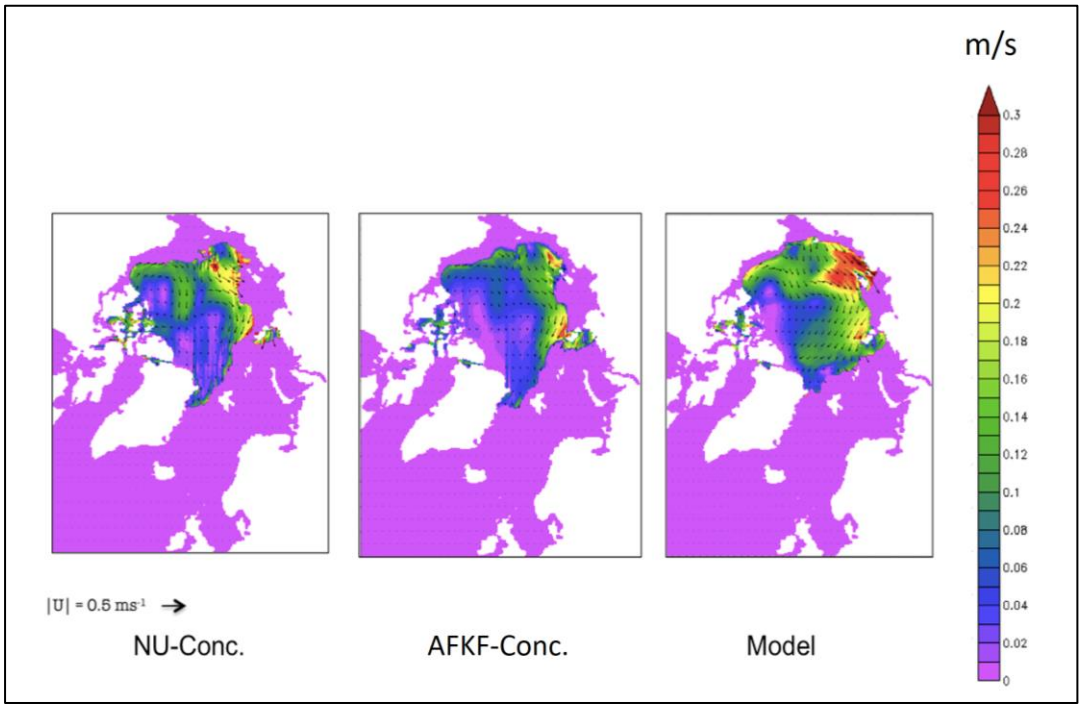

Figure 6-9: Sea ice velocity in m/s from nudging assimilation (left) from AFKF assimilation (center) from model (right)

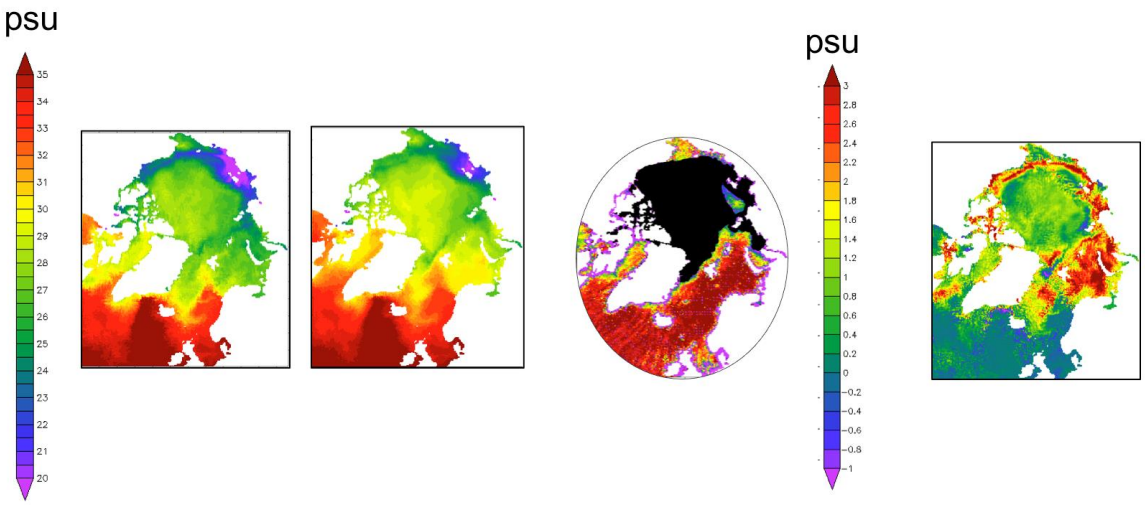

Figure 6-10: from left Sea surface salinity in psu of model, assimilation(AFKF-Conc), Observation-Aquarius data set(area in black is where there is no data), salinity difference (assimilation-model) respectively in September

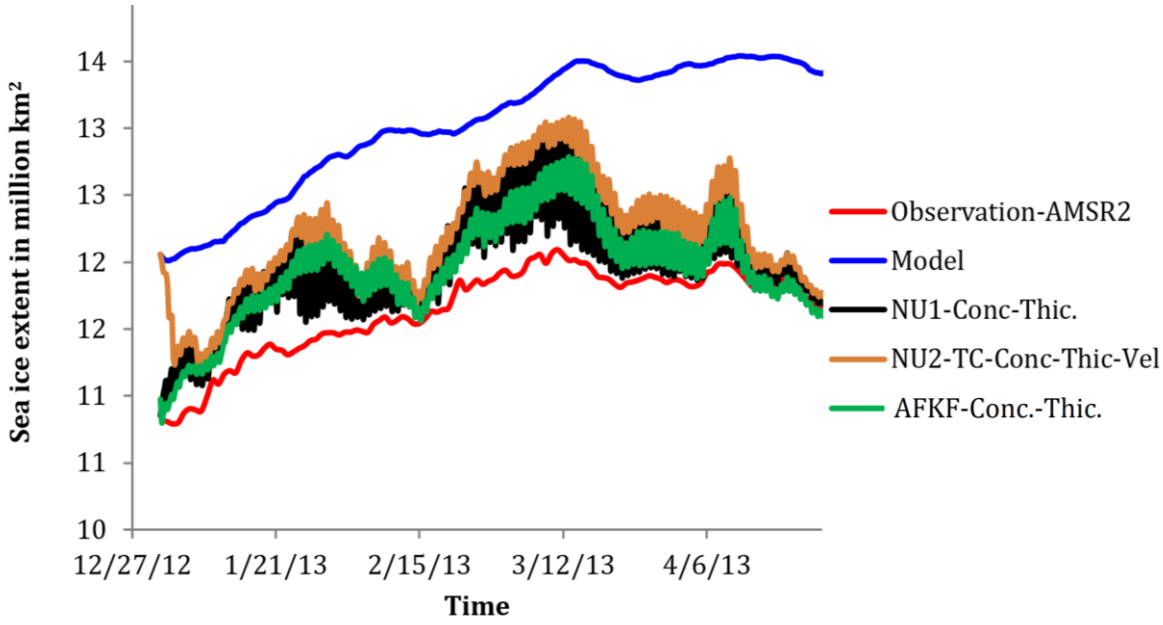

Figure 6-11: Sea ice extent time series from AFKF-Conc-Thic,NU1-Conc-Thic, NU2-TC-Conc-Thic-vel model and observations

This is a result of sea ice being removed from the model as a correction for sea ice extent as discussed before.

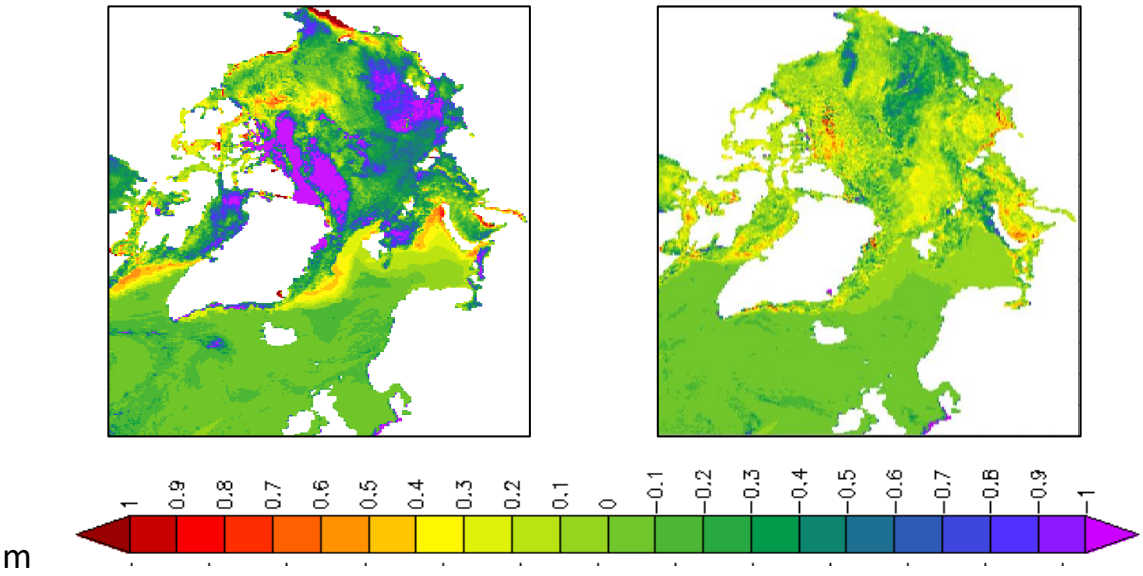

Figure 6-12: Sea ice thickness difference in meter in winter, (model - observation) on left, (AFKF-Conc.-Thic. - observation) on right

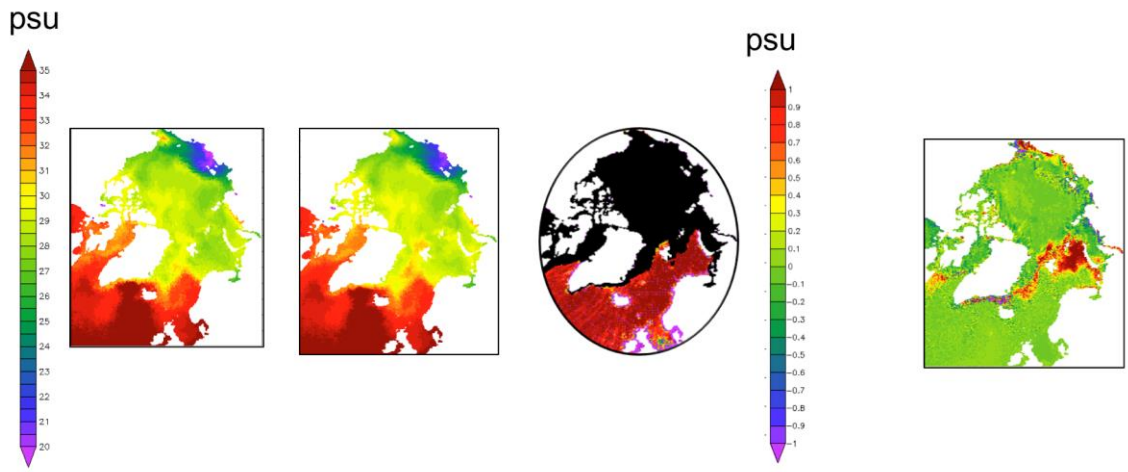

Figure 6-13: from left Sea surface salinity in psu of model, assimilation (AFKF-Conc-thic), Observation-Aquarius data set (area in black is where there is no data), salinity difference (assimilation-model) respectively in February

6.4 Sea ice concentration and velocity AFKF assimilation

In this experiment sea ice concentration and sea ice velocity are assimilated simultaneously. Sea ice concentration and velocity gridded data (Kimura N. 2016) based on

AMSR-2 satellite are assimilated daily. Satellite observations are introduced each day at midnight. Assimilation experiment is executed for the year 2013 winter since the velocity data set is not reliable in summer.

This experiment well reproduces sea ice extent and sea ice thickness. This is presented in figure 6-14 and figure 6-15. Similar to 6.3 section, sea ice extent from AFKF method shows less variance due to the influence of seven ensemble members (figure 6-14). Sea ice thickness from assimilation is comparable with that of the observations (figure 6-15). Sea surface salinity is also improved locally by the assimilation (figure 6-16). This is a result of improved sea ice extent.

6.5 Sea ice concentration, sea ice thickness and sea ice velocity AFKF assimilation

In this experiment sea ice concentration, sea ice thickness and sea ice velocity are assimilated simultaneously in a daily interval. Satellite observations are introduced each day at midnight. Sea ice thickness and sea ice velocity are assimilated only during winter since they are not reliable in the winter. Sea ice concentration is assimilated throughout the year.

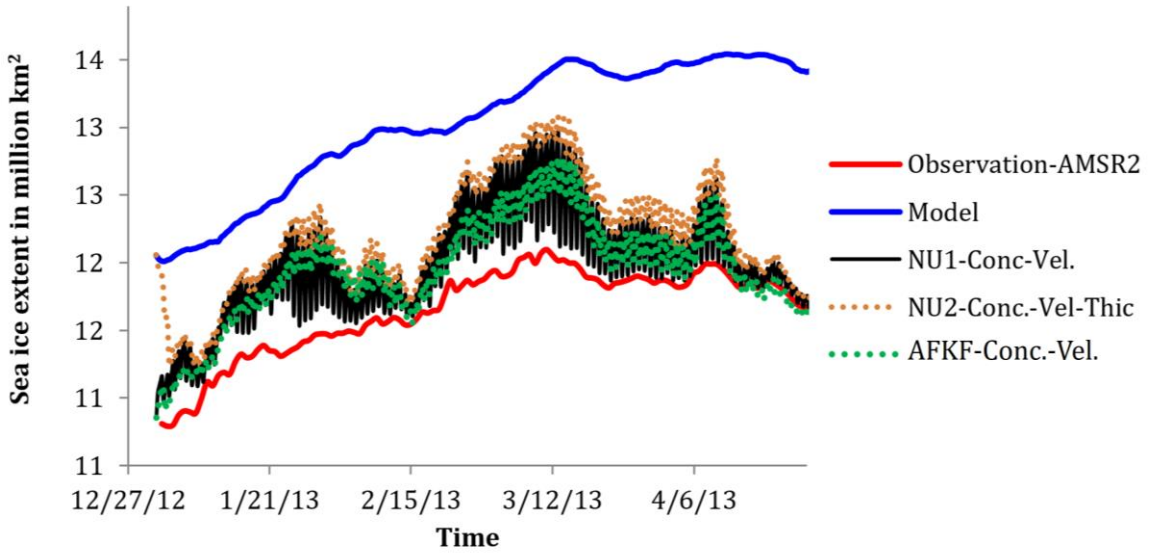

Figure 6-14: Sea ice extent from AFKF-Conc-Vel experiment, NU-Conc-Vel experiment, model and observations

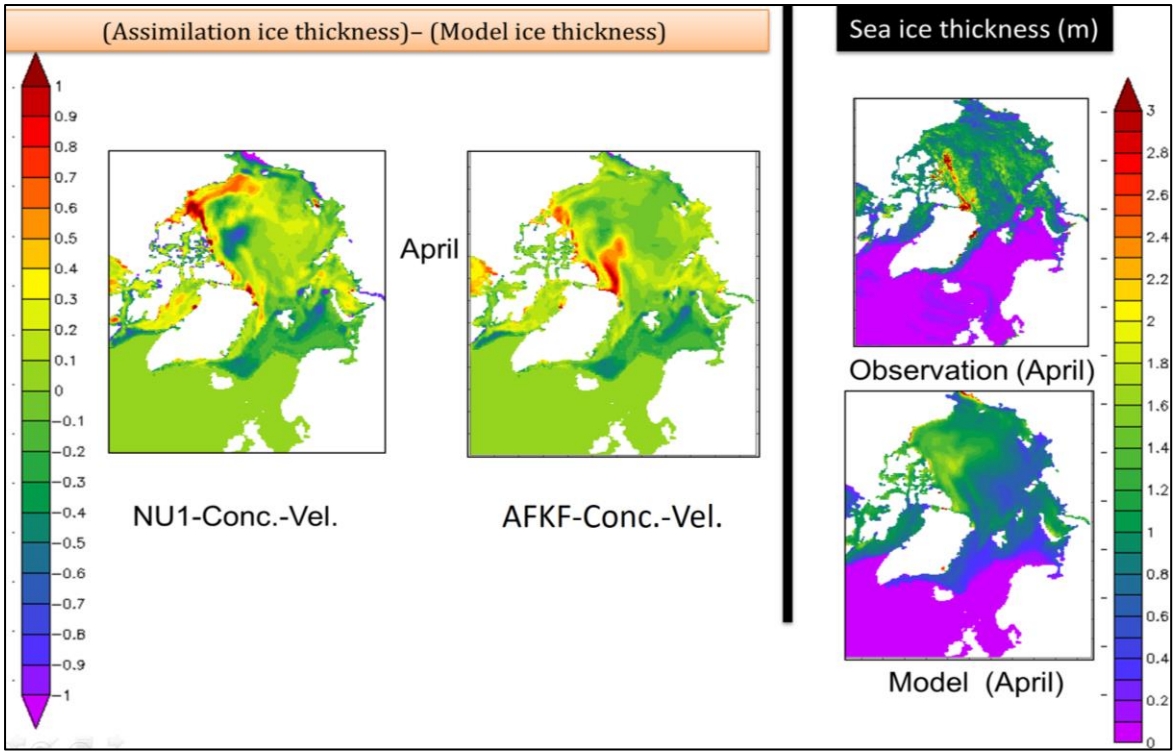

Figure 6-15: Sea ice thickness difference in meter (assimilation –model) on left. Observation sea ice thickness on top right. Model sea ice thickness on bottom right.

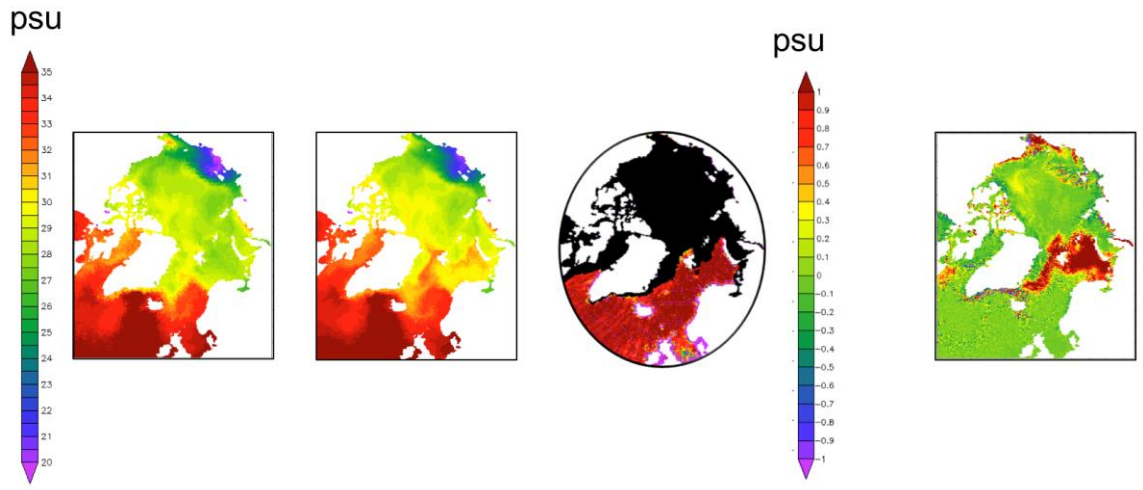

Figure 6-16: from left Sea surface salinity in psu of model, assimilation(AFKF-Conc-vel), Observation-Aquarius data set(area in black is where there is no data), salinity difference (assimilation-model) respectively in September

Figure 6-17 and figure 6-18 show how the ensemble spreads. The difference between the maximum and minimum sea ice extent is plotted in figure 6-18. It shows that the ice extent difference ranges between 0.1 million km^2 and 1 million km^2. It's an indication that the ensemble spreads properly. According to figure 6-17 the experiment can reproduce the sea ice extent for the entire year.

Figure 6-19 presents the magnitude of the Kalman gain matrix when sea ice concentration is assimilated. It is presented as the Frobenius norm. Frobenius norm is calculated to be the trace of the squared of the diagonal components of the Kalman gain matrix. It is an indication of the model error. Model error grows gradually in winter and the freezing season. Model error is a maximum in summer where the uncertainty of the forcing data is high.

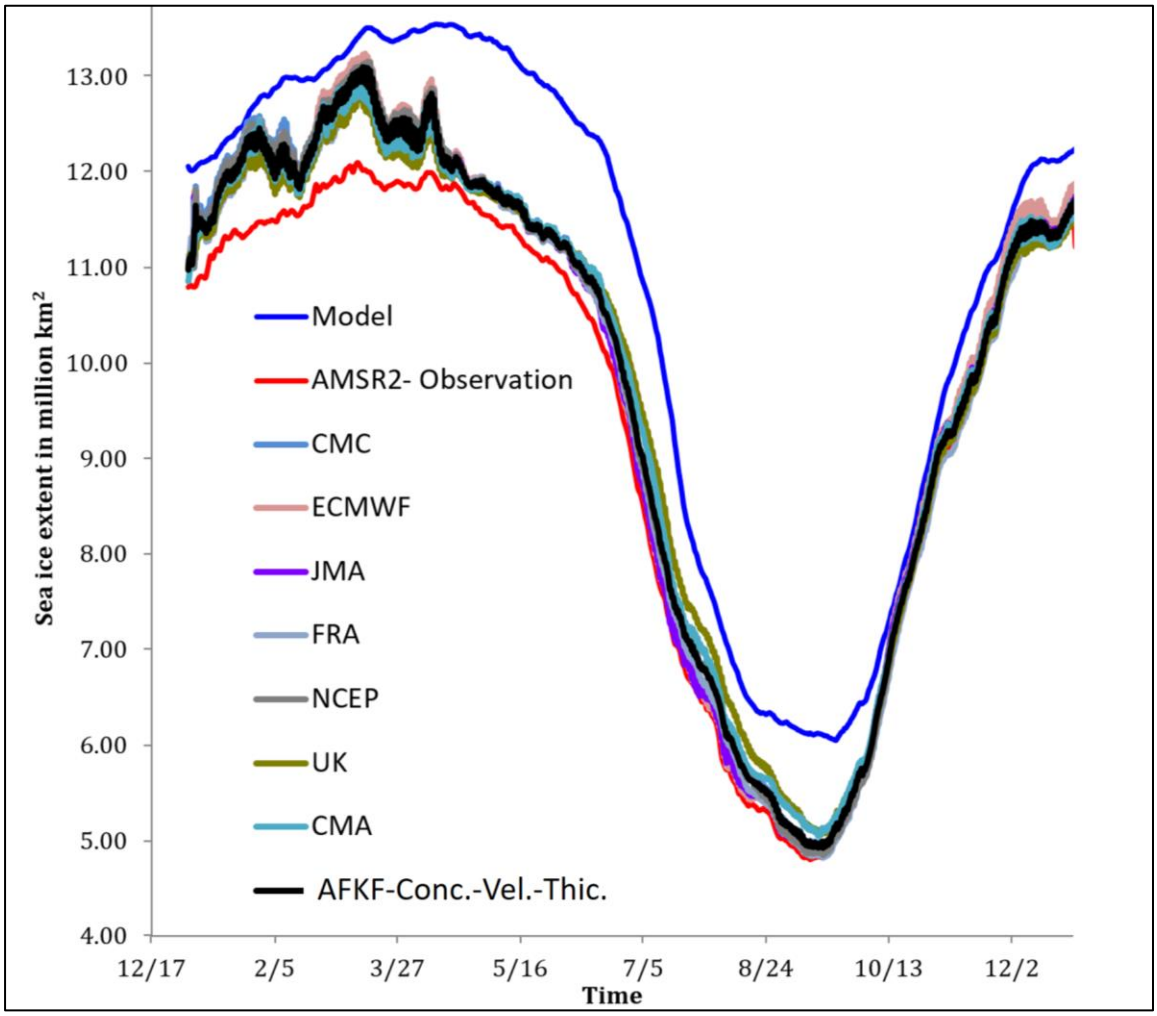

Figure 6-17: Time series of sea ice extent from different ensemble members, model run and AMSR2 observation data

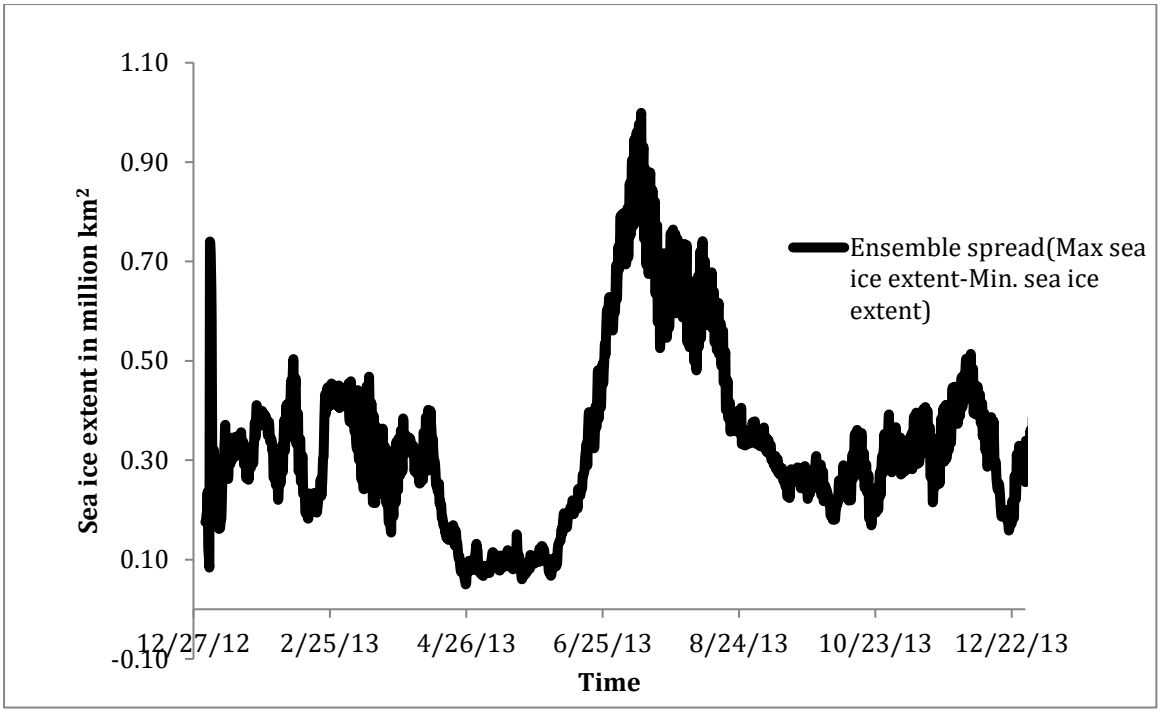

Figure 6-18: Time series of difference between the maximum and minimum sea ice extent

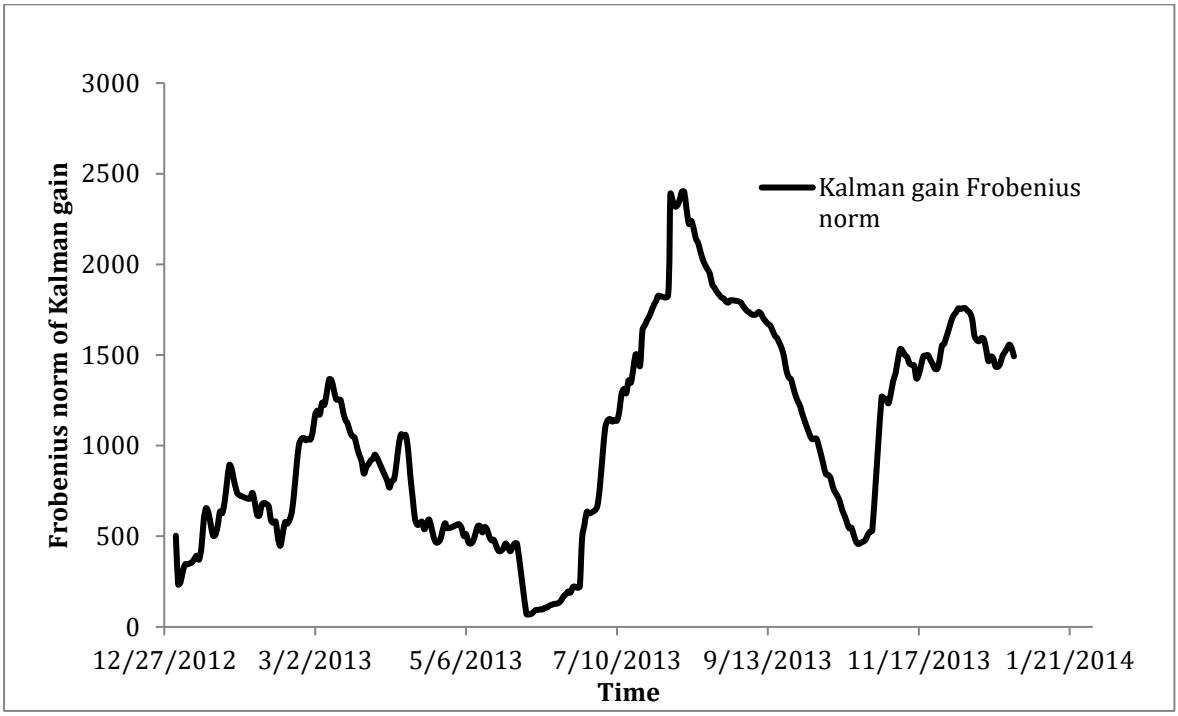

Figure 6-19:Time series of Frobenius norm of the Kalman gain matrix for AFKF-Conc-Vel-thic experiment sea ice concentration

The comparison of 6-18 and 6-19 indicates that when the spread of the sea-ice extent estimate is large, there is more weight on the observation. Figure 6-20 and Figure 6-21 present the time series of difference between the maximum and minimum of the temperature and pressure in the atmospheric data sets. In figure 6-20 the temperature difference trend roughly resembles the trend in Frobenius norm in figure 6-19 in some months. The similarity prevails because the atmospheric temperature directly affects the sea ice creation and melting processes. It is also visible in figure 6-21 that the temperature difference between maximum and minimum has even reached 3.5 degrees. Due to this amount of large difference in temperature the sea ice extent produced in different ensemble members can vary significantly leading to assign more weight on sea ice observations.

Figure 6-22 presents the structure of the Kalman gain matrix. The Kalman gain is an indication of how model error and the observation error are reflected in the assimilation. In winter, assimilation has the strongest impact on sea ice edge. Due to similarity between observation and model in ice pack, in winter, assimilation has very little impact on sea ice concentration in the ice pack.

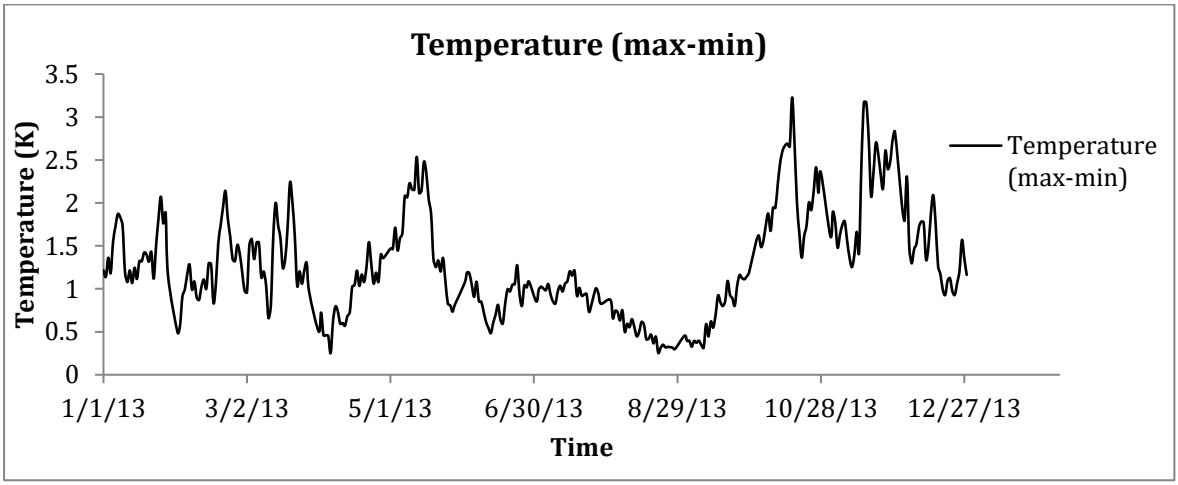

Figure 6-20: Time series of difference between the maximum and minimum temperature of the atmospheric forcing data sets

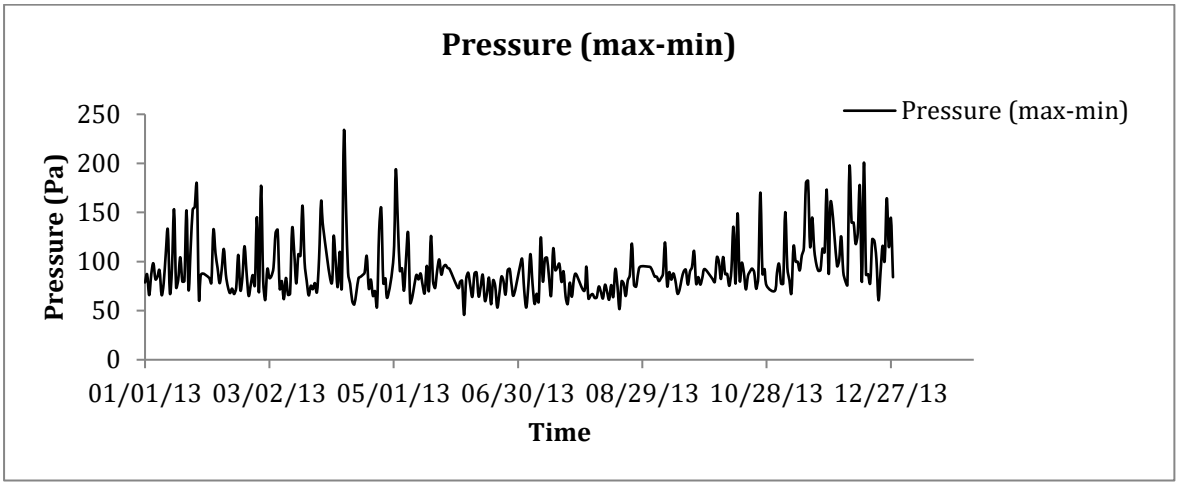

Figure 6-21: Time series of difference between the maximum and minimum pressure of the atmospheric forcing data sets

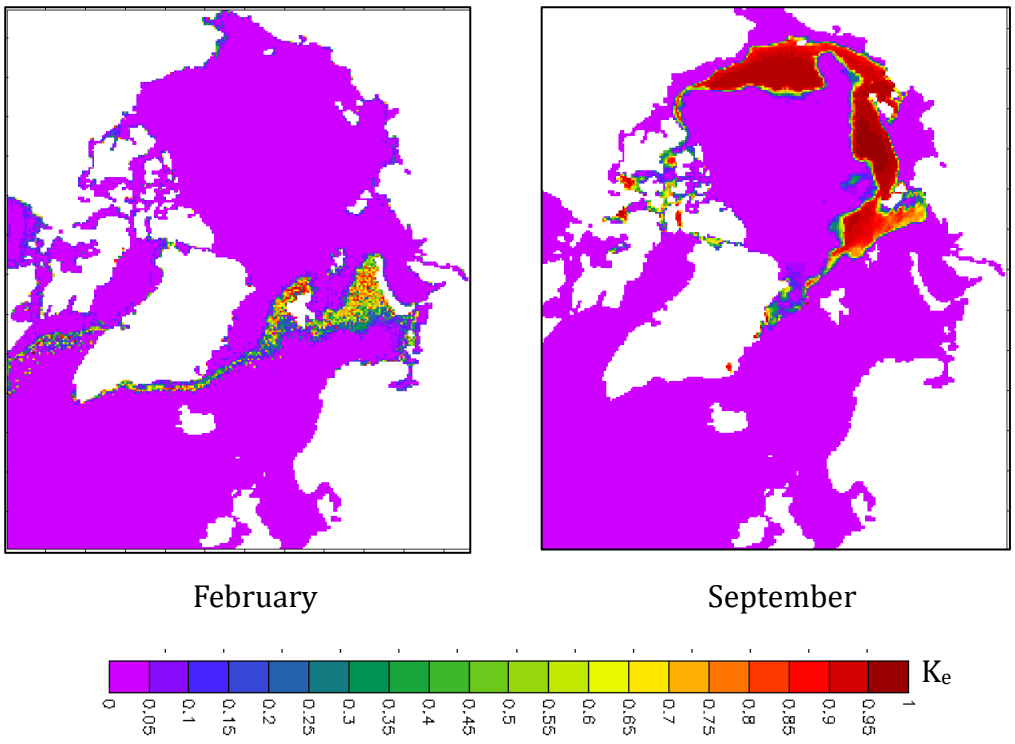

Figure 6-22: Diagonal components of Kalman gain matrix of AFKF-Conc-Vel-thic experiment sea ice concentration. 02/2013 on left(a) 09/2013 on right(b)

In summer uncertainty of forcing data is high, especially along the sea ice edge increasing the model error along the sea ice edge. This is reflected in the Kalman gain in figure 6-22(b) where observations are weighted along the sea ice edge. Due to similarities in model and observations in the ice pack, assimilation has little impact on sea ice concentration of the ice pack. This also confirms that the sea ice thickness differences observed as a result of assimilation in the ice pack (figure 6-8) are related to sea ice velocity changes rather than the corrections to the sea ice thickness.

Figure 6-23 presents the diagonal components of the sea ice thickness Kalman gain matrix. Assimilation has a high impact in Polar area where model has under estimated sea ice thickness. In February assimilation has affected the sea ice edge and the Polar area. The model error has increased with time, that after two months both marginal areas and Polar area show higher Kalman gain.

Figure 6-24 compares resulting sea ice thickness from the experiment. Model under estimates sea ice thickness in the polar area (figure 5-4) compared to the Cryosat data set. This is improved with the assimilation run. Figure 6-25 presents the root mean squared difference(RMSD) between the assimilation and the cryostat data from October 2013 to December 2013 in the same area. While nudging methods show a growth in RMSD, atmospheric forcing Kalman filter method shows a decline. It can be seen that the sea ice thickness hasn't grown abnormally in atmospheric forcing Kalman filter method.

The reason for this sea ice thickness rise is the improved sea ice velocity in the Polar area as presented in figure 6-26. Sea ice velocity has decreased in the area increasing sea ice thickness.

Ocean salinity is also affected by assimilation. As discussed in previous experiments with the sea ice extent decrease in the Barents Sea, sea surface salinity and ocean salinity are increased. This will be discussed further in Chapter 7.

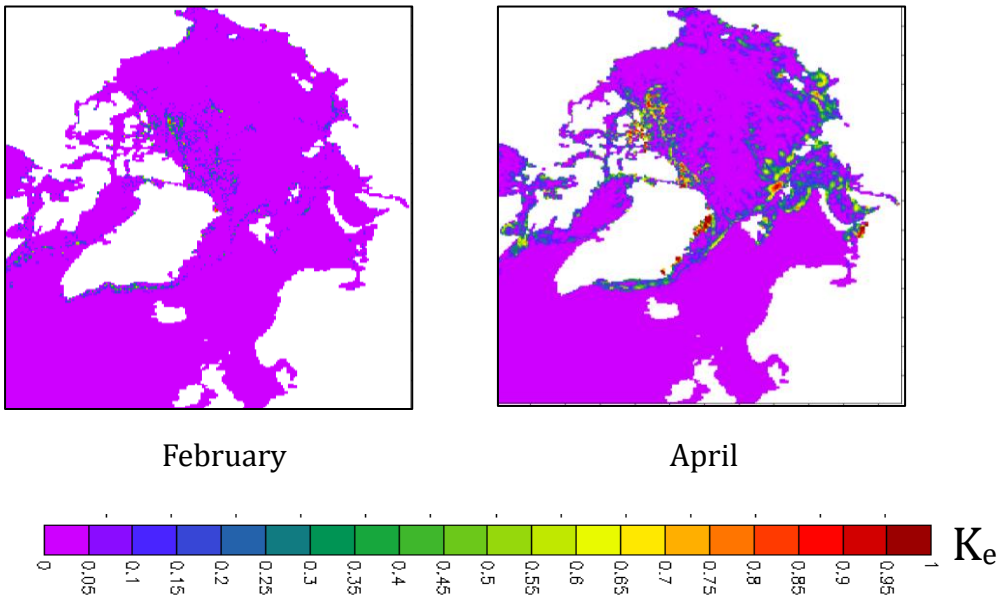

Figure 6-23: Diagonal components of Kalman gain matrix of AFKF-Conc-Vel-thic experiment sea ice thickness in 02/2013 on left(a) 04/2013 on right(b)

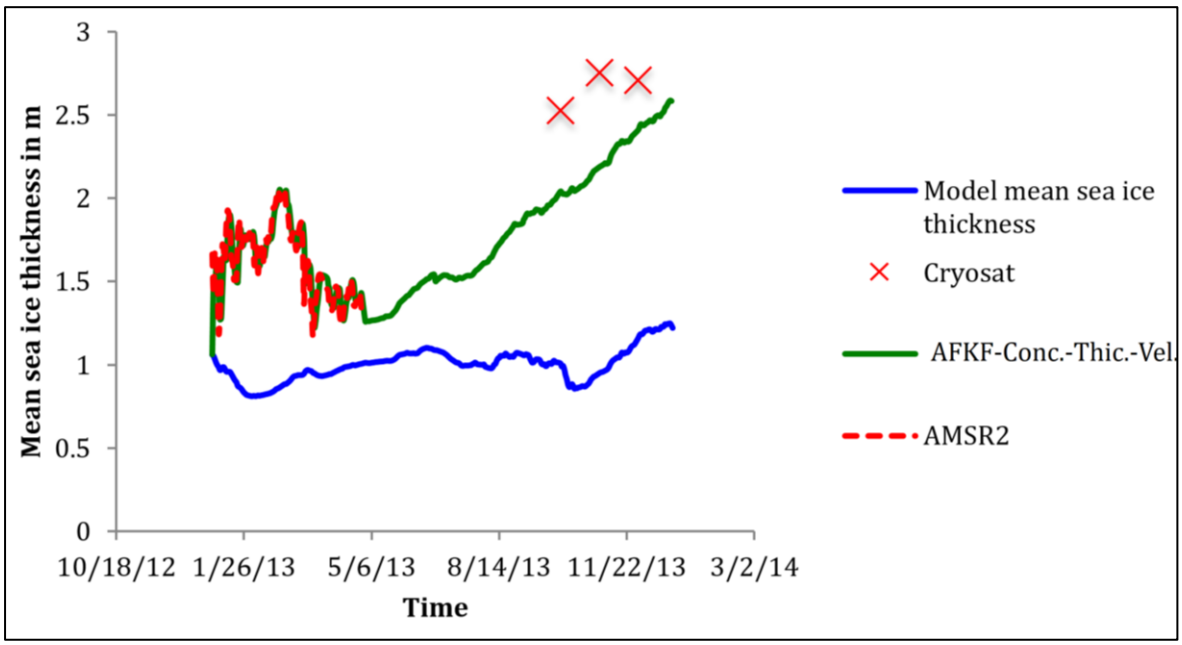

Figure 6-24: Mean sea ice thickness in the polar area (figure 5-4) from model, AMSR2 observation, cryosat observation and AFKF-Conc-Thic-Vel experiment.

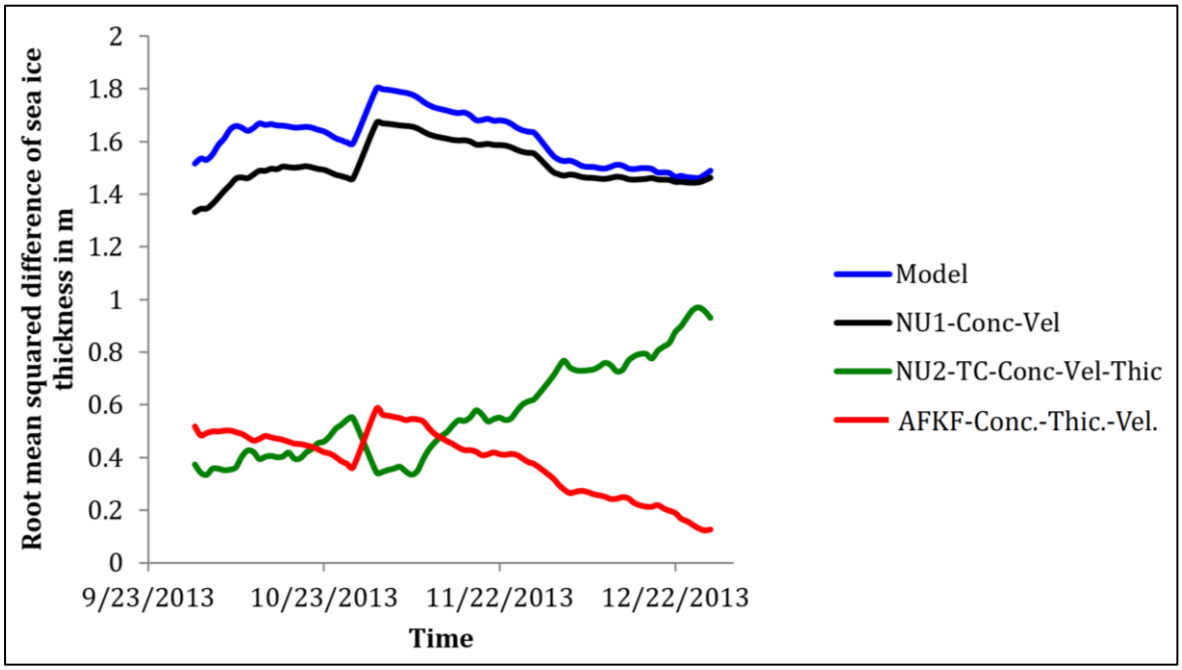

Figure 6-25: Root mean squared difference of sea ice thickness in the polar area

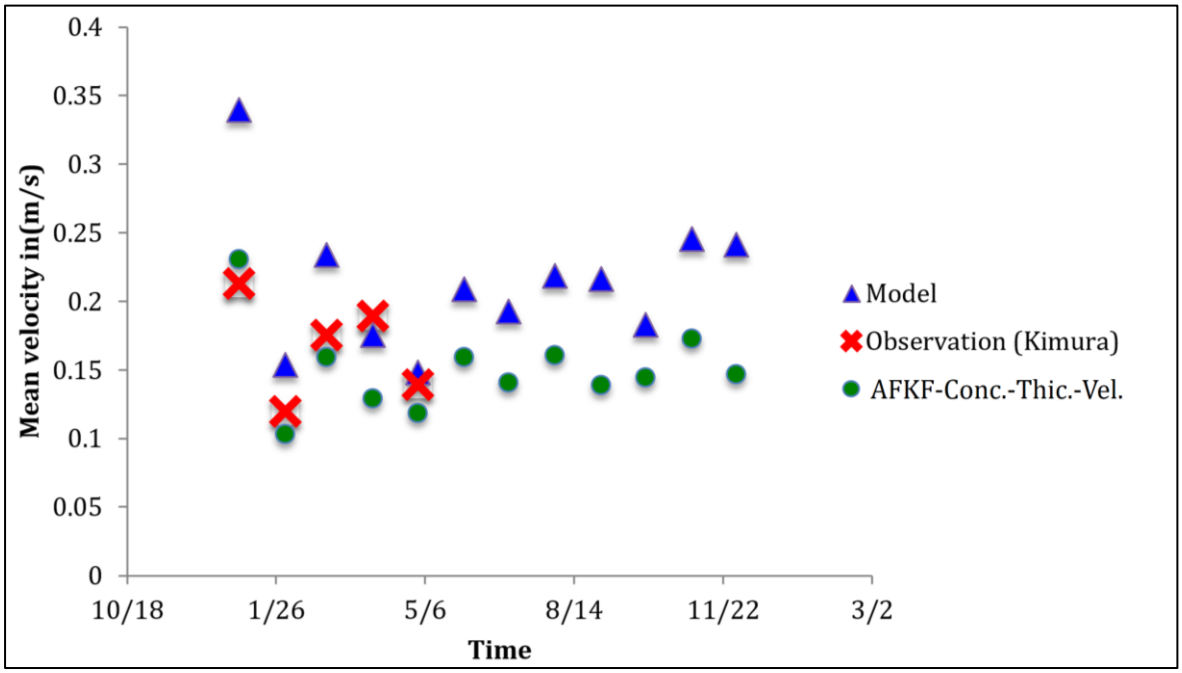

Figure 6-26: monthly mean sea ice velocity magnitude from model, Kimura observation data set and AFKF-Conc-Thic-Vel experiment in m/s in polar area (figure 5-4

7. Validation of assimilation

This chapter evaluates the effectiveness of different assimilation techniques and presents their local effect.

7.1 Local impact of assimilation

Sea ice thickness in the polar area is examined. Selected area is presented in figure 7-1. This area is an important area for Arctic Sea Route with a higher political interest in navigating along the North Pole where no country holds the geographical ownership. Furthermore, part of ASR falls along the Canadian Archipelago.

One of the issues with the whole Arctic model predictions is that sea ice thickness is under predicted in the polar area. Figure 7-2 compares sea ice thickness in the area using different methods while figure 7-3 presents the root mean squared difference between sea ice thickness from different methods and independent Cryosat sea ice thickness data set.

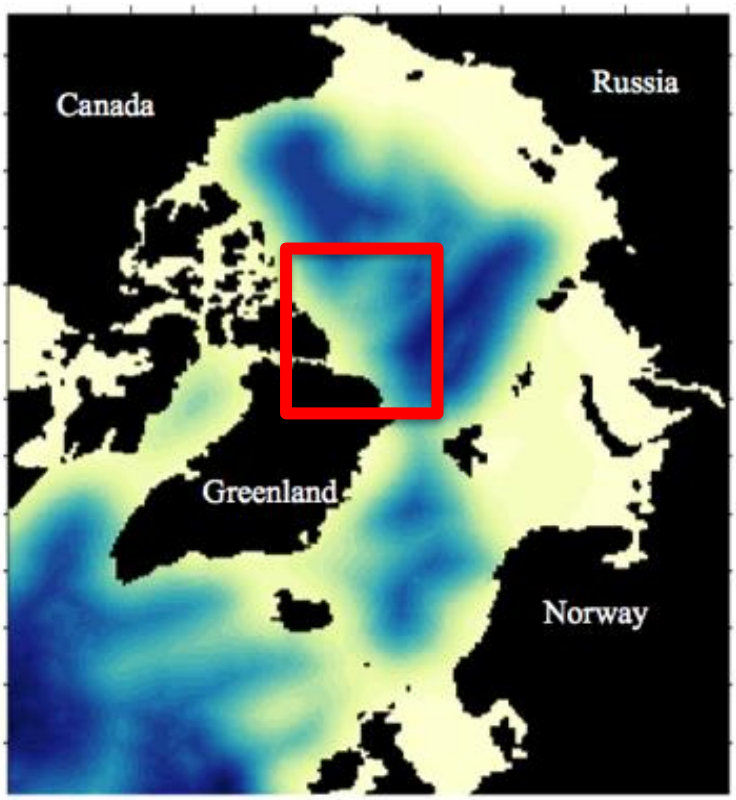

Figure 7-1: Polar area used for comparison

There are disparities between AMSR2 sea ice thickness data set and cryostat data set. However, cryostat data is considered to be more accurate with an overall standard deviation close to 14cm where AMSR-2 sea ice thickness data set has an overall standard deviation of 15-42cm. Hence Cryosat data is used in calculating root mean squared error.

According to figure 7-3 all the assimilation experiments have improved sea ice thickness estimation in polar area compared to the model with time. Nudging method with time constant and nudging-2 methods shows the common flaw of many existing data assimilation approaches by over estimating sea ice thickness in the area.

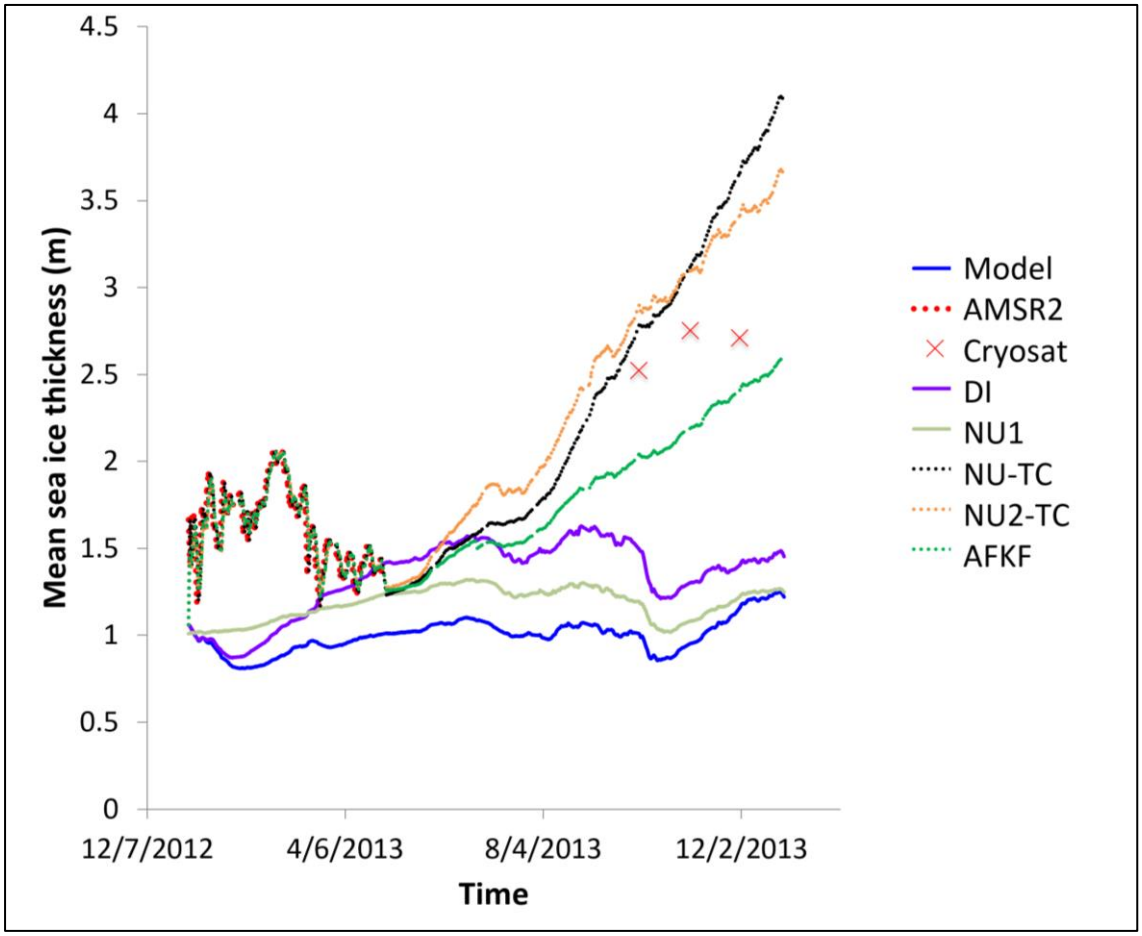

Figure 7-2: Comparison of mean sea ice thickness in the polar area(figure 7-1) from different assimilation methods; direct insertion, nudging1, nudging 2, nudging with time constant, atmospheric forcing Kalman filter method, model, Cryosat observations and AMSR 2 observations

In nudging method with time constant (NU-TC-Conc-Thic-Vel), the observation error is not considered. Therefore, the nudging weight is 1. In nudging-2 method, the nudging weight is formulated according to equation 3-8. The term $|C_{obs} + C_{bias} - C_{model}|$ in equation 3-8 accounts for the observation bias. However, bias is insignificant compared to the difference between observation and the model estimate. Therefore, in equation 3-8 the term $|C_{obs} + C_{bias} - C_{model}|$ is the dominating term that drives nudging weight closer to 1. When the nudging weight is close to one, rapid alterations occur in the model. Thereby affecting the accuracy of the estimate.

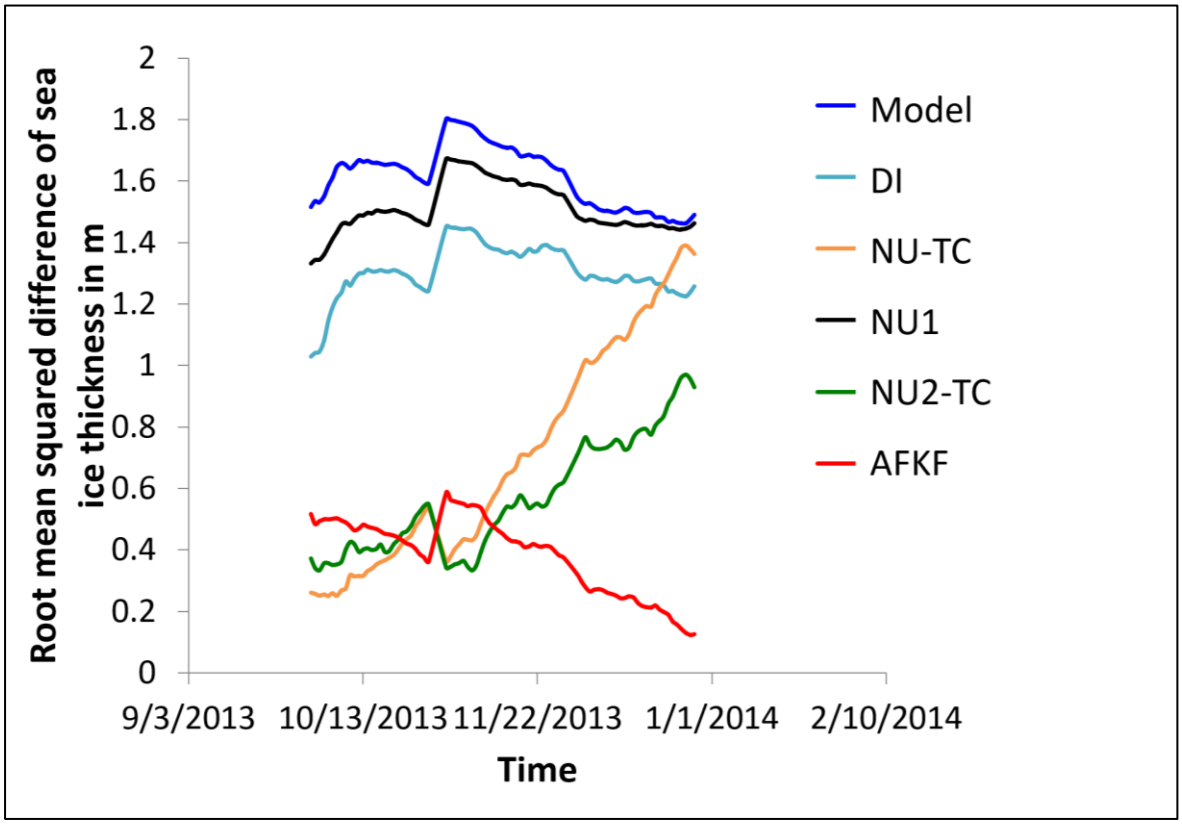

Figure 7-3: Comparison of root mean squared difference of mean sea ice thickness in the polar area(figure 7-1) between cryostat dataset and other datasets; model free run, direct insertion, nudging1, nudging 2, nudging with time constant and Atmospheric forcing Kalman filter method from October to December

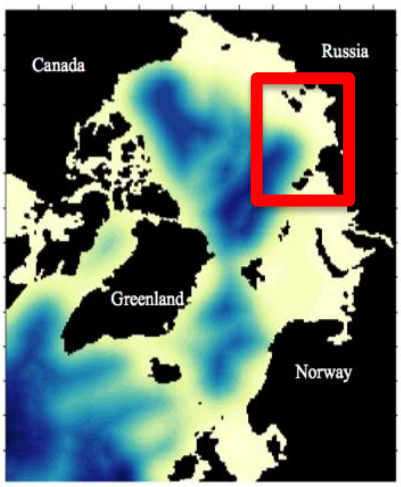

Figure 7-4: Laptev Sea area that is used for comparison is highlighted with a red square

According to table 7-1 and Figure 7-3 atmospheric forcing Kalman filter experiment makes a more accurate estimate with the lowest RMSD sea ice thickness in the polar area.

The area marked with a red square in figure 7-4 includes Laptev Sea. This area is also important as a part of ASRs. Figure 7-5 compares sea ice extent in this area while figure 7-6 presents the RMSD between sea ice extent from each method and AMSR2 observations. It can be observed that the sea ice extent from all methods have improved compared to that of the model other than the direct insertion method and nudging 1 method. All the other methods well reproduce sea ice extent in the area. However, it should be noted that the AMSR2 observations also contains errors. This is reflected in atmospheric forcing Kalman filter method and Nudging-2 methods where the mean RMSD is not too low or too high as the other methods (table 7-1).

Direct insertion method and nudging method-1 do not use a time constant. Therefore, observations are introduced in a single time step. This leads to creating a shock in the system. All the other nudging methods use a time constant; hence they smoothly incorporate observation in to the model. This graph shows the importance of the time constant in nudging method.

Same can be observed with sea ice extent in the Barents Sea (figure 7-7). As presented in figure 7-8 all methods produce similar sea ice extent that is closer to observation. Sea ice edge lies in the Barents Sea.

Table 7-1: Comparison of different assimilation methods

Method comparison	Model free run	DI	NU-1	NU-TC	NU-TC-2	AFKF
Sea ice thickness(m) in polar area (RMSD with Cryosat data)	1.61	1.3	1.51	0.71	0.57	0.38
Sea ice extent ($km^{2)}$ in Laptev Sea (RMSD with AMSR2 data)	166,414	138,501	186,046	19,350	23,881	24,349
Sea ice extent ($km^{2)}$ in Barents Sea (RMSD with AMSR2 data)	164,030	31,191	33,070	22,212	27,430	34,632
Sea ice extent (million $km^{2)}$ in Whole Arctic region (RMSD with AMSR2 data)	1.28	0.13	0.15	0.16	0.31	0.33
Sea ice concentration estimation error standard deviation	N/A	N/A	N/A	N/A	N/A	Winter:0.056 Summer:0.078
Sea ice thickness estimation error standard deviation	N/A	N/A	N/A	N/A	N/A	Winter:11cm

Computational hours required for 1-year computation	518	547	576	633	662	6048
Cores used for computation	12	12	12	12	12	84

In this area observation error is higher than in other areas. Therefore, sea ice extent in the area is not the same as in AMSR2 observations.

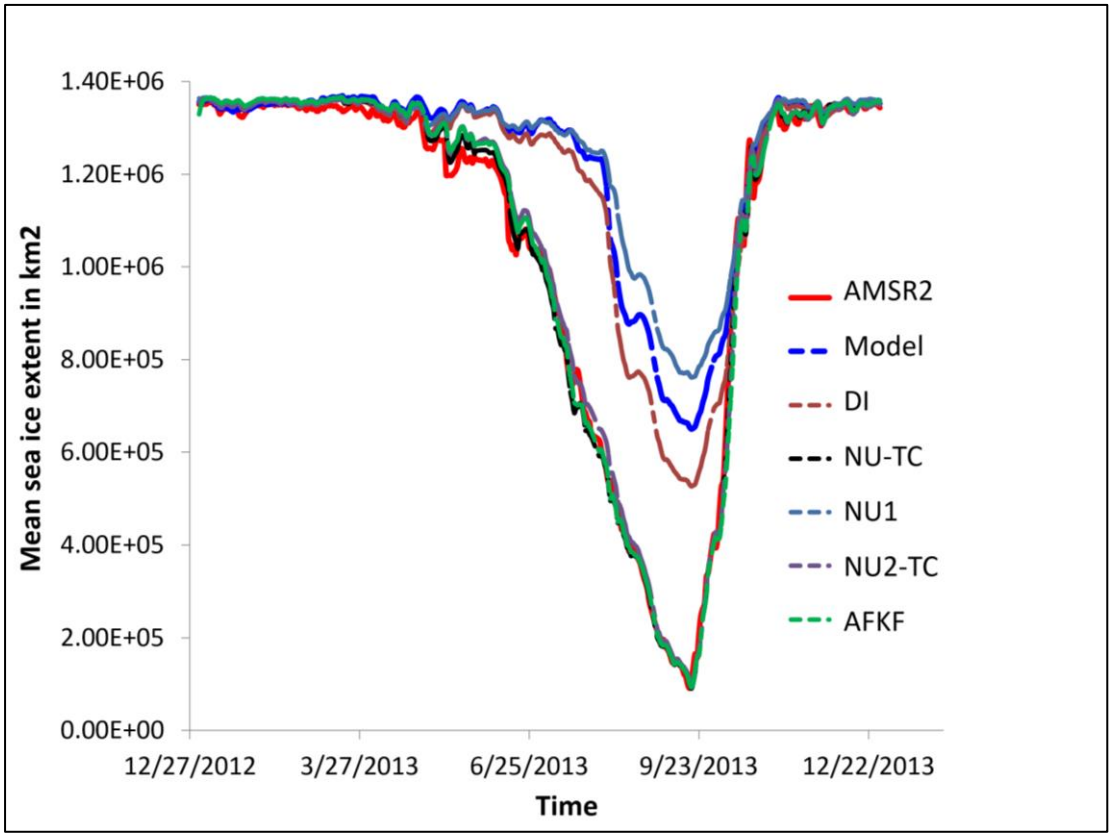

Figure 7-5: Comparison of sea ice extent in Laptev Sea area (figure 7-4) from different assimilation methods

According to mean RMSD values presented in table 7-1 and figure 7-9, Atmospheric forcing Kalman filter method, NU-1 and NU-TC-2 methods consider the bias of observation therefore having a slightly higher RMSD compared to other methods such as DI and NU-TC.

Changes in salinity are observed as a result of assimilation experiments. This is specifically highlighted in the areas where there is a significant sea ice extent difference between the model and the assimilation (figure 7-10 and 7-11).

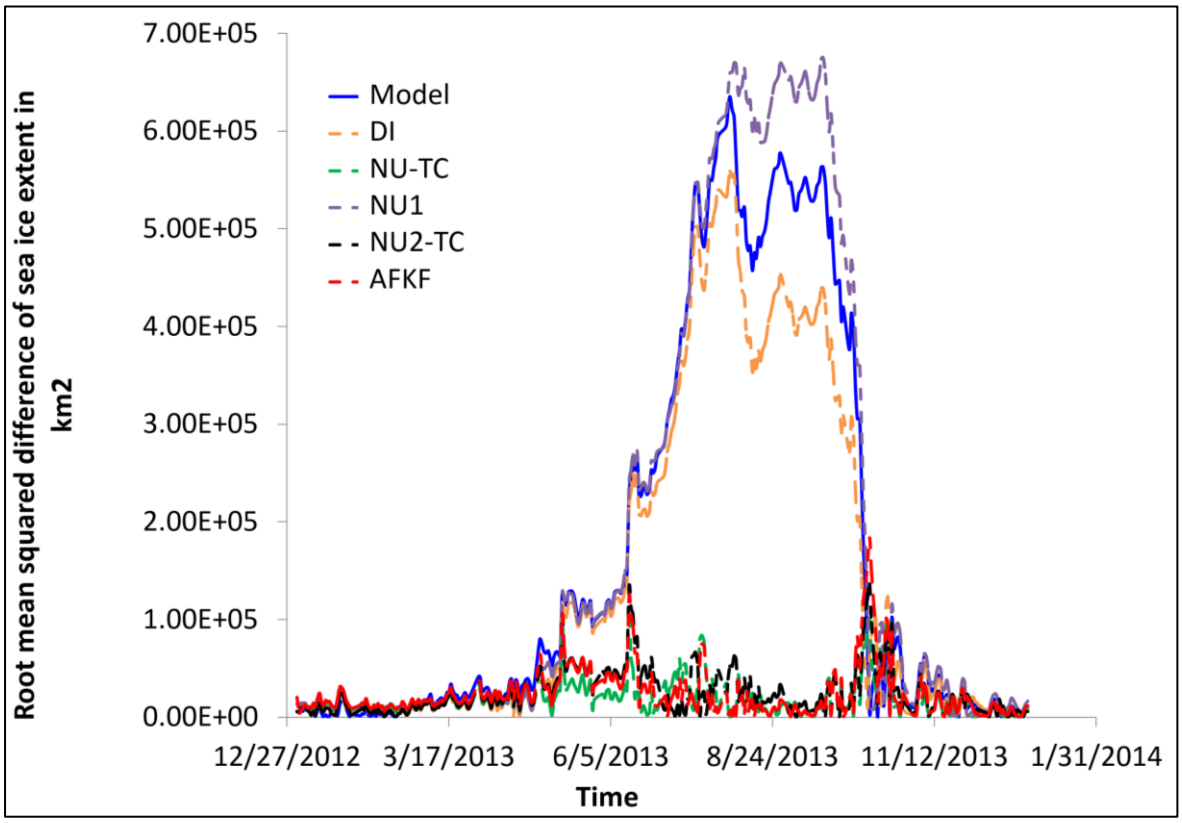

Figure 7-6: Comparison of root mean squared difference of mean sea ice extent in the Laptev Sea area (figure 7-4) between AMSR2 dataset and other datasets; model free run, direct insertion, nudging1, nudging 2, nudging with time constant and Atmospheric forcing Kalman filter method

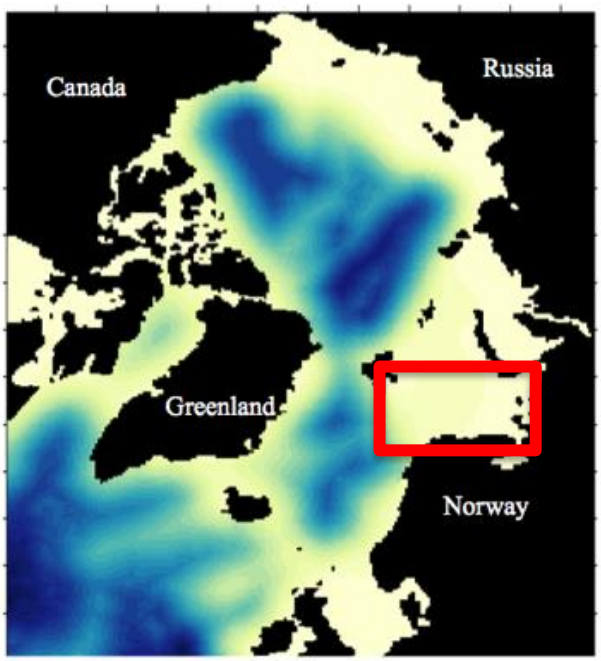

Figure 7-7: Area that includes Barents Sea that is used for comparison is highlighted with a red square

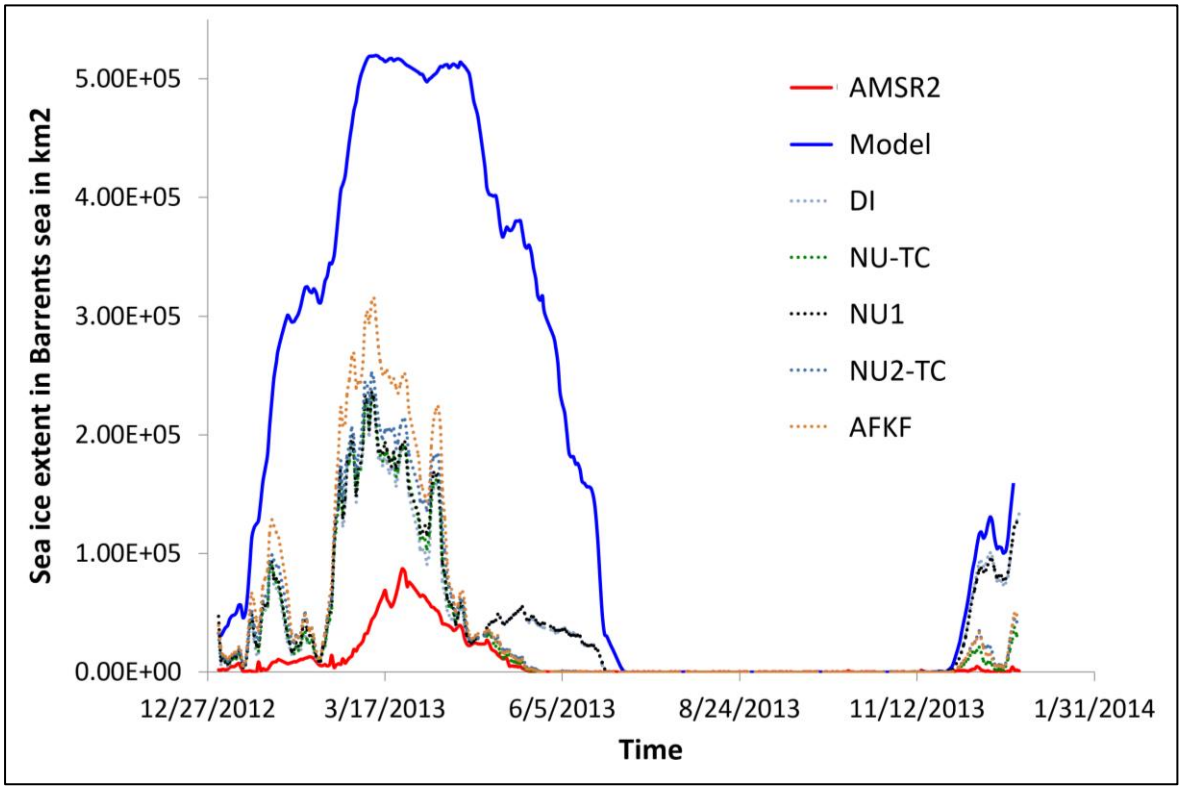

Figure 7-8: Sea ice extent in Barents Sea (figure7-5) from different assimilation methods, model and AMSR2 observations

There are two possible reasons for the rise in sea surface salinity. When the sea ice is removed as a correction done by assimilation, freshwater is being removed as a result. This is the reason where the salinity difference is highlighted in areas like Barents Sea where there are disparities between model sea ice extent and AMSR2 sea ice extent.

For the same reason the SSS bias becomes a maximum in summer. In the model with no assimilation sea ice melts in summer and therefore sea surface salinity is low in summer but in the assimilation, there is no ice to melt hence the bias is larger in summer. Another reason for the rise in SSS is evaporation. When there is open ocean, surface albedo is about 0.06 where in sea ice the value can vary between 0.5-07. Therefore, more heat is absorbed by the ocean and freshwater is evaporated increasing the salinity in those areas. Effect of salinity extends beyond the surface vertically due to the corrections that are done to inner ocean as presented in figure 7-12 and 7-13.

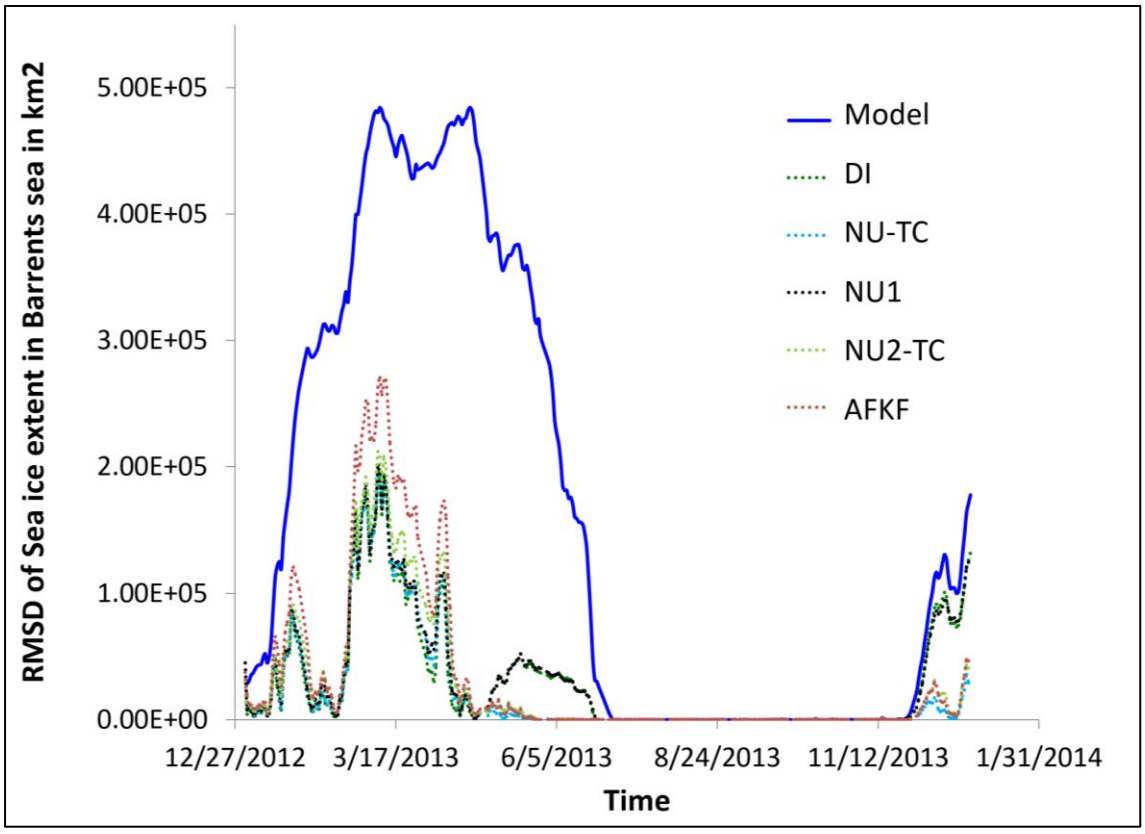

Figure 7-9 Comparison of root mean squared difference of mean sea ice extent in the Barents Sea area (figure 7-7) between AMSR2 dataset and other datasets; model free run, direct insertion, nudging1, nudging 2, nudging with time constant and Atmospheric forcing Kalman filter method

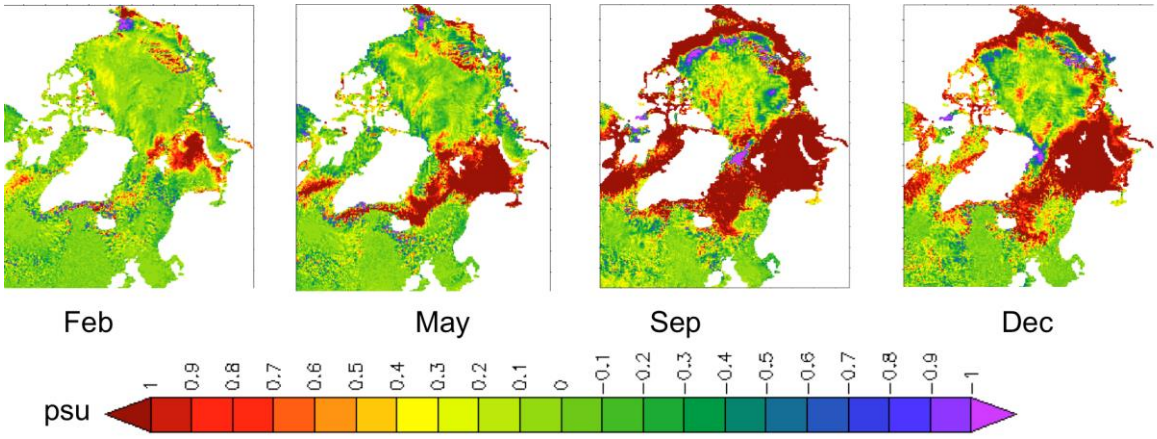

Figure 7-10: Sea surface salinity bias(AFKF assimilation SSS-model SSS) in different months

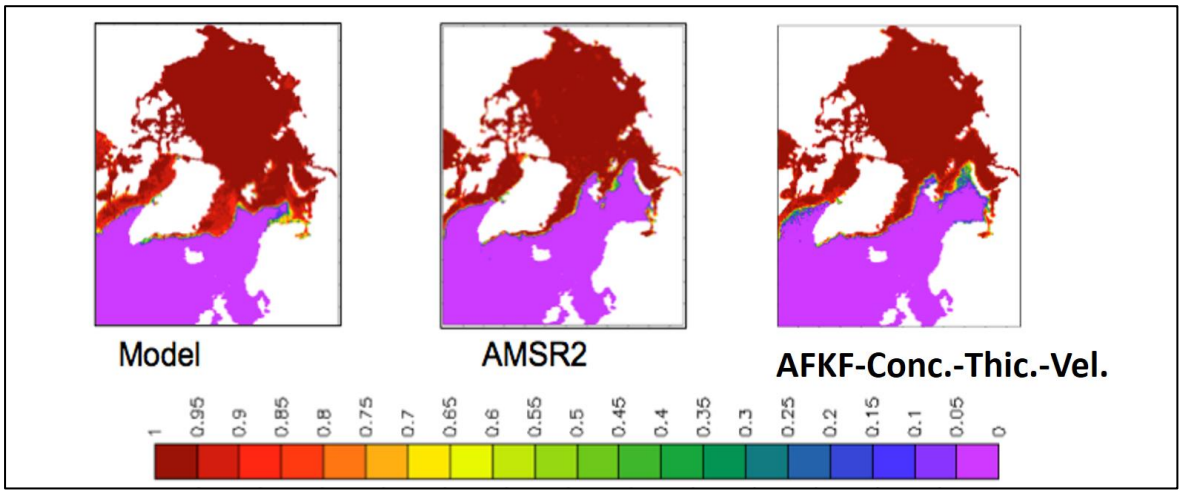

Figure 7-11: Comparison of sea ice extent in February from Model, AMSR2 and AFKF assimilation

7.2 Overall impact of assimilation

As presented in chapter 4, 5 and 6, sea ice extent in the entire whole Arctic model is improved by the assimilation. Figure 7-14 compares the sea ice extent from all the methods while figure 7-15 presents the RMSD of sea ice extent between different methods and AMSR2 observations. Overall all the methods show similar skills of reproducing sea ice extent in the whole Arctic region. However according to figure 7-15 and table 7-1, methods that introduce bias in observation such as AFKF, NU-2 and NU-1 show slightly higher mean RMSD.

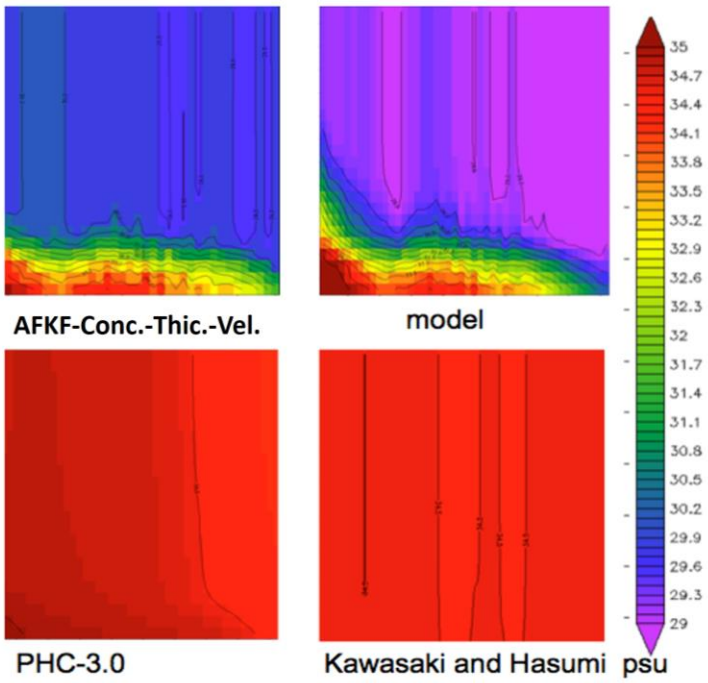

Figure 7-12: Vertical profile of ocean salinity in March AFKF-Conc-vel-thic (top-left) model(top-right) PHC3.0 (bottom-left) Kawasaki and Hasumi salinity (bottom-right)

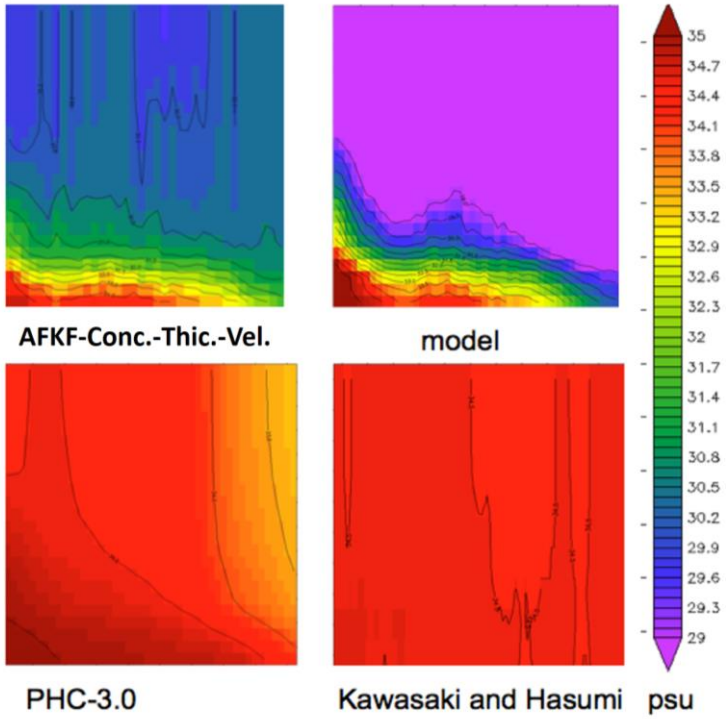

Figure 7-13: Vertical profile of ocean salinity in September AFKF-Conc-vel-thic(top-left) model(top-right) PHC3.0 (bottom-left) Kawasaki and Hasumi salinity (bottom-right)

Another set of experiments are performed to see the predictability of model once the assimilation is relaxed. In these experiments sea ice concentration is assimilated for 6 months. Sea ice thickness and sea ice velocity are assimilated for four months and the assimilation is relaxed after six months.

Figure 7-16 presents the sea ice extent from the experiments that are relaxed six months after assimilation. All methods are able to reproduce observed sea ice extent more accurately than the model. Until one month after relaxation, all experiments well reproduce observations.

Figure 7-17 presents sea ice thickness in December after one year assimilation run. They are compared with cryosat sea ice thickness data and the model.

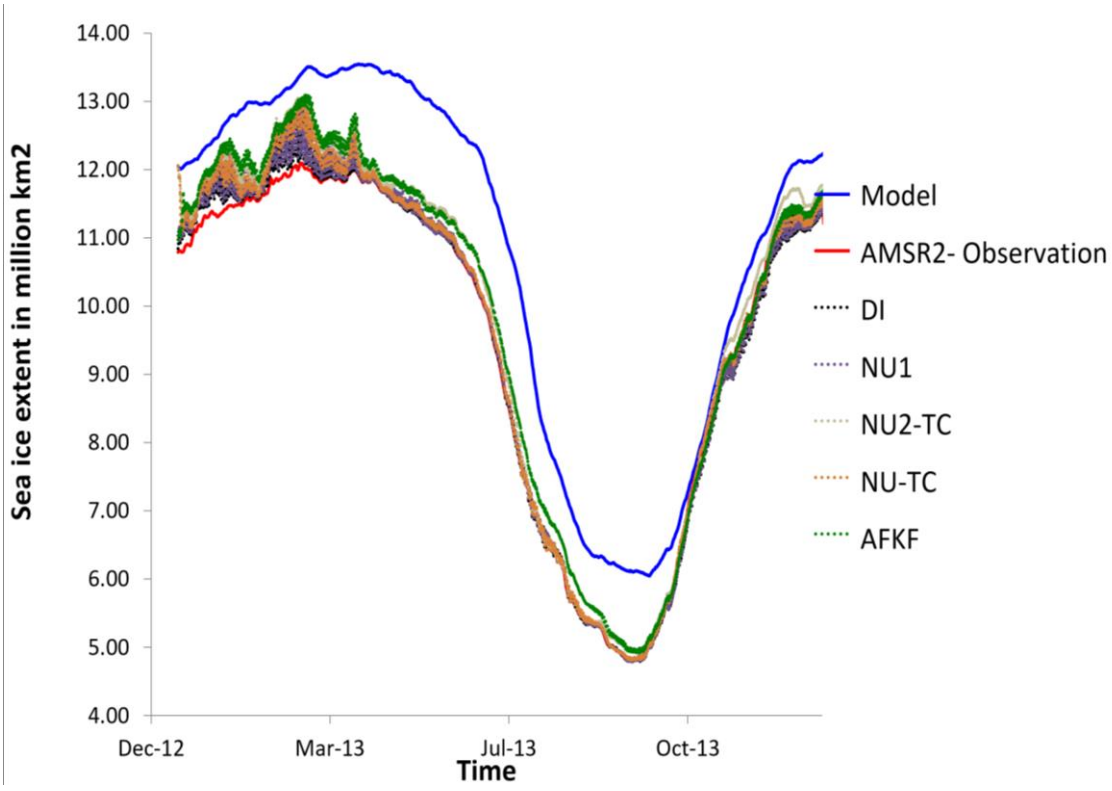

Figure 7-14: Sea ice extent from different assimilation methods, model and observation

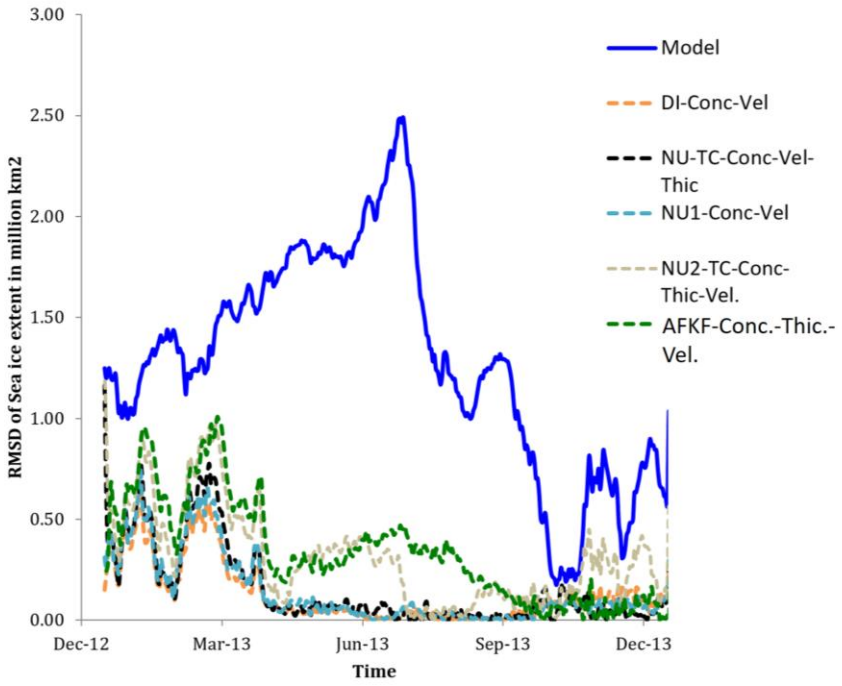

Figure 7-15: Comparison of root mean squared difference of mean sea ice extent in the whole Arctic region between AMSR2 dataset and other datasets; model free run, direct insertion, nudging1, nudging 2, nudging with time constant and Atmospheric forcing Kalman filter method

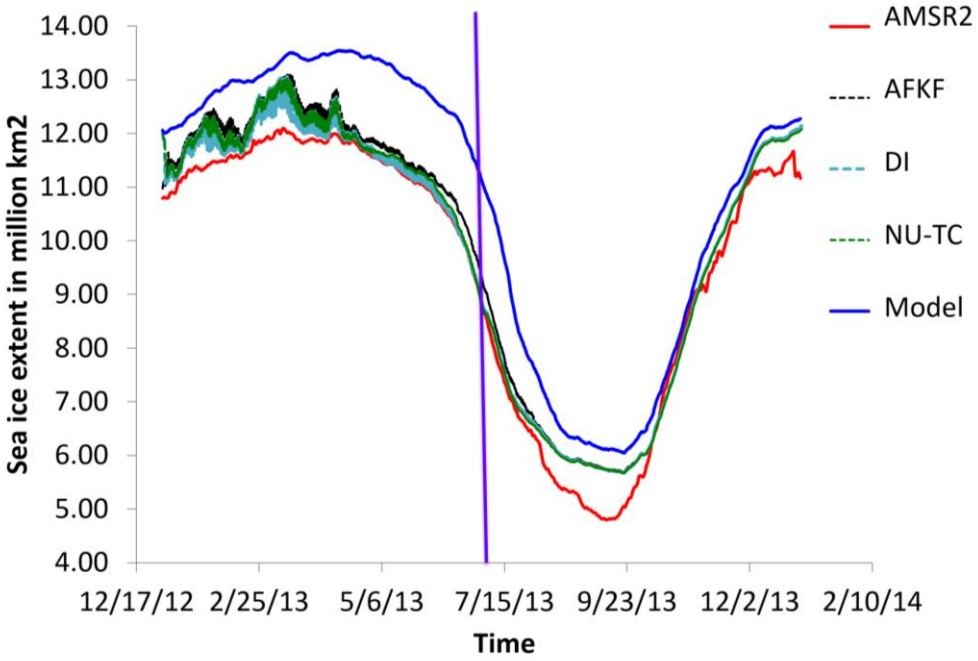

Figure 7-16: Time evolution of total sea ice extent from AMSR2 satellite observation, model prediction, assimilation experiments using different methods that relaxed the assimilation after 6 months. Purple vertical line indicates the time that relaxed the assimilation

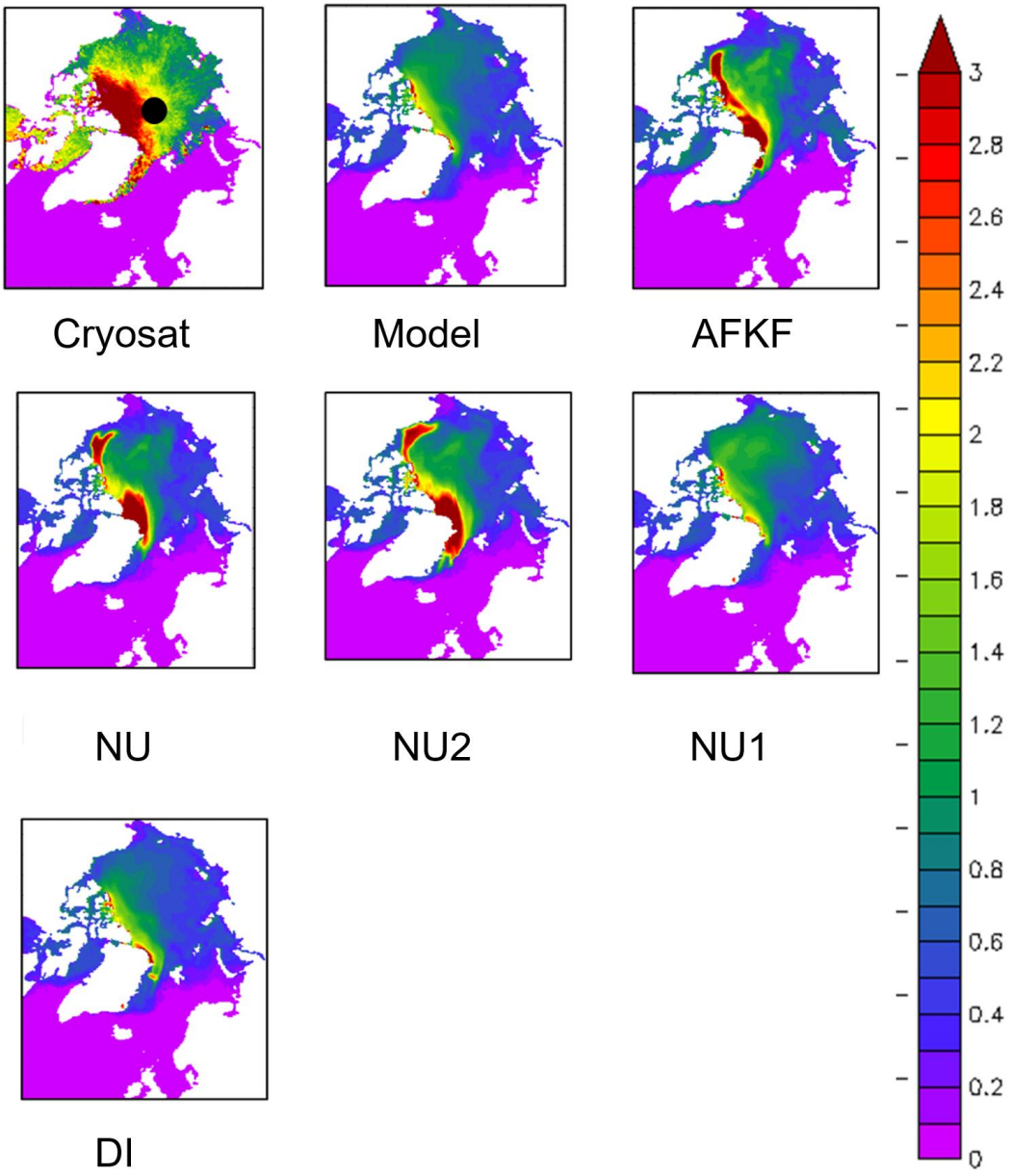

Figure 7-17: Sea ice thickness distribution in December from different assimilation methods, model and Cryostat observation (data not available is in black)

It can be clearly seen that sea ice thickness distribution is improved with assimilation compared to the model. Sea ice thickness from AFKF method is comparable with the cryosat sea ice thickness. NU-TC and NU-TC-2 methods also produce sea ice thickness that is comparable to the cryosat sea ice thickness. However according to figure 7-2 the sea ice thickess near the pole is overestimated from those two methods.

Sea surface temperature is also affected by the assimilation. As already explained in section 2.5.4, model under estimates sea surface temperature in marginal areas due to overprediction of sea ice extent. This has been improved as a result of improved sea ice extent according to figure 7-18. When there is open ocean, surface albedo is about 0.06 where in sea ice the value can vary between 0.5-07. Therefore, more heat is absorbed by the ocean with the absence of sea ice and the sea surface temperature rises as a result

In chapter 4, an experiment is performed to investigate how the assimilation time interval affects the lead time of the assimilation. In the first experiment assimilation is relaxed after four months of assimilation. In the second experiment assimilation is relaxed after six months. Running through the melting season improves the accuracy of sea ice extent considerably according to figure 4-18. Even after the assimilation is seized, the model produces results that are closer to observation.

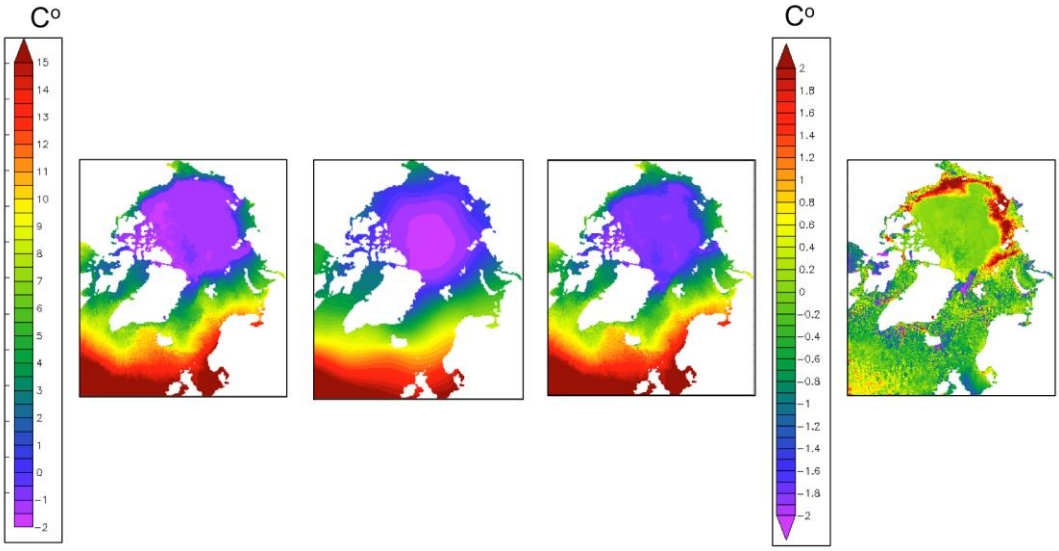

Figure 7-18: Sea surface temperature distribution in September from left model, PHC3.0,AFKF-Conc-Vel-Thic, and temperature difference(Assimilation-model) respectively

This could be explained by the figure 7-18. It can be observed that the sea surface temperature is increased in the marginal areas due to removal of sea ice in the marginal areas by the assimilation. This elevated temperature is a result of low surface albedo in the ocean where sea ice is removed. This increased sea surface temperature helps the model to retain the ice-free conditions even after the assimilation is seized. After 6 months assimilation, this elevated sea surface temperature continues to rise with the increased atmospheric temperature in the summer

7.3 Comparison of assimilation methods

Performance comparison of different assimilation methods are presented in this section. Several factors are taken in to account. Local representation of sea ice thickness, sea ice extent, estimation accuracy and computational economy are some factors considered. They are presented in table 7-1.

As already discussed in previous two sections, local sea ice thickness in the polar reigion is accurately presented by the atmospheric forcing Kalman filter method. It also fairly estimates overall sea ice extent as well as local sea ice extent considering the observation error. Another advantage of using the atmospheric forcing Kalman filter is computing the error covariance of estimate error (thereby providing information such as standard deviation), which cannot be done with the other methods. It should also be noted that atmospheric forcing Kalman filter method requires additional computational power which is about 10 times higher than the other methods.

Nudging method-2 is also effective in making sea ice extent and sea ice thickness estimations both locally and in the whole Arctic region. The method overestimates sea ice thickness in some areas, which is considered to be a common flaw in data assimilation of sea ice variables. This method can be considered as a computationally economical method to estimate sea ice conditions with a fair accuracy.

Nudging method 1 and direct insertion method is effective in predicting overall sea ice extent however it is not very effective in predicting local sea ice thickness and sea ice extent.

8. Regional model

The whole Arctic model with 25km resolution cannot be used to investigate the fine details of sea ice dynamics such as ice edge positions and extents accurately for applications such as navigation in ASRs. Therefore, regional models are required for those applications. Figure 8-1(b) consists of the area with 50E:165E longitude and 68N:85.5N latitudes. The region consists of Laptev Sea, part of Kara and East Siberian Seas.

The basic mechanisms of the model used in these high-resolution computations are same as those used in whole Arctic computation. The resolution of zonal and meridional directions are set to be about 2.5km×2.5km in horizontal plane and 33 sigma layers in the vertical direction. Initial ice, ocean conditions and boundary conditions are given by the output of the whole Arctic AFKF-Conc.-vel.-thick assimilation.

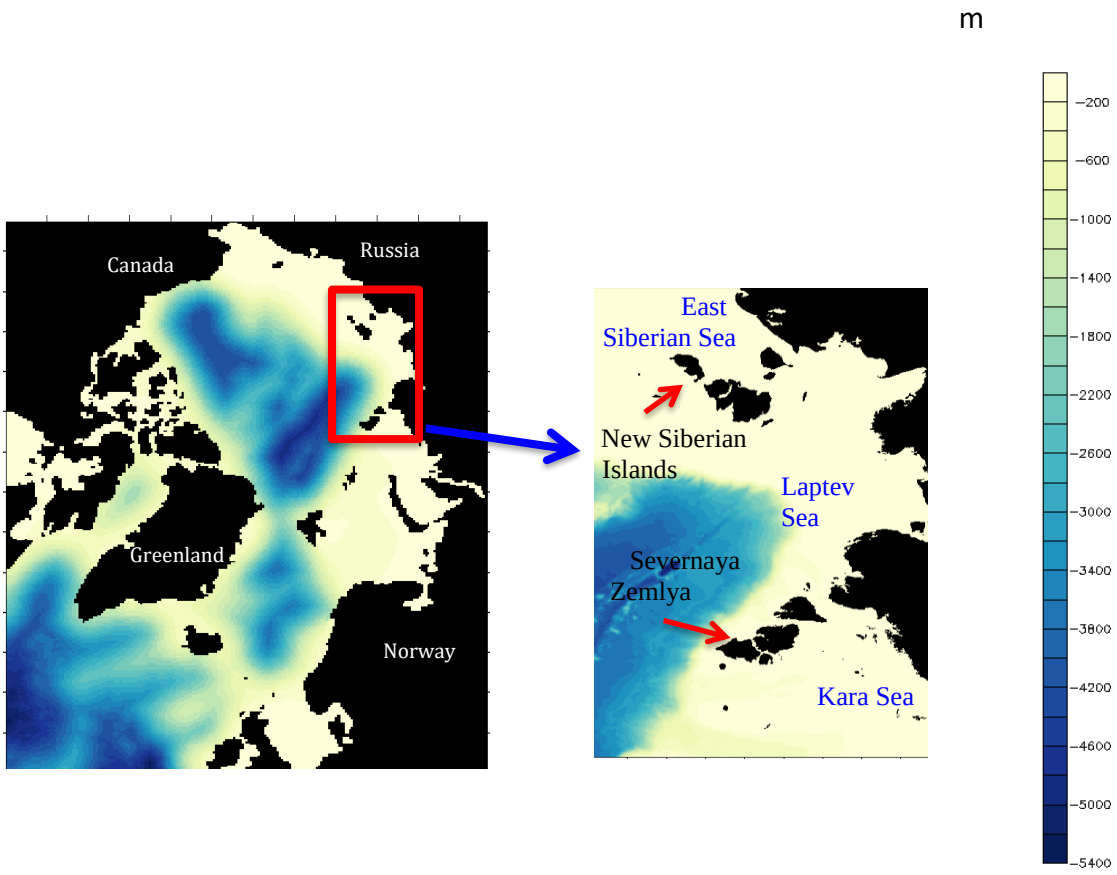

Figure 8-1: (a) Whole Arctic coarse model on left (b) regional model on right

The atmospheric forcing is taken from ERA interim data and NCEP data same as whole Arctic model. In the marginal regions of model domain, radiation boundary condition is applied and in coastal regions no-slip boundary condition is adopted.

For the regional model incremental analysis update method discussed in section 3-4 and Lindsay (2006) nudging method are used. Only AMSR2 sea ice concentration data is used in assimilation since other data sets aren't reliable in summer. Regional model run starts at the end of August (28th August 2013) and runs until the end of freezing season (November 2013).

Figure 8-3 compares sea ice extent from the regional model run, regional NU-TC-Conc assimilation run, Regional nudging-1 assimilation run, 25km AFKF-Conc.-Vel.Thic assimilation run, 25km model run and AMSR2 observations. One of the issues mentioned in De Silva (2013) PhD thesis is that the regional model isn't creating adequate ice in the freezing season (figure 8-2) as mentioned in section 2.5.4.

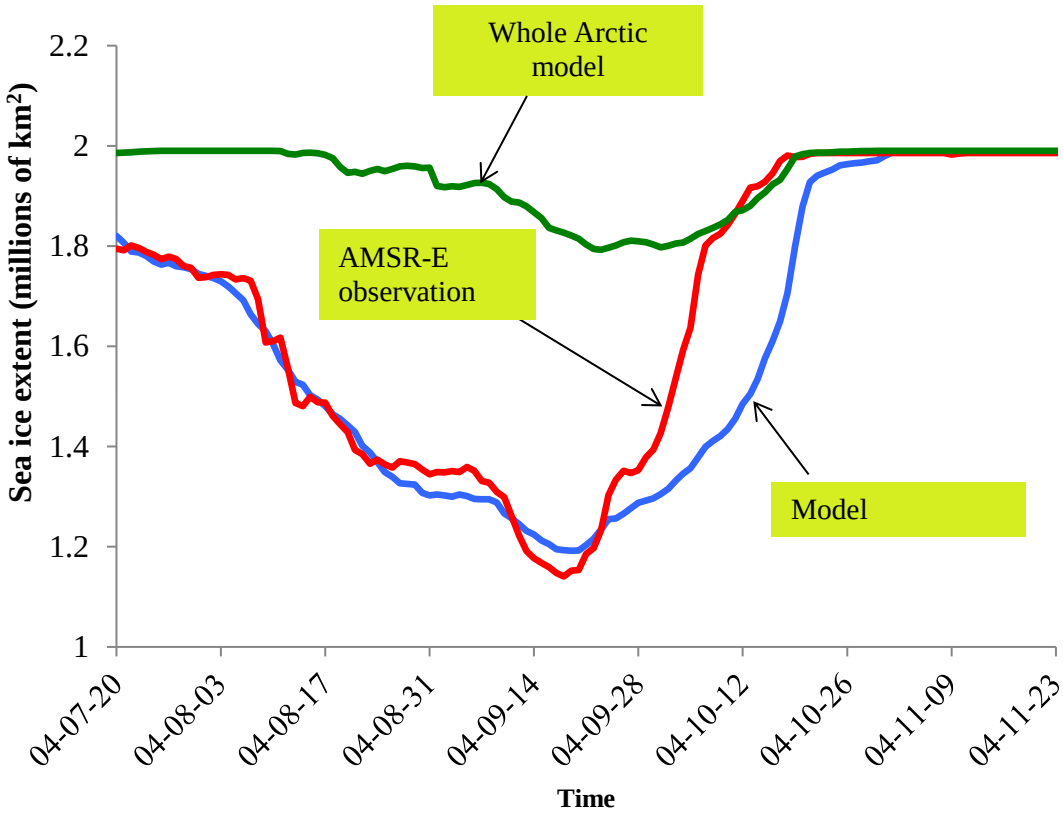

Figure 8-2: Comparison of sea ice extent from regional model run, 25km model and AMSR-2 observation. (De Silva 2013)

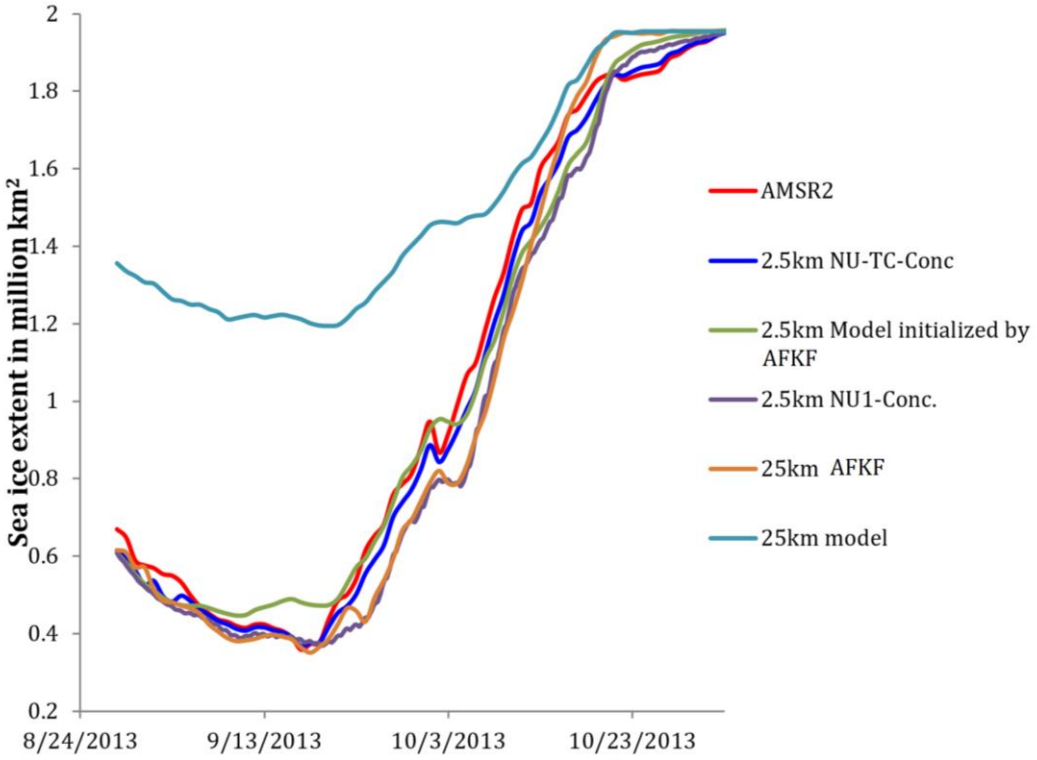

Figure 8-3: Comparison of sea ice extent from regional model run(initialized by AFKF-Conc-Vel-Thic), regional NU-TC-Conc assimilation, regional NU1-Conc assimilation, 25km AFKF-Conc-Vel-Thic, 25km model and AMSR-2 observation.

According to figure 8-3 and 8-4 it's clear that the regional model initialized by whole Arctic AFKF-Conc.-Vel-Thic assimilation can reproduce sea ice extent that is in line with observations. It can also be observed that 25km assimilated coarse model can also reproduce sea ice extent with enough accuracy. Regional IAU assimilation sea ice extent well reproduces AMSR2 sea ice extent.

However, it must be noted that AMSR2 sea ice concentration data set contains higher error in summer. The error is greater in the area used in regional model, which focuses on ice edge area. Therefore, regional model that uses nudging method-1 incorporating observation error under predicts sea ice extent compared to the other regional model computations.

According to figure 2-11 taken from De Silva (2013), the maximum bias between regional model and AMSR-2 observation is about 0.4 million km^2 however, the bias from the regional model (figure 8-3 green line) is about 0.13 million km^2 in the freezing season. The

value is lower for regional model assimilation experiments. Ice edge produced by regional model is presented in figure 8-3.

Sea ice edge is well represented in both regional model initialized by the AFKF assimilation and the regional model assimilation.

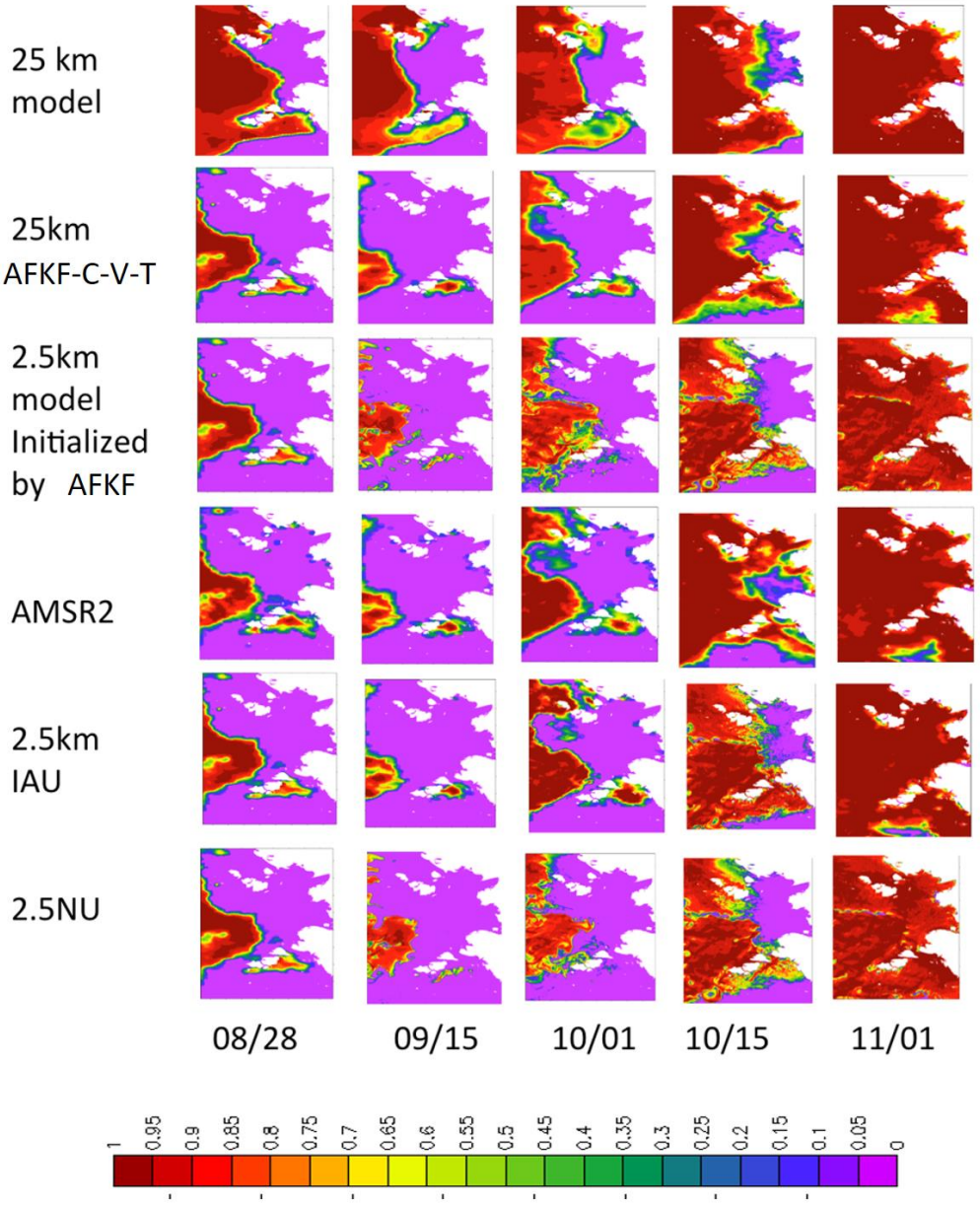

Figure 8-4: Comparison of sea ice concentration from regional model run(initialized by AFKF-Conc-Vel-Thic), regional NU-TC-Conc assimilation, regional NU-Conc assimilation, 25km AFKF-Conc-Vel-Thic, 25km model and AMSR-2 observation

9. Conclusions and Future work

This study is a first attempt to implement a data assimilation system to ice-POM model. In this study data assimilation is introduced to ice-POM model with the aim of accurately predicting short-term sea ice distribution along the NSRs.

Sea ice concentration, sea ice thickness and sea ice velocity are assimilated in the study.

Assimilating sea ice variables improved ocean and ice conditions as expected. It is evident from the changes in sea ice extent, sea ice thickness, ocean temperature and ocean salinity. Non-assimilated sea ice variables have also been indirectly improved by assimilation. Improvements in sea ice variables are emphasized in the Barents Sea and near the pole.

Sea ice thickness is improved near the pole as a result of decreased sea ice velocity near the pole. Sea ice extent is improved in the whole domain with assimilation. Atmospheric forcing Kalman filter and introducing a time constant have led to less assimilation shock compared to direct insertion method.

It can be observed that sea surface salinity is altered in the places where sea ice concentration is improved. This is a result of correcting sea ice extent in over predicted areas where freshwater is being removed from the model and increased evaporation in open ocean areas. Sea surface temperature has also improved as a result of improved sea ice extent.

Compared to single variable assimilation, multiple variable assimilation produces more accurate results. Sea ice concentration assimilation improves the accuracy more effectively than sea ice thickness or sea ice velocity.

In addition to improving the accuracy of prediction, another aim of this study was to investigate the effect of different parameters that govern the effectiveness of data assimilation.

In the investigation of the impact of time interval, it was evident that daily assimilation produces results that are closer to observations throughout the year, while weekly and monthly-assimilation experiments produce results with adequate accuracy during the summer. This is favorable in real-time computations where observation data is not immediately available.

When observations are directly introduced into the model large fluctuations can be observed in the results. To minimize the shock and to improve the numerical stability, nudging time constant τ is introduced. Time constant in nudging experiments is proven to be effective in improving the quality of prediction. Initial fluctuations in sea ice extent have reduced when τ is introduced .

The impact of nudging weight was also investigated. Assimilated variables were close to the observations regardless of the size of nudging weight. However, the assimilated variables reached observations two months faster when the nudging weight was closer to 1 compared to the experiments that used nudging weight close to 0. It can be observed that it takes a longer time for the experiments with lower weight to reach observations. After this initial period, all the experiments produce similar results. Even though the assimilated variable is not considerably sensitive to the nudging weight, non-assimilated variables are sensitive to nudging weight, where the experiments that used larger nudging weight (close to 1) had improved the accuracy of non-assimilated variables more than that of nudging weight close to 0.

AFKF method produces better sea ice thickness compared to nudging methods and direct insertion method in the polar area. With AFKF method it is also possible to determine the error covariance of estimate error (thereby providing information such as standard deviation), which cannot be done with the other methods. However, the computational power required for the assimilation is about 10 times higher than the nudging and direct assimilation methods. Nudging method-2 is ahead of other nudging methods and direct insertion method in terms of the accuracy of local sea ice extent and sea ice thickness predictions using lower computational hours.

The whole Arctic assimilation run is used to initialize regional model with 2.5km resolution. Regional model initialized by the whole Arctic AFKF-Conc.-Vel-Thic assimilation can reproduce sea ice extent that is in line with observations. Specifically, accuracy has been improved in the freezing season. Regional model assimilation has further improved the prediction of the ice extent.

Overall in one-year span data assimilation improves the predictability of Ice-POM model. It also enhances the accuracy of regional model predictions.

One of the limitation of this study is providing accurate boundary conditions for ocean variables. Even though, ocean salinity and temperature observations are available ocean velocity observations are infrequent. Further study can be performed on how to set more accurate ocean velocity. This could be extended to include assimilating ocean variables.

In this study, investigation was limited to one-year assimilation run. Further study should be done to further investigate long-term effect of data assimilation on the accuracy of predictions.

The model used for computations consists of one sea ice thickness category. This could be improved by introducing more sea ice thickness categories in to the ice model. Since assimilation imposes corrections to sea ice thickness, sea ice concentration and sea ice velocity, introducing more sea ice thickness categories will increase the effectiveness of assimilation model.

References

Bennett, A. F. (1992). *Inverse methods in physical oceanography.* Cambridge university press.

Bloom, S. C. (1996). Data assimilation using incremental analysis updates. . *Monthly Weather Review, 124*(6), 1256-1271.

Caya A., M. B. (2010). Analysis and forecasting of sea ice conditions with three-dimensional variational data assimilation and a coupled ice-ocean model. *Journal of Atmospheric and Oceanic Technology, 27*, 353-369.

De Silva, L. W. (2013). *Ice-ocean coupled computations for the sea ice prediction to support ice navigation in the Arctic Ocean.* Tokyo: The University of Tokyo .

De Silva, L. W. A., Mudunkotuwa, D. Y., & Yamaguchi, H. (2016). Short-term sea ice prediction for ice navigation in the Arctic sea routes using TIGGE data. In Final Symposium on GRENE-Arctic Climate Change Research Project (pp. 3-4).

Efimova, N. A. (1961). On methods of calculating monthly values of net longwave radiation (in Russian) . Meteorol. Gidrol , 10, 28-33.

Evensen, G. (2009). *Data Assimilation: The ensemble Kalman filter.* Bergen, Norway: Springer.

Evensen, G. J. (1994). Sequential data assimilation with a nonlinear quasi-geostrophic model using Monte Carlo methods to forecast error statistics. *ournal of Geophysical Research: Oceans , 99*, 10143-10162.

Fujisaki, A. H. (2007). Improvement of short- term sea ice forecast in the southern Okhotsk Sea. *Journal of Oceanography* (63).

Haltiner, G. J. (1957). *Dynamical and Physical Meteorology.* McGraw-Hill.

Hunke E.C. (2001). Viscous–plastic sea ice dynamics with the EVP model: linearization issues. *Journal of Computational Physics, 170*, 8–38.

Ikeda, M. (2009). Mechanisms of the recent sea ice decay in the Arctic Ocean related to the Pacific-to-Atlantic pathway . *Influence of Climate Change on the Changing Arctic and Sub-Arctic Conditions* , 161-169.

Ikeda, M. J. (2003). Importance of Clouds to the Decaying Trend and Decadal Variability in the Arctic Ice Cover. *Japanese Meteorok Society Japan, 81*, 179-189.

Inoue, J., Enomoto, T., & Hori, M. E. (2013). The impact of radiosonde data over the ice‐free Arctic Ocean on the atmospheric circulation in the Northern Hemisphere. Geophysical Research Letters, 40(5), 864-869.

Inoue, J., Yamazaki, A., Ono, J., Dethloff, K., Maturilli, M., Neuber, R., ... & Yamaguchi, H. (2015). Additional Arctic observations improve weather and sea-ice forecasts for the Northern Sea Route. Scientific reports, 5.

Japan Aerospace Exploration Agency (JAXA). (n.d.). *National Snow and Ice Data Center*. Retrieved 01 21, 2016, from AMSR-E Instrument Description: https://nsidc.org/data/docs/daac/amsre_instrument.gd.html

Jun Ono, J. I. (2016, 02). The impact of radiosonde data on forecasting sea-ice distribution along the Northern Sea Route during an extremely developed cyclone. *Journal of Advances in Modeling Earth Systems*.

Kawasaki, T. a. (2015, 12 04). The inflow of Atlantic water at the Fram Strait and its interannual variability. *Journal of Geophysical Research: Oceans*.

Kimura N., A. N. (2016). Influence of winter sea-ice motion on summer ice cover in the Arctic. . *Polar Research [Online], 32*.

Krishfield, R. A. (2014). Deterioration of perennial sea ice in the Beaufort Gyre from 2003 to 2012 and its impact on the oceanic freshwater cycle. *Journal of Geophysical Research:Oceans , 119.2*, 1271-1305.

Laevastu, T. (1960). Factors affecting the temperature of the surface layer of the sea: A study of the heat exchange between the sea and the atmosphere, the factors affecting temperature structure in the sea and its forecasting. *Helsingfors*.

Lindsay R. W., a. Z. (2006). Assimilation of ice concentration in an ice-ocean model. Journal of Atmospheric and Oceanic Technology . *Journal of Atmospheric and Oceanic Technology, 23*, 742-749.

Lindsay R., H. C. (2012). Seasonal forecasts of Arctic sea ice initialized with observations of ice thickness. *Geophysical research letters, 39*(21).

Lindsay, R., Wensnahan, M., Schweiger, A., & Zhang, J. (2014). Evaluation of seven different atmospheric reanalysis products in the Arctic. Journal of Climate, 27(7), 2588-2606.

Lorenc, A. C. (1991). The Meteorological Office analysis correction data assimilation scheme. *Quart. J. Roy. Meteor. Soc*(117), 59-89.

Ludovic Brucker, M. I. (2014, 11). NASA Team 2 Sea Ice Concentration Algorithm Retrieval Uncertainty. *IEEE TRANSACTIONS ON GEOSCIENCE AND REMOTE SENSING, 52*.

McPhee, M. G. (2008). Revisiting heat and salt exchange at the ice-ocean interface: Ocean flux and modeling considerations . *Journal of Geophysical Research , 113*.

Mellor G, H. ,. (2002). A Generalization of a Sigma Coordinate Ocean Model and an Intercomparison of Model Vertical Grids. *Ocean Forecasting: Conceptual Basis and Applications*, 55-72.

Mellor, G. L. (2003, June). *Users guide for a three-dimensional, primitive equation, numerical ocean model.* Princeton University,.

Mudunkotuwa D.Y., D. S. (2015). Parametric study of assimilating sea ice concentration in a coupled ice-ocean model using nudging. *International Symposium on Okhotsk Sea & Sea Ice (Mombetsu-15 Symposium),*, *30*, pp. 64-67. Mombetsu, Hokkaido, Japan,.

Murray, F. W. (1967). On the Computation of Saturation Vapor Pressure . *Journal of Applied Meteorology , 6*, 203-204.

National Snow and Ice Data Center. (2015, 10). *arctic sea ice news*. Retrieved 02 2016, from nsidc.org: http://nsidc.org/arcticseaicenews/files/2015/10/monthly_ice_09_NH.png

NCAR Advanced Study Program. (n.d.). Retrieved 2016, from http://www.asp.ucar.edu/colloquium/1992/notes/part1/node125.html

Overland, J. E. (2013). When will the summer Arctic be nearly sea ice free? *Geophysical Research Letters*.

Parkinson, C. L. (1979). A large-scale numerical model of sea ice. . *Journal of Geophysical Research , 84*, 311.

Rheem C.K., Y. H. (1997). Distributed mass/discrete floe model for pack ice rheology computation. *Journal of Marine Science and Technology*, 101–121.

Rothrock, D. A. (2005). Arctic Ocean sea ice volume: What explains its recent depletion? . *Journal of Geophysical Research* , 110.

Sagawa, G. (2007). *Development of ice dynamic model that takes account of floe collision and its validation in numerical sea ice forecast in the Sea of Okhotsk. (In Japanese.).* Tokyo: University of Tokyo.

Sakov, P. C. (2012, August). TOPAZ4: an ocean-sea ice data assimilation system for the North Atlantic and Arctic. *Ocean Science, 8(4)*, 633.

Scott K. A., B. M. (2012). Direct assimilation of AMSR-E brightness temperatures for estimating sea ice concentration. *Monthly Weather Review, 140*(3), 997-1013.

Shimada, K. T. (2006). Pacific Ocean inflow: Influence on catastrophic reduction of sea ice cover in the Arctic Ocean. *Geophysical Research Letters*, 33.

Smagorinsky, J. (1963). General circulation experiments with primitive equations. *Monthly Weather Review, 91*, 99-164.

Steele M., M. R. (2001). PHC: a global ocean hydrography with a high-quality Arctic Ocean. . *Journal of Climate* .

Steele, M. W. (2008). Arrctic Ocean surface warming trends over the past 100 years . *Geophysical Research Letters* , 35.

Talagrand, O. a. (1987). Variational assimilation of meteorological observations with the adjoint vorticity equation. I: Theory. *Quarterly Journal of the Royal Meteorological Society*(113), 1311-1328.

Toyoda, T. A. (2011). Impact of the assimilation of sea ice concentration data on an atmosphere-ocean-sea ice coupled simulation of the Arctic Ocean climate. *SOLA, 7*, 37-40.

Wang, M. J. (2012). A sea ice free summer Arctic within 30 years: An update from CMIP5 models. *Geophysical Research Letters*.

Watanabe, E. (2013). Linkages among halocline variability, shelf-basin interaction, and wind regimes in the Beaufort Sea demonstrated in pan-Arctic Ocean modeling framework . *Ocean Modelling* .

Weathernews. (2008, January 08). *Toward the Arctic Ocean route support*. Retrieved 07 26, 2016, from https://weathernews.com/ja/nc/press/2008/080708.html

Wongittilin, S. J. (2000). *Alaska Traditional Knowledge and Native Foods Database*. Retrieved 2016, from Alaska Native Science Commission and Institute of Social and Economic Research : http://www.nativeknowledge.org/

Zhang J., R. D. (1998). Warming of the Arctic Ocean by a strengthened Atlantic inflow: model results. *Geophysical Research Letters, 25*, 1745–1748.

Zhang, J. a. (1997). On an efficient numerical method for modeling sea ice dynamics. *Journal of Geophysical Research, 102*.

Zillman, J. (1972). A study of some aspects of the radiation and heat budgets of the southern hemisphere oceans. . *Meteorolog. Australian Government Publishing Service* .